Universitat Autònoma de Barcelona

GEOCHEMICAL BEHAVIOUR OF URANIUM AND THORIUM IN THE WASTE OF A URANIUM CONVERSION FACILITY

Teresa Fernandes

UNIVERSITAT AUTÒNOMA DE BARCELONA

INSTITUT DE CIÈNCIA I TECNOLOGIA AMBIENTALS

GEOCHEMICAL BEHAVIOUR OF URANIUM AND THORIUM IN THE WASTE OF A URANIUM CONVERSION FACILITY

Teresa Fernandes

PhD thesis, 2017

Directors: Dr. Lara Duro Pérez

Dr. Pere Masqué Barri

ABSTRACT

The waste contained in the decantation basins of the uranium conversion plant of Comurhex-Malvési, France, was characterised to investigate the behaviour of uranium and thorium in this specific environment. The waste is a succession of heterogeneous strata comprising a mixture of the process effluent with soil (arising from the re-construction of the basins' dykes), the sludge effluent, and the former sulphur mine tailings and flotation waste over which the basins have been sited. The original sludge effluent has a heterogeneous chemical composition that varies spatially and with depth in the basins due to the evolution of the conversion process over time and due to the different raw material received from mines around the world.

In this thesis, a detailed examination of waste cores and pore waters, static batch and kinetic column test work, and geochemical modelling was combined to characterise the composition of the material and the geochemical speciation of uranium and thorium.

The data reported in this thesis have elucidated the geochemical mechanisms that control the migration of these elements and how this migration can be affected in the long term.

Uranium in the stratum of sludge is present under more than one speciation: as a silicate phase, as a uranyl-oxide phase, adsorbed to iron oxy-hydroxides and associated with major minerals, such as gypsum and calcite. Uranium in the other strata of waste is present at concentrations that were not quantifiable by spectroscopic techniques. The release of U(VI) and its transport within the oxidising strata of sludge is dominated by kinetically-limited dissolution and transformation of uranophane, or a similar uranyl-silicate phase. Aqueous uranium concentrations under experimental conditions are controlled by a mineral phase. schoepite (dehydrated) was found to be the most common solubility limiting mineral. However, at the field scale, and due to the heterogeneous nature of the waste in the basins, it is possible that, locally, other uranium phases may be the main solubility controlling minerals.

Thorium is homogeneously distributed in the sludge, and occasionally correlated with uranium, as a U-Th oxide. Thorium concentrations in solution are controlled by ThO_2.

This work has put in evidence the importance of an approach comprising complementary techniques in the characterisation of the solid speciation of uranium and thorium in a heterogeneous material. The use of multiple techniques is required to identify different

phases and in order to establish multiple lines of evidence for the presence of a certain physical form.

RESUMEN

Los residuos contenidos en las balsas de decantación de la planta de conversión de uranio de Comurhex - Malvési, Francia, han sido caracterizados con el objectivo de investigar el comportamiento de uranio y torio en este entorno específico. El residuo es una sucesión de estratos heterogénea que comprende una mezcla de los efluentes del proceso con el suelo (que han tenido su origen en la re-construcción de los diques de las balsas, el efluente de lodo, y los antiguos desechos de las minas de azufre y de flotación de residuos sobre las que las balsas han sido localizadas. El efluente de lodo original tiene una composición química heterogénea que varía espacialmente y con la profundidad en las balsas debido a la evolución del proceso de conversión con el tiempo y debido a la materia prima recibida de diferentes minas del mundo.

En esta tesis, se combinó un examen detallado de los desechos y del agua intersticial, experimentos de batch y en columna, y el modelado geoquímico para caracterizar la composición del material y determinar la especiación geoquímica del uranio y el torio.

Los datos presentados en esta tesis han elucidado los mecanismos geoquímicos que controlan la migración de estos elementos y cómo esta migración puede verse afectada en el largo plazo.

El uranio en el estrato de los lodos está presente en más de una especiación: como una fase de silicato, como una fase de óxido de uranilo, adsorbido en oxihidróxidos de hierro y asociados a los principales minerales, tales como yeso y calcita. Uranio en los otros estratos de residuos está presente en concentraciones más bajas que las cuantificables mediante técnicas espectroscópicas. La liberación de U (VI) y su transporte dentro de los estratos oxidantes de los lodos está dominado por disolución limitada cinéticamente - y transformación de uranofana, o una fase similar de uranilo - silicato. Las concentraciones de uranio acuoso bajo condiciones experimentales son controladas por una fase mineral. La fase mineral limitante de solubilidad más común en condiciones experimentales ha sido la schoepita (deshidratada). Sin embargo, a escala de campo, y debido a la naturaleza heterogénea de los residuos en las balsas, es posible que, a nivel local, otras fases de uranio pueden ser los principales minerales de solubilidad control.

El torio se distribuye homogéneamente en los resíduos, y se encuentra, ocasionalmente correlacionado con el uranio como óxido de U-Th. Las concentraciones de torio en solución son controladas por ThO_2. Este trabajo ha puesto en evidencia la importancia de un enfoque que comprenda técnicas complementarias en la caracterización de la especiación sólida de uranio y torio en un material heterogéneo.

ACKNOWLEDGMENTS

I would like to thank, first and foremost, to Dr. Lara Duro and Dr. Pere Masqué, without whom this thesis would never have been carried through to completion. Their guidance, direction and patience helped keep this project in the right path and see the light of day. I would also like to thank Dr. Anne Delos, who nurtured this project and got it off the ground.

This project would not exist if it weren't for the financial support of AREVA and the technical guidance of Walter Van Hecke, Gerard Videau and Jean-Sébastien Flinois at the site of Malvési. Their assistance with all queries relating to the site and waste management aspects of the basins, as well as assistance with access to the basins and collection of samples, are especially appreciated.

Part of this thesis was carried out at the Karlsruhe Institute of Technology Institute for Nuclear Waste Disposal (KIT INE), in Germany, where a large part of the data presented in this study were obtained. For that, I would like to thank Dr. Thorsten Schäfer who provided technical direction both during and after my stay and facilitated access to the Institute's laboratory resources and the ANKA Synchrotron Radiation Facility. I am forever indebted to everyone at the Institute who kindly assisted with laboratory analysis of the samples, including Dieter Schild, Stephanie Heck, Eva Soballa, Conny Walschburger, Stefanie Hilpp, Kerstin Bender, Dr. Kathy Dardenne and Dr. Joerg Rothe; to Dr. Florian Huber for providing guidance throughout my stay; and to my office colleagues, Yury and Louie, for always being ready for a laugh. The research stay could not have been completed without the financial support of the European FP7 TALISMAN project (grant number TALI_C01_09) under contract with the European Commission.

I would also like to thank my colleagues at the UAB: Valentí, Viena, Muntsa, Giada, Maxi, Jordi and especially Núria and Joan Manel for their help throughout the thesis, both in and outside of the laboratory. A big thank you goes to my colleagues and friends at Amphos, especially Vanessa, Marek and Flávia for being always ready to help resolve issues with the Phreeqc models. Thank you to Mireia for making me feel part of a team right from the start of the project, even if I was rarely at Amphos for the first few years of the project.

Finally, I would like to thank my friends Rafa, Joana G. and Joana L. for reminding me of the important things in life, Inês for helping put things in perspective and Carlos for never doubting I could take this adventure to the end. Last, but not least, thank you Mum, Dad, Sérgio, João, Xuca and Dino for always being there for me.

LIST OF CONTENTS

LIST OF FIGURES

LIST OF TABLES

LIST OF ABBREVIATIONS

ADU – Ammonium DiUranate precipitation process

ANDRA – *Agence Nationale pour la Gestion des Déchets Radioactifs*

ASN –*Autorité de Sûreté Nucléaire*

B1/**B2** – Decantation basins B1 and B2 of the AREVA NC Site of Malvési

BTC – Breakthrough Curve

C – Contaminant Concentration

C_0 – Initial Contaminant Concentration

CDE – Convection-Dispersion Equation

COMURHEX – Société pour le Conversion de l'URanium en metal et en HEXafluoride

EDS – Energy Dispersive X-ray

EGME – Ethylene Glycol Monoethyl Ether

EXAFS – Extended X-ray Absorption Fine Structure

FA – Fulvic Acids

HA – Humic Acids

HTO – Tritiated Water

IAEA – International Atomic Energy Agency

ICP-MS – Inductively Coupled Plasma – Mass Spectrometry

K_D – Partition Coefficient

MIM – Mobile-Immobile Model

PNGMDR –*Plan National de Gestion de Déchets et Matières Radioactives*

PV – Pore Volume

PVC – Polyvinyl Chloride

SEM – Scanning Electron Microscopy

SF – Stop Flow

SRU – *Sociéte de Raffinage de l'Uranium*

SUCP – *Société des Usines Chimiques de Pierrelatte*

TICTOC – Total Inorganic Carbon Total Organic Carbon

UV - Ultraviolet

XAFS –X-ray Absorption Fine Structure

XANES – X-ray Absorption Near Edge Structure

XAS – X-ray Absorption Spectroscopy

XRD – X-ray Diffraction

XRF – X-ray Fluorescence Spectroscopy

XPS – X-ray Photoelectron Spectroscopy

1. Introduction

1.1 Overview

Nuclear activities produce large amounts of waste that require appropriate management and disposal. In addition to posing a threat to human health and the environment, if not properly controlled, nuclear and radioactive waste can arise sentiments of fear and rejection, leading to a generally negative public perception. The purification and conversion of natural uranium into uranium tetrafluoride results in large quantities of liquid waste effluents that contain ^{238}U, ^{235}U, ^{234}U and ^{230}Th, and their daughter products. Due to their long half-lives, uranium and thorium will persist in the environment. As emitters of alpha particles, they present a direct health hazard, either directly or via their daughter products.

One of the largest uranium conversion facilities in the world, operating since 1959, is the Malvési plant, located in Narbonne, France, and operated by AREVA NC. In 2013, it had an annual production of nearly 12,500 tonnes of UF_4 (AREVA NC Malvési, 2013), representing 16% of the world conversion capacity (IAEA, 2014). Since 1959, the waste effluents from this facility have been managed by decantation and subsequent natural evaporation in basins. In 2004, two of the decantation basins (B1 and B2, Figure 1.1) ceased operation and, with no supernatant remaining, were covered with a layer of soil to minimise wind dispersion of contaminated dust. The facility occupies the site of a former sulphur mine and the basins are located on what were once the sulphur tailings and sulphur flotation waste basins. There is no liner isolating the conversion waste from the former sulphur mine tailings and the potential for downward percolation of contaminants towards the sulphur waste and subsequently to the environment are poorly understood. Furthermore, the basins occupy an elevated position with relation to the surrounding landscape posing an increased risk of contaminant migration towards the environment.

The objective of this work is to advance the understanding of the speciation and mobility of uranium and thorium in the waste contained in basins B1 and B2 of the AREVA NC Malvési plant.

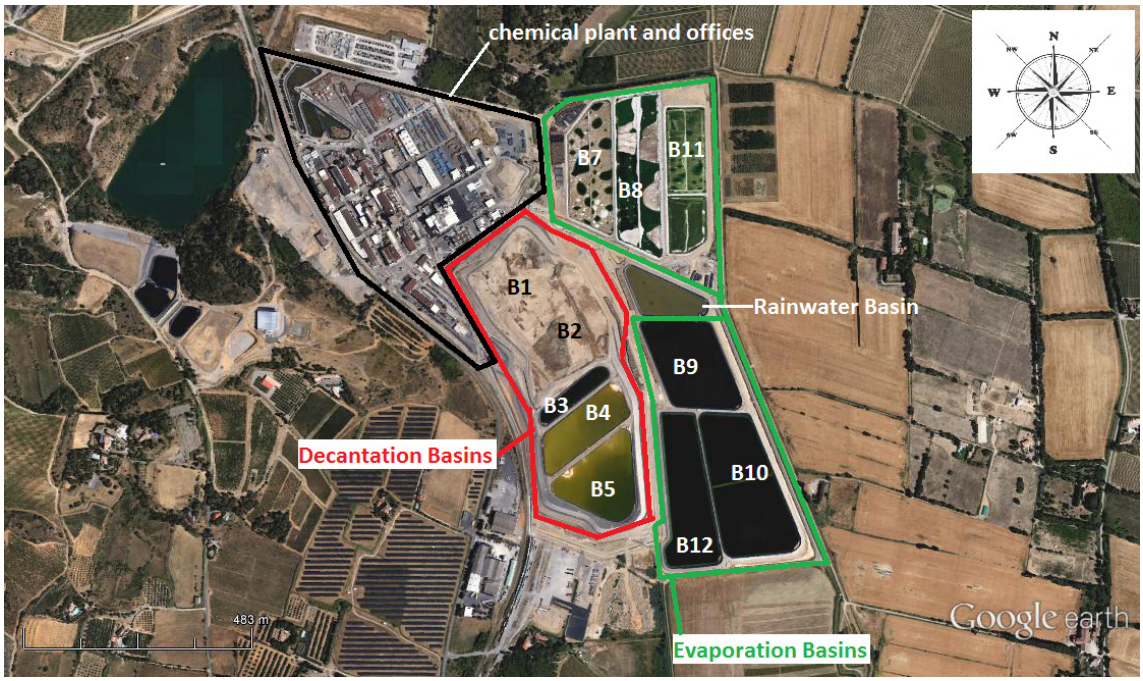

Figure 1.1: Aerial view of the AREVA NC Malvési site showing the location of the chemical plant and offices, the decantation and the evaporation basins. Basins B1 and B2 are no longer operational and currently provide interim storage of the waste.

1.2 Background

1.2.1 The Nuclear Fuel Cycle

At the end of 2015, there were 441 nuclear power reactors in operation worldwide, with a global generating capacity of 382.9 GWh (IAEA, 2016). In addition, 68 reactors were under construction at the same time. Most these reactors are fuelled by enriched uranium, which contains 3 to 5% ^{235}U, the remaining uranium comprising ^{238}U. The processing, use and disposal/recycling of the nuclear fuel comprises several chemical and physical steps, a simplified diagram of it is presented in Figure 1.2.

The cycle can be divided in the “front end”, i.e. the preparation of the fuel, the “service period”, in which fuel is used during reactor operation to generate electricity, and the “back end”, which comprises the management of the spent fuel, be it reprocessing and reuse or its disposal.

The processes of mining, milling, conversion and enrichment form the “front end” of the nuclear fuel cycle. Uranium ore *mining* is carried out either by excavation (underground or open pit) or by *in situ* techniques that consist in circulating oxygenated groundwater

(with sulphuric acid or sodium bicarbonate-carbonate solutions) through the porous orebody to dissolve the uranium oxide and bring it to the surface.

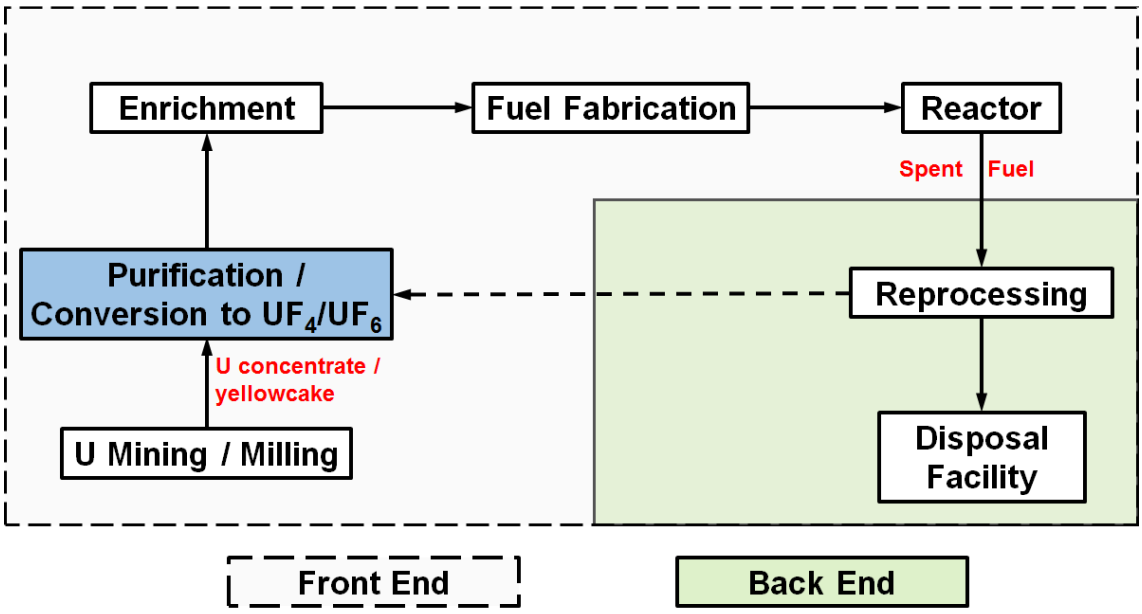

Figure 1.2: Simplified diagram of the nuclear fuel cycle.

In the *milling stage*, the concentrated uranium oxide is extracted from the ore by crushing, grinding and chemical treatment followed by oxidation of U(IV) to U(VI). This produces a powder of concentrated uranium (as uranium oxide or as uranates) known as yellowcake. Following the milling process, the yellowcake is *purified* from impurities and *converted* into uranium tetrafluoride (UF_4). If enrichment is required, the UF_4 is further converted to the gaseous uranium hexafluoride (UF_6), otherwise it is converted to uranium dioxide (UO_2). The enrichment stage comprises mass separation of the lighter $^{235}UF_6$, either by centrifugation or diffusion. The product containing enriched ^{235}U is then reconverted to produce enriched uranium oxide, which in turn is compressed and sintered at the *fuel fabrication* plant to make 1 cm long *pellets*. The pellets are encased in metal tubes, forming fuel rods, which are arranged into a fuel assembly. Several hundred of these fuel assemblies make up the core of a nuclear reactor.

In a nuclear reactor core, when ^{235}U absorbs a neutron, it may split (or fission) into two radioactive fission products giving off energy as heat and a few more neutrons to continue this nuclear chain reaction. Uranium-238 is not fissile, however, some ^{238}U nuclei can capture a neutron and be transformed into ^{239}Pu, which is fissile and can generate energy through nuclear fission. A small fraction of ^{239}Pu can also be transformed into other plutonium isotopes by neutron capture mechanisms and produce

minor actinides, such as neptunium-237, americium-241, americium-243, curium-242 through to -248 and californium-249 through to -252.

At the end of a lifetime of 3-6 years, the fuel assemblies are removed from the reactor core, albeit still containing large amounts of fissile material, in particular uranium and plutonium. In a closed nuclear fuel cycle, the spent fuel is reprocessed in order to recover the uranium (about 96%) and plutonium (≈1%). The uranium, the plutonium and the remaining 3% comprising high level radioactive waste products are chemically separated. Uranium and plutonium can be used to fabricate mixed oxide fuel. The uranium can also be recovered into the “front end” of the nuclear fuel cycle. The high level waste is vitrified and disposed in a high level waste disposal facility.

1.2.2 Natural uranium conversion plants

Currently, five countries operate commercial scale plants for the conversion of yellowcake to uranium hexafluoride (UF_6) (IAEA, 2016): Canada, China, France, Russian Federation and USA, as summarised in Table 1.1. The UK ceased conversion of uranium in its Springfields facility in 2014. All plants, except in the USA, follow a two facility model where oxidation to UF_4 and fluorination to UF_6 are carried out in separate facilities (Schneider, Carlsen and Tavrides, 2010). In addition, seven other countries operate small conversion facilities: Argentina, Brazil, India, Islamic Republic of Iran, Japan and Pakistan. In total, there was an annual conversion capacity of approximately 60,000 tonnes of uranium as UF_6 per year in 2015 (IAEA, 2016).

Table 1.1: Commercial scale uranium conversion plant operators.

Company	Facility	Country	Status	Capacity (tonnes U / year)	Notes
AREVA	COMURHEX I Malvési	France	Operating since 1959	14,000 as UF_4	1
	COMURHEX I Pierrelatte	France	Operating since 1961	14,000 as UF_6	1
	COMURHEX II Malvési	France	Operating since 2016	15,000 as UF_4	1
	COMURHEX II Pierrelatte	France	Operating since 2016	15,000 as UF_6	1
	URT II Pierrelatte	France	Under study	-	2
TVEL (Atomenergoprom)	Angarsk	Russia	Closed 2014	(18,700)	3
	Glazov	Russia	Closed 1990’s	-	5
	SCC Seversk	Russia	Operating	12,500 as UF_6	3, 6, 7
Cameco	Port Hope	Canada	Operating since 1984	12,500 as UF_6	1

Company	Facility	Country	Status	Capacity (tonnes U / year)	Notes
China National Nuclear Corporation (CNNC)	Lanzhou	China	Operating since 1980	5,000	3, 8
ConverDyn (Honeywell)	Metropolis	USA	Operating since 1958	15,000 as UF_6	1
Westinghouse	Springfields	UK	Closed 2014	6,000 as UF_4/UF_6	4

1 – plant capacity as publicly available in the operator website: www.areva.com (AREVA), www.cameco.com/annual-report/2015 (Cameco), converdyn.com/metropolis (ConverDyn);
2 - (White *et al.*, 2010);
3 – plant capacity as per information held by the World Nuclear Association: www.world-nuclear.org/information-library/country-profiles/countries-a-f/china-nuclear-fuel-cycle.aspx (CNNC), and www.world-nuclear.org/information-library/country-profiles/countries-o-s/russia-nuclear-fuel-cycle.aspx (TVEL);
4 – plant capacity as per the IAEA: https://infcis.iaea.org/NFCIS/FacilityDetails/583 (Westinghouse);
5 – capacity prior to closure unknow;
6 – data of start of operation unknown;
7 – capacity to increase to 20,000 tonnes U (as UF_6) per year in 2016;
8 – final product unknown

The conversion process used in all facilitites, except in the USA, is the wet fluoride volatility process, which comprises the dissolution of yellowcake, purification by solvent extraction and conversion in a series of denitration, reduction, hydrofluorination and fluorination steps to UF_6 or uranium metal (Raffo-Caiado *et al.*, 2009). The flow diagram in Figure 1.3 depicts the steps of the “wet” process.

1.2.3 Uranium conversion effluents

Liquid waste effluents are generated at various points of the uranium conversion process, with the higher volume of waste arising from the purification and hydrofluorination steps. The effluents from the purification stage contain uranium and thorium and the daughter radionuclides of their decay chains, in particular of the ^{238}U decay chain. The sludge arising from the hydrofluorination step contains small amounts of uranium and calcium fluoride that results from neutralisation of unreacted HF by lime (IAEA, 1999).

Both uranium and thorium pose a concern for environmental management due to their long half-lives ($4.5 \cdot 10^9$, $245.5 \cdot 10^3$ and $75.7 \cdot 10^3$ years for ^{238}U, ^{234}U and ^{230}Th respectively) and emission of alpha particles. Figure 1.4 presents the natural decay chain of ^{238}U, the half-life and the type of decay of each isotope. The alpha particles cannot penetrate the skin but they pose a health risk when taken into the body by inhalation or ingestion, as the energy of the ionisations can damage tissue and DNA, inducing cancer. Moreover, uranium is chemically toxic. Uranium can damage kidney tubular cells, when ingested, and the respiratory tract, when inhaled. In addition, it can target the

reproductive system and the developing organism (ATSDR, 2013). Thorium, like other heavy metals, is toxic in the body although its chemical toxicity is low (ATSDR, 1990b; Keith and Wohlers, 2014). The main risk posed by thorium is the additional impact of its daughter products ^{226}Ra and ^{222}Rn. Radium-226 presents a radiation risk from its gamma emissions. Radon-222 is chemically inert, however, as a gas, it can escape the waste and be transported by wind. Its progeny, which includes lead, bismuth and polonium, can be inhaled via contaminated dust and deposit in the respiratory system. Radon daughters, in particular the alpha emitting isotopes ^{218}Po and ^{214}Po, pose a significant health hazard in relation to lung cancer (ATSDR, 1990a).

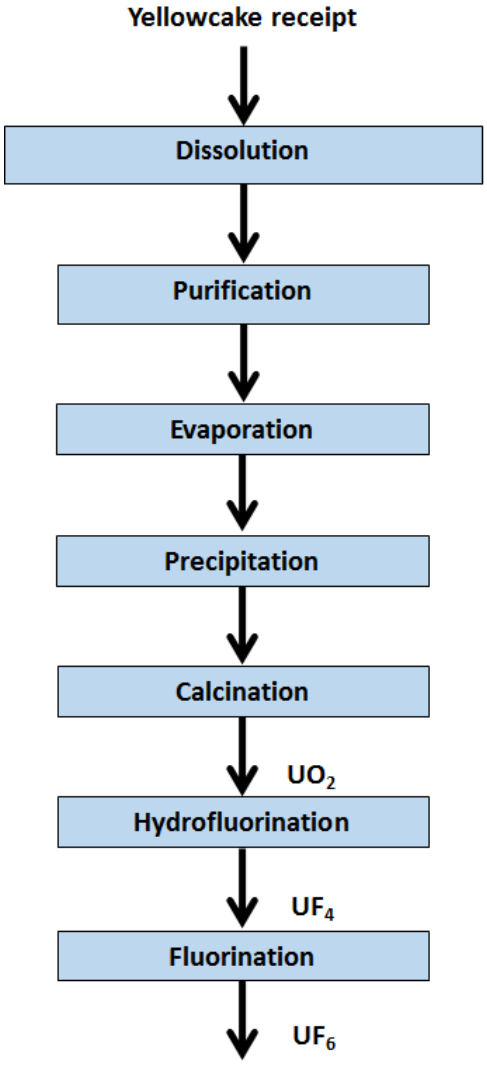

Figure 1.3: Simplified flow diagram of the "wet" conversion process (adapted from Raffo-Caiado et al. 2009).

Other concerns associated with management of uranium conversion effluents include the presence of artificial radionuclides, namely ^{236}U, $^{239+240}Pu$, ^{241}Am and ^{99}Tc, when reprocessed uranium is used as feed material, and high concentrations of heavy metals associated with the uranium ore. In addition, the use of large quantities of hazardous chemicals in the process such as nitric acid, ammonia and hydrofluoric acid, pose management problems. According to Areva (Schneider, Carlsen and Tavrides, 2010), the production of 1 tonne of UF_6 requires 0.69 tonnes of hydrofluoric acid, 2.07 tonnes of nitric acid and 0.54 tonnes of ammonia. These chemicals, together with calcium hydroxide added to the liquid effluent in the pH neutralisation step, can form salts of nitrate, ammonia and fluoride in the final effluent, increasing the effluents' ionic strength.

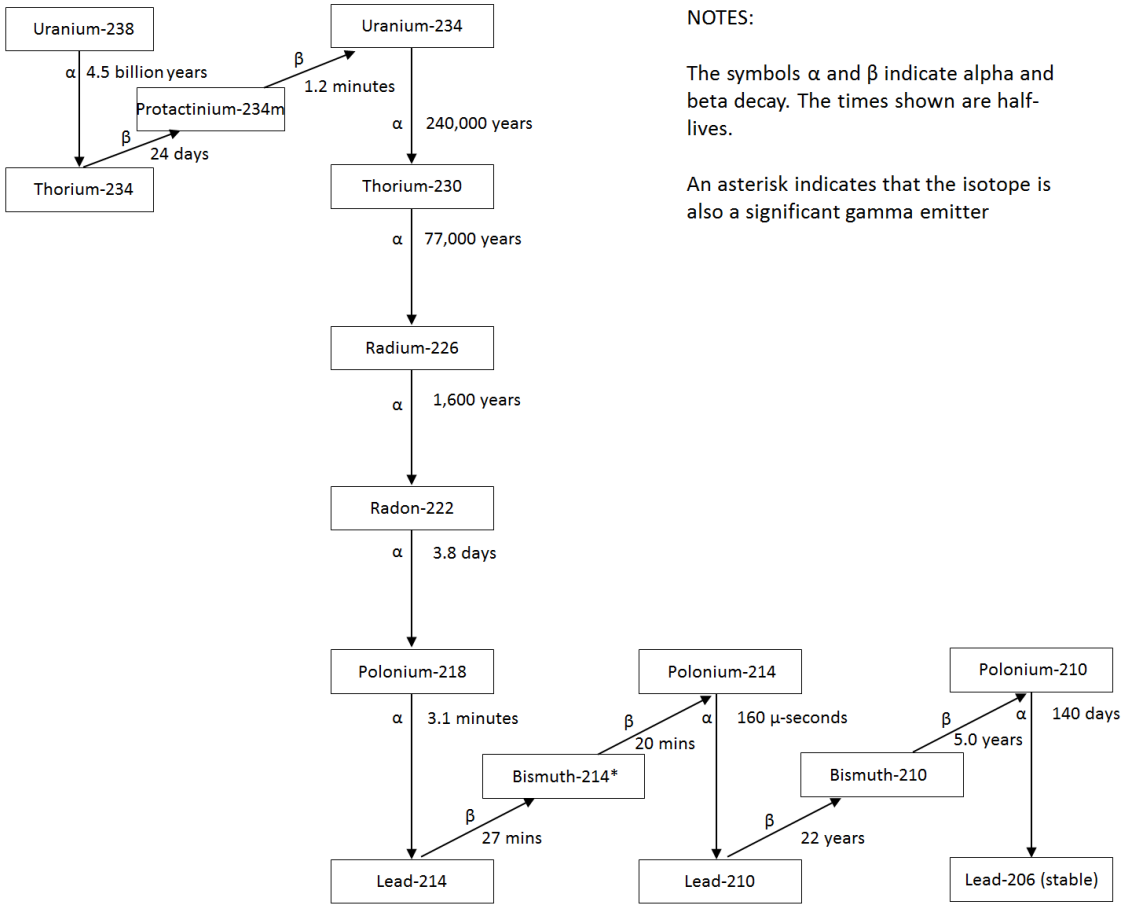

Figure 1.4: Natural decay chain of uranium-238.

1.2.4 Decantation waste stored in basins B1/B2 of the AREVA NC Malvési plant

Due to its low activity (between 10^2 and 10^5 Bq/g) and presence of long-lived radionuclides (i.e. with a half-life of more than 31 years), the waste contained in basins B1 and B2 is classified as Low Activity-Long Life (FA-VL, faible activité-vie longue) under the French Radioactive Waste Classification. However, the radiological characteristics

of the waste (elevated activity in thorium (50% of total alpha activity) and presence of artificial radionuclides (1% of total activity)) result in failure of the acceptance criteria for disposal at the French low level waste storage centre (Cires) (ASN, 2013).

The French Nuclear Security Authority (ASN, Autorité de Sûreté Nucléaire) produces, every three years, the National Plan for the Management of Radioactive Waste and Radioactive Materials (PNGMDR - Plan National de Gestion des Déchets et Matières Radioactives), where the national inventory of radioactive waste is compiled. The PNGMDR for the period comprising 2013 to 2015 (ASN, 2013) lists the B1/B2 waste as waste that does not have a regulated management approach. The ASN therefore requires that AREVA NC undertakes feasibility studies on the options for final disposal of this waste.

Arcadis (Bary *et al.*, 2010a, 2010b) and Burgeap (Burgeap, 2009a) have carried out initial characterisation studies of the waste. However, due to the complex waste composition, the solubility mechanisms controlling uranium and thorium behaviour could not be established. Release and retention kinetics of uranium and thorium in the waste have not been investigated.

1.2.5 Studies of uranium and thorium behaviour in the environment

The speciation, migration and retention of uranium and thorium has been investigated in soils contaminated by nuclear activities, such as the soils underlying or in the vicinity of large nuclear complexes such as the Hanford site, US (Cantrell, Serne and Last, 2002; Liu *et al.*, 2004; Qafoku *et al.*, 2005; Wang *et al.*, 2005; Catalano *et al.*, 2006; McKinley *et al.*, 2006; Um *et al.*, 2007), and the Savannah River site, US (Kaplan and Serkiz, 2001; Serkiz *et al.*, 2007), and in uranium mill tailings (Landa *et al.*, 2000; Kelly *et al.*, 2003; Landa, 2004; Zachara *et al.*, 2013). Studies of the geochemical behaviour of uranium and thorium have also been carried out in former uranium conversion facilities such as the Weldon Spring Chemical Plant, US (Seeley and Kelmers, 1985), the Fernald site, US (Rautman *et al.*, 1994), and the Itteville disposal site (France) which received the waste of the dismantled Le Bouchet uranium ore treatment plant (Phrommavanh, 2008). However, the studies investigated the behaviour of these elements in the soils in the vicinity of the sites, and not in the waste itself. Characterisation of the waste arising from the currently operational commercial scale uranium conversion facilities, such as the plants listed in Table 1.1, if existent, are not publicly available.

Characterisation of the geochemical behaviour of uranium and thorium in environments where these radionuclides naturally occur in elevated concentrations has been advanced by studies of the Poços de Caldas site, Brazil (Miekeley and Küchler, 1987; MacKenzie *et al.*, 1992; Miekeley *et al.*, 1992; Cera *et al.*, 2002), the Palmottu natural analogue site, Finland (Cera, Bruno and Duro, 1999; Ahonen *et al.*, 2004), the Koongarra uranium deposit, Australia (Short, 1988; Yanase, 1991; Payne *et al.*, 1992; Sato *et al.*, 1997; Murakami *et al.*, 2005), or the San Joaquin Valley evaporation ponds, US (Duff *et al.*, 2000).

1.3 Research Scope, Objectives and Approach

The questions being addressed in this study are:

1. What are the chemical and physical characteristics of the waste contained in basins B1/B2, including typical concentrations of uranium and thorium? How do these characteristics affect the retention and release of uranium and thorium?
2. What is the predominant form (solid and liquid speciation) of uranium and thorium in the waste contained in the B1/B2 basins? How does the speciation affect mobility of these elements in the waste?
3. What are the main geochemical processes and mechanisms contributing to the retention and release of uranium and thorium from the waste?

To meet the objectives discussed above, a series of controlled experiments was designed and conducted along the following four points:

1. Characterisation of the waste, including its solid and liquid fractions;
2. Characterisation of uranium and thorium in samples of waste;
3. Investigation of the elution of uranium and thorium under static (batch) conditions; and
4. Investigation of the elution of uranium and thorium under dynamic (column) conditions.

The experiments were carried out in two laboratories, the Environmental Radioactivity Laboratory (LRA) of the Autonomous University of Barcelona (UAB), Spain, and at the Institute of Nuclear Waste Management (INE) of the Karlsruhe Institute of Technology (KIT), Germany.

The study started with the characterisation of existing solid samples collected by Arcadis (Bary *et al.*, 2010a, 2010b) during their 2009 investigation of the basins. These samples

are referred throughout the text as “2009” or “aged” samples and were subjected to analysis in both laboratories. In 2012, AREVA NC provided the opportunity to collect additional samples and borehole SC429 was drilled in basin B1. Core samples from this borehole were transported to the KIT-INE laboratory for analysis. A separate visit to site was undertaken to collect groundwater samples from existing groundwater wells.

1.3.1 Thesis structure

This thesis is structured in the following order; Chapter 2 presents the AREVA NC Malvési facility. The objective of the chapter is to describe the aspects that are relevant to understanding the current composition of the waste, such as the chemical conversion process and the history of the decantation basins. In addition, previous investigations carried out to characterise the waste and their results are summarised.

Chapter 3 provides a summary of the current state of knowledge of the geochemistry of uranium and thorium under environmental conditions (low pressure and ambient temperature), and mechanisms that may contribute to retention or mobilisation of these elements.

The experimental approach followed (Chapter 4) integrated bulk and molecular scale characterisation of the solid samples with solution chemistry measurements. Multiple techniques were used to probe specific aspects of the system at different spatial scales. Bulk characterisation of the solid samples comprised measurement of density, moisture content, total surface area, chemical composition and mineralogy. Sequential extraction was used to investigate the mineral phases capable of retaining uranium and thorium. Prior to the use of spectroscopic and synchrotron techniques, areas of enhanced activity of the samples were identified by autoradiography. Scanning Electron Microscopy (SEM) with energy dispersive X-ray (EDS) analysis was used to image individual areas containing uranium and Raman spectroscopy was used to investigate the molecular bonding environment of uranium. Synchrotron techniques were applied for the determination of the uranium oxidation state and its elemental composition in the samples (micro X-ray absorption spectroscopy, µ-XAS) and to map the distribution of uranium and thorium in the samples and determine their spatial correlation with other elements (X-ray fluorescence spectroscopy, µ-XRF). Solution chemistry was analysed for a range of parameters. The techniques used depended on the laboratory were the analysis were carried out, but generally comprised measurement of pH, Eh, dissolved carbon and alkalinity, and analysis of cations, anions, Fe(2)/Fe(3) and NO_2/NO_3 pairs, uranium and thorium. Solution chemistry was speciated in Phreeqc. The methodology

and main findings of the intrusive investigation and groundwater sampling campaign are described in Chapter 5.

Chapter 6 presents the results of the characterisation of the solid samples and the predominant solid speciation of uranium and thorium. The speciation of uranium and thorium in groundwater and porewater samples is also presented and discussed.

The findings of the batch experiments, such as characterisation of uranium and thorium mobility in the colloidal form, rates of release, fraction of total initial uranium and thorium released, speciation and dependency on other elements is presented in Chapter 7.

Chapter 8 presents the findings of the investigation of the retention of uranium and thorium in the solid samples under column experimental conditions, such as the rate and fraction released, and geochemical speciation. One of the questions being addressed in this study is whether, and how fast, uranium and thorium migrating downwards from the sludge is being retained in the tailings. This is investigated in Chapter 8.

Finally, in Chapter 9, the main findings of this study are summarised. Important accomplishments are highlighted, and areas for future research are identified.

2. The Malvési Site

This chapter describes the AREVA NC Malvési uranium conversion facility, its environment, the chemical process, the management of the liquid effluents and the waste contained in the decantation basins.

2.1 Location

The Malvési site is located 3 km to the north-northwest of Narbonne, in the southwest of France (Figure 2.1). It occupies an area of approximately 100 ha, with the built area occupying 2.2 ha in the northern part of the site, and the decantation and evaporation basins occupying approximately two thirds of the total area in the southern and eastern parts of the site (Figure 2.2). The site is bordered by the Livière alluvial plain to the north and east, wetlands to the south and the Hills of Narbonne to the west.

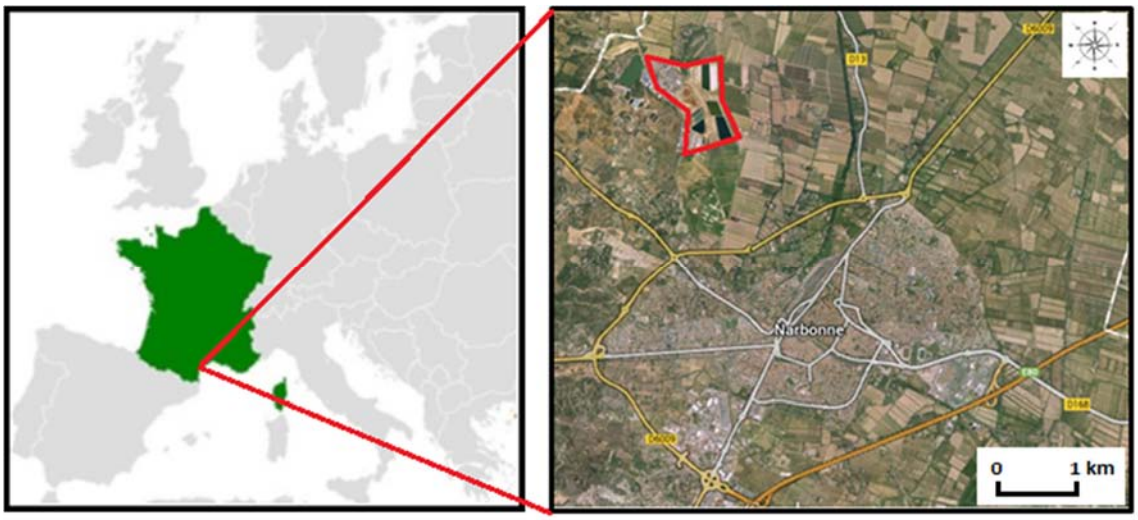

Figure 2.1: Location of the Malvési site, Narbonne, France.

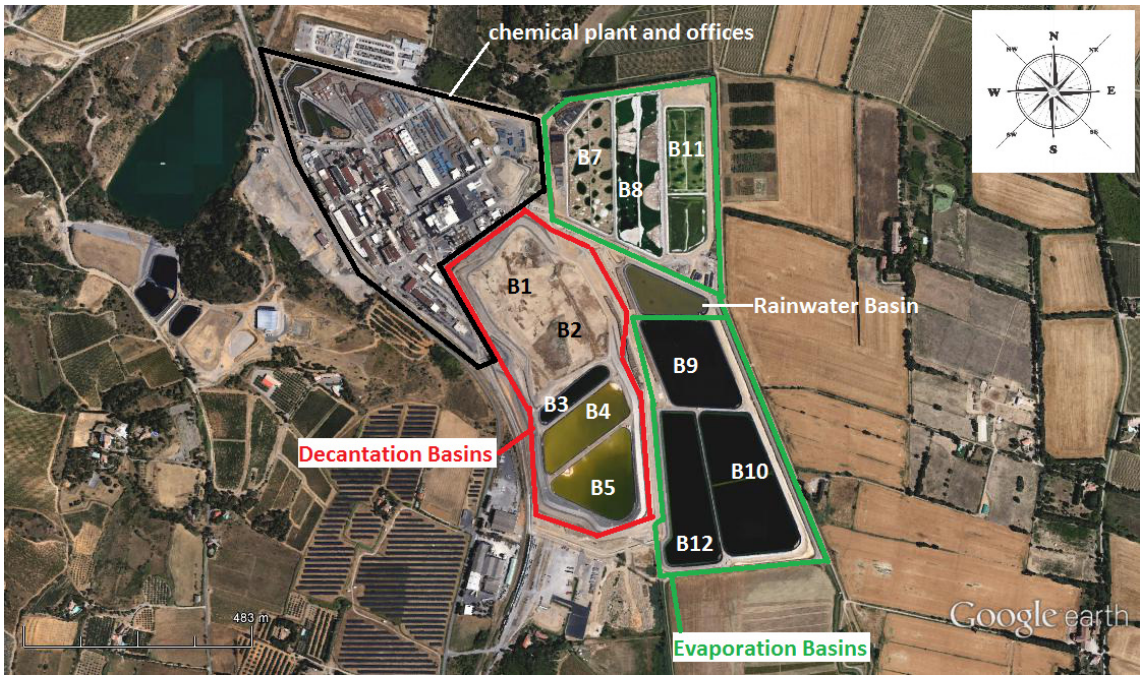

Figure 2.2: Aerial view of the site showing the location of the chemical plant and offices, the decantation and the evaporation basins.

2.2 Geology and Hydrogeology

The geology of the site comprises the Quaternary Alluvium of silty clay of increasing thickness to the east that overlies the Upper Oligocene (red Shale). The alluvium is generally of low permeability (10^{-6} to 10^{-4} m/s), although more permeable (10^{-4} to 10^{-3} m/s) sandy layers of about 2-3 m thickness are found at depths of 5 to 8 m below surface level (Burgeap, 2010). The underlying Upper Oligocene is characterised by uncontinuous sandy / silty marl layers and by conglomerate channels at its base. Its thickness can exceed 75 m. At depth, the Upper Jurassic of grey limestone comprises the karstic aquifer.

Various geological faults aligned in a northeast-southwest direction are present to the northwest of the site. The closest of these faults is located approximately 200 m to the northwest of the B1 basin.

Two aquifers are present beneath the site:

- The 'semi-permeable' alluvial aquifer of the Tauran plain with its highest piezometric levels directly beneath the plant and basins, and
- The karstic aquifer contained in the Upper Jurassic strata. This aquifer is encountered at depth beneath the site but it discharges immediately to the north

of the site in the spring of Oeillal. This suggests that the aquifer is confined from the superficial aquifer by the Oligocene marl, which provides some protection from contaminant migrating from the alluvium.

The Oligocene strata comprises clays and shale of very low permeability ($1 \cdot 10^{-7}$m/s) and, due to its thickness of around 100 m, is an effective separation medium between the two aquifers described above. However, it is not unlikely that the waters from the two aquifers mix along the geologic faults. The permeability of the various strata on site is presented in Table 2.1.

Table 2.1: Permeability of the natural strata as measured by Burgeap (2010) beneath or in the vicinity of the site.

Strata	Permeability (m/s)
Upper Alluvium (clays)	$1 \cdot 10^{-8}$ to $6 \cdot 10^{-4}$
Lower Alluvium (gravelly sands)	$2 \cdot 10^{-6}$ to $4 \cdot 10^{-6}$
Oligocene (Dolomite)	$3 \cdot 10^{-6}$
Oligocene (Marl)	$1 \cdot 10^{-9}$ to $7 \cdot 10^{-7}$
Montlaurès Hills (Limestone)	$4 \cdot 10^{-5}$

2.3 The AREVA NC Malvési uranium conversion facility

In 1959, the Malvési Uranium Refining Company (SRU, Société de Raffinage de l'Uranium) was established for the chemical transformation of uraniferous compounds, in particular the conversion of uranium mining concentrates (yellowcake) in uranium tetrafluoride (UF_4) and uranium metal. Between 1960 and 1983, the facility also carried out recycling of low quantities of reprocessed uranium originated from the Marcoule nuclear site (France).

In 1971, SRU merged with SUCP (Société des Usines Chimiques de Pierrelatte or Pierrelatte Chemical Plant Company) specialised in the conversion of uranium tetrafluoride to uranium hexafluoride (UF_6) to become the COMURHEX Company (Société pour le COnversion de l'URanium en metal et en HEXafluoride). The main mission of COMURHEX is the conversion of yellowcake into uranium hexafluoride.

Originally hold by majority (51%) by the group ALUMINIUM PECHINEY, from 1992 to 2007, the company was a subsidiary of COGEMA (Compagnie Générale des Matières Nucléaires), which in turn was a subsidiary at 100% of AREVA. In 2007, COGEMA became AREVA NC and in 2013, AREVA NC created AREVA NC Malvési via a merger.

2.4 The uranium conversion process

Until 2016, the yellowcake received at the plant would be converted to UF_4 via the ADU (precipitation to Ammonium DiUranate) process (in 2016, and with the introduction of the Comurhex II process, conversion changed to a thermal denitration method). Fluorination to UF_6 is carried out in a separate facility, at the COMURHEX site of Pierrelatte.

Each batch of yellowcake (uranium concentrate) contains 70 to 75% of uranium in various chemical forms (magnesium, sodium and ammonium uranates and uranium oxides). On arrival to the plant, the concentrates were dissolved in nitric acid at 90ºC before being purified by solvent extraction with tributyl phosphate (TBP, $C_{12}H_{27}PO_4$). The extraction of uranium was undertaken according to the following reaction:

$$UO_2^{2+} + 2NO_3^- + 2\overline{TBP} \Leftrightarrow \overline{UO_2(NO_3)_2TBP_2} \quad \textbf{(2.1)}$$

The purified uranyl nitrate was then precipitated by injection of gaseous ammonia. The reaction formed insoluble ammonium diuranate (ADU, $(NH_4)_2U_2O_7$), which was separated from the mother liquor (a very pure solution of ammonium nitrate). The reaction describing this step is:

$$2UO_2(NO_3)_2 + 6NH_3 + 3H_2O \rightarrow (NH_4)U_2O_7 + 4NH_4NO_3 \quad \textbf{(2.2)}$$

The insoluble ammonium diuranate was dried and calcined at 400ºC in a furnace where it was transformed into uranium trioxide UO_3. The hydrofluorination process comprised a series of several furnaces in parallel to produce UF_4. In these furnaces, two successive reactions occurred:

i. Reduction of UO_3 to UO_2 by hydrogen formed by thermal cracking of ammonia gas:

$$UO_3 + H_2 \rightarrow UO_2 + H_2O \quad \textbf{(2.3)}$$

ii. Hydrofluorination of the uranium dioxide in tetrafluoride where the hydrogen fluoride travelling in counter current transforms the UO_2 to UF_4:

$$UO_2 + 4HF \rightarrow UF_4 + 2H_2O \quad \textbf{(2.4)}$$

The UF_4 was kept in storage silos until transportation to the plant of Pierrelatte for further fluorination prior to enrichment in ^{235}U.

Liquid waste effluents were generated at various points of the process although most of the volume arised from the solvent extraction process and the hydrofluorination step. The process (in black arrows) and the waste effluents (in red arrows) are shown schematically in Figure 2.3.

2.4.1 The Uranium Recovery Unit

The recovery unit receives the effluents containing uranium from the various chemical processes in order to recycle them back into the process. It also receives low content uranium bearing material from other installations (French and foreign) and byproducts from COMURHEX Pierrelatte. This introduced a number of impurities into the plant, including fission products The uranium depleted solution is disposed as waste effluent.

2.4.2 The Waste Effluents

The final effluent contains all elements of the uranium concentrates left after the extraction of uranium, such as heavy metals and the radionuclides of the natural radioactive chains, as well as artificial radionuclides originated from the treatment of recycled uranium. In addition, as part of the conversion process or treatment of the effluents with acids (HNO_3) and bases (NH_3, NaOH, KOH and $Ca(OH)_2$), various salts, including uranium and thorium salts, can be found in the final waste, i.e. nitrate, ammonium, fluoride and potassium salts, as well as chemicals such as sodium carbonate and tributyl phosphate (Perez, 1980) After uranium separation, the final waste effluent, containing less than 1 mg U/l is neutralised with lime, $Ca(OH_2)$, and discharged to decantation basins, where particles precipitate and accumulate. The effluent's quantity and quality are not well characterised. The supernatant solution is transferred to neighbouring basins for evaporation by natural action of the sun and wind.

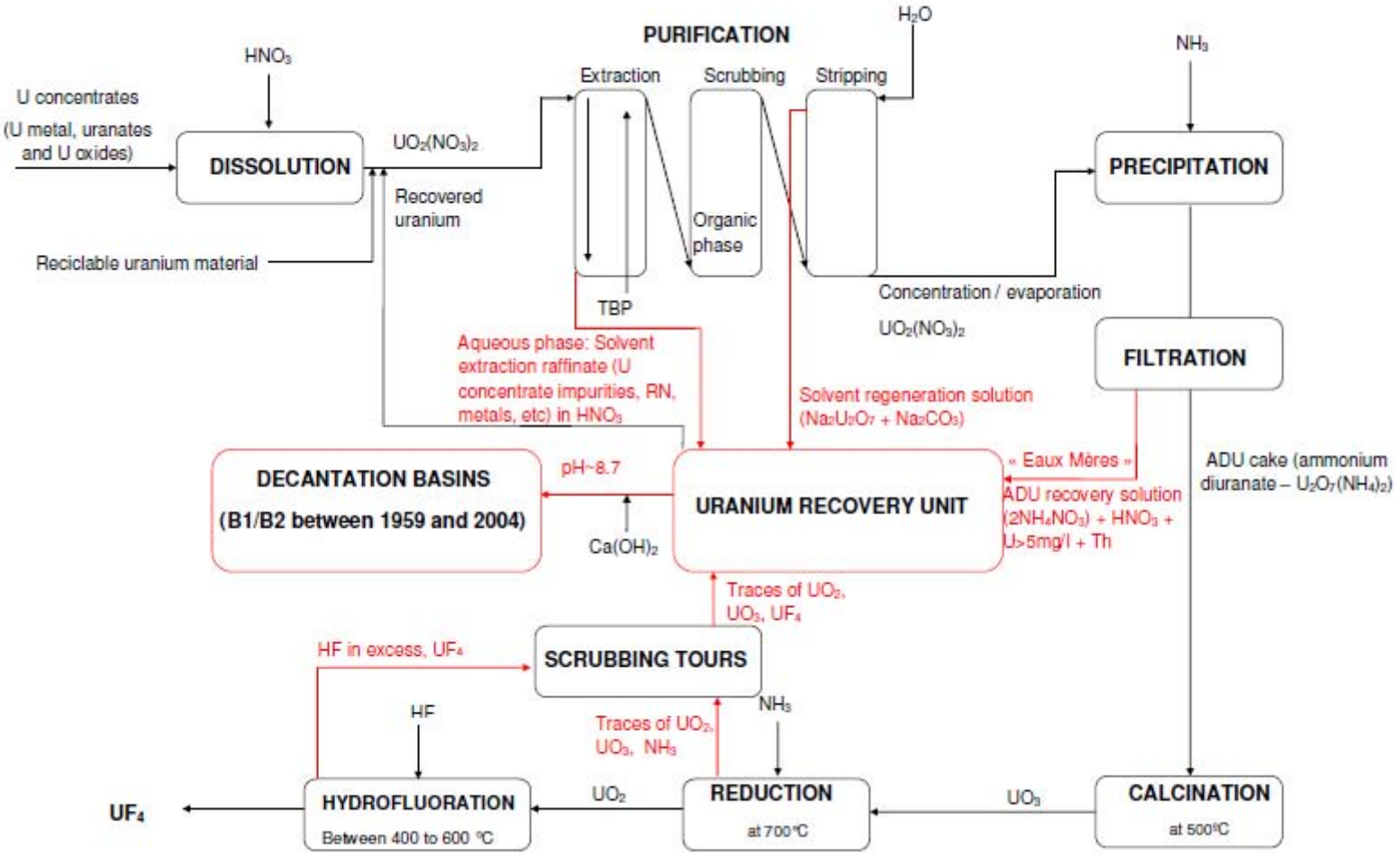

Figure 2.3: Main stages of the conversion process of uranium into UF_4. Black arrows denote the conversion process, red arrows denote waste effluents.

2.5 The Waste Basins

The five decantation basins, B1 to B6 (B4 has been merged with B5 and no longer exists), are located on the elevation formed by the sulphur mine tailings (Figure 2.3). Basins B1 to B5 have ceased operation and the process effluent is currently discharged to basin B6. The evaporation basins, B7 to B12, were constructed on the alluvial plain, to the east.

2.5.1 History of the decantation basins

Between 1945 and 1959, a sulphur mine occupied the Malvési site and the current decantation basins were constructed to receive the flotation waste arising from the mine activity. The sulphur mine tailings were used to build the basins and dykes directly on the alluvial plain (Schmitt, 1998). Aerial photographs of the site show basin B1, in 1946, as the first to be constructed (Figure 2.4). However, by 1956 (Figure 2.5), the whole B1-B6 massif had been built. At the time, the massif consisted of three basins, corresponding to the current B1, B2 and B3-B6 basins. The sulphur mine flotation waste was disposed in two phases (Schmitt, 1998), forming two cones of decantation. The first was disposed from the northwest corner of B1 and spread on B1 only, as shown in the 1946 aerial photograph. Later, the waste was discharged to the southwest corner of basin B2, forming a semi-cone of decantation around the southwest corner of B2 and the northwest corner of B3 (Schmitt, 1998).

When the uranium processing activity of SRU started, in 1959, the effluents were disposed directly to the north part of the basin, in what are currently basins B1 and B2. No barrier was constructed between the former sulphur mine flotation waste and the uranium conversion effluents. Initially, the uranium sludge was decanted in basin B1 and the supernatant transferred to basin B2 (Figure 2.6). From 1992 onwards, basin B2 also started to receive the sludge effluents (Bary *et al.*, 2009). By 1992 (Figure 2.7), the internal dyke separating basins B1 and B2 had been submerged by supernatant. In 2003, the dyke was raised by an estimated 2 m with material sourced from basin B3 (Bary *et al.*, 2010b) (Figure 2.8).

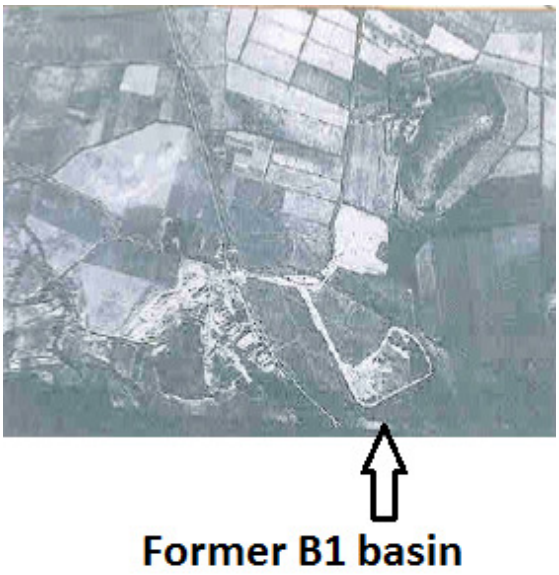

Figure 2.4: 1946 aerial photograph of the site showing the creation of the B1 decantation basin (extracted from (Schmitt, 1998).

Figure 2.5: 1956 aerial photograph of the site showing the B1/B6 massif and the semi-cone of decantation from the SW corner of B2 and NW corner of B3 (Bary et al., 2010b).

In 2004, the eastern dyke of the B2 basin broke, and the liquid sludge dispersed onto the alluvial plain, where nowadays are B10, B12 and the rainwater basin (Figure 2.9). Basins B1 and B2 immediately ceased operation. In 2006, a new dyke was constructed further to the east of the original dyke (Figure 2.10). The sludge spread on the plain was recovered, together with the sulphur mine waste, the broken dyke and the soils affected by contamination. It is estimated that the sludge represents 5% to 25% of this mixture (Bary *et al.*, 2010b), which is called 'mixture of soil and sludge'. This mixture was deposited in the area between the former and the new eastern dyke of B2, called East of B2, and on top of the remaining sludge on B1/B2. Bary et al. (2010b) estimate that around 70-80% of this material was disposed in B1/B2 with the remaining 20-30% disposed to the new East of B2. There is no protection of the alluvium beneath East of B2. A final layer of uncontaminated soils was deposited on top of B1, B2 and East of B2 to minimise contaminated dust emission, as show in the aerial photograph of the reconstructed basins, Figure 2.11. The basins B1/B2 will be used for intermediate storage of waste for the next 30 years. AREVA plans to construct a disposal cell for the waste arising from the emptying of decantation basins B5 and B6 in the south of B2 and to place a bituminous cover on top of basins B1/B2.

Figure 2.6: 1971 aerial photograph extracted from (Bary *et al.*, 2010b).

Figure 2.7: 1992 aerial photograph extracted from (Bary *et al.*, 2010b).

Figure 2.8: 2003 aerial photograph (Source: Google Earth).

Figure 2.9: Aerial view of the B1, B2 and B3 basins showing the rupture of the B2 eastern dyke, March 2004 (Source: AREVA).

The decantation basins B3 to B6 were constructed in the 1970s. These were initially built directly on the B1/B6 massif but were progressively equipped with geomembranes at the bottom. The evaporation basins that receive the nitrate solution are all equipped with a geomembrane at the bottom for prevention of contamination by infiltration. Basin B3 was operational between 1975 and 1985. From 1985 to 1996, when it ceased operation, the basin was drained and used to dispose all types of domestic and technological waste,

such as restaurant/canteen refuse, tyres, glass and plastic, old furniture, combustible material and asbestos (Bary *et al.*, 2010b).

Figure 2.10: Aerial view of the B1 and B2 basins showing the construction of the new B2 east dyke and emplacement of mixture of soil and sludge within the B1/B2 basins, March 2007 (Source: AREVA).

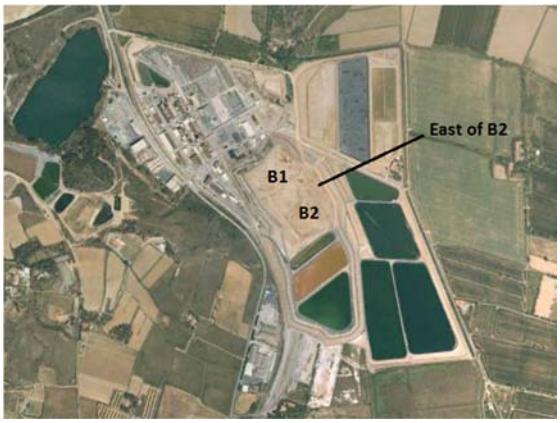

Figure 2.11: 2008 aerial photograph of the site showing the reconstructed B1/B2 basins (Source: Google Earth).

2.5.2 Piezometry within the basins

The piezometric level in B1/B2 is at 17 m NGF (*nivellement général de la France*), and is likely to represent the water level in the perched aquifer of the tailings. The groundwater level contours then follow the topography of the basins flowing along and with the basins' dykes (

Figure 2.12).

The alluvial aquifer beneath the B1/B6 massif is at a maximum level of 9.5 m NGF in the east/southeast of B5. From this maximum level, the water flows in all directions with the main flow towards the east and decreasing to a level of 5.5 m NGF beneath East of B2 (

Figure 2.12).

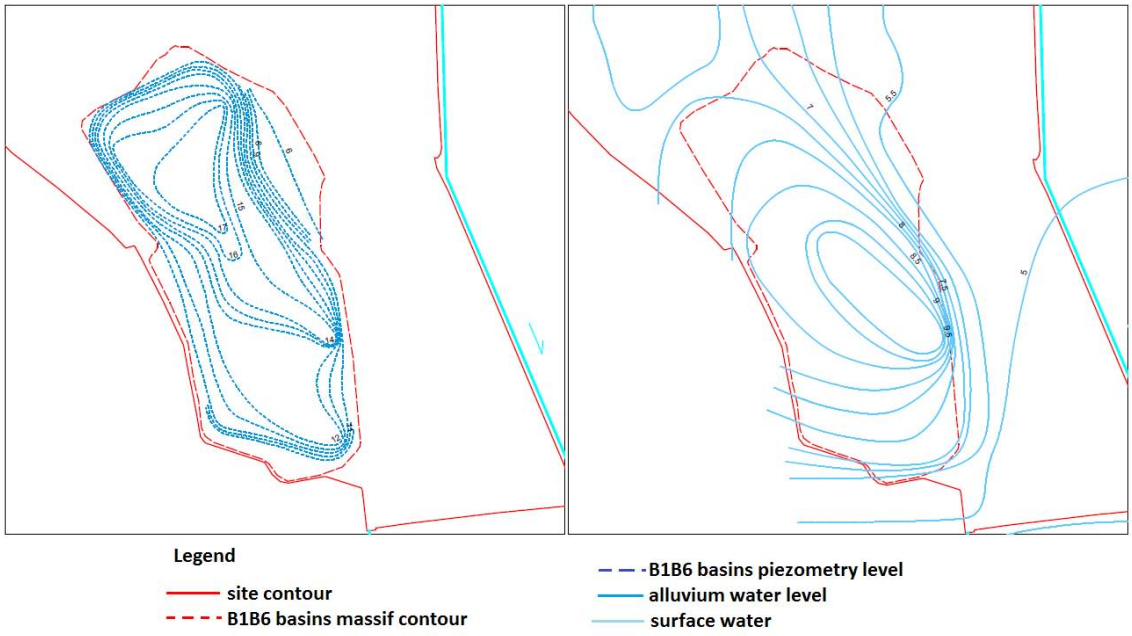

Figure 2.12: Piezometry beneath the basins in March 2010 – groundwater/perched water level in the B1B6 massif (on the left) and in the alluvium (on the right). Source (AREVA NC - Comurhex, 2010).

2.5.3 Characterisation of the waste contained in B1/B2

The sludge effluent contained in the B1/B2 basins is chemically heterogeneous due to the evolution of the conversion process and the different yellowcake feed received from various mines around the world. The uranium conversion process has evolved since the start of operations to both improve efficiency of recovery and adapt to the final product required: initially and until 1991 production of uranium metal and from 1964 onwards production of uranium tetrafluoride (UF_4). The raw material comprises a wide variety of uranium concentrates, including triuranium octoxide (U_3O_8), uranates (U_2O_7X, where X can be Ca, Mg, $(NH_4)_2$, Na, etc) and uranium oxides (UO_2, UO_3).

The sulphur mine tailings are also heterogeneous due to the disposal of the flotation waste in two successive cycles, as described in 2.5.1 above. Periods of inactivity of the sulphur mine allowed growth of vegetation resulting in thin layers of organic matter within the tailings.

As a result of the rupture of the east dyke of B2, various lithologies of waste are present within the basins. These are the ***cover layer***, the ***sludge***, the ***mixture of soil and sludge*** and the ***East of B2 (mixture of soil, sludge and tailings)***, in addition to the ***mine tailings***, containing the former sulphur mine tailings and flotation waste. A

schematic cross-section of the B1/B2 basins illustrating the strata of waste they contain is presented in Figure 2.13.

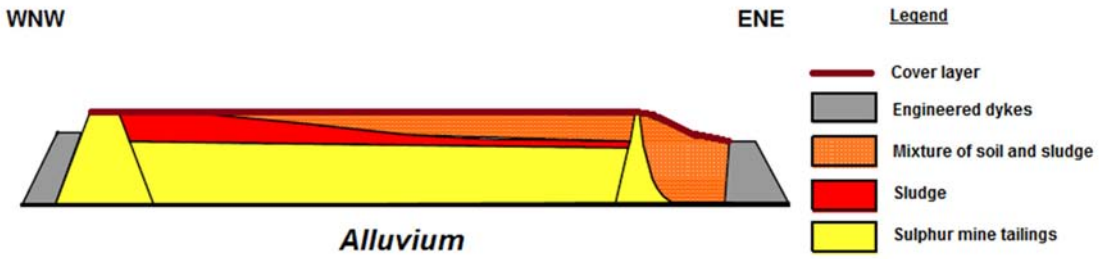

Figure 2.13: Schematic representation of the main strata present in the B1/B2 basins. Adapted from (Burgeap, 2009b).

The volume of waste contained in B1/B2 is approximately 240,000m^3 (Bary *et al.*, 2010b). The total volume of the mine tailings, i.e. the B1/B6 massif is 1,300,000m^3 (Van Hecke *et al.*, 2009).

2.5.4 Previous B1/B2 Waste Characterisation Studies – Arcadis 2009

Arcadis carried out an environmental investigation of the waste contained in the basins during the summer of 2009 (Bary *et al.*, 2009, 2010a, 2010b). The works comprised intrusive ground investigation, with a total of 41 window sampling locations drilled across B1 and B2, and laboratory analysis of solid and water samples (170 solid samples and 8 water samples) for chemical and radiochemical characterisation. The main findings of the study are described below.

2.5.4.1 Chemical Composition

As described in section 2.3, the basins receive large amounts of nitrate, carbonate and fluoride from the processing of the yellowcake. In addition, the original sulphur deposit from which the sulphur mine tailings result consisted of shale, limestone, marl, gypsum and sulphur (SLREM, 1952). It is then expected that large concentrations of carbonate and sulphates be found in this stratum. Bary and co-workers (2010a; 2010b) found that salts of carbonate and sulphate comprise approximately a third of the total dry weight of the waste. Average concentrations of main salts and their profile with depth along selected boreholes are presented in Figure 2.14 and Figure 2.15, respectively.

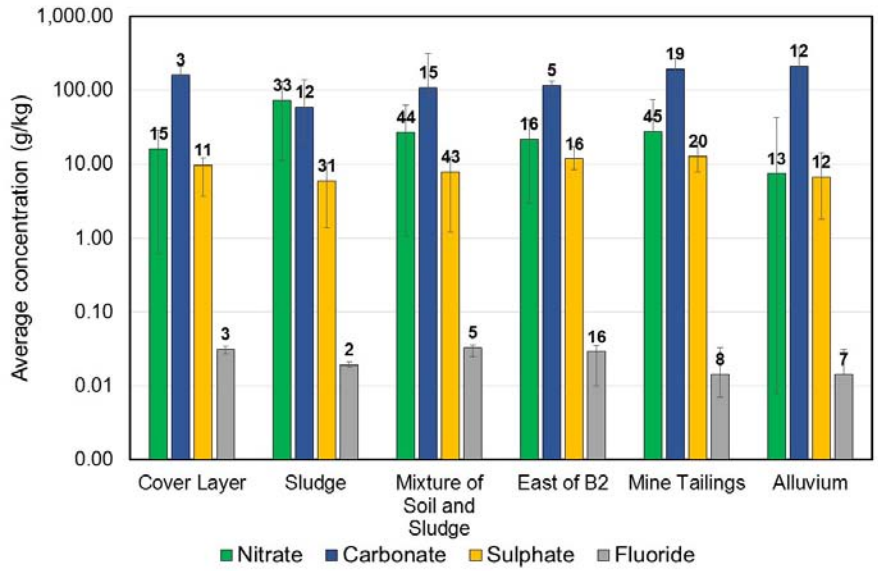

Figure 2.14: Average concentrations of nitrate, carbonate, sulphate and fluoride measured in B1/B2 (error bar represents range of concentration, label on each column represents number of samples analysed). Source of data: (Bary et al. 2010b).

The concentrations of nitrate range between less than 1 g/kg in the cover layer, alluvium and mine tailings to a maximum of 129 g/kg in the sludge. The sludge is the stratum with the highest concentration of nitrates, at an average of 73 g/kg. The average concentration in the other strata varies between 7 g/kg in the alluvium to 27 g/kg in the mixture of soil and sludge and 28 g/kg in the mine tailings.

The concentration of carbonates is less variable across the different strata, ranging from a minimum of 120 g/kg in the cover layer to a maximum of 380 g/kg in the alluvium. The average concentration of carbonates increases with depth, going from 60 g/kg in the sludge, to 200 g/kg in the mine tailings and to 220 g/kg in the alluvium.

Due to the origin of the mine tailings, higher concentrations of sulphate are contained in this stratum (average of 13 g/kg) than in the waste (6 g/kg in the sludge) or in the alluvium (7 g/kg).

Fluoride concentrations average 15 mg/kg in the mine tailings and 30 mg/kg in the mixture of soil and sludge. The average concentration in the samples of sludge (20 mg/kg) may not be representative of the whole strata as only two samples of sludge were analysed for fluoride concentrations.

The two strata comprising mixture of soil and sludge (East of B2 and mixture of soil and sludge) contain similar average chemical concentrations of the main salts, confirming their similar origin.

Figure 2.15: Selected chemical profiles of the main salts contained in B1/B2, nitrate, carbonate, fluoride and sulphate (mg/kg) (Bary et al., 2010b).

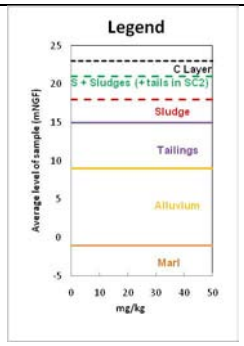

Location of boreholes:

SC2 – East of B2

SC417 – Basin B1

SC416 – Basin B2

Nitrate	Carbonate	Fluoride	Sulphate
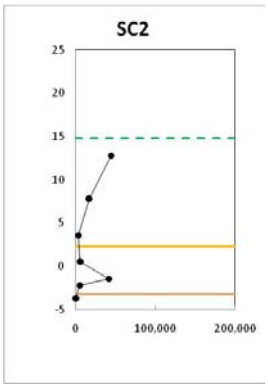	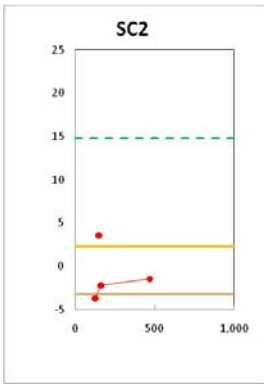	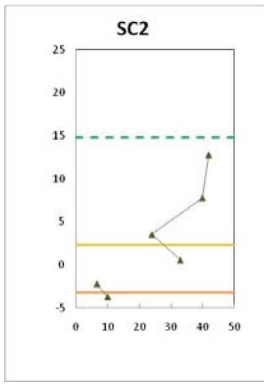	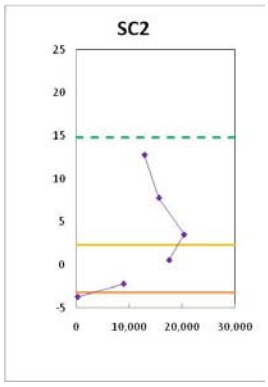
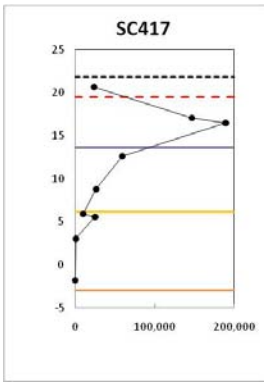	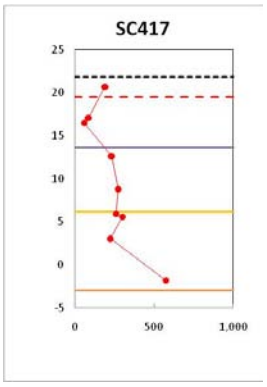	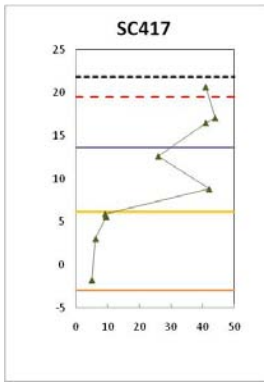	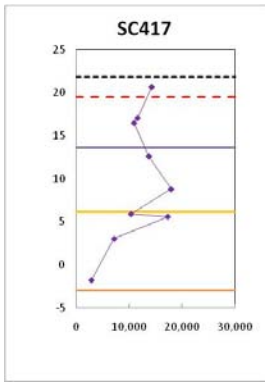
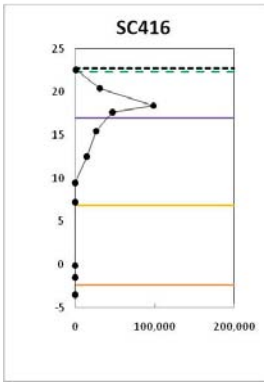	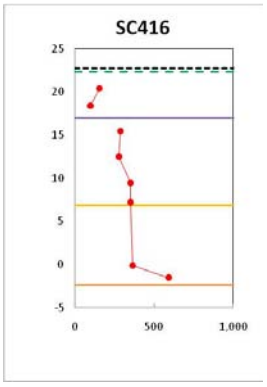	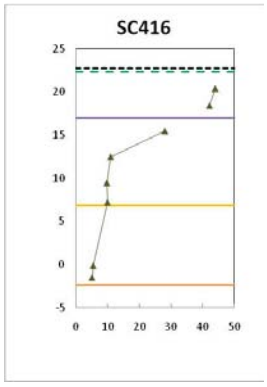	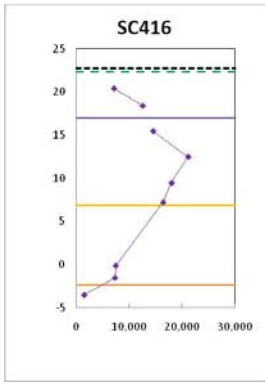

The pore water composition of five samples (one collected from the sludge, two from East of B2 and two from the mine tailings) collected by Burgeap in 2009 (Burgeap, 2009a) indicates less variability of the concentrations of salts. Nitrates vary between 1.7 and 2.6 mol/l in East of B2 and in the sludge respectively, whilst 2.3 mol/l were measured in the tailings. The average concentration of carbonates was $3.4 \cdot 10^{-2}$ mol/l in the sludge, $1.3 \cdot 10^{-2}$ mol/l in East of B2 and $1 \cdot 10^{-2}$ mol/l in the tailings. Sulphates were measured in marginally higher concentrations in the tailings than in the sludge and East of B2: $2.3 \cdot 10^{-2}$ mol/l in the tailings compared with $9.4 \cdot 10^{-3}$ mol/l in the sludge and $1.3 \cdot 10^{-2}$ mol/l in East of B2. Fluoride was not analysed on these samples although a sample collected from the tailings' dyke (location Pz12), contained $1 \cdot 10^{-4}$ mol/l of fluoride.

2.5.4.2 Radiological characteristics

The radioactivity in the waste arises mostly from alpha emitters and ranges between 50 and 400 Bq/g across the different strata (Bary *et al.*, 2010a). The main contributors to the alpha activity are ^{230}Th (50%) and the natural uranium isotopes (30%) (

Table 2.2). The beta activity is given mainly by ^{234}Th and ^{234m}Pa (≈60%) and ^{210}Pb and ^{210}Bi (15-20%).

Artificial radionuclides represent less than 2% of the alpha activity (^{237}Np, ^{238}Pu, $^{239+240}$Pu and ^{241}Am) and less than 0.5% of the beta activity (^{90}Sr, ^{99}Tc, ^{137}Cs and ^{241}Pu) (Bary *et al.*, 2010a).

The sulphur mine tailings have lower average alpha and beta activities (8 Bq/g and 5 Bq/g, respectively) than the waste (Bary *et al.*, 2010a). However, the wide range of activity measured (1-60 Bq/g of alpha and 1-20 Bq/g of beta) confirms the presence of areas where the mine tailings have been impacted by the waste. The high contribution of ^{99}Tc, a highly mobile radionuclide, to the beta activity (17%) also suggests that contamination has migrated from the overlying strata of waste.

Lower average alpha and beta activities(1 Bq/g and 2 Bq/g, respectively) are found in the natural alluvium (Bary *et al.*, 2010a).

Table 2.2: Main radiological characteristics of the waste, mine tailings and alluvium. Source: (Bary et al. 2010b).

Strata	No of analysis	Average activity (Bq/g)			% alpha activity				% beta activity		
		Alpha	Beta	Art. RNs*1*2	U	^{230}Th	Art. RNs*1	Other*3	Main contributors	Art. RNs*2	Other*3
Cover Layer	16	60 (5 – 180)	20 (2 – 60)	1 (<1 – 10)	27	45	<2	26	53 (^{234}Th + ^{234m}Pa) 15 (^{210}Pb + ^{210}Bi)	<1	31
Sludge	33	400 (15 – 1300)	110 (10 – 350)	5 (<1 – 10)	27	53	<2	18	58 (^{234}Th + ^{234m}Pa) 18 (^{210}Pb + ^{210}Bi)	2	22
Mixture Soil and Sludge	44	100 (1 – 430)	40 (1 – 140)	1 (<1 – 10)	33	45	<2	22	60 (^{234}Th + ^{234m}Pa) 14 (^{210}Pb + ^{210}Bi)	4	23
East of B2	16	45 (<1 – 130)	20 (<1 – 40)	1 (<1 – 2)	29	48	<2	22	55 (^{234}Th + ^{234m}Pa) 16 (^{210}Pb + ^{210}Bi)	2	28
Mine Tailings	46	8 (<1 – 60)	5 (<1 – 20)	-	32	31	<2	-	49 (^{234}Th + ^{234m}Pa) 36 (^{238}U decay)	17 (^{99}Tc)	-
Alluvium	13	1 (<1 – 10)	2 (<1 – 15)	-	37	47	<2	-	47 (^{234}Th + ^{234m}Pa) 32 (^{99}Tc + ^{238}U decay)	<1	21

*1Art. RNs = Artificial Radionuclides contributing to alpha activity comprise: ^{237}Np, ^{238}Pu, $^{239+240}$Pu and ^{241}Am.

*2Art. RNs = Artificial Radionuclides contributing to beta activity comprise: ^{90}Sr, ^{99}Tc, ^{137}Cs, ^{241}Pu in the waste and ^{99}Tc and ^{137}Cs in the mine tailings and alluvium

*3Other radionuclides contributing to alpha and beta activity include alpha and beta emitters of the ^{238}U and ^{235}U decay chains, when not included under main contributors

2.5.4.3 Uranium and Thorium

The average concentration of uranium found in the sludge (5,804 mg/kg), in the mixture of soil and sludge (1,847 mg/kg) and in the East of B2 (507 mg/kg), as shown in Figure 2.16. The average concentration of uranium is one order of magnitude lower in the tailings (134 mg/kg) and two orders of magnitude lower in the alluvium (10.2 mg/kg). However, the concentrations of uranium in the tailings show a wide variability with the higher concentrations found in the upper part of the tailings and decreasing concentrations with depth, as seen in Figure 2.17.

Thorium is also found heterogeneously distributed in the basins. Its average concentration in the sludge is 109 mg/kg, but ranges from 5.4 to 299 mg/kg (Bary *et al.*, 2010a). Lower average concentrations are found in the mixture of soil and sludge (31 mg/kg) and in the East of B2 (17 mg/kg). The concentrations of thorium then decrease to an average of 8 mg/kg in the tailings, where no attenuation is apparent with depth (Figure 2.17), and 5 mg/kg in the alluvium.

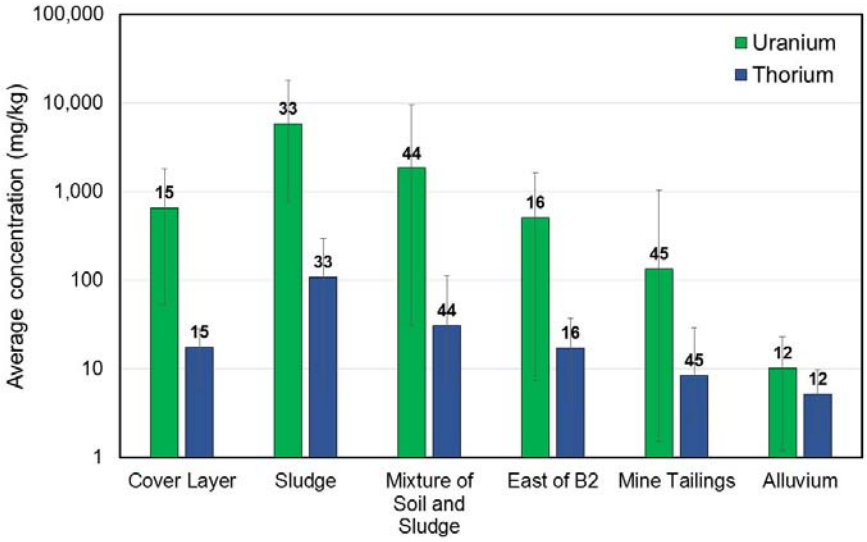

Figure 2.16: Average concentrations of uranium and thorium measured in B1/B2 (error bar represents range of concentration, label on each column represents number of samples analysed). Source of data: (Bary et al. 2010b).

The total uranium and thorium mass contained in the B1/B2 basins is estimated by Arcadis (Bary *et al.*, 2010b) in 677 and 13.5 tonnes respectively (Table 2.3). The mine tailings are mostly contaminated on the upper 7 metres, where they contain 65 tonnes of uranium and 3.8 tonnes of thorium.

Table 2.3: Mass of uranium and thorium contained in the B1/B2 basins. Source: (Bary *et al.*, 2010b).

Strata	Uranium (tonnes) ($^{234}U + ^{235}U + ^{238}U$)	Thorium (tonnes) ($^{227}Th + ^{230}Th + ^{232}Th + ^{234}Th$)
Cover Layer	41	1
Sludge	308	6
Mixture of Soil and Sludge	277	4.5
East of B2	51	2
Total in waste	677	13.5
Mine Tailings (top 7m depth)	65	3.8

The analysis of samples of pore water carried out by Burgeap (Burgeap, 2009a) indicated lower concentrations of uranium in the sludge ($1.1 \cdot 10^{-6}$ mol/l) than in the East of B2 ($1.1 \cdot 10^{-4}$ mol/l) or even in the tailings ($4.9 \cdot 10^{-5}$ mol/l). The average concentration of thorium in the pore water was $1.3 \cdot 10^{-6}$ and $2.9 \cdot 10^{-6}$ mol/l in the tailings and in East of B2 respectively, and one order of magnitude higher within the sludge ($1.7 \cdot 10^{-5}$ mol/l).

Figure 2.17: Selected profiles of uranium and thorium in B1/B2 waste (mg/kg).

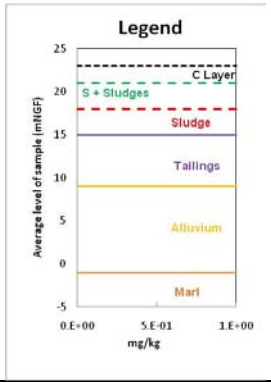

Location of boreholes:

SC2 – East of B2

SC417 – B1 Basin

SC416 – B2 Basin

Uranium

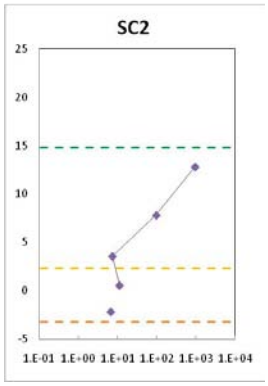

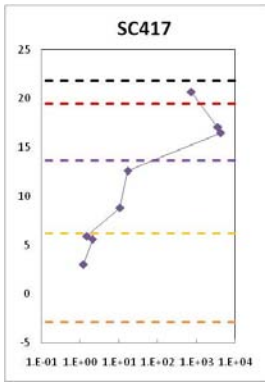

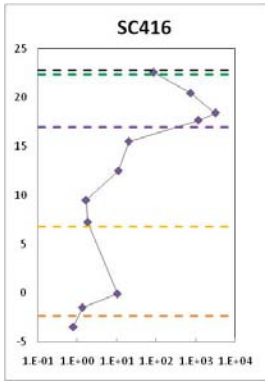

Thorium

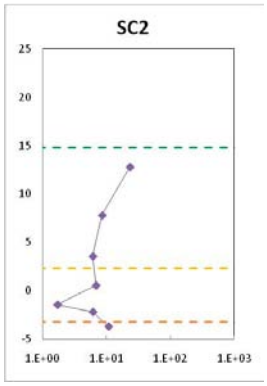

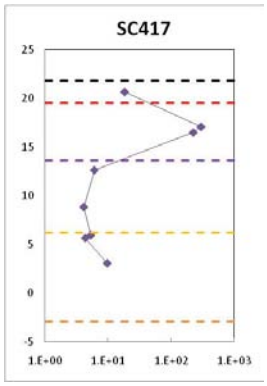

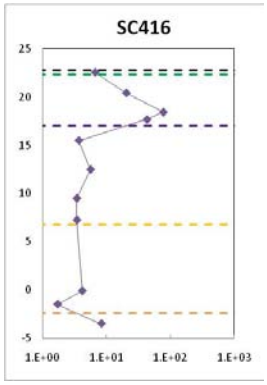

3. Uranium and Thorium Geochemistry

3.1 Environmental Geochemistry of Uranium

3.1.1 Uranium in the Environment

Uranium is a radioactive element that occurs naturally in soil, rock, surface water and groundwater in low concentrations. It has a crustal abundance of 2.7 mg/kg ($1.13 \cdot 10^{-5}$ mol/kg) (Taylor, 1964). In seawater the uranium concentration is about $13.5 \cdot 10^{-9}$ mol/l (Whitfield and Turner, 1987). In natural waters, the uranium concentration was found to vary between 10^{-7} and 10^{-5} mol/l in the UK, to 10^{-9} mol/l in CO_2-rich waters from Valles-Bains, in France (Bruno *et al.*, 1997).

Uranium is the heaviest naturally occurring element, with an atomic number of 92. It is most abundant as ^{238}U (>99%) and ^{235}U (0.72%). The isotope ^{234}U, with an abundance of only 0.0055%, occurs naturally as a daughter in the ^{238}U radioactive decay series. Two other isotopes, ^{233}U and ^{236}U, can also be found in nature. Uranium-233 is an artificial nuclide resulting from nuclear transformations. Uranium-236 found in the environment mostly results from anthropogenic production (estimated at an amount of 10^6 kg) although a small amount (estimated at 30 kg) is produced naturally by cosmogenic and nucleogenic neutrons (Steier *et al.*, 2008; Casacuberta *et al.*, 2014). The main characteristics of the uranium isotopes are presented in Table 3.1.

The bulk of uranium production comes from seven uranium minerals (Nordberg *et al.*, 2008): reduced minerals uraninite (well crystallised UO_2) and pitchblende (microcrystalline UO_2) and oxidised minerals tyuyamunite ($Ca(UO_2)_2(VO_4)_2.6H_2O$), carnotite ($K_2(UO_2)_2(VO_4)_2.3H_2O$), autunite ($Ca(UO_2)_2(PO_4)_2.10\text{-}12H_2O$), torbernite ($Cu(UO_2)_2(PO_4)_2.12H_2O$) and comminite. Oxidation and loss of uranium by radioactive decay may increase the oxygen-uranium ratio, so uraninite and pitchblende rarely have a precise UO_2 composition, approaching a composition of U_3O_8 (Krauskopf and Bird, 1995). Due to their higher solubility, oxidised minerals will be transported in water before precipitating (as pitchblende or coffinite, $USiO_4.nH_2O$, for example) in reducing environments (Krauskopf and Bird, 1995).

Table 3.1: Radioactive properties of key uranium isotopes (Peterson *et al.*, 2007).

Isotope	Half-Life (years)	Natural Abundance (%)	Specific Activity (kBq/g)	Decay Mode	Radiation Energy (MeV)		
					Alpha (α)	Beta (β)	Gamma (γ)
^{232}U	72	0	$81.4 \cdot 10^{+7}$	α	5.3	0.017	0.0022
^{233}U	160,000	0	$36.26 \cdot 10^{+3}$	α	4.8	0.0061	0.0013
^{234}U	240,000	0.0055	$23.31 \cdot 10^{+4}$	α	4.8	0.013	0.0017
^{235}U	700 million	0.72	81.4	α	4.4	0.049	0.16
^{236}U	23 million	0	$24.0 \cdot 10^{+2}$	α	4.5	0.011	0.0016
^{238}U	4.5 million	>99	12.58	α	4.2	0.010	0.0014

Industrial activities may contribute to increasing the concentration of uranium in soils, surface and ground waters by releasing large quantities of this element at a local scale. Uranium contaminated wastes can be found in a variety of sites around the world, usually as a result of nuclear related activities such as uranium mining, milling, conversion, enrichment and fuel reprocessing. Other non-nuclear industries, such as phosphate and heavy metal mining, coal use, inappropriate waste disposal and research and development activities also contribute to the presence of uranium containing materials in the environment (Gavrilescu, Pavel and Cretescu, 2009).

3.1.2 Uranium oxidation state and speciation

Uranium can exist in the +3, +4, +5 and +6 oxidation states in the aqueous environment. However, the U(V) aqueous species (UO_2^+) readily disproportionates to U(IV) and U(VI) and, in reducing conditions, U(III) easily oxidises to U(IV). The most common states in the natural environment are, therefore, U(IV) and U(VI) species, which predominate under reducing and oxidising conditions respectively. The pentavalent uranium species UO_2^+ has a small stability field at slightly acidic and weakly reducing conditions (Altmaier and Vercouter, 2012).

When present under reducing conditions, uranium is relatively immobile. The predominant U(IV) species (Figure 3.1) are U^{4+} and $U(OH)^{3+}$ for pH values below 1, $U(OH)_2^{2+}$ and $U(OH)_3^+$ for pH values between 1 and 5, and the neutral species $U(OH)_4$ for neutral and alkaline conditions. Under oxidising and mildly reducing conditions, the uranyl species [U(VI)] will dominate. In the absence of complexing ligands, other than hydroxide, the dominant aqueous U(VI) species are UO_2^{2+} at pH values below 5.5, UO_2OH^+ and $UO_2(OH)_2(aq)$ at neutral pH values, and $UO_2(OH)_3^-$ and $UO_2(OH)_4^{2-}$ at pH values above 8.1. With increasing concentrations of total dissolved uranium, for instance $4.2 \cdot 10^{-6}$ mol/l (1,000 µg/l), polynuclear species such as $(UO_2)_3(OH)_5^+$ and $(UO_2)_3(OH)_7^-$

begin to dominate the hydrolysis of uranium, as shown in Figure 3.1. For even higher concentrations of uranium, such as above 10^{-4} mol/l, the species $(UO_2)_2(OH)_2^{2+}$ is a major species under slightly acidic conditions (Grenthe *et al.*, 2006).

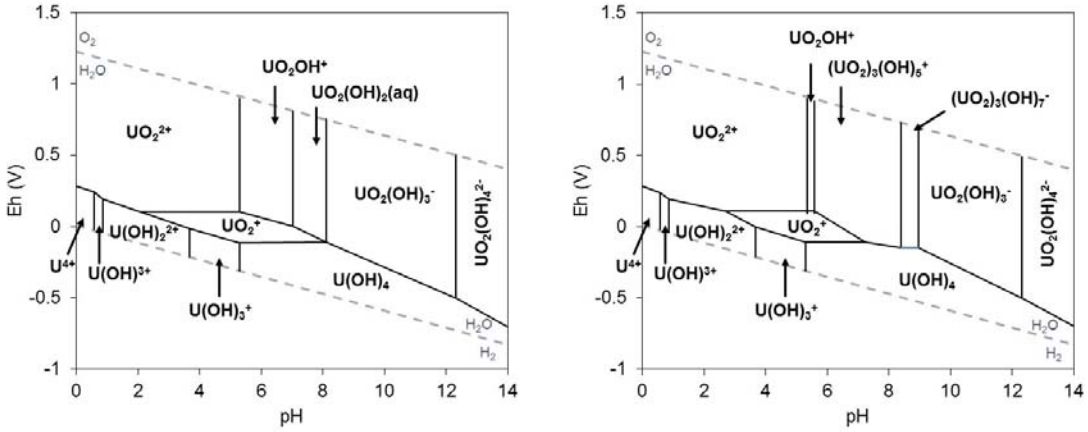

Figure 3.1: Eh-pH diagram showing the hydrolysis of uranium in the absence of other complexing ligands at total dissolved U concentrations of 10^{-7} mol/l (on the left) and $4.2 \cdot 10^{-6}$ mol/l (on the right). Diagram calculated with MEDUSA (Puigdomenech, 2010) at 25ºC and I = 0 mol/l, using the NEA-TDB selections (Guillaumont, 2003). Solid phase formation is not considered.

In natural waters, the speciation of uranium is governed by the concentration of dissolved carbonate. At low pH values (pH<5), the hydrolysed uranyl species $[(UO_2)_p(OH)_q^{2p-q}]$ will dominate. However, an increase in the pH value will lead to the stabilisation of uranium carbonate complexes, such that, at neutral pH, the predominant species will be $(UO_2)_2CO_3$ and for even higher pH values polycarbonate complexes will form. Under reducing conditions, hydroxide complexes will predominate under most pH conditions due to the prevalence of the tetravalent uranium. If there is an increase in the dissolved carbonate concentration, the environmental conditions for which carbonate complexes are stable is broader. In the presence of typical groundwater calcium concentrations (> 1 mmol/l), dissolved uranium will form calcium-uranyl-carbonate complexes $[Ca_2UO_2(CO_3)_3(aq)$ and $CaUO_2(CO_3)_3^{2-}]$ (Guillaumont, 2003; Dong and Brooks, 2006; Fox, Davis and Zachara, 2006) (Figure 3.2). Even though the stability constants for these complexes are likely overestimated (Kalmykov and Choppin, 2000; Bernhard *et al.*, 2001), their formation will play a major role in uranium migration in calcium rich alkaline waters due to their weak adsorption to sediments (Fox *et al.*, 2012). Other ligands may contribute to aqueous speciation, such as fluoride, phosphate and organic ligands, if present at elevated concentrations and at certain pH conditions (Langmuir, 1978).

Under the chemical composition of the groundwater beneath the AREVA NC Malvési site, uranium speciation will be dominated by sulphate complexes at low pH values

(below pH 5), and by carbonate complexes under neutral and alkaline conditions (Figure 3.2).

The speciation of uranium affects its solubility and hence, its mobility in water. Under oxidising conditions, the uranyl ion and its complexes are soluble and mobile, enhancing uranium transport. However, as these are positively charged species they will also be easily sorbed to the negatively charged surfaces of minerals and organic matter, therefore being retained by sediments. Simultaneously, the strong affinity of carbonate ligands for the uranyl ion will form negatively charged complexes that will not easily sorb and will again increase the solubility of uranium.

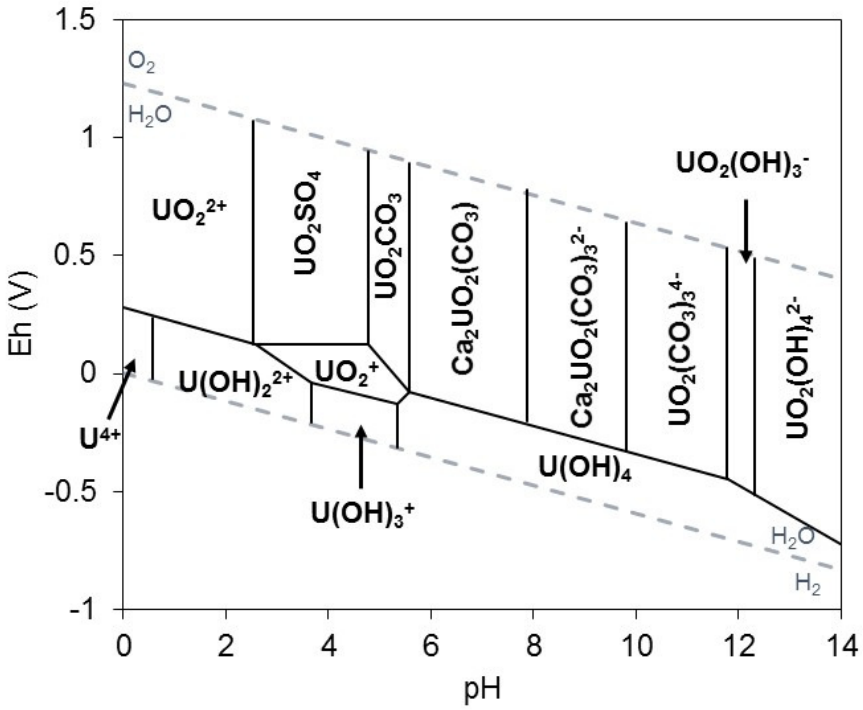

Figure 3.2: Eh-pH diagram showing the hydrolysis of uranium ($2.9 \cdot 10^{-8}$ mol/l) in the presence of Ca^{2+} ($3.2 \cdot 10^{-3}$ mol/l), CO_3^{2-} ($6.9 \cdot 10^{-3}$ mol/l), SiO_4^{4-} ($1.7 \cdot 10^{-4}$ mol/l), NO_3^- ($1.6 \cdot 10^{-5}$ mol/l), Cl- ($8.5 \cdot 10^{-3}$ mol/l) and SO_4^{2-} ($1.4 \cdot 10^{-3}$ mol/l). Aqueous concentrations based on the composition of the alluvium groundwater beneath the AREVA NC Malvési site, borehole S65 (Burgeap, 2009a). Diagram calculated with MEDUSA (Puigdomenech, 2010) at 25ºC and I=0 mol/l, using the NEA-TDB selections (Guillaumont, 2003). Solid phase formation is not considered.

3.1.3 Uranium Sorption

Sorption of uranium is strongly influenced by pH and concentration of dissolved ligands, in particular carbonates. Ionic strength and mineralogy also affect uranium sorption.

The pH has a significant impact on uranium sorption because it defines U(VI) speciation in solution and it changes the surface species and the surface charge of solids (Dzombak and Morel, 1990) such as Fe- and Al-oxides and natural organic matter. Sorption is low for pH values less than 3, where the uranyl cation predominates (Arnold *et al.*, 1998). With increasing pH, more negatively charged binding sites become available on mineral surfaces due to the release of protons, and the uranium sorption increases rapidly up to a maximum at pH 5 to pH 8. With increasing pH values, in natural waters, the fraction of uranium complexed with the carbonates increases, decreasing sorption (Tripathi, 1984; Hsi and Langmuir, 1985; Wazne, Korfiatis and Meng, 2003; Jang, Dempsey and Burgos, 2007). In fact, the mobility of uranium in natural waters is strongly influenced by the presence of dissolved carbonates. Waite and co-workers (Waite *et al.*, 1994) observed that an increase in the partial pressure of CO_2 from $10^{-3.5}$ atm to 10^{-2} atm, resulted in a decrease in U(VI) sorption onto ferrihydrite in the pH range 7-9, as shown in Figure 3.3. However, the increase in partial pressure had no effect in U(VI) sorption in the acidic pH range. Um and co-workers (2007) showed that sorption of U(VI) decreases with increasing concentrations of dissolved carbonate in batch tests carried out with aquifer sediments collected at the Hanford Site. They showed that strong anionic aqueous uranium-carbonate complexes formed at high pH (>7.8) and high alkalinity conditions (>140 mg/l as $CaCO_3$). Under field conditions, Zhou and Gu (2005) observed that the presence of small quantities of carbonate/bicarbonate could result in rapid and increased leaching, and the mobilisation of U(VI) from contaminated soil from the field research centre at the National Security Complex in Oak Ridge (USA).

Fox et al (2006) highlighted the importance of taking into account the effects of calcium on uranium aqueous speciation when predicting the sorption and mobility of uranium at contaminated sites by demonstrating that the presence of Ca^{2+} in solution can decrease U(VI) sorption on ferrihydrite and quartz when the $Ca_2UO_2(CO_3)_3(aq)$ species dominates U(VI) aqueous speciation.

Sorption of uranium has been studied onto a variety of minerals and phases: clays (Arnold *et al.*, 1998; Catalano and Brown, 2005; Singer, Zachara and Brown, 2009), oxides and silicates (Sylwester, Hudson and Allen, 2000; Massey *et al.*, 2014), and organic matter (Glaus, Hummel and Van Loon, 1997; Saito *et al.*, 2004).

It has been shown that U(VI) forms strong surface complexes with Fe (oxy)hydroxides (Hsi and Langmuir, 1985; Waite *et al.*, 1994; Payne, 1999; Nico, Stewart and Fendorf, 2009). Waite and co-workers (Waite *et al.*, 1994) showed that increasing concentrations of Fe in solution result in sorption over a wider pH range.

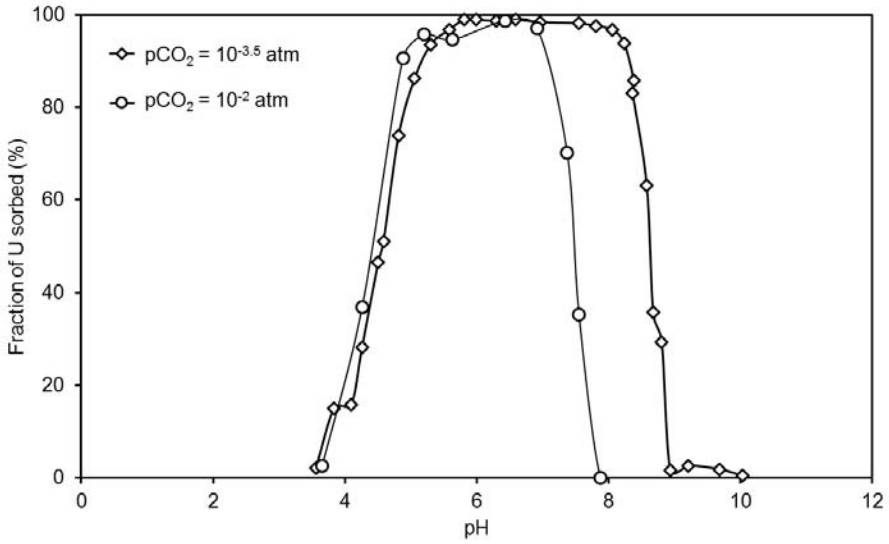

Figure 3.3: Adsorption of 10^{-6} mol/l U(VI) on ferrihydrite (10^{-3} mol/l as Fe) as a function of pH and partial pressure of CO_2 in 0.1 mol/l $NaNO_3$. Source: (Waite et al., 1994).

3.1.4 Uranium Solubility

Under oxidising conditions and low concentrations of dissolved uranium, U(VI) solubility is still likely to be controlled by sorption instead of dissolution, especially in the presence of carbonate which will form aqueous U(VI) carbonate complexes. However, for high concentrations of dissolved uranium, such as the oxidation dissolution of an ore deposit or near a disposal site of uranium-contaminated material, mineral solubility will become increasingly important. Langmuir (1997) described various potentially important mineral solubility phases of U(VI): compreignacite ($K_2U_6O_{19}.11H_2O$), uranophane [$Ca(UO_2)_2(SiO_3)_2(OH)_2.5H_2O$], boltwoodite [$K(H_3O)UO_2(SiO_4).1.5H_2O$], sklodowskite [$Mg(UO_2)_2(SiO_3)_2(OH)_2.5H_2O$], becquerelite ($CaU_6O_{19}.10H_2O$), carnotite [$K_2(UO_2)_2(VO_4)_2.3H_2O$], schoepite [$(UO_2)_8O_2(OH)_{12}.12H_2O$], rutherfordine ($UO_2CO_3$), tyuyamunite [$Ca(UO_2)_2(VO_4)_2.5\text{-}8H_2O$], autunite [$Ca(UO_2)_2(PO_4)_2.10\text{-}12H_2O$] and potassium autunite [$K_2(UO_2)_2(PO_4)_2.10\text{-}12H_2O$].

Under reducing conditions, or in the presence of high concentrations of uranium, mineral dissolution, precipitation and coprecipitation become increasingly important due to the low solubility of U(IV). For example, under the reducing conditions of the uncontaminated groundwater in the alluvium beneath Malvési (Figure 3.4), uranium will precipitate as uraninite. However, there are no solubility controls for U(VI). Increasing the uranium concentration will expand the uraninite stability field to lower pH values and slightly

higher oxidising conditions and will result in the oversaturation and precipitation of U(VI) phases under oxidising conditions.

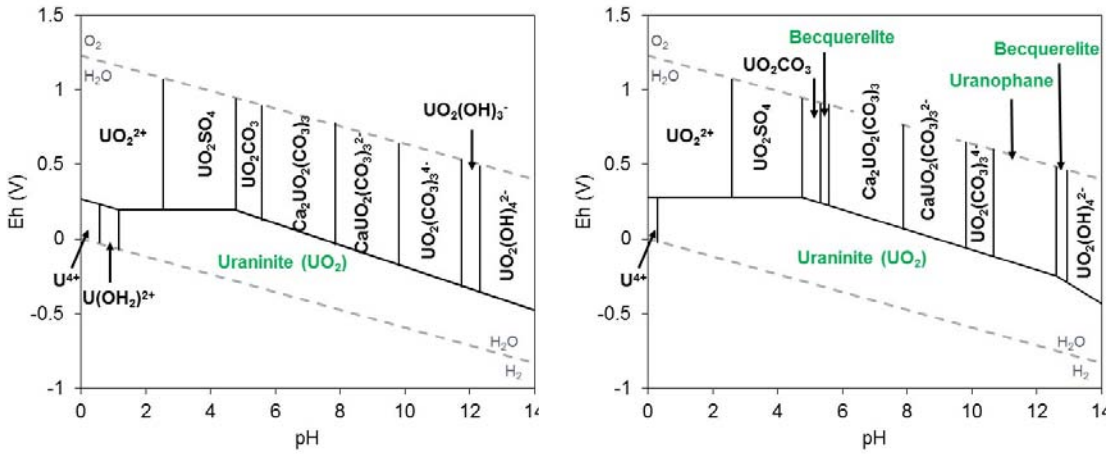

Figure 3.4: Eh-pH diagrams showing the hydrolysis of uranium ([U] = $2.9 \cdot 10^{-8}$ mol/l on the left and [U] = $5 \cdot 10^{-6}$ mol/l) in the presence of Ca^{2+} ($3.2 \cdot 10^{-3}$ mol/l), CO_3^{2-} ($6.9 \cdot 10^{-3}$ mol/l), SiO_4^{4-} ($1.7 \cdot 10^{-4}$ mol/l), NO_3^- ($1.6 \cdot 10^{-5}$ mol/l), Cl^- ($8.5 \cdot 10^{-3}$ mol/l) and SO_4^{2-} ($1.4 \cdot 10^{-3}$ mol/l). Aqueous concentrations based on the composition of the groundwater in the alluvium beneath the AREVA NC Malvési site, borehole S65 (Burgeap, 2009a). Diagram calculated with MEDUSA (Puigdomenech, 2010) at 25ºC and I=0 mol/l, using the NEA-TDB selections (Guillaumont, 2003) and without considering solid phase formation.

Solubility processes can also be important in partially saturated sediments, for instance vadose zone soils and sediments, as the concentration of uranium in the residue pore fluids may exceed the solubility limits for U(VI)-containing minerals or coprecipitates with other minerals, such as iron oxides (Krupka and Serne, 2002).

3.1.5 Uranium concentrations in Malvési

The background concentration of uranium in the soils around the site of Malvési is 2.4-2.6 mg/kg, increasing to 4.9 mg/kg downwind of the site, suggesting some impact of the plant on the natural soils (Pourcelot, 2008; Pourcelot *et al.*, 2011). Pourcelot and co-workers (2011) measured enhanced activities of actinides in cypress needles collected at the edge of the Malvési facility. They concluded that these enhanced activities resulted in part from the release of uranium from basins B1/B2 when the sludge dried out and/or when earthworks were carried out at the ponds, such as, for example, during reinforcement of dykes.

The concentrations of uranium measured in the B1/B2 basins by Arcadis in 2009 (Bary *et al.*, 2010a, 2010b) are three to four orders of magnitude higher: 650 mg/kg in the cover layer, 5,800 mg/kg in the sludge and 130 mg/kg in the tailings. Airborne particulate matter, probably originated from the B1/B2 basins was observed on leaf surfaces in the

vicinity of the Malvési site (Gieré, Kaltenmeier and Pourcelot, 2012). The particulate matter comprised nahcolite (a Na-rich carbonate typically occurring in evaporates and other saline environments), calcium sulphate, halite and fluorite. Other basin-derived material observed included U-fuel impurities, such as uranium decay daughter isotopes (e.g., ^{230}Th and ^{226}Ra) and artificial actinides (Pu isotopes and ^{241}Am), that resulted from the introduction of reprocessed fuel in the recovery unit (see Chapter 2).

The groundwater in the natural strata beneath the AREVA NC Malvési site, i.e., in the alluvium, is in the order of 10^{-7} mol U/l. Within the B1/B2 basins, the concentration of uranium rises to 10^{-6} mol/l in the sludge, 10^{-5} mol/l in the tailings and as high as 10^{-4} mol/l in the mixture of soil and sludge (Burgeap, 2009a). In surface waters, the concentration of uranium ranges between 10^{-7} and 10^{-9} mol/l (Bary *et al.*, 2010a).

Pourcelot and co-workers (2011) determined concentrations of uranium in surface waters in the vicinity of the site. The lowest concentrations of uranium (as ^{238}U) were observed at the spring of l'Oeillal ($1.6 \cdot 10^{-3}$ to $7.4 \cdot 10^{-3}$ mg/l) while the highest concentrations were observed downstream of the site, at the Tauran Canal ($3.4 \cdot 10^{-3}$ to $5.1 \cdot 10^{-2}$ mg/l). At the Cadariège Canal, which received discharge water from the retention basin up to the year 2000, the concentrations of uranium were low and similar to what was observed in the spring of l'Oeillal ($8.2 \cdot 10^{-4}$ to $3.3 \cdot 10^{-3}$ mg/l).

3.2 Environmental Geochemistry of Thorium

3.2.1 Thorium in the Environment

Thorium is a radioactive element that occurs naturally in low concentrations in the earth's crust (soils, rock, surface waters, groundwaters, plants and animals). It is about three times more abundant than uranium, having a crustal abundance of 9.6 mg/kg (Krauskopf and Bird, 1995). In surface waters, the average concentration of thorium can go from as high as 0.043 to as low as $4.3 \cdot 10^{-9}$ mol/l (Bruno *et al.*, 1997). In the ocean, the concentrations can range between $5 \cdot 10^{-14}$ mol/l and $148 \cdot 10^{-14}$ mol/l (Bruno *et al.*, 1997).

In its pure form, thorium is a silvery-white heavy metal that is about as dense as lead. There are 26 known isotopes of thorium, however, only 12 of them have half-lives longer than one second and of these, only three have half-lives above years to warrant an environmental concern, ^{232}Th, ^{230}Th and ^{229}Th (Table 3.2).

The dominant thorium isotope in nature is ^{232}Th, which is the head of the thorium decay chain, and has a natural abundance of nearly 100%. However, ^{230}Th is the most important thorium isotope in the ^{238}U decay series and the most important thorium

isotope in terms of radioactivity in uranium mill tailings and groundwaters affected by uranium mining, milling and tailings disposal (Langmuir and Herman 1980; and references therein). Because ^{230}Th is the longest-lived ^{238}U daughter product that remains with the tailings and it decays to ^{226}Ra, the parent of ^{222}Rn, radon emanation will persist for the period governed by decay of ^{230}Th (half-life of 77,000 years) (Landa, 1980). Thorium-234, the direct daughter of ^{238}U, has a half-life of 24 days. It is rapidly in secular equilibrium and is a good tracer of ^{238}U. Thorium-229 is produced as a daughter of artificial ^{233}U, although very low natural concentrations can result from the decay chain of ^{237}Np in uranium ores. It is generally not considered a radionuclide of concern in environmental contamination (Peterson *et al.*, 2007).

Table 3.2: Radioactive properties of key thorium isotopes (Peterson *et al.*, 2007).

Isotope	Half-Life (years)	Natural Abundance (%)	Specific Activity (kBq/g)	Decay Mode	Radiation Energy (MeV)		
					Alpha (α)	Beta (β)	Gamma (γ)
^{232}Th	14,000,000	>99	4.07	α	4.0	0.012	0.0013
^{230}Th	77,000	<<1	740,000	α	4.7	0.015	0.0016
^{229}Th	7,300	<<1	8,140,000	α	4.9	0.12	0.096

In contrast with uranium, which occurs predominantly in uraniferous secondary minerals and as a small fraction in primary rock-forming minerals, thorium occurs almost exclusively in minor accessory minerals (thorite, huttonite, zircon). It occurs as a major species only in a few rare minerals such as thorianite (ThO_2) and thorite ($ThSiO_4$), isomorphous minerals with uraninite and zircon, respectively. A large part of the naturally occurring thorium is consequently found incorporated in the zircon structure (Langmuir and Herman, 1980). Thorium-232 is generally associated with the rare earths, particularly cerium (Ce), yttrium (Y), lanthanum (La), and sometimes also with zirconium (Zr) and uranium (Short, 1988). The most common source of thorium is the rare earth phosphate mineral monazite ((Ce, Y, La, Th)PO_4) which contains 6.0 to 8.5 wt% thorium oxide (Herring, 2004).

3.2.2 Thorium Speciation

The two most important ligands for thorium aqueous complexation are hydroxide and carbonate. In the absence of complexing ligands other than water, the formation of hydroxide complexes $Th_x(OH)_y^{4x-y}$ is governed by the reaction (Neck and Kim, 2001):

$$xTh^{4+} + yOH^{-} \leftrightarrow Th_x(OH)_y^{4x-y} \quad \textbf{(3.1)}$$

At pH values below 3, the predominant species in solution is Th^{4+}. For pH values between 3 and 6.5, the 1:1, 1:2 and 1:3 hydroxy complexes predominate, while for higher pH values, $Th(OH)_4$ will be the major species (M Altmaier *et al.*, 2005). Figure 3.5 below shows the distribution of thorium-hydroxy complexes with pH in water.

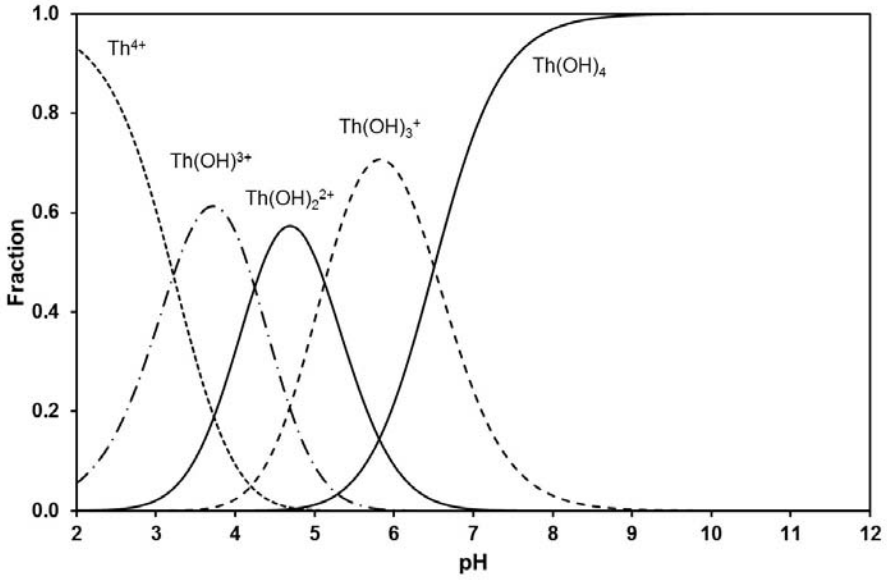

Figure 3.5: Speciation diagram of 10^{-8} mol/l Th(IV) in the absence of complexing ligands at I = 0.1 mol/l NaCl and 25ºC. Calculations performed in Phreeqc 3.3.2 (Parkhurst and Appelo, 2015) using the thermodynamic database ANDRA – Thermochimie version 9a (Giffaut et al., 2014) and the SIT (specific ion interaction theory) model. Solid phase formation is not considered.

Carbonate is the most important ligand under environmental conditions. Altmaier et al (2005) showed the most important ternary Th(IV) complexes to be $Th(OH)(CO_3)_4^{5-}$ and $Th(OH)_2(CO_3)_2^{2-}$, followed by $Th(OH)_2(CO_3)(aq)$, $Th(OH)_3(CO_3)^-$ and $Th(OH)_4(CO_3)^{2-}$. At high carbonate concentrations ($[CO_3)^{2-}] \geq 1M$) and neutral pH (pH 7-10), $Th(CO_3)_5^{6-}$, $Th(OH)(CO_3)_4^{5-}$ and possibly $Th(OH)_2(CO_3)_4^{6-}$ can also form. Inorganic ligands such as fluoride, phosphate and sulphate will also form complexes enhancing the solubility and mobility of thorium (Langmuir and Herman, 1980; Osthols, Bruno and Grenthe, 1994), although it will depend on their concentrations in natural waters.

Under the groundwater conditions of the uncontaminated alluvium beneath the site of Malvési, thorium inorganic complexation is expected to change from a predominance of fluoride speciation at pH below 5.5 to carbonate speciation at neutral and slightly alkaline pH values (Figure 3.6). At pH values above 11, $Th(OH)_4$ will be the predominant species.

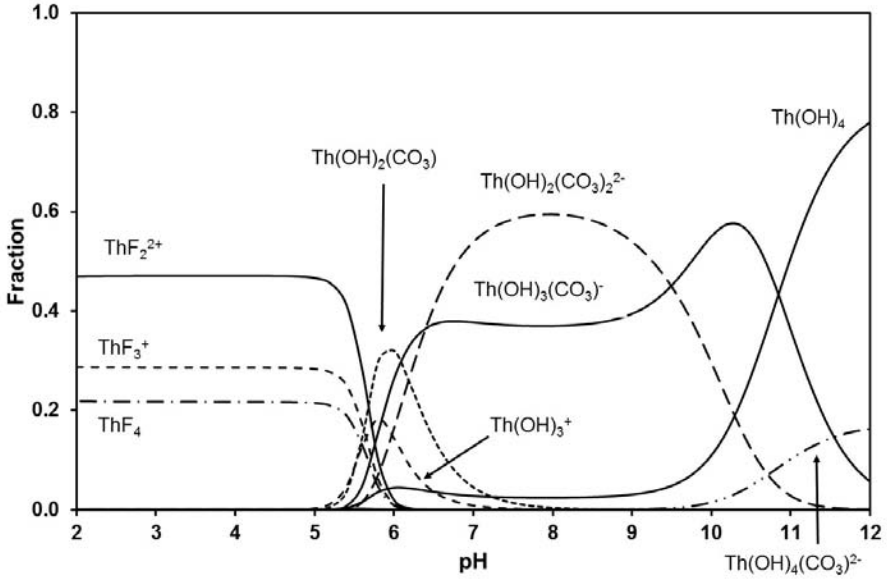

Figure 3.6: Speciation diagram of 10^{-8} mol/l Th(IV) in the uncontaminated groundwater in the alluvium beneath the AREVA NC Malvési site at I = 0.1 mol/l NaCl and 25ºC ($[Ca^{2+}]$ = $3.2 \cdot 10^{-3}$ mol/l, $[CO_3^{2-}]$ = $6.9 \cdot 10^{-3}$ mol/l, $[SiO_4^{4-}]$ = $1.7 \cdot 10^{-4}$ mol/l, $[NO_3^-]$ = $1.6 \cdot 10^{-5}$ mol/l, $[SO_4^{2-}]$ = $1.4 \cdot 10^{-3}$ mol/l). Calculations performed in Phreeqc 3.3.2 (Parkhurst and Appelo, 2015) using the thermodynamic database ANDRA – Thermochimie version 9a (Giffaut et al., 2014) and the SIT (specific ion interaction theory) model. Solid phase formation is not considered.

3.2.3 Thorium Solubility

In the absence of other complexing ligands, the solubility of thorium in aqueous solution is controlled by the solubility of thorium oxide/hydroxide (Neck *et al.*, 2003). Above pH 3, the solubility of thorium is independent of the solid phase (ThO_2(c) or $ThO_2.xH_2O$(am)) and it is independent of pH. With the onset of hydrolysis, the predominant aqueous species above this pH value is $Th(OH)_4$(aq).

Solubility studies (Ryan and Rai, 1987; Moon, 1989; Neck *et al.*, 2003) reported the experimental solubility values for crystalline ThO_2(c) in excess of the thermodynamic calculation by various orders of magnitude, approaching those of the amorphous solid. Fanghänel and Neck (2002) suggested that the sorption or precipitation of the hydroxide complex $Th(OH)_4$(aq) on the surface of crystalline ThO_2(c) would lead to an amorphous surface layer that controls the solubility of the crystalline solid.

The presence of carbonate in solution greatly increases the solubility of thorium oxide/hydroxide (Osthols, Bruno and Grenthe, 1994; Neck *et al.*, 2002; M Altmaier *et al.*, 2005), with this effect becoming evident at pH > 4.5 (Figure 3.7). The solubility is

increased by the formation of mononuclear complexes $Th(OH)_Y(CO_3)_Z^{4-Y-2Z}$ and colloidal Th(IV) species (M Altmaier *et al.*, 2005). In the pH range from 8 to 10 and with an increase in the carbonate concentration from 0 to 0.1mol/l, the formation of mono- and penta-carbonate complexes leads to an increase in solubility of 5 orders of magnitude (Osthols, Bruno and Grenthe, 1994). Thorium concentrations exceeding the solubility of crystalline ThO_2 in water by several orders of magnitude were measured in highly alkaline environments, such as in the waters of Soap Lake (USA) and Mono Lake (USA) due to strong carbonate complexation (Santschi et al. 2006 and references therein).

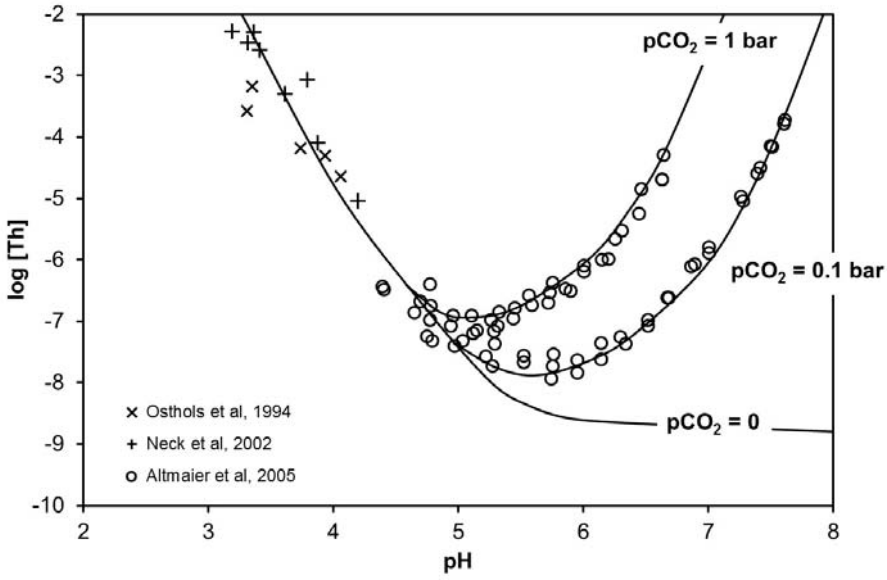

Figure 3.7: Solubility of amorphous Th(IV) oxyhydroxides at I = 0.5 mol/l at pCO_2 = 0, pCO_2 = 0.1 bar and pCO_2 = 1 bar. Adapted from (M Altmaier et al., 2005).

Other factors, such as particle size, presence of colloids and ionic strength can affect the solubility of thorium. Schindler (1967) showed that differences in particle sizes in oxides and hydroxides relate to differences in the Gibbs energy of the solids and hence can affect solubility. Neck and Kim (2001) estimated the effect of particle size on the solubility product using the equations of Schindler (Schindler, 1967). Their results indicated that the solubility product of a bulk ThO_2(cr) crystal is expected to be about 1.2 orders of magnitude lower than that of the observed ThO_2 colloids. Bitea et al. (2003) investigated the formation of thorium colloids. They observed small crystalline (<10 nm) colloids at pH values 1.5-2.5. At pH 3-5, the colloids observed were very small (2-5 nm size) under low saturation, or between 50 and 100 nm, under a high degree of saturation. The 50-100 nm colloids presented an amorphous structure composed of smaller substructures which in turn could comprise a crystalline structure. Rothe et al. (2002) hypothesized the formation of small microcrystalline $ThO_2.H_2O$(s) colloids that subsequently agglomerate

to a microcrystalline precipitate at pH values between 1.5 and 2.5. At pH 3-5, the formation of amorphous thorium hydroxide colloids would be caused by hydrolysis and poly-nucleation. Increasing ionic strength increases the solubility of ThO_2(am). Above pH 7 in 3mol/l NaCl solutions, the solubility is approximately three orders of magnitude higher than that measured in 0.1mol/l $NaClO_4$ solution (Felmy, Dhanpat and Mason, 1991).

3.2.4 Thorium Sorption

Thorium(IV) ions are extremely particle reactive (Santschi *et al.*, 2006). Thorium adsorption onto Fe-hydroxides is higher than that of U, and can be stronger, even at pH values as low as 2 (Chabaux, Riotte and Dequincey, 1992). Quigley and co-workers (1996) determined that sorption of Th onto hematite is rapid and equilibrium is attained within a few minutes. Under acidic conditions (pH values between 3 and 4.2), thorium forms bidentate-corner sharing arrangements to the [FeO_6] octahedra and [FeO_4] tetrahedra on the surface of magnetite and shares one O atom with each of the two coordinated octahedra on the surface of ferrihydrite (FeOOH) (Rojo *et al.*, 2009). Thorium is strongly sorbed to gibbsite (Hongxia, Zheng and Zuyi, 2006).

In the neutral to alkaline pH range, the hydrolysis of thorium is strong enough to cause thorium desorption from the silica surface, and sorption to silica is therefore important only in the pH range 3 to 6 (Östhols, 1995). The exact pH region where Th is sorbed to silica will depend on the ratio of Th concentration to silica surface. However, it will rarely be present as sorbed silica above pH 5-6. It is unlikely that silica will act as efficient scavenger in the neutral to alkaline pH range. The sorption of Th onto silica is further decreased by the formation of meta-stable Th-silica colloids at pH above 7, resulting in concentrations higher by a factor of 10^3 than concentrations observed for pure Th(IV) oxyhydroxides (Hennig *et al.*, 2013).

Thorium is also known to sorb to clays. It sorbs primarily by surface complexation (Wu *et al.*, 2007; Schmidt *et al.*, 2012) although additional contribution by cation exchange has been identified in some studies (Xu *et al.*, 2007; Yu *et al.*, 2008).

Humic (HA) and fulvic acids (FA) were shown to enhance Th(IV) sorption at low pH and decrease Th sorption at intermediate and high pH on a variety of substrates including silica (C. Chen and Wang, 2007), γ-Al_2O_3 (C. L. Chen and Wang, 2007), rectorite (Xu *et al.*, 2007; Yu *et al.*, 2008) and TiO_2 nanoparticles (Tan *et al.*, 2007). They attributed the positive influence of HA/FA on sorption at pH values 2 to 4 to strong surface binding of HA/FA on SiO_2 and subsequently the formation of ternary surface complexes such as

≡MO-O-HA-Th or ≡MO-O-FA-Th. Sorption was strongly dependent on the concentration of HA/FA. Righetto et al (1991) have also observed increased thorium adsorption in the low pH-region and decrease in adsorption at high pH values on both alumina and silica in the presence of HA. Reiller et al. (2002) also observed a decrease of Th sorption onto the surface of hematite (α-Fe2O3) and goethite (α-FeOOH) in the presence of humic acids (HA) in the pH range 3.5-9.5. These authors attributed the decreased sorption to competition between hematite sites, sorbed HA sites and "free" HA sites in the case of excess HA sites compared to hematite sites.

Jernstrom and co-workers (2002) investigated the solubility of thorium in 0.1 mol/l NaCl solution and in saline and fresh anoxic synthetic reference groundwater (I = 0.5 mol/l and 0.002 mol/l respectively) containing 10^{-6} and 10^{-5} mol/l total carbonate. The low carbonate concentrations of 10^{-5} and 10^{-6} mol/l had no effect on the solubility and aqueous thorium speciation, but IR spectrometry gave an indication that carbonate might be sorbed onto the solid phase. LaFlamme and Murray (1987) showed a dependence between the sorption of Th onto goethite and carbonate alkalinity. Thorium (at a total concentration of 10^{-13} mol/l) in the presence of 5.22 mg/l α-FeOOH and 0.1 mol/l $NaNO_3$ has an adsorption edge from pH 2-5. At pH 9.0 ± 0.6 the percent Th adsorbed on the solid began to decrease from 100% at 100 meq/l carbonate alkalinity and exhibited no adsorption above 300 meq/ l. The rise in solubility can be explained by the decrease in thorium adsorption due to competition of HCO_3^- and CO_3^{2-} ions for surface sites and by the increase of thorium in solution due to dissolved thorium carbonate complexes (LaFlamme and Murray, 1987). Jakobsson (1999), on the other hand, found no measurable desorbing influence on the sorption of Th onto TiO_2 in the pH interval 5 to 10.5 for a carbonate concentration lower than 10^{-2} mol/l.

3.2.5 Thorium concentrations in Malvési

The concentration of thorium isotopes of the ^{238}U chain in the soils around Malvési is very low to the north of the site, but increases in the East of the site where the soils are likely to be impacted by the plant, see Table 3.3, (Pourcelot and Le Roux, 2008). Thorium-234 concentrations, found in equilibrium with ^{238}U, are three orders of magnitude higher in the sludge and two orders of magnitude higher in the tailings and cover layer compared with the background soils. The enhanced concentrations of ^{230}Th in the basins represent an increase in concentration of four orders of magnitude in the sludge and two orders of magnitude in the tailings. The study (Pourcelot and Le Roux, 2008) did not investigate background concentrations of ^{232}Th.

Table 3.3: Measured concentrations and activities of ^{230}Th and ^{234}Th in the soils around the site and in B1/B2 (Pourcelot and Le Roux, 2008).

Location	^{234}Th		^{230}Th	
	Mass (mg/kg)	Activity (Bq/kg)	Mass (mg/kg)	Activity (Bq/kg)
North of site	$3.2 \cdot 10^{-11}$ - $3.9 \cdot 10^{-11}$	27 – 33	<DL	
East of site	$3.8 \cdot 10^{-11}$ – $7.3 \cdot 10^{-11}$	32 - 62	$6.1 \cdot 10^{-5}$ – $8.3 \cdot 10^{-5}$	43 - 58
C. Layer	$7.2 \cdot 10^{-9}$	$6.1 \cdot 10^{+3}$	$4.2 \cdot 10^{-2}$	$3.0 \cdot 10^{+4}$
Sludge	$6.6 \cdot 10^{-8}$	$5.6 \cdot 10^{+4}$	$6.8 \cdot 10^{-1}$	$4.8 \cdot 10^{+5}$
Mix soil and sludge	$1.8 \cdot 10^{-8}$	$1.5 \cdot 10^{+4}$	$9.1 \cdot 10^{-2}$	$6.4 \cdot 10^{+4}$
Mix East of B2	$6.9 \cdot 10^{-9}$	$5.8 \cdot 10^{+3}$	$3.4 \cdot 10^{-2}$	$2.4 \cdot 10^{+4}$
Tailings	$1.6 \cdot 10^{-9}$	$1.3 \cdot 10^{+3}$	$4.4 \cdot 10^{-3}$	$3.1 \cdot 10^{+3}$

<DL: below detection limit

As it is eliminated from the ore concentrates during the uranium conversion process, ^{230}Th is expected to be present in elevated concentrations in the liquid effluents of the Malvési facility. However, as there is poor monitoring of the effluent quality and quantity (AREVA NC Malvési, personal communication) the final concentration of thorium is not known. In the basins B1/B2, ^{230}Th contributes with approximately 45-50% of the total alpha activity of the B1/B2 waste.

The concentration of thorium in the groundwater underlying the Malvési site was found to be in the range of 10^{-11} to 10^{-10} mol/l in both the natural soils (alluvium) and in the waste contained in B1/B2 (mixture of soil and sludge, sludge and tailings) (Burgeap, 2009a).

4. Materials and Methods

4.1 Introduction

As seen in Chapter 3, the geochemistry of U and Th is complex. This complexity presents analytical challenges in the investigation of the processes contributing to the mobility of these elements in the basins. In this thesis, a multi-technique approach was used in order to obtain complementary information on:

- The geochemical environment of the waste;
- The speciation of U and Th in the waste; and
- The release behaviour of U and Th from the waste under different conditions.

The following activities were carried out:

Field Sampling

- Retrieval of solid samples collected by Arcadis in 2009 (Bary *et al.*, 2010a) from the B1/B2 basins as part of their ground investigation, referred to as ***2009 samples***. These samples permitted laboratory testing of samples covering a broad horizontal and vertical distribution within the basins;
- Drilling and collection of a core sample in the B1 basin with sampling along its depth. These samples are referred to as ***2012 samples***; and
- Groundwater sampling and collection from existing piezometers located in the basins (Bary *et al.*, 2010a).

Laboratory Methodology

- Bulk solid sample characterisation, comprising moisture content, total surface area, wet and dry bulk density, total chemical composition, and mineralogy by X-ray powder diffraction (XRD);
- Investigation of the mineral phases capable of retaining U and Th by sequential extraction techniques;
- Investigation of the solid speciation of uranium and thorium, comprising particle isolation by autoradiography, by analysis under UV light or by sample

suspension, followed by analysis of these areas by electron microscopy, Raman spectroscopy and synchrotron techniques;

- Groundwater and pore water analysis;
- Investigation of the release and retention of U and Th with static (batch) and dynamic (column) experiments; and
- Investigation of the colloidal fraction of U and Th.

Modelling

- Geochemical speciation modelling; and
- U and Th dynamic release and retention modelling.

4.2 Field sampling

4.2.1 Overview

The solid samples used in this work comprised material collected from the decantation basins B1 and B2 of the site of AREVA NC Malvési in 2009 by Arcadis (Bary *et al.*, 2010a), prior to the start of this thesis and samples collected specifically for this research in 2012.

4.2.2 2009 sampling campaign

The 2009 investigation comprised the drilling of 44 boreholes across the basins, on a 40m by 40m horizontal grid. These samples had been dried, homogenised and the fraction smaller than 2mm saved for laboratory analysis. Six samples, chosen to represent different locations and depths along the basins, were selected for the sequential extraction and batch experiments and analysed by XRD (Table 4.2). The location of the samples is shown in Figure 4.1

4.2.3 2012 sampling campaign

In 2012, AREVA NC organised an additional ground investigation for the drilling of one borehole (borehole SC429, see location in Figure 4.1) and collection of samples. The core samples, undisturbed and within the PVC liner were sealed at both ends with paraffin and transported to the laboratory. Samples for analysis were collected at discrete depths along the cores. Chapter 5 presents details of the site observations. The samples selected from this new borehole were used for bulk characterisation and analysed by

spectroscopy methods. Table 4.2 summarises the experiments carried out on each sample.

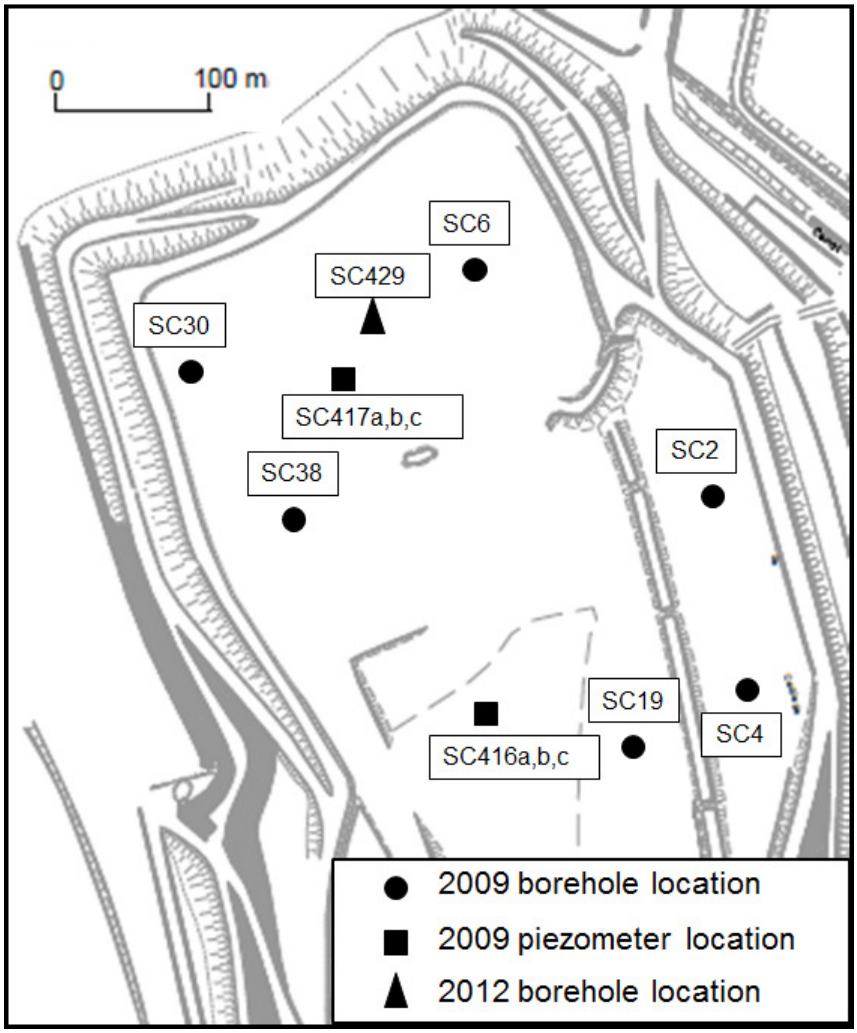

Figure 4.1: Location of boreholes drilled and piezometers installed as part of the 2009 ground investigation carried out by Arcadis (Bary et al., 2010a) and location of borehole drilled in the 2012 ground investigation.

Pore water samples were extracted from the solid samples at three depths, corresponding to the three strata: mixture of soil and sludge (3.2 m), sludge (6.8 m) and tailings (8.8 m). The samples were extracted as follows: a 20 mL polyethylene vial containing approximately 10-15 g of solid sample was centrifuged for 40 minutes at 18,000 rpm, followed by ultracentrifugation at 90,000 rpm for 1 hour. Sample pre-treatment and analysis is described in Section 4.5.

4.2.4 Groundwater sampling campaign

Groundwater samples were collected from the piezometers installed during the 2009 ground investigation (Bary *et al.*, 2010a). The response zones of the piezometers were

within the mixture of soil and sludge, the sludge, the tailings and the alluvium, as detailed in Table 4.1. The location of the piezometers is shown in Figure 4.1. Measurements of pH and Eh were carried out *in situ* during sampling and again in the AREVA NC laboratories, no more than 24h after sampling. Sample pre-treatment and analysis is described in Section 4.5.

Table 4.1: Response zone of piezometers.

Piezometer name	Response zone (m depth)	Strata monitored
SC416a	1.0 – 5.8	Mixt. S+S
SC416b	6.0 – 16.0	Tailings
SC416c	19.0 – 26.8	Alluvium
SC417a	3.0 – 7.5	Sludge
SC417b	7.0 – 16.5	Mixt. S+S and Tailings
SC417c	19.5 – 25.5	Alluvium

4.3 Laboratory Methodology

4.3.1 Overview

A multi-technique approach was required to adequately characterise the Malvési samples and the U and Th distribution in the samples. The diagram in Figure 4.2 illustrates the techniques used.

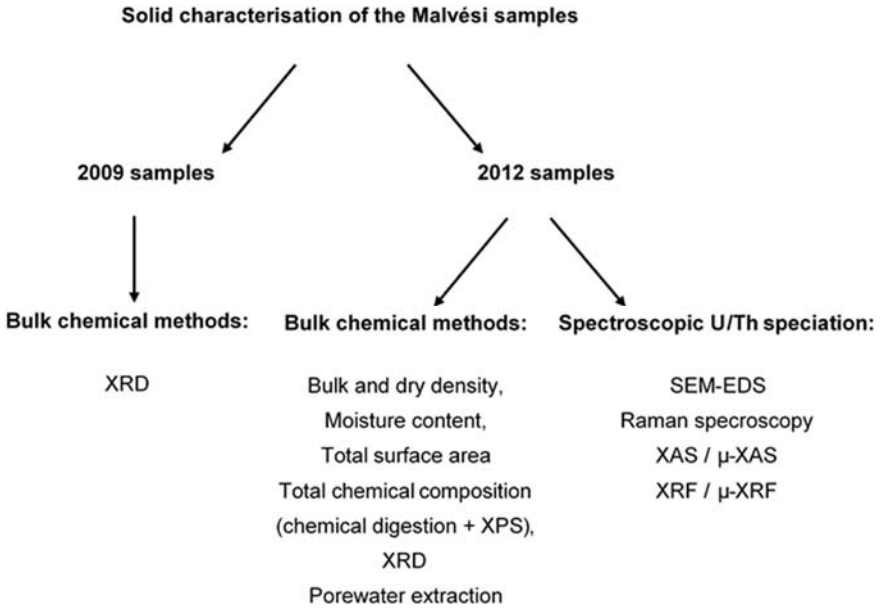

Figure 4.2: Diagram of the bulk chemical and spectroscopic U and Th speciation methods used in the characterisation of the Malvési samples.

Table 4.2: Summary table of analysis carried out for each solid sample.

Year	Sample ID /Location	Depth (m)	Strata	Bulk Solid Characterisation			Identification of area of enhanced activity	Microscopy	Synchrotron techniques	Release and retention of U and Th
				Bulk analysis	Elemental composition	Mineralogy				
2009	SC30	0-2.15	Mixt S+S	-	-	XRD	-	-	-	Batch
	SC416b	0.45-4.3	Mixt. S+S	-	-	XRD	-	-	-	SE
	SC30	2.4-5.6	Sludge	-	-	XRD	-	-	-	SE
	SC6	8.6-9.3	Sludge	-	-	XRD	-	-	-	SE
	SC19	2.5-3.8	Sludge	-	-	XRD	-	-	-	SE, batch
	SC417b	8.2-10.2	Tailings	-	-	XRD	-	-	-	SE, batch
	SC417a	1.5-3.0	Sludge	-	-	-	-	-	-	Batch, column
	SC416b	5.8-7.3	Tailings	-	-	-	-	-	-	Batch, column
2012	SC429	3.2	Mixt. S+S	MC, TSA	Digestion, XPS	-	-	-	-	Pore water, batch
	SC429	6.8	Sludge	MC, TSA	Digestion, XPS	-	AR(c), UV (6.9m)	SEM-EDS; RS	XAS, XRF	Pore water, batch
	SC429	8.0	Sludge	MC, TSA	XPS	-	-	-	-	-
	SC429	8.1	Sludge	density	Digestion, XPS	XRD	AR(c), UV (8.15m), SS	SEM-EDS; RS	XAS, XRF, µ-XAS, µ-XRF	Column
	SC429	8.4-8.5	Tailings	MC, TSA, density	Digestion, XPS	-	-	-	XAS, XRF	Column
	SC429	8.8	Tailings	MC, TSA	Digestion, XPS	-	AR(c)	-	-	Pore water, batch
	SC429	11.8	Tailings	MC, TSA, density	Digestion, XPS	-	-	-	-	Column

MC: moisture content at 105°C; Density: sample density according to method BS1377-2 (1996); TSA: total surface area by EGME adsorption (Cerato et al., 2002); Digestion: determination of total elemental composition by acid digestion with HNO_3, HCl and HF (all acids to suprapur standard) followed by ICP-MS analysis; XPS: ULVAC-PHI, Inc., model PHI 5000 VersaProbe II XP spectrometer equipped with a scanning microprobe X-ray source (monochromatic Al Kα (1486.6 eV) X-rays); AR(c): Autoradiography carried out with a Packard Bioscience Company Cyclone, interpretation with the OptiQuant software; UV: desk table UV lamp emitting light at 250 nm; SS: sample suspension in alcohol; SEM-EDS: FEI Quanta 650 FEG SEM. NORAN System 7 (Thermo Fisher Scientific) EDS; RS: Bruker Senterra Raman microscope; XAS: X-ray absorption spectroscopy; µ-XAS: micro-X-ray absorption spectroscopy; XRF: X-ray fluorescence spectroscopy; µ-XRF: micro-X-ray fluorescence spectroscopy; SE: sequential extraction; Pore water:pore water analysis; Batch: batch experiments; Column: column experiments.

4.3.2 Bulk solid characterisation

4.3.2.1 Moisture content

The moisture content of the samples was obtained gravimetrically by measuring the percentage of change in mass of the soil before and after drying the samples in an oven at 105^0C to constant mass.

4.3.2.2 Bulk density and surface area

The wet and dry bulk densities were calculated by the linear measurement method based on British Standard BS1377-2 *(British Standard, 1996)*.

Total surface area was measured by EGME adsorption (Cerato and Lutenegger, 2002). The method consists in wetting a sample with a polar liquid, EGME (ethylene glycol monoethyl ether), equilibrating and then removing the excess liquid by evacuation at 0.15 bar. The total surface area is computed from the mass of the liquid retained under the assumption that a monomolecular layer of EGME is adsorbed to the surface. This method has the advantage of including the area of the internal surfaces of clays, which are not measured by the BET (from Brunauer, Emmett and Teller) method (Payne *et al.*, 2011).

4.3.2.3 Total elemental composition of solid samples

Total elemental composition of the sediment samples was determined by treating the samples by acid digestion followed by inductively coupled plasma mass spectrometry (ICP-MS) on a PerkinElmer ELAN 6100 machine. The methodoloy comprised heating 100 to 150 mg of dry sample at 150 ºC in a hot plate with 3 ml of HNO_3, 100 µl HCl and 1.5 ml HF (all acids to suprapur standard). After 2 hours, the digested sample was purified from vestigies of HF and HCl by allowing the solution to evaporate, at a temperature of approximately 80 ºC, and adding 2 ml of HNO_3. This step was repeated three times, after which 1 ml of HNO_3 was added to the sample which in turn was transposed to a graduated flask and was filled to the graduated mark with deionised water.

Uranium and thorium were analysed in quantitative mode, whilst cations and trace metals were analysed in semi-quantitative mode, which has an uncertainty of around 30%.

Additional elemental characterisation was carried out by X-ray photoelectron spectroscopy (XPS), as described below.

4.3.2.4 X-ray Photoelectron Spectroscopy (XPS)

The samples collected during the 2012 sampling campaign were analysed by X-ray photoelectron spectroscopy (XPS) at room temperature. The samples, without any pre-treatment, were pressed onto indium foil, mounted on the sample holder and allowed to dry at room temperature. The uppermost surface layers (up to ~10 nm) were analyzed with an XP spectrometer (ULVAC-PHI, Inc., model PHI 5000 VersaProbe II) equipped with a scanning microprobe X-ray source (monochromatic Al Kα (1486.6 eV) X-rays) in combination with an electron flood gun and a floating ion gun generating low energy electrons and low energy Ar ions for charge compensation (dual beam technique). This technique allows a semi-quantitative analysis of the elemental composition of the samples as well as a determination of their redox state. With monochromatic Al Kα X-ray excitation, the bremsstrahlung induced background intensity and X-ray satellites are absent, yielding a detection limit for U of about 0.04 atom percent. The spectrometer was equipped with a hemispherical capacitor analyzer (mean diameter 279.4 mm) and the detector consisted of a microchannel detector with 16 anodes. Calibration of the binding energy scale of the spectrometer was performed using well-established binding energies of elemental lines of pure metals (monochromatic Al Kα: Cu $2p_{3/2}$ at 932.62 eV, Au $4f_{7/2}$ at 83.96 eV) (Seah, Gilmore and Beamson, 1998). Standard deviations of binding energies of isolating samples were within ±0.2 eV. The spectra were collected at a take-off angle of 45° (angle between sample surface and analyzer) and the pressure inside the spectrometer was about $2 \cdot 10^{-7}$ Pa.

Survey scans were recorded with an X-ray source power of 33 W and a pass energy of 187.85 eV of the analyzer, to identify the elements and to determine their atomic concentrations at the sample surface. The X-ray beam diameter was adjusted to 200 µm and scanned over an area of 1 x 0.5 mm^2. To retrieve information about the chemical state of the elements, narrow scan spectra of elemental lines were recorded at a pass energy of 46.95 eV. All spectra were charge referenced to the C 1s elemental line of adventitious hydrocarbon (C_xH_y) at 284.8 eV. Data analysis was performed using PHI MultiPak program, Version 9.4. The elemental lines (Shirley background subtracted) were fitted by applying a non-linear least-squares optimization procedure using Gaussian–Lorentzian sum functions. Chemical bonding states were identified by comparison of the binding energies of the elemental lines with reference values reported in the literature.

4.3.2.5 Mineralogy

The mineralogy of each bulk sample (<2 mm) was determined using X-ray powder diffraction analysis (XRD). The samples were homogenised and grinded before preparation for analysis. The analysis was carried out on a Philips X-Pert XRD unit using monochromated CuKα radiation (wavelength 1.5418). Randomly oriented samples were scanned from 5^0 to 60^0 2θ with a step size of 0.03^0. Scans were collected electronically and processed using commercial software (HighScore Plus XRD pattern processing software). Mineral identification was based on powder diffraction files published by the International Centre for Diffraction Data (ICDD).

4.3.3 Investigation of mineral phases capable of retaining uranium and thorium

The retention of U and Th in the material was studied by treating the samples with a series of chemical reagents in order to partition the U and Th contained in various phases by sequential extraction.

The method, summarised in Table 4.3, is based on the work of Payne (Payne, 1999) and Yanase (Yanase, 1991) for the study of the distribution of uranium in mineral phases at the Koongarra uranium deposit in Australia, which in turn is an adaptation of the original method by Tessier (Tessier, Campbell and Bisson, 1979). The five fractions studied are: 1) exchangeable; 2) amorphous minerals and secondary U minerals; 3) crystalline iron minerals; 4) clay minerals and U oxides; and 5) resistate.

This method is particularly useful for estimating the amount of mineral phases capable of retaining U and Th, such as amorphous or crystalline iron minerals in the sediments. The amount of U and Th extracted within the first two phases, is considered to be “labile” and gives an indication of the fraction of total U and Th that could be easily released to the groundwater under natural conditions. Duplicates of a sample of sludge (sample SC6) were extracted to study the reproducibility of the technique. The liquid samples were analysed for Al, Si, Fe, Mg, Ti, Mn, ^{238}U and ^{232}Th in a Thermo Elemental XSeries 2 ICP-MS machine.

Table 4.3: Extraction methodology.

Fraction No.	Reagent	Main phases dissolved	Extraction Conditions (for 1g of soil)
1 – Soluble salts, exchangeable ions	Morgan's solution	Carbonate minerals, adsorbed trace elements	40 ml, shake for 4 hrs
2 – Amorphous oxide minerals	Tamm's acid oxalate (TAO)	Amorphous minerals of Fe, Al and Si; secondary U minerals	40 ml, shake in dark for 4 hrs
3 – Crystalline iron minerals	Citrate / dithionite / bicarbonate (CDB) reagent	Crystalline iron oxides, hydroxides and oxyhydroxides	60 ml stirred for 30 min at 85ºC Repeat extraction until all the iron colouration is removed from the residue
4 – Amorphous Al and Si compounds	6M HCl	Clay minerals, uranium oxides	Stirred for 2 hrs at 85ºC
5 – Resistate material	Digestion and Fusion	Remaining resistate minerals (quartz, muscovite)	HF / $HClO_4$ digestion, evaporation. Make up solution with oversaturated boric acid.

Morgan's solution: 1M NaOAc adjusted to pH 5.0 with acetic acid

TAO: 10.9g/l oxalic acid + 16.1 g/l ammonium oxalate

CDB: 0.3M tri-sodium citrate, 0.2M $NaHCO_3$, 1 g/g sample of sodium dithionite

4.4 Investigation of the solid speciation of uranium and thorium

A variety of methodologies were used to investigate the source terms of U and Th in the material. To guide the selection of spots for source term characterisation, the areas of enhanced activity were first identified. These areas were then analysed by SEM-EDS (scanning electron microscope – energy dispersive x-ray spectroscopy) and Raman spectroscopy. Synchrotron techniques were used to study the oxidation state of U and the elemental distributions in the samples.

4.4.1 Identification of areas of enhanced activity

One of the main difficulties encountered during characterisation of the Malvési samples derived from the complexity of the matrix, which masked the presence of the U and Th particles. In order to identify areas of enhanced activity that could then be investigated by spectroscopic methods, a variety of techniques were used, which included autoradiography, analysis of the sample material under UV light and preparation of sample suspensions.

Autoradiography was used to guide the selection of hotspots for additional spectroscopy measurements. The samples were pressed onto microscope glass slides and left in

contact with a storage phosphor screen for a duration of between 4 days and 3 weeks. The phosphor screens captured the emissions of radiation of the samples and were analysed with a Cyclone machine (Packard Bioscience Company) and interpreted using the OptiQuant software. Areas of enhanced radioactivity were identified in the samples of sludge at 6.8m and 8.1m depth. These areas were further analysed by SEM-EDS, Raman spectroscopy, μ-XRF and μ-XANES. A sample of tailings at 8.8m depth was also investigated but no areas of enhanced activity were encountered even after a contact time of 3 weeks.

An attempt to identify U particles was made using a UV lamp by taking advantage of the fact that many U and Th minerals are fluorescent. For example, under UV light, the fluorescent minerals of uranophane and schoepite would show a weak yellow-green and a pale green colour respectively. However, it should be noted that not all U and Th minerals are fluorescent and hence, this technique could discriminate against certain U particles. A desk table UV lamp emitting light at 250 nm was used to investigate samples of sludge at 6.9m and 8.15m depth. These samples were prepared by pressing a thin layer of sample onto microscopy glass slides (the same methodology used for the autoradiography analysis). No fluorescent particles were identified in the sample of sludge at 6.9m depth. In the sample at 8.15m depth, fluorescent particles were identified and they were prepared for SEM analysis by sub-sampling the particles into self-adhesive carbon pads fixed to standard ESCA sample holders.

Another attempt was made to separate the particles from the matrix so that EDS spectra could be obtained for U particles without matrix interference. This was carried out by preparing suspensions of the wet sample of sludge at 8.1m depth in alcohol. The suspension was allowed to air dry in a self-adhesive carbon pad fixed to a standard ESCA sample holder.

4.4.2 Scanning Electron Microscopy – Energy Dispersive Spectrometry (SEM-EDS)

A FEI Quanta 650 FEG scanning electron microscope (SEM) was used for high-resolution imaging of the morphology and composition of U and Th containing particles. The energy-dispersive spectrometry (EDS) system, NORAN System 7 (Thermo Fisher Scientific) with dry detector, provided qualitative elemental analysis of scanned areas of particles. Operating conditions consisted of 30 keV for both SEM imaging and EDS analysis. To help identify particles that contained elements with large atomic number (high electron density), such as U and Th, the SEM was operated in backscattered

electron (BSE) mode. Because no coating was applied, charge compensation of the sample surface was achieved by 70 Pa of water vapour within the analysis chamber (variable pressure mode). The electron beam ionized water molecules compensated the negatively charged sample surface caused by implantation of electrons by the beam.

4.4.3 Raman Spectroscopy

A Bruker Senterra Raman microscope was used for analysing mineral phases containing uranium previously located by SEM-EDS. Two laser wavelengths, 532 nm and 785 nm, were used consecutively to identify Raman active lines at the spectra. Calibration of the wavenumber scale was checked by measurement of polystyrene. During measurement of the samples, continuous wavenumber calibration was automatically performed by SureCal technique.

4.4.4 Synchrotron techniques - bulk analysis

Synchrotron techniques are a group of techniques that are becoming increasingly used as complementary methods in the characterisation of contaminated sediments. In this project, absorption and fluorescence synchrotron techniques were applied in the determination of the U oxidation state and in the elemental composition of the samples. The X-ray Absorption Spectroscopy (XAS) process is characterised by an absorption edge (a sharp increase in absorption of X-rays by matter over a narrow energy range), which is caused by the excitation of an electron from a deep core state of an atom to either an empty or a continuum state. The absorption edge only occurs when the energy of the incident X-ray photons equals the energy required for excitation. In ionic bonds, a shift in the position of the edge features to higher energies is observed as metal becomes more oxidised. The region in the vicinity of the edge, the X-ray Absorption Near Edge Structure (XANES) provides information on the oxidation state, as well as geometry and bonding of the nearest neighbour environment, while the Extended X-ray Absorption Fine Structure (EXAFS) region, which comprises the oscillations above the edge, is used for qualitative determination of bond length and coordination number.

The absorption of X-rays can also cause fluorescence of a sample. In this case, the incident X-ray knocks out an electron from one of the orbitals surrounding the nucleus, which produces a hole in the orbital, resulting in a high energy, unstable configuration for the atom. To restore equilibrium, an electron from a higher energy, outer orbital, falls into the hole, emitting energy in the form of a fluorescent X-ray. The energy difference between the expelled and replacement electrons is characteristic of the element atom in

which the fluorescent process is occurring. The energy of the emitted fluorescent X-ray is therefore, directly linked to a specific element being analysed.

Wet samples were prepared for bulk measurements on 400 µl vials. The samples prepared were: 2 samples of sludge at 6.9/7.0m depth; 2 samples of sludge at 8.1m depth; and 1 sample of tailings at 8.5m depth, Figure 4.3. Bulk samples were prepared in polyethylene vials for XANES / XRF measurements. Scanning XRF using a monochromatic X-ray beam focused to 600 µm was performed at an incident energy above the U and Th L3 edges. Figure 4.4 shows the microprobe set-up for the thin film samples (on the left) and three of the bulk samples (on the right).

XANES and XRF spectra of U and Th were obtained at the INE beamline of the ANKA synchrotron light source facility at the INE Karlsruhe Institute of Technology (KIT) in Germany.

Figure 4.3: Three 400 µl sample vials (sludge at 6.9m, sludge at 8.15m and tailings at 8.5m depth) for bulk XANES and XRF measurements.

4.4.5 Synchrotron techniques - microprobe

The investigation of a sample microscopic environment can be carried out at a synchrotron beamline by focusing the beam to achieve smaller beam sizes. These microprobe techniques are gaining importance in the application to the X-ray absorption and X-ray fluorescence processes. At the INE beamline of the ANKA synchrotron (Karlsruhe, Germany), for example, the usual beam spot size is 600 µm x 600 µm, while

the size achieved by the focused beam is 25 µm x 25 µm, allowing the study of a sample at a much smaller scale.

Micro-X-ray fluorescence spectroscopy (µ-XRF) was performed at the INE-Beamline of the ANKA synchrotron on the regions of interest with high local U concentration identified from SEM images in the sample of sludge at 8.1m depth. Scanning 2D µ-XRF using a monochromatic X-ray beam focused to a 25 µm spot was performed at an incident energy above the U L3 edges to allow locating U hot spots in the thin films. A polycapillary optic mounted on a hexapod positioning unit was used to focus monochromatic radiation delivered by the double crystal monochromator equipped with a pair of Ge<422> crystals into a beam spot-size of ~25 µm at the sample surface. The sample holder was mounted on a three-axis positioning stage with the thin film sample surface at a 45° angle to the incident beam (Figure 4.4). The y and z stage axes (the x-axis determines the focus) were used to scan selected areas and precisely position the samples in the beam path. A silicon drift detector (SIINT Vortex-60EX) was used for collecting X-ray fluorescence radiation.

U hotspots identified in element distribution maps reconstructed from the scanning µ-XRF measurements were selected for µ-XANES scans. U L3 µ-XANES spectra were recorded by registering the windowed U Lα fluorescence intensity.

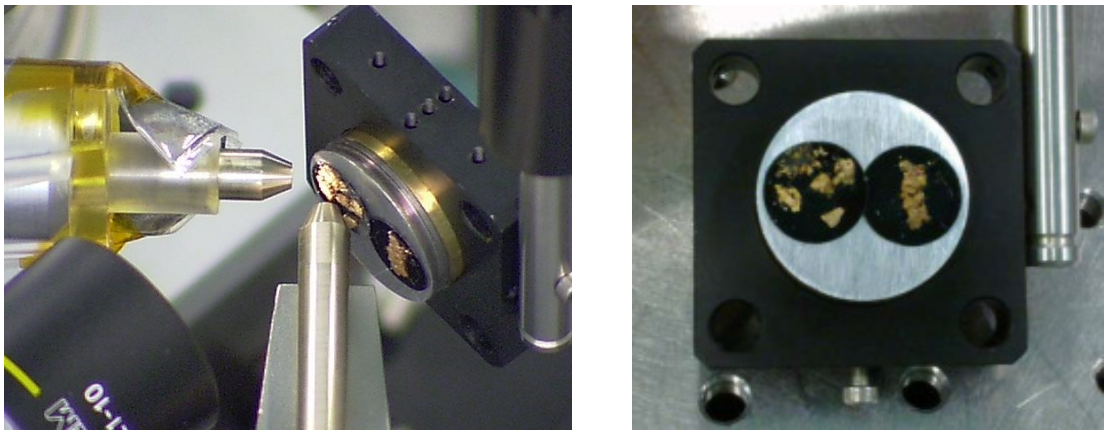

Figure 4.4: Polycapillary setup for the µ-XRF measurements at the INE-Beamline – the silicon drift detector is depicted with a secondary capillary mounted for confocal measurements (in-depth resolved) (left). Dried and lacquer-fixed sample 8.1 (sample of sludge at 8.1m depth), mounted on sample holder (right).

4.5 Analysis of groundwater and pore water samples

4.5.1 Groundwater samples

The pH and Eh of the groundwater samples was measured, the samples were filtered through a 0.22 µm nitrocellulose membrane Millipore filter and acidified with HNO_3 prior to analysis (except samples for carbon analysis). The list of analysis carried out and equipment used is presented in Table 4.4.

4.5.2 Pore water samples

Pore water samples were extracted as described in Section 4.2.3. The pH of the samples was measured prior to acidification with HNO_3. The Eh and redox pairs were not analysed as the samples were treated in atmosphere. The list of analysis carried out and equipment used is presented in Table 4.4.

Table 4.4: Analytical measurements of chemical parameters carried out in groundwater and pore water samples.

Chemical parameter	Groundwater samples	Pore water samples
pH	√ (a)	√ (b)
Eh	√ (c)	-
Alkalinity	-	-
Total inorganic carbon	√ (d)	-
Total organic carbon	√ (d)	-
Total carbon	√ (d)	-
Total Fe, Fe(II) and Fe(III	√ (e)	-
Anions	√ (f), F^-, Cl^-, NO_2^-, NO_3^-,SO_4^{2-}, PO_4^{2-}	√ (f), Cl^-, SO_4^{2-}, NO_3^-
Major cations and trace elements	√ (g), Na, Ca, Mg, K, Si	√ (h)
U and Th	√ (i), ^{234}U, ^{235}U, ^{238}U, ^{232}Th	√ (j), ^{238}U, ^{232}Th

(a) measured with a pH glass electrode of Ag/AgCl (Crison ref. 5012). (b) with a pH (Ross pH combination electrode of Pt and Au). (c) with a glass platinum Eh electrode (Crison ref. 5058). (d) with a total inorganic carbon total organic carbon (TICTOC) analyser, OI Analytical Model 1020A. (e) by UV-visible spectrophotometry. (f) by ion-chromatography (IC). (g) by inductively-coupled plasma optical emission spectrometry (ICP-OES), Perkin-Elmer Optima 4300DV. (h) by inductively-coupled plasma mass spectrometry (ICP-MS) with a Perkin-Elmer ELAN 6100, running in semi-quantitative mode (uncertainty ±30%). (i) by ICP-MS with a Thermo Elemental XSeries 2. (j) by ICP-MS with a Perkin-Elmer ELAN 6100 running in quantitative mode.

4.6 Investigation of the release and retention of U and Th

The release of U and Th was investigated under static (batch) and dynamic (column) conditions. The potential formation of U and Th colloids was investigated in selected aliquots of the batch experiments.

4.6.1 Procedure for batch experiments

Batch experiments were carried out on a 1:5 and 1:10 solid to liquid ratio (S:L) with either MilliQ water or with 0.1M $NaClO_4$. Contact time ranged between 15 minutes and 150 days. At collection, pH and Eh of the supernatant were measured, and samples were either filtered through a 0.22 µm nitrocellulose membrane Millipore filter or centrifuged at 18,000 rpm for 40 minutes and the liquid aliquot collected with a disposable syringe. The aliquot was then prepared for analytical testing. Table 4.5 details the experimental set-up for each sample.

Table 4.5: Batch experimental set-up.

Group	Year	Sample	Strata	S:L ratio	Liquid solution; filtered vs centrifuged	Comments
Dry	2009	SC30 @ 0-2.15m	Mixt. of soil and sludge	1:10	0.1M $NaClO_4$; Filtered	Samples dried, homogenised and the size fraction smaller than 2 mm used
		SC19 @ 2.5-3.8m	Sludge	1:10 and 1:5	0.1M $NaClO_4$; Filtered	
		SC417b @ 8.2-10.2m	Tailings	1:10 and 1:5	0.1M $NaClO_4$; Filtered	
		SC417a fraction size <0.5mm	Sludge	1:10	MilliQ water; centrifuged	The aggregates of the samples were gently grinded and mixed with mortar and pestle and the two size fractions separated (sample not oven dried)
		SC417a fraction size 0.5-1.0mm	Sludge	1:10	MilliQ water; centrifuged	
	2012	SC429 @ 3.2m	Mixt. of soil and sludge	1:10	MilliQ water; centrifuged	The samples were oven dried at 105ºC and the aggregates gently grinded with mortar and pestle before the experiment
		SC429 @ 6.8m	Sludge	1:10	MilliQ water; centrifuged	
		SC429 @ 8.8m	Tailings	1:10	MilliQ water; centrifuged	
Wet	2012	SC429 @ 3.2m	Mixt. of soil and sludge	1:10	MilliQ water; centrifuged	No pre-treatment was applied to these samples. The samples were collected directly from the PVC liner into the Zinsser vial*
		SC429 @ 6.8m	Sludge	1:10	MilliQ water; centrifuged	
		SC429 @ 8.8m	Tailings	1:10	MilliQ water; centrifuged	

* The sample moisture content (as measured during the bulk characterisation) was taken into account in the calculation of the S:L ratio

4.6.2 Procedure for column experiments

Four packed columns were prepared (two with samples of sludge, two with samples of tailings). The Plexiglas columns had a length L = 8 cm and an internal diameter Ø = 2 cm. They were packed uniformly with the size fractions of 0.5-1.0 mm of samples SC417A (aged sludge, 2009), SC429 (fresh sludge, 2012) and SC416 (aged tailings, 2009) and eluted with artificial rainwater. Sample SC429 (fresh tailings, 2012) was eluted with artificial sludge effluent.

Tracer tests were carried out with tritiated water (HTO), which was pumped through the column with a syringe pump. A three-way valve allowed injection of artificial rainwater /artificial sludge effluent, HTO or both. The pressure drop in the columns was measured with pressure sensors located at the inlet and at the outlet of the columns. At the outlet, the liquid aliquots were either automatically collected by a fraction collector or disposed off as waste. Master variables were monitored via inline pH and Eh electrodes and additionally measured in samples sent for analytical analysis. Filters of 0.22 µm pore diameter were used at the top and bottom of each column to uniformly distribute the leaching solution at the inlet and prevent removal of sediments from the column at the outlet. The column set up is shown in Figure 4.5.

Table 4.6: Flow rates used in column experiments.

Column ID	Sample / Depth	Strata	Flow rates (ml/min)*	Eluted with:
Packed column of aged sludge	SC417a / 1.5-3.0 m	Sludge	0.036 ± 0.002 (12) 0.146 ± 0.003 (11) 0.357 ± 0.005 (8) 0.129 ± 0.010 (11)	Artificial rainwater
Packed column of aged tailings	SC416b / 5.8-7.3m	Tailings	0.037 ± 0.003 (3) 0.126 ± 0.009 (9) 0.331 ± 0.006 (6) 0.396 ± 0.081 (6)	Artificial rainwater
Packed column of fresh sludge	SC429 / 8.1 m	Sludge	0.156 ± 0.018 (25)	Artificial rainwater
Packed column of fresh tailings	SC429 / 11.75 – 11.85 m	Tailings	0.154 ± 0.020 (31)	Artificial sludge effluent

*figure in parentheses are the number of flow rate experimental measurements

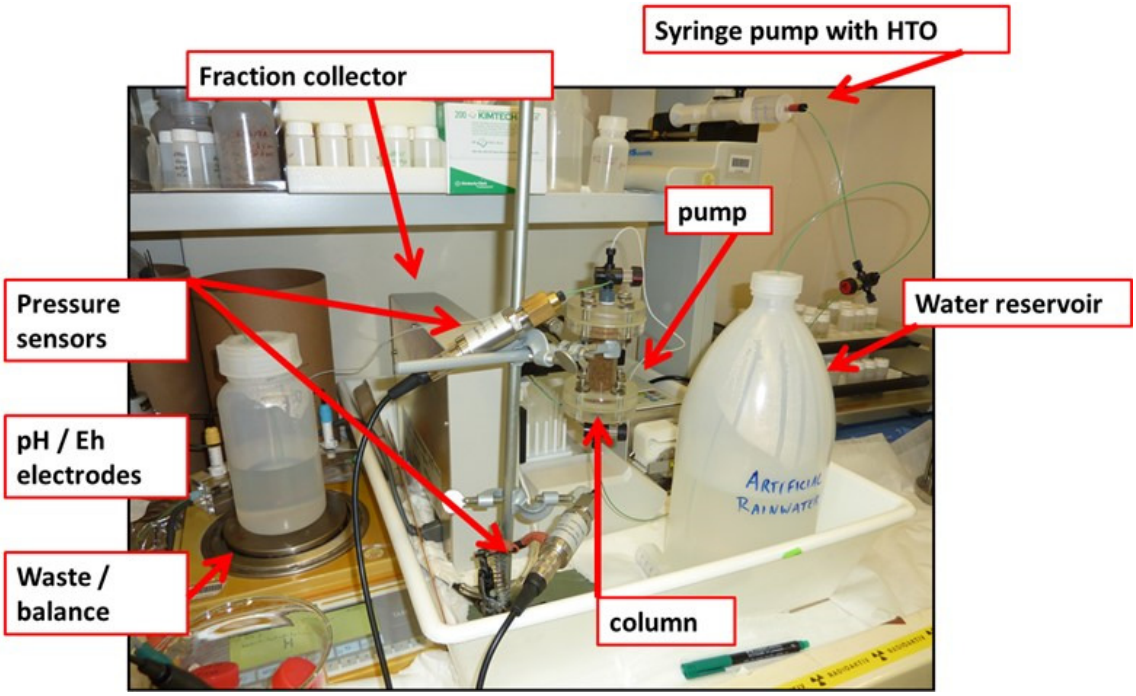

Figure 4.5: Column experimental set-up.

4.7 Analytical techniques

4.7.1 Elemental composition

The elemental composition of solid samples was determined by acid digestion with HNO_3, HCl and HF (all acids to suprapur standard), followed by ICP-MS analysis.

4.7.2 Investigation of the uranium and thorium colloidal fraction

4.7.2.1 Ultracentrifugation

Liquid aliquots of the wet batch experiments, collected at 1 and 7 days contact time, were divided in two sub-aliquots. One sub-aliquot was centrifuged at 18,000 rpm for 1 hour, one sub-aliquot was ultracentrifuged at 90,000 rpm for 1 hour.

4.7.2.2 Ultrafiltration

Selected aliquots of the batch and column experiments were centrifuged using Microsep Advance Centrifugal Filters (Pall Corporation) at up to 3,000 rpm for periods of time ranging from 5 to 20 minutes. Filter sizes used were 3kD, 10kD, 30kD, 100kD, 0.2 µm and 0.45 µm.

4.7.3 Liquid samples and aliquots

Liquid samples and aliquots collected in the experiments described above were measured for pH and Eh with pH and Eh electrodes, organic and inorganic carbon with a TICTOC analyser or alkalinity by the Gran titration method, anions by ion-chromatography, the Fe(II)/Fe(III) and NO_2/NO_3 pairs by UV-visible spectrophotometry, cations, U, Th and trace metals by inductively coupled plasma mass spectrometry (ICP-MS) or inductively coupled plasma optical emission spectrometry (ICP-OES). Details of the equipment used in each analysis is provided in Table 4.2.

4.7.3.1 Gran titration method

Alkalinity was determined by titration with a HCl solution (0.01 M) and pH measurement. The volume of HCl added was plotted against the Gran function in order to find the equivalence point, after which all the HCO_3^- is converted to H_2CO_3.

4.8 Modelling approach

4.8.1 Geochemical speciation

Redox potential, ionic strength, U and Th speciation and the saturation indices of minerals in aqueous samples were calculated using the geochemical code Phreeqc (Parkhurst and Appelo, 1999). Phreeqc is a computer model developed by the U.S. Geological Survey that can perform a wide variety of aqueous geochemical calculations. The model is based on an ion-association aqueous model and has capabilities for i) speciation and saturation index calculations, ii) batch reaction and one-dimensional (1D) transport calculations and iii) inverse modelling.

The thermodynamic database used was ThermoChimie version 9a (Giffaut *et al.*, 2014), which is the database created and developed by ANDRA (Agence Nationale pour la Gestion des Déchets Radioactifs). The ThermoChimie domain of application is mainly within a pH range of 6 to 13, Eh of -0.5V to +0.5V and for temperatures below 80ºC.

4.8.2 Column hydrodynamic parameters

The transport of the nonreactive tracer (tritiated water, HTO) was modelled using the computer code CXTFIT (Toride, Leij and Van Genuchten, 1995). This program combines the convective-dispersive equation (CDE) and a non-linear least squares parameter optimization method, in order to estimate transport parameters from observed

concentrations. Parameters obtained with the modelling are the volumetric water content, θ, the dispersivity, λ, the mobile water fraction, β, and the mass transfer coefficient, ω.

5. Sampling

5.1 Field Sampling Campaigns

This chapter summarises the key aspects of the two field sampling programs, one for groundwater collection and one for collection of solid samples. It presents the observations of the borehole drilling and groundwater sampling campaigns. Detailed analysis and interpretation of the laboratory measurements carried out are presented in Chapter 6.

5.2 2012 Field Sampling Campaign

The soil sampling campaign was carried out in February 2012 and comprised the drilling of one core in the B1 basin (core SC429 at x,y = 652466.3, 101666.9). See Figure 4.1 in Chapter 4 for borehole location. All the cores were left unopened in their PVC liners so logging of the material was done through a visual examination of the open ends of each core, as shown in Figure 5.1.

The borehole intersected the three strata of mixture of soil and sludge, sludge and tailings as shown in the borehole log included in Appendix 1. The interface between the sludge and the tailings was encountered at 8.3m depth. The depth and description of each strata is summarised in Table 5.1. Samples were collected at discrete depths for bulk characterisation, spectroscopy measurements and investigation on the retention and release behaviour of uranium and thorium. Photographs of selected samples are presented in Figure 5.2.

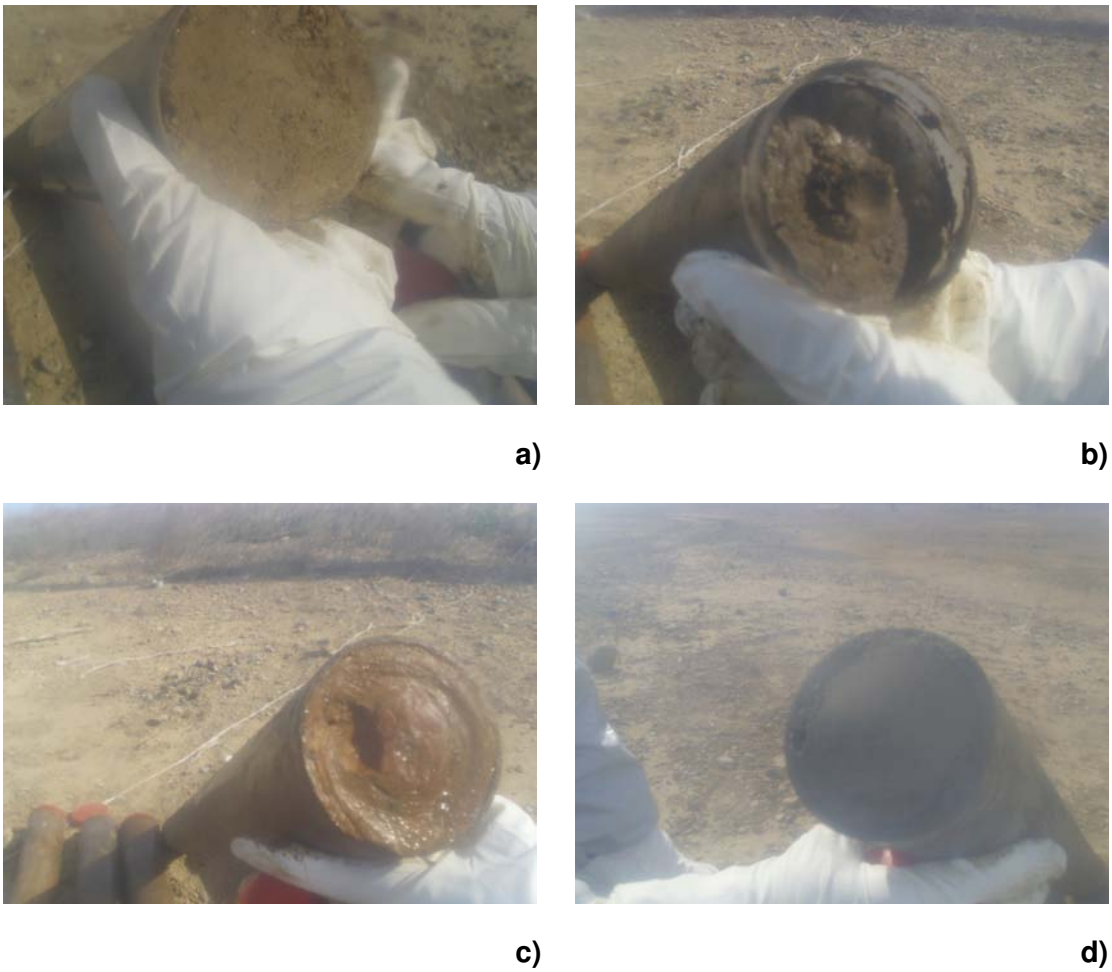

Figure 5.1: Photographs of the cores retrieved from borehole SC429 showing the different strata: (a) mixture of soil and sludge at 3 m depth; (b) sludge at 7 m depth; (c) sludge at 8 m depth; and (d) tailings at 11 m depth.

Table 5.1. Depth and description of strata intersected by core SC429 and samples selected for bulk characterisation and spectroscopy measurements.

Borehole Identification	Depth (m)	Strata	Description	Selected samples (depth in m)[b]
SC429	0-1	Cover Layer	Light brown SAND	-
SC429	1-5.2	Mixture of soil and sludge	Brown slightly sandy CLAY	3.2
SC429	5.2-8.3	Sludge	Light brown to brown SILT to CLAY	6.8; 8.0-8.1
SC429	8.3-13.2[a]	Tailings	Dark grey SAND with pockets of CLAY	8.4-8.5; 8.8; 11.8

[a] bottom of tailings not found; [b] samples selected for bulk characterisation and spectroscopy measurements.

a) Sludge at 6.8m depth

b) Sludge at 8.0 m depth

c) Sludge at 8.1 m depth

d) Interface between sludge and tailings at 8.3 m depth

e) Tailings at 8.4 m depth

f) Tailings at 11.8 m depth

Figure 5.2: Photographs of samples selected for analysis.

5.3 Groundwater Sampling Campaign

Groundwater collection and monitoring took place in the B1/B2 basins on the 18th and 19th of October 2011. Samples were collected from the existing piezometers, installed in 2009 by Arcadis (Bary *et al.*, 2010a). The locations of these piezometers are shown in Figure 4.1 (Chapter 4).

Prior to sampling, and whenever possible, the boreholes were purged to remove stagnant water. Due to the slow refill of water, the boreholes were pumped dry on the 18th October 2011 and sample collection was usually carried out the following day, after a 15-30 second purge, in which the water sampled was disposed of. Table 5.2 below summarises the *in situ* observations relating to purging, water depth and other water quality observations.

Table 5.2: *In situ* observations during groundwater monitoring and collection.

BH ID	Total depth of bh (m)	Depth to level of water (m)	Purging time
SC417a	7.58	3.37	18.10.11: 18 min (no water after 12 min). 19.10.11: 30 sec purge followed by sampling.
SC417b	10.71	5.35	18.10.11: 23 min (dry after 13 min). 19.10.11: 5 min purge followed by sampling. Many sediments in the water.
SC417c	24.70	13.56	18.10.11: purging not possible 19.10.11: 15 sec purge followed by sampling. Very dirty water. Strong smell to H_2S.
SC416a	6.20	4.70	18.10.11: 7 min (dry after 3 min). Waited for 5 min, then purged another 1 min. 19.10.11: 10 sec purge followed by sampling.
SC416b	11.00	5.81	18.10.11: 20 min (dry after 5 min), waited for 3 min, purge another 2 min and dry, waited 10 min, then purge for 6 min (then dry), waited 8 min, then purge for 1 min. 19.10.11: 1 min purge followed by sampling. Obs: can hear the water at the bottom of the hole. Presence of air (can be seen in the pumping tube).
SC416c	>25	15.87	3 min purge - relatively clean water.

6. Results of Analysis of Solids and Pore Waters

6.1 Solids texture, total elemental composition and mineralogy

6.1.1 Solids texture: moisture content, sample density and total surface area measurements

The moisture content of the samples increases along the depth of the stratum of sludge, from 34 to 90% and decreases slightly (from 42 to 31%) along the depth of the tailings (Table 6.1). The total surface area reveals the same tendency, increasing with the depth of the sludge and then decreasing along the depth of the tailings, Table 6.1 and Figure 6.1.

Table 6.1: Density, moisture content and total surface area of samples of SC429.

Sample	ρ_{wet} (g/cm^3)	ρ_{dry} (g/cm^3)	ω (%)	TSA (m^2/g)
Mixt. of Soil and Sludge 3.2m	ND	ND	33.9	180(20)
Sludge 6.8m	ND	ND	48.1	200(10)
Sludge 8.1m	2.43	1.28	89.8	480(80)[a]
Tailings 8.5m	1.70	1.20	41.9	300(15)
Tailings 8.8m	*ND*	*ND*	*ND*	95(15)
Tailings 11.8m	1.62	1.24	31.1	50(15)

ρ_{wet}: wet bulk density; ρ_{dry}: dry bulk density; ω: moisture content; TSA: Total Surface Area;

ND: Not Determined, [a] error calculated from four replicates

The high surface areas measured indicate the sediments to be rich in amorphous or clay minerals, which typically exhibit higher surface areas than crystalline minerals and have higher sorption capcity. Surface areas of common soil minerals can range between 1.8 m^2/g for hematite to 800m^2/g for montmorillonite (Langmuir, 1997). Uranium has strong affinity to adsorb onto Fe oxides such as ferrihydrite (Waite *et al.*, 1994; Bruno *et al.*, 1995; Um *et al.*, 2008), which has a surface area of 250 to 600 m^2/g (Dzombak and Morel, 1990).

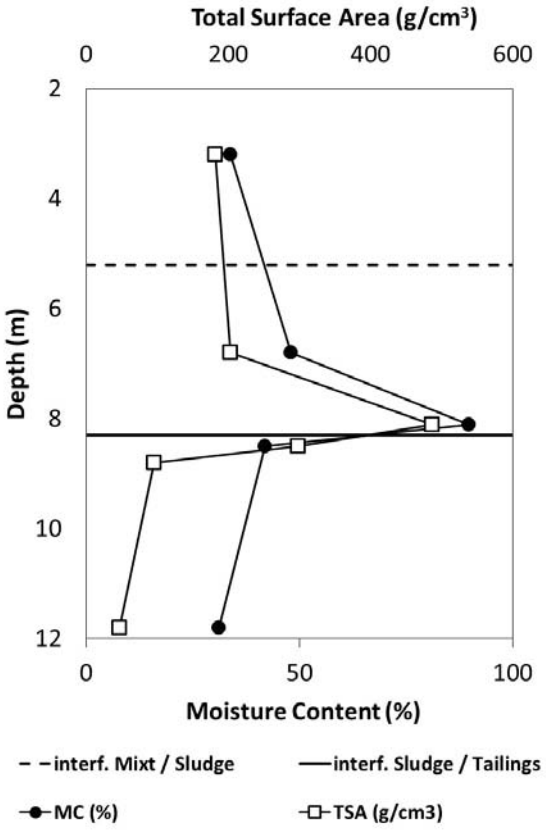

Figure 6.1: Moisture content (MC) and total surface area (TSA) with depth in samples of borehole SC429.

The values of moisture content and wet density (Table 6.1) of the samples of mixture of soil and sludge and tailings are within the range of values obtained in previous investigations (Bary *et al.*, 2010a), 13-48% and 14-28% moisture content, and 1.38-2.15 and 1.60-2.11 g/cm^3 for the mixture of soil and sludge and tailings, respectively. The samples of sludge analysed indicated slightly higher moisture content and wet density than previously measured (37-83% and 1.22-2.07 g/cm^3).

6.1.2 Total elemental composition

The semi-quantitative and qualitative information provided by XPS (Table 6.2) and XRF (Figure 6.2) analyses, respectively show that oxygen (60%), aluminium and silicon (20%), and total carbon and nitrogen (15%) represent 90-95% of the total weight of the samples. The remaining 5-7% consists of sodium, magnesium, potassium, calcium, iron, fluorine and sulphur.

The XRF technique cannot detect elements of low atomic mass (lighter than Ar) found by XPS to comprise the majority, in atomic concentrations, of the samples' elemental

composition. The qualitative results given by this technique show that samples contain Fe, Ca, Zn, Cu, Ni, Pb, Se and Sr (Figure 6.2). U and Th were detected only in samples where their concentrations were sufficiently high, as was the case of the sample of sludge at 8.15m depth. ICP-MS measurements discussed below revealed that this sample contained 4,200 mg/kg U and 86 mg/kg Th.

Table 6.2: Atomic concentration of the solid samples of SC429 measured by XPS[a] (%).

Strata	Depth (m)	C	N	O	F	Na	Mg	Al	Si	P	S	K	Ca	Fe	Zn
Mixt. S+S	**3.2**	4.7	2.2	65.1	1.1	0.7	1.0	7.3	13.6	–	–	1.0	2.0	1.4	–
Sludge	**6.8**	10.0	5.0	60.5	0.8	0.4	2.4	5.0	13.0	–	–	0.4	1.3	1.3	–
	8.0	8.3	6.7	57.4	5.4	0.9	1.0	3.2	5.2	0.4	0.6	0.2	7.1	3.2	0.22
	8.1	8.6	4.9	59.0	2.6	0.3	1.0	5.0	12.2	–	0.9	0.6	3.7	1.3	–
Tailings	**8.5**	13.8	4.0	59.0	0.2	0.4	1.1	4.6	12.3	–	1.0	0.5	1.9	1.3	0.02
	8.8	12.4	3.8	59.5	0.3	0.2	1.3	4.9	13.6	–	1.2	0.3	1.4	1.1	–
	11.8	7.2	2.1	64.0	0.3	0.3	1.5	4.4	15.5	–	1.2	0.2	1.5	1.7	–

Mixt. S+S: Mixture of soil and Sludge; [a] the relative error of the measurements is ±(10-20)%

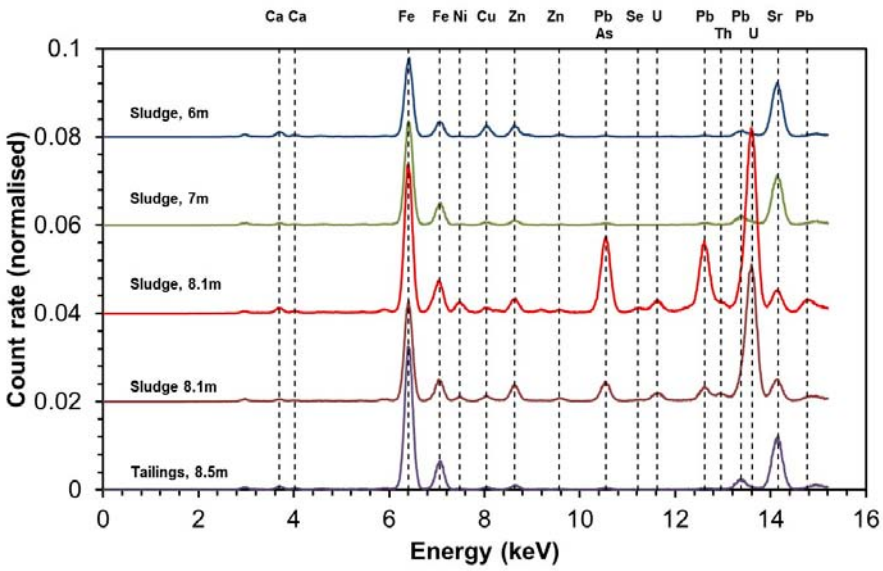

Figure 6.2: XRF elemental composition of bulk samples of sludge and tailings.

The atomic concentrations of Ca and F (Figure 6.3) are higher in the sludge and increase with depth along this stratum, increasing to 7% Ca and 5% F at 8.0m depth. The proportions of these two elements drop between the strata of sludge and the tailings, to 2% Ca and 0.2% F directly beneath the interface at 8.5m depth. The increased proportions of Ca and F are a direct result of the chemical process used for uranium conversion. F-rich effluents are a result of UF_4 production whilst the Ca content arises from the neutralisation of the waste effluent with calcium oxide. Fluorite (CaF_2) is likely to be present in the sludge. Increased relative concentrations of Mg, as observed in the sample of sludge at 6.8m depth, result from the production of U metal before 1991. These two elements provide a good indication of the degree of contamination of the material, as seen from their relation with the concentrations of U and Th (Figure 6.3).

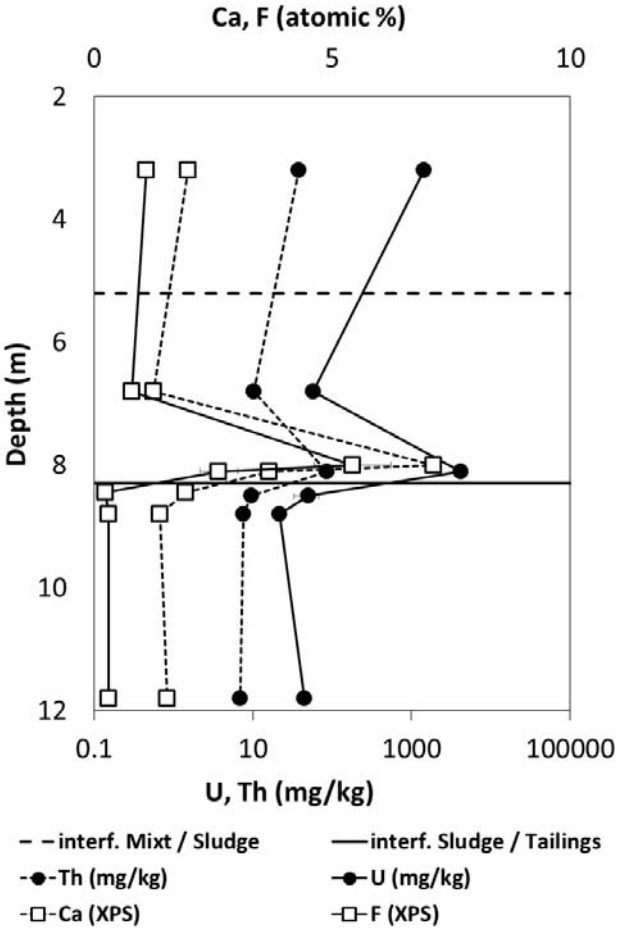

Figure 6.3: Relative atomic concentrations (%) of Ca and F and concentrations (mg/kg) of U and Th along the depth profile of borehole SC429.

Sludge

The interface between the sludge and the tailings, at 8.3m depth, is clearly seen from the difference in composition of the samples of sludge (above 8.3m depth) and tailings (below 8.3m depth). A general tendency of increasing concentrations of Ca, F, N, Na and Mg throughout the depth of the sludge and up to the interface of the sludge with the tailings can be seen (Table 6.2). The increased gradients throughout the sludge are a result of seepage from the upper layers and accumulation at depth. However, this stratum can still be highly heterogeneous, as indicated by the variability in concentrations of F, Ca, Si and Fe between samples 8.0m and 8.1m. This variability is a result of both the chemical process (F and Ca) and the origin of the U ore (Si and Fe). Below the interface, as the stratum of tailings becomes less contaminated, the concentrations of these elements decrease with depth.

Mixture of Soil and Sludge

The sample of mixture of soil and sludge shows some signs of contamination, e.g. with F, although generally less than in the stratum of sludge.

Tailings

The tailings are characterised by higher fractions of carbon, which can be as high as 14% at the top of the stratum and decrease with depth to 7% at 11.8m depth. An increase in the oxidation state of carbon (Table 6.3) indicates anaerobic decomposition of the organic material with depth along the tailings. The carbon content in the former sulphur mine tailings originates both from the original ore (SLREM, 1952) and from periods of inactivity during the sulphur mine operation, when vegetation would grow on top of the tailings, resulting in thin layers of organic matter within the tailings.

Table 6.3: Elemental distribution by oxidation state (in % of total element for oxidation states, in % atomic concentration measured by XPS for element (total)).

Sample	N (-III)	N (+III)	N (+V)	Total N	C (0)	C (+II)	C (+IV)	Total C	S (0)	S (+VI)	Total S
Sludge 8.1m	8.2	17.7	74.1	**4.85**	79.2	13.2	7.6	**8.64**	39.2	60.8	**0.91**
Tailings 8.8m	9.3	28.7	62.1	**3.79**	79.4	12.9	7.7	**12.44**	70.5	29.6	**1.19**
Tailings 11.8m	25.2	74.8	0	**2.09**	62.7	14.2	23.1	**7.18**	36.8	63.2	**1.24**

The sharp decrease in N(+V) concentration with depth (Table 6.3) indicates that NO_3^- reduction is significant in the tailings. Constantin and co-workers (Constantin *et al.*, 1996; Constantin and Fick, 1997) studied the denitrification process in the effluent of the site using microorganisms collected from the sludge of the settling basins. At the time, the basins were still operational, contained sludge covered by liquid effluent and exhibited bacterial activity characterised by gas emissions. In their work, Constantin and co-workers found that, even for the high concentrations of nitrate in the effluent (600mM), two strains of bacteria could carry out total denitrification. *Pseudomonas cepacia* reduced nitrates to nitrites and gaseous nitrogen, while *Staphylococcus hominis* reduced nitrites to gaseous nitrogen. This process may still be occurring in the basins.

The weight percent of S increases slightly with depth along the tailings, from 0.95% at 8.45m to 1.24% at 11.8m. However, no tendency concerning its oxidation state is apparent. It is possible that the sample of tailings at 8.8m depth contained dolomite with sulphur nodules, the original source rock for the former sulphur mine, thereby locally decreasing the oxidised fraction of S.

Uranium, thorium and iron

Uranium concentrations increased with depth and were as high as 4,200 (±20) mg/kg dry sample at 8.1 m depth (Figure 6.3). In the tailings, the concentration of uranium was significantly reduced by two orders of magnitude to 50 (±17) mg/kg (at 8.3 m depth). The two samples collected within the tailings did not confirm the trend of decreasing uranium concentrations observed by Bary and co-workers (2010b) in this stratum. Uncontaminated soils in a remote area, 5 km from the site, were found to contain on average 2.7 mg/kg uranium (Pourcelot *et al.*, 2011), an order of magnitude lower than what is found in the tailings and in line with the average and range of background concentrations in soils of 2 mg/kg (Kabata-Pendias and Pendias, 1985) and between 0.7 and 10.7 mg/kg (Herring, 2004), respectively, suggesting that uranium is migrating downwards and contaminating this stratum.

The concentrations of thorium show a similar tendency of increasing concentrations with depth along the sludge followed by a decrease in concentrations directly beneath the interface of the sludge and the tailings. The mixture of soil and sludge contains elevated concentrations of uranium (1,400 (±20) mg/kg) and thorium (40 (±1) mg/kg), although lower than the concentrations found at the bottom of the stratum of sludge.

The concentrations of iron decrease slightly with depth. The Fe(III)/Fe(II) ratio was not determined since samples were prepared at atmosphere where Fe could be oxidised at the surface during drying.

The concentrations of U, Th and Fe with depth are compared with the four nearest boreholes drilled in 2009 (Bary *et al.*, 2010a), see Figure 6.4. The results are within the same order of magnitude as the values previously obtained. The decrease in U and Th concentrations from the sludge to the tailings and within the tailings with depth is a feature observed at all locations.

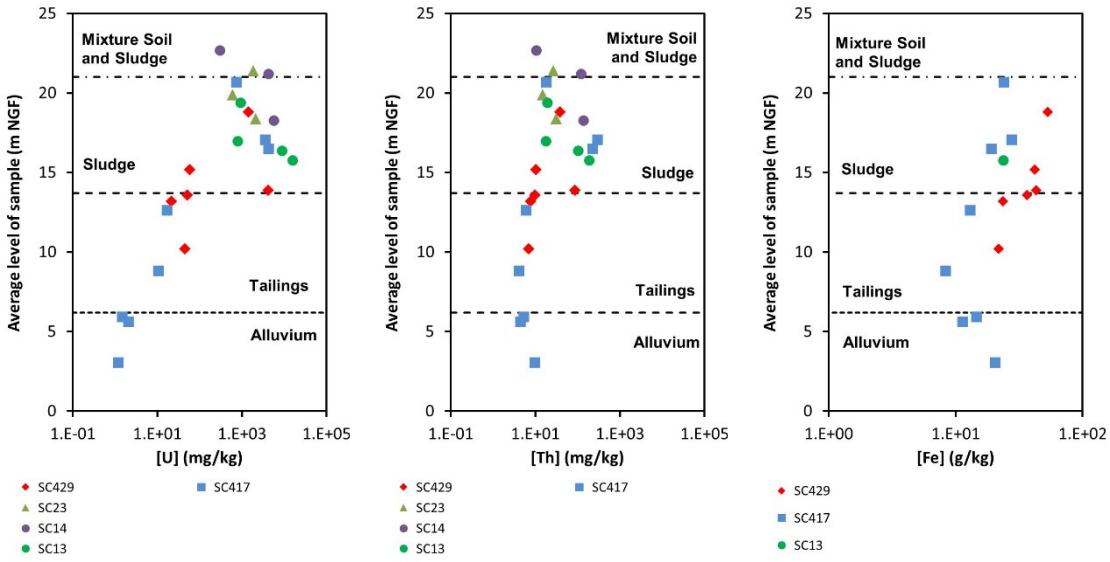

Figure 6.4: Distribution of U, Th and Fe with depth (expressed as level of sample). New results are shown in red (SC429).

6.1.3 Mineralogy

Main crystalline phases such as calcite, quartz and gypsum were present in all samples (Figure 6.5 to Figure 6.8). Common features across the diffractograms of the same strata showed that the mixture of soil and sludge (Figure 6.5) is characterised by quartz, calcite, muscovite and low contents of gypsum, while the old sulphur mine tailings (Figure 6.6) are, as expected, dominated by gypsum, dolomite and muscovite, with variable contents of quartz and calcite. Sample SC417b (tailings) shows smaller relative amount of gypsum and calcite compared with sample SC38. This sample, however, has a higher content of dolomite, as expected for the stratum of tailings.

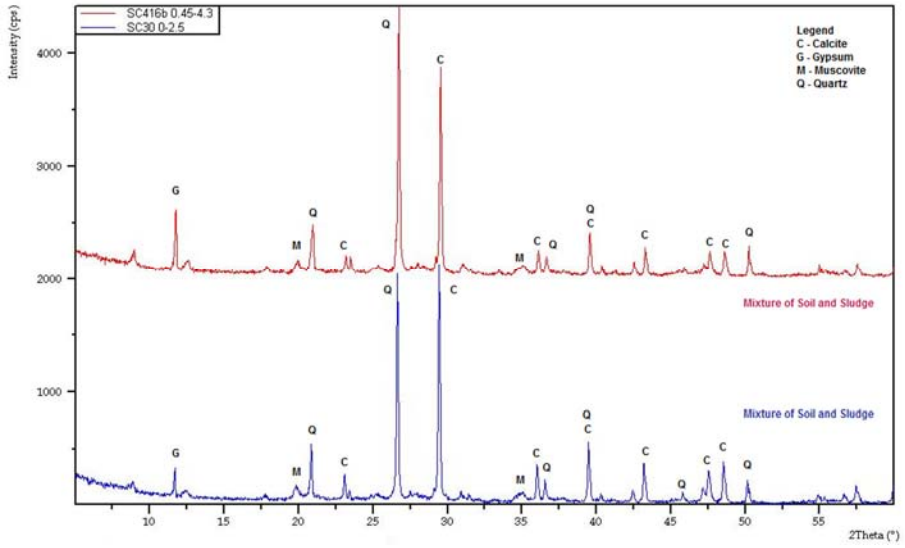

Figure 6.5: X-ray powder diffractograms of the samples of mixture of soil and sludge (samples SC416b at 0.45-4.3m and SC30 at 0-2.5m).

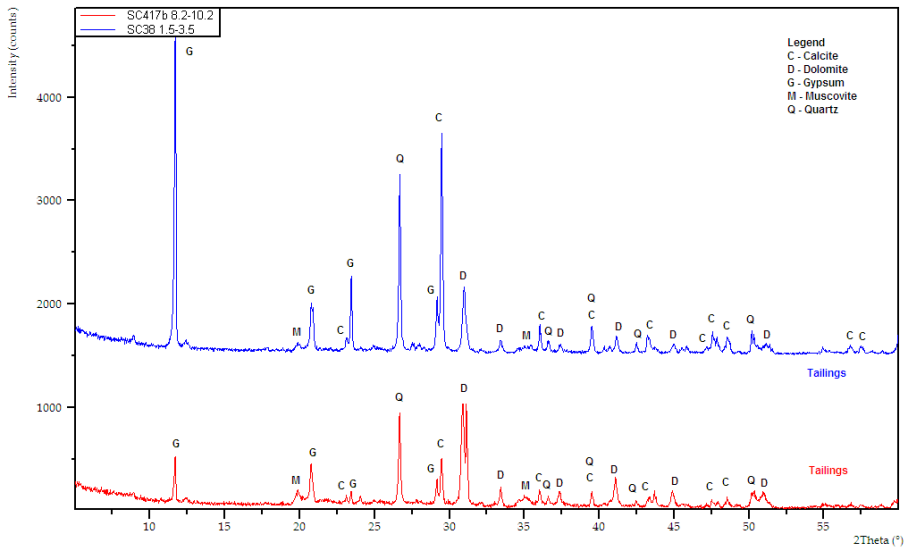

Figure 6.6: X-ray powder diffractograms of the samples of tailings (samples SC417b at 8.2-10.2m and SC38 at 1.5-3.5m).

The samples of sludge (Figure 6.7 and Figure 6.8) are characterised by a wide variability in relative proportions of quartz, calcite, dolomite and gypsum. One sample (SC30) comprised only calcite and gypsum as crystalline phases. Sample SC429 at 8.1m depth contains higher contents of gypsum together with calcite, quartz and dolomite.

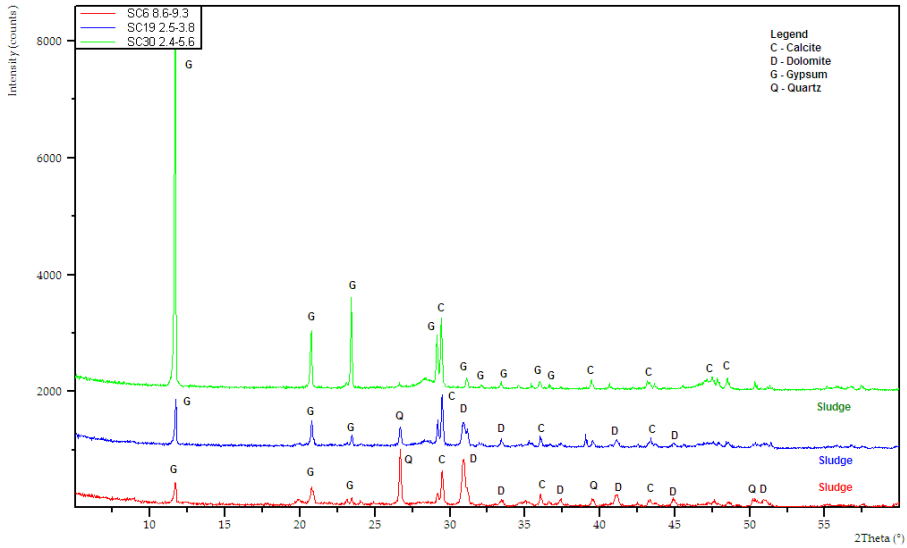

Figure 6.7: X-ray powder diffractograms of the samples of sludge (samples SC6 at 8.6-9.3m, SC19 at 2.5-3.8m and SC30 at 2.4-5.6m).

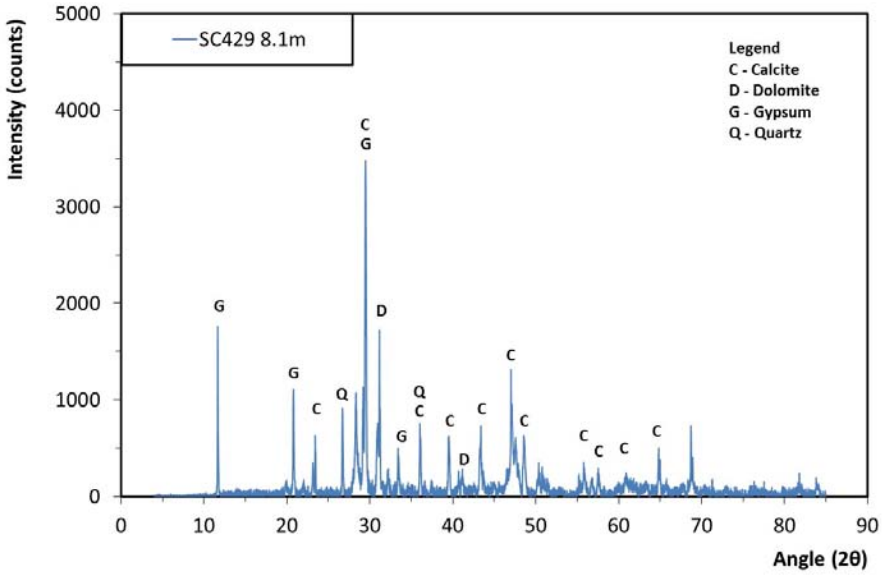

Figure 6.8: X-ray powder diffractograms of the sample of sludge SC429 at 8.1 m depth.

The XRD diffractograms did not indicate the presence of iron minerals. This is due to their low concentration in the samples and the fact that one third of the iron is present in the amorphous phase (see chemical partition results below). The clay-size fraction of the samples could include other clays (smectite, illite, montmorillonite) not detected by XRD due to their low concentrations in the samples, that could play a role in U adsorption. Catalano et al. (2006), for instance, identified uranium sorbed onto phyllosilicates in the vadose zone of process ponds which received U(VI)-Cu(II) waste streams from the dissolution of nuclear fuel at the Hanford site.

6.2 Investigation of the mineral phases capable of retaining Uranium and Thorium

The retention of U and Th was investigated by sequential extraction of mineral phases as described in Section 4.4.

6.2.1 Main elements: Aluminium, Silicon, Iron, Uranium and Thorium containing phases

The sequential extraction results (Figure 6.9) showed that aluminium is contained predominantly in the clays and resistate fractions of the sludge (80%) and in the mixture of soil and sludge (92%) and in its majority (98%) in the resistate fraction of the tailings. Similarly, silicon was mostly contained in the clays and resistate fractions of the sludge (72%) and mixture of soil and sludge (98%), and present only in the resistate fraction (100%) of the tailings.

Fe concentrations varied between samples, but were generally comprised by the amorphous and crystalline Fe minerals and contained in the resistate material (31%, 35% and 32% respectively in the sludge and 38%, 30% and 32% respectively in the tailings). In the sample of mixture of soil and sludge, iron was mainly contained in the fraction of clays (76%), suggesting a high percentage of soil in this sample.

Uranium was predominantly contained within the first two phases, soluble salts (mostly of Al) and amorphous minerals (mostly of Fe). Around 90% of the uranium in the sludge and mixture of soil and sludge and 70% of the uranium in the tailings was contained in these fractions.

The majority of the uranium contained in the sample of mixture of soil and sludge was present as secondary uranium minerals (25%) and adsorbed or associated with the carbonate minerals (69%).

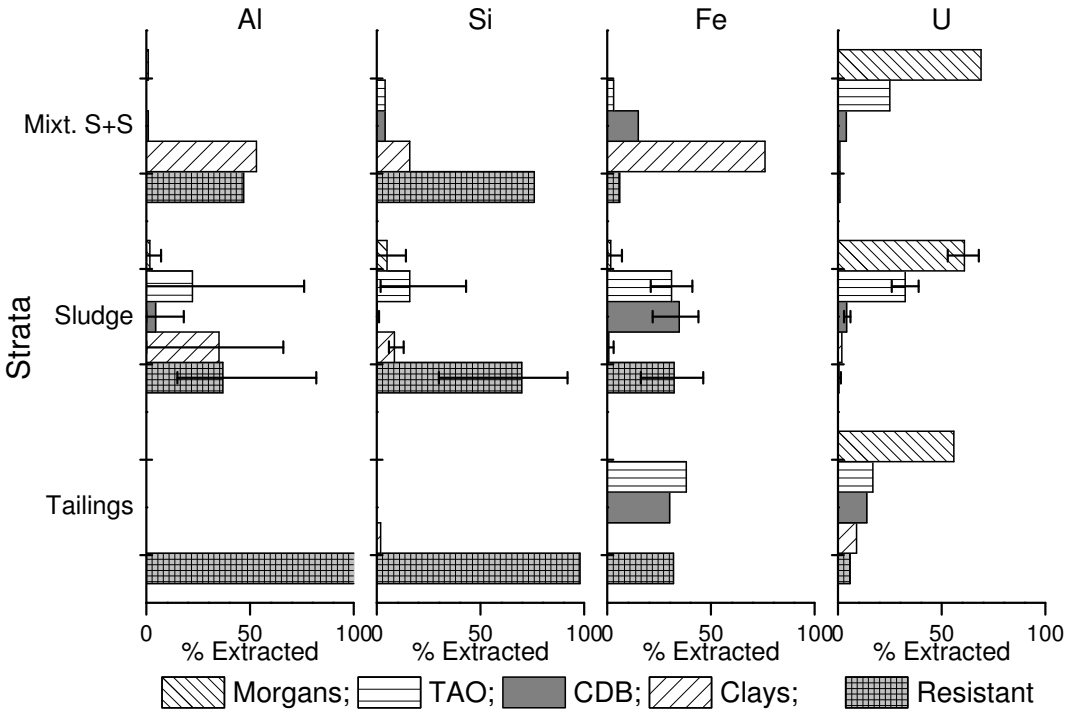

Figure 6.9: Percentage of Al, Si, Fe and U desorbed by sequential extraction of the samples of mixture of soil and sludge, sludge and tailings. The five fractions studied are: 1) Morgans - soluble salts and exchangeable ions; 2) TAO - amorphous oxide minerals; 3) CDB - crystalline iron minerals; 4) Clays - amorphous Al and Si compounds; and 5) resistant material, such as quartz and muscovite.

The thorium contained in the sample of tailings was too low to investigate its distribution among the various fractions (below the detection limit of 3.2 mg/kg). In the samples of sludge, the majority of the Th was associated with the crystalline Fe oxides, hydroxides and oxyhydroxides. This phase comprised 60-70% of the Th in the mixture of soil and sludge and in the sludge. The second fraction containing most Th were the amorphous minerals of Fe, Al and Si (TAO fraction), which contained 10-20% of thorium. Total thorium extracted in each fraction are presented in Table 6.4 and Table A3.1.

6.2.2 Distribution of uranium and thorium per strata

The samples of sludge containing a higher fraction of amorphous minerals of Al, Si and Fe also contained higher concentrations of U (samples SC19 and SC30 with U concentrations of 3,000 and 4,300 mg/kg respectively) (Table A2.1 and Table A2.2). Circa 30-40% of the total U in these samples was present as secondary U minerals and / or associated with the amorphous minerals of Al, Si and Fe. The samples with lowest total uranium concentration, i.e. SC6 (sludge), SC416b (mixture of soil and sludge) and SC417b (tailings) had a very small percentage (<5%) of Si and Al as amorphous minerals, indicating that the 20-30% uranium extracted with this phase was either

adsorbed to amorphous minerals of Fe or present as secondary U minerals. In all the samples of sludge, the remaining ~60% uranium was present as adsorbed phases or associated with carbonate minerals. Only 5 to 8% of U was extracted with the crystalline, clays or resistant material.

In the stratum of tailings, the concentration of U was at least one order of magnitude lower than in the samples from the other strata (13 mg/kg). Of the total content, about 30% (4 mg/kg) was associated with the crystalline, clays and resistant fractions, considered to represent background uranium concentration. The remaining uranium, found associated with the carbonate and amorphous Fe minerals, is likely a result of the downward migration from the contaminated layer of sludge.

Table 6.4: Percentage of Al, Si, Fe and U extracted with the TAO phase (amorphous minerals of Al, Si, Fe and secondary U minerals) and total U concentration present in each sample used for sequential extraction.

Sample; depth (m)	Strata	Al (%)	Si (%)	Fe (%)	U (%)	Th (%)	U total (mg/kg)	Th total (mg/kg)
SC416b; 0.45-4.3	Mixt.SS	4	0	3	25	22	820±20	22.8±13.5
SC6-1; 8.6-9.3	Sludge	3	0	21	26	16	640±20	24.3±14.1
SC6-2; 8.6-9.3	Sludge	2	0	29	29	17	610±20	23.7±13.6
SC19; 2.5-3.9	Sludge	16	13	41	39	19	3,000±80	96.2±50.2
SC30; 2.4-5.6	Sludge	43	76	33	36	11	4,300±120	87.3±44.4
SC417b; 8.2-10.2	Tailings	0	0	38	17	-	13±0.4	<3.2

Mixt. SS: Mixture of Soil and Sludge

6.3 Solid state speciation of Uranium and Thorium

6.3.1 Distribution of Uranium and Thorium in the solid state

Identification of areas of enhanced activity

When measured by autoradiography, the samples of sludge at 6.8 m and 8.1 m depth presented areas of enhanced activity (Figure 6.10 and Figure 6.11). Sub-samples collected from the areas circled in red in Figure 6.10 and Figure 6.11 were further analysed by SEM-EDS and Raman spectroscopy, and the results are presented and discussed below. Sub-samples of the areas of enhanced activity circled in Figure 6.11 were collected from the duplicate samples of sludge at 8.1 m depth and measured by XRD. The results did not indicate the presence of U or Th. Section 6.1.3 above presents the mineralogy of this sample. The sample of tailings, despite having been in contact

with the storage film for 3 weeks, did not exhibit areas of enhanced activity. The sample of mixture of soil and sludge was not autoradiographed.

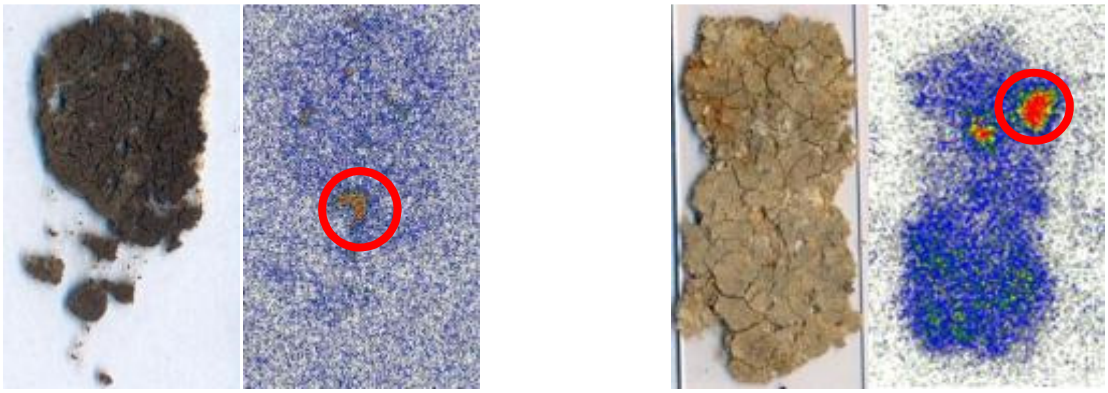

Figure 6.10: Photograph (left) and autoradiographic image (right) of the samples of sludge at 6.8m depth (left) and 8.1m depth (right) – highlighted areas analysed by SEM-EDS and Raman spectroscopy.

Alcohol suspensions of wet samples of sludge at 8.15m depth were analysed by SEM-EDS with the objective of obtaining EDS spectra of U and Th free from the interference of matrix elements. This sample also exhibited fluorescent particles when investigated with the desk table UV lamp, which were analysed by SEM-EDS.

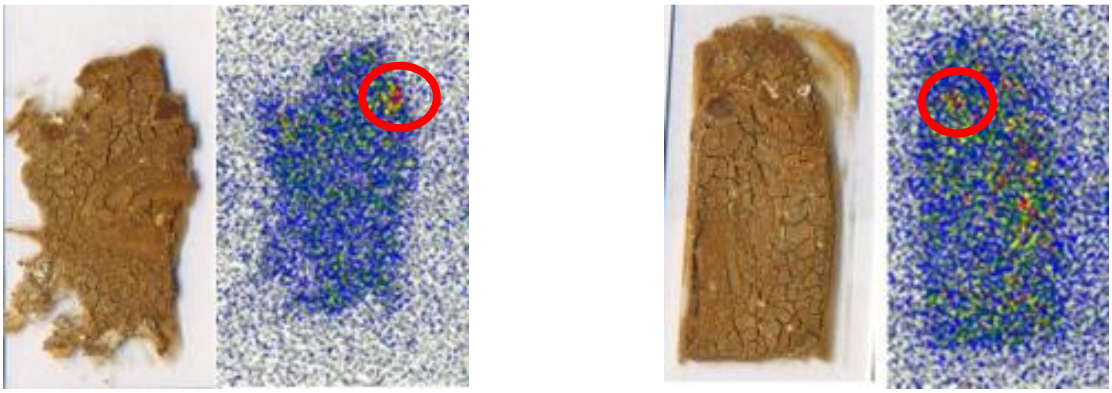

Figure 6.11: Photograph (left) and autoradiographic image (right) of duplicate samples of sludge at 8.1m depth - highlighted areas analysed by XRD.

Scanning Electron Microscopy – Electron Dispersive X-ray Spectroscopy Results

The electron microscopy analysis of the sludge identified uranium under various forms (Figure 6.12). In the sample of sludge at 6.8m depth, uranium was observed as a phase deposited on major minerals, such as gypsum and calcite, and as isolated uranium phases with dimensions of 10-20 µm length. The composition of these particles, obtained by EDS was predominantly U, Si, C and O, with minor amounts of Na, Mg, Ca and Al.

Fe was not present at detectable levels in the samples. However, in the adsorbed phases, minor amounts of iron were identified (less than 0.15 atom %). Uranium coprecipitated with calcite has been found in waste disposal ponds neutralized with NaOH (Catalano *et al.*, 2006). The analysis identified the major phases of gypsum and calcite, as well as barite ($BaSO_4$).

In the sample of sludge at 8.1m depth, uranium was observed as groups of finely dispersed particles of submicrometer dimensions (Figure 6.12). The EDS spectra for these particles showed their main composition to comprise Na, Mg, K and Ca, as well as Si, Al, C and O and up to 0.2 atom % Fe. This suggests the presence of both aluminosilicate clays and iron oxides combined in the coatings where uranium is adsorbed or precipitated. Other elements were identified in several particles, such as (in atom %): F (0 to 19%), P (0 to 3.4%), S (0 to 4.2%) and N (0 to 8%). Thorium phases were not identified in the samples analysed.

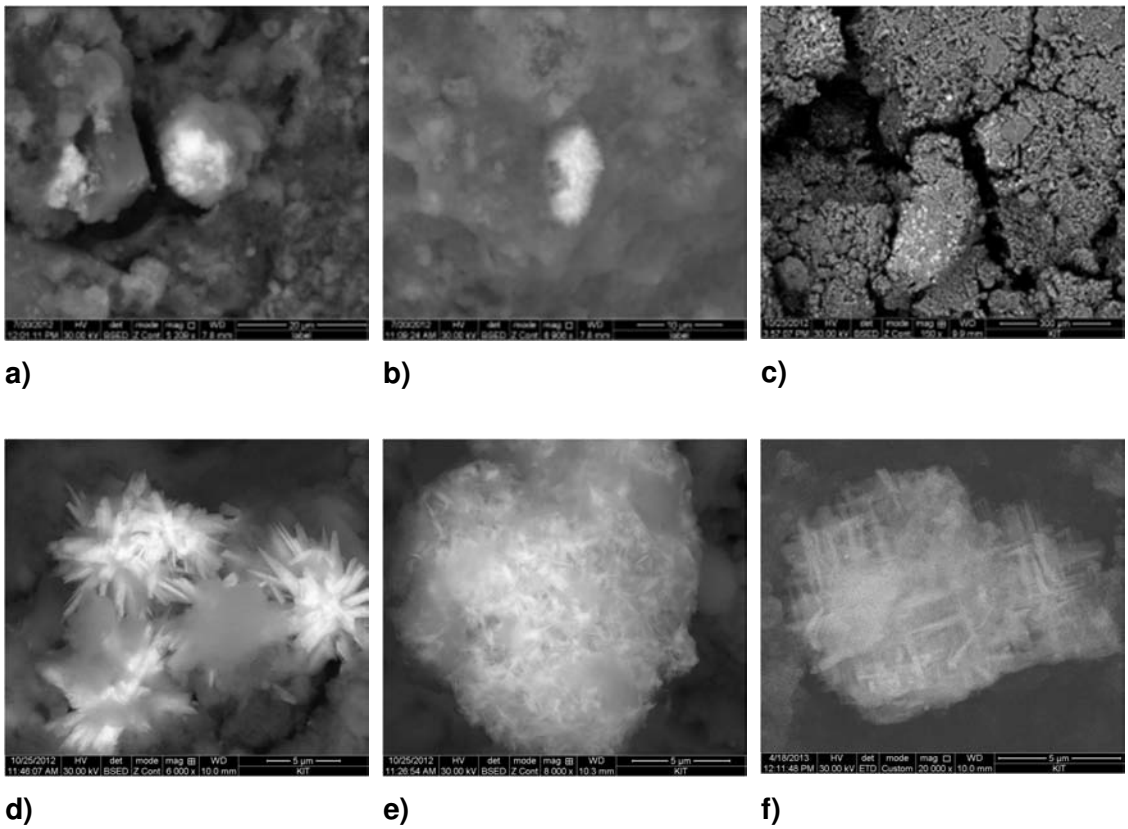

Figure 6.12: Scanning electron micrographs in backscattered mode of sludge at 6.8m depth (a and b) and at 8.1m depth (c, d, e and f). Image a) uranium deposited on gypsum (on the left) and on calcite (on the right). Image b) isolated phase at 6.8m depth. Image c) dispersed U particles. Images d), e) and f) U aggregates found at 8.1m depth. The greyish areas indicate accessory minerals from the sediment matrix.

Brown and co-workers (2010) also identified uranium simultaneously present in different chemical forms in uranium-contaminated sediments collected near a nuclear waste storage and processing facilities at Hanford, Washington. These authors encountered particles with uranium enriched areas that appeared to have formed as coatings on existing sediment particles. Similarly to the Malvési samples, the particles investigated by Brown et al. (2010) contained Si, Al, Ca and lower amounts of Fe, P and Cu. They found that the second most common occurrence of U was as smaller U-enriched grains (of 5 µm) occurring as discrete particles in the sediment.

Raman Spectroscopy Results

Particles of uranium identified by electron microscopy which were sufficiently large (> 10 µm) were analysed by Raman spectroscopy. One particle identified by microscopy from the sample of sludge at a depth of 6.8m (Figure 6.12b) and various other particles from the sample of sludge at 8.1m depth were measured. Both at 6.8m and 8.1m, the particles had the characteristic peaks at wavenumbers of 789 cm^{-1} and 959 cm^{-1}, corresponding to the spectral regions assigned to UO_2^{2+} at 750-800 cm^{-1}, and to the vibrations of the SiO_4^{4-} tetrahedra at 950-1000 cm^{-1} (Frost *et al.*, 2006). The spectrum (Figure 6.13) is similar to the reference spectra of various uranyl-silicate phases, such as uranophane $[Ca(UO_2)_2(SiO_3OH)_2{\cdot}5H_2O]$ and natroboltwoodite $[(H_3O)(Na,K)(UO_2)SiO_4{\cdot}H_2O]$. The spectra could also be fit by an uranium oxide mineral, such as calciouranoite $(Ca,Ba,Pb)U_2O_7{\cdot}5H_2O$, which can contain significant amounts of SiO_2 (Zhao and Ewing, 2000). In several particles, an additional peak was observed at 1054 cm^{-1}, corresponding to the sulphate region. However, we could not fit the three peaks (uranyl, Si tetrahedral and sulphate) to any of the reference spectra. It is likely that the sulphur peak originated from the sediment matrix. Uranium mobility has been found to be limited by precipitation of U-silicate phases in uranium-contaminated sites (Liu *et al.*, 2004; Um *et al.*, 2010).

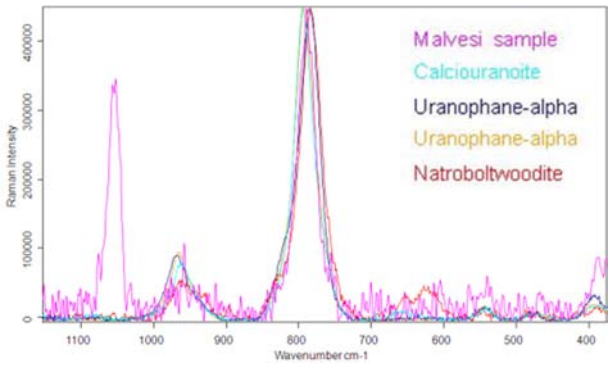

Figure 6.13: Raman spectroscopy image of the sludge at 6.8m depth (in pink) and reference spectra for selected U phases.

6.4 Results of beamline measurements

According to the XAFS measurements results, uranium was present as the uranyl(VI) compound. Good spectral fingerprints were obtained for uranium (Figure 6.14) in the samples of sludge at 6.9 m and 8.15 m depth and for thorium (Figure 6.15) in the sample at 8.15m depth. Figure 6.14 shows the spectral fingerprint of three natural uranium minerals measured as references for comparison, soddyite [$(UO_2)_2(SiO_4).2(H_2O)$], boltwoodite [$(K,Na)(UO_2)(HSiO_4).0.5(H_2O)$] and Cu-sklodowskite [$Cu(UO_2)(HSiO_4)_2.6(H_2O)$], all uranium-silicate minerals. The spectral fingerprint points to a similar uranium speciation in the samples.

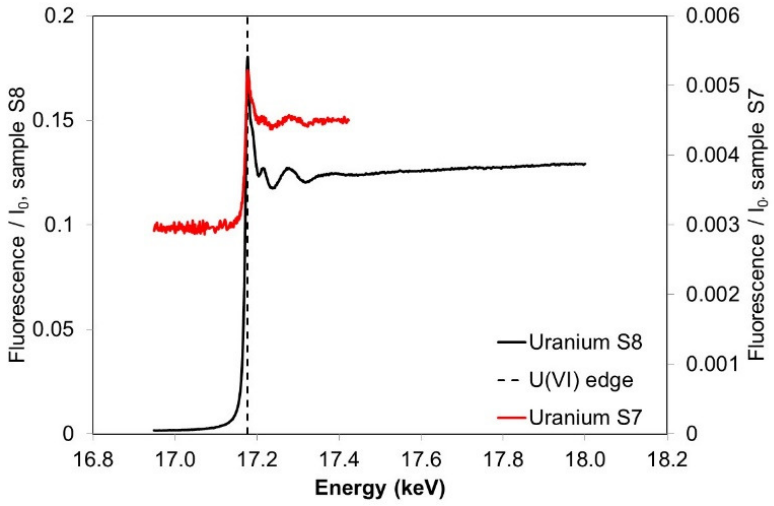

Figure 6.14: Normalised U L3-XANES spectra of the bulk sample of sludge at 8.15m depth (in black) and at 7 m depth (in red).

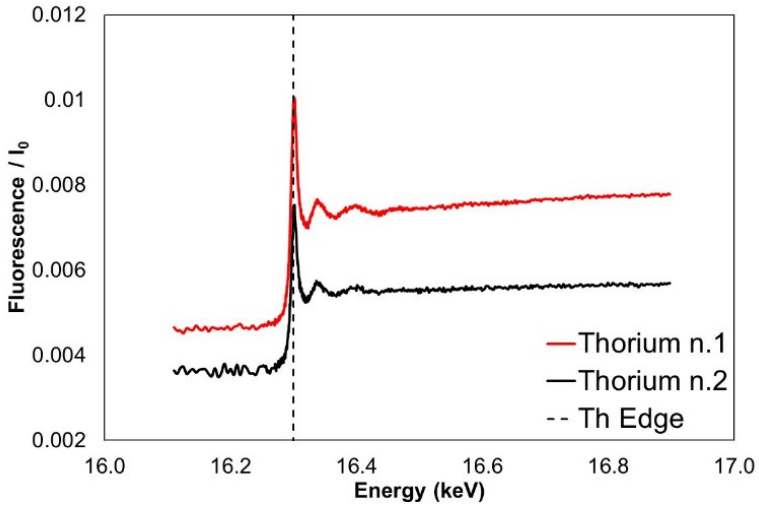

Figure 6.15: Normalised Th L3-XANES spectra (2 measurements) of the bulk sample of tailings at 8.5m depth.

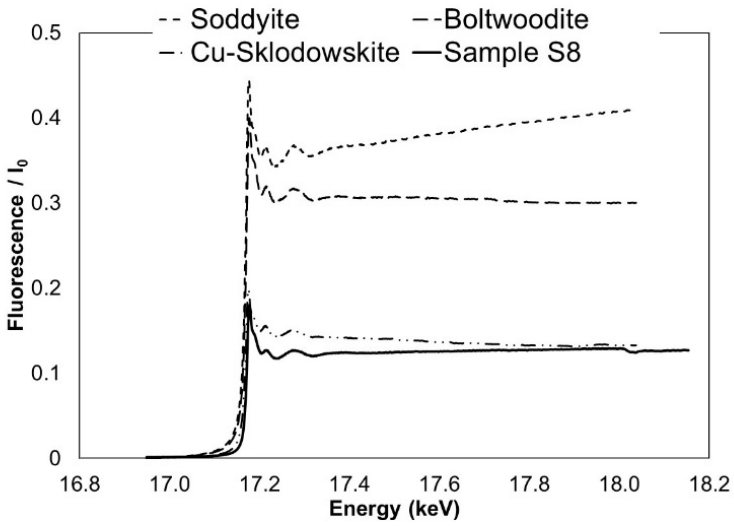

Figure 6.16: Normalised U L3-XANES spectra of the bulk sample of sludge at 8.15m depth and three uranyl-silicate mineral references.

Micro-XAS were carried out in the thin film samples to investigate whether the speciation of U and Th was the same in different areas of the samples and whether they were the same as in the bulk samples. The two thin film samples selected (spots b and aa, both from the sample of sludge at 8.15m depth) had been previously identified by SEM-EDS as shown in Figure 6.19. Comparison of these spectra with the references again points to a uranyl-silicate speciation (Figure 6.17 and Figure 6.18). The thorium µ-XRF map was obtained for spot b (Figure 6.22). However, a good spectral fingerprint could not be obtained by µ-XAS, even when the micro-beam was focused at areas of higher concentration.

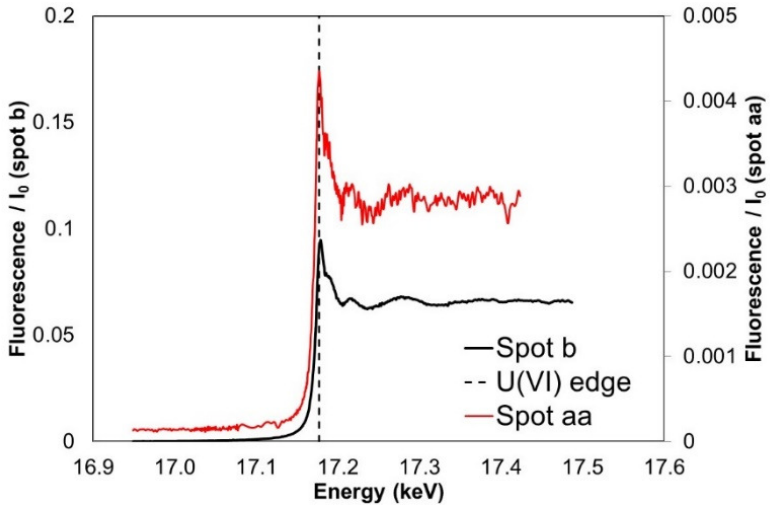

Figure 6.17: Normalised U L3-µ-XAS spectra of the thin sample of sludge at 8.15m depth: spot b, point U1_1 with high concentration of U (black) and spot aa (red).

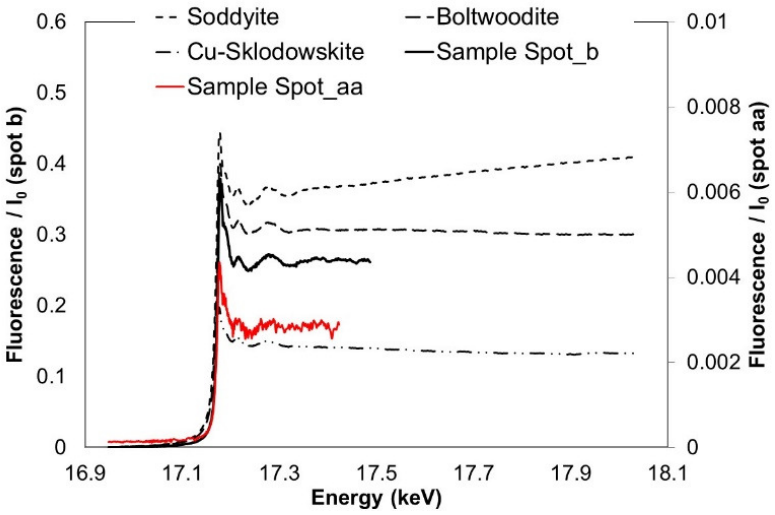

Figure 6.18: Normalised U L3-µ-XAS spectra of the thin sample of sludge at 8.15m depth (spots aa and b) and three uranyl-silicate mineral references.

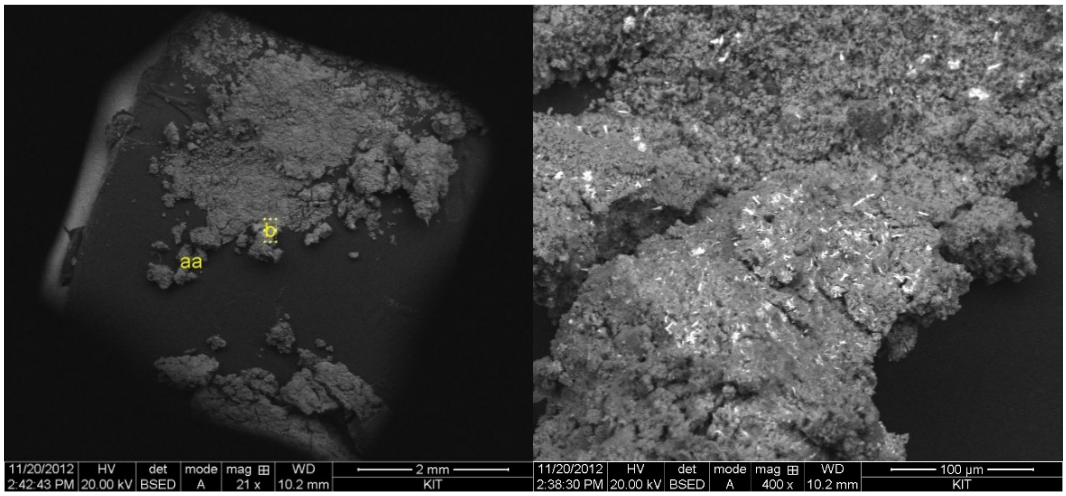

Figure 6.19: SEM image of sample of sludge at 8.15m depth with spots aa and b (left) and zoom in on spot b (right) – bright spots indicate increased concentrations of uranium.

6.4.1 Measurement of thin film samples, µ-XRF mapping

Three regions with areas ranging from 3000µm^2 to 4200µm^2 of the sample of sludge at 8.1m were investigated by µ-XRF. Figure 6.20 shows the elemental maps in spot aa. The figure illustrates Fe, K, Ni and Zn to be well correlated together and in some extend with Ca. On the contrary, Cu shows an anticorrelation with Fe. U is distributed as discrete small hot spots located mainly at the border between Fe and Cu. This may indicate a prominent role of Fe in the adsorption of U. In this spot, the elemental map for Th shows

this element to be homogeneously distributed in the sample. There is no correlation in its distribution with any other element.

On the map of spot a (Figure 6.21), a different region of the same sample, the uranium distribution is more diffuse but it is still at the border of Fe. However there are two areas of highest U concentration, two U hot spots (red dots on the U map) whose distribution correlates only with K (spot around coordinate 40µm horizontal, 9µm vertical). Again, no correlation between U and Th is observed.

Figure 6.22 shows the elemental maps for spot b, where a particle of U was observed. Here also, higher concentrations of Ca and Fe are present next to the U particle. Fe, Ca, K, Ni and Zn are also well correlated together. On the contrary, Cu and Mn are in anticorrelation with these elements. The Th distribution can be clearly seen to correlate with U, potentially showing a mixed U-Th oxide.

The preferential precipitation of U in the vicinity of Fe indicates a prominent role of Fe in the adsorption of U. Um et al (2007) demonstrated that Fe(III) oxyhydroxide coatings on soils and sediments are one of the most important factors in controlling the adsorption and transport of U(VI) in the subsurface. It is unclear whether the iron oxides are present as coatings on other geomedia or as discrete minerals.

It has been shown that uranium may be immobilised by first sorbing onto mineral grains and then precipitating as coatings or intergrowths with non-U-bearing phases, or as discrete U particles (Brown *et al.*, 2010). The µ-XRF results suggest a variety of chemical forms of uranium. It should be noted, however, that this technique cannot confirm the presence or absence of U-silicates or adsorption to clays, as Si and Al are too light to be detected at the beamline operated in air for µ-XRF and µ-XAS. The beamline could detect elements heavier than (and including) Ar.

XANES spectra at different positions in the sample (not presented) showed U to be always present as a uranyl(VI) compound.

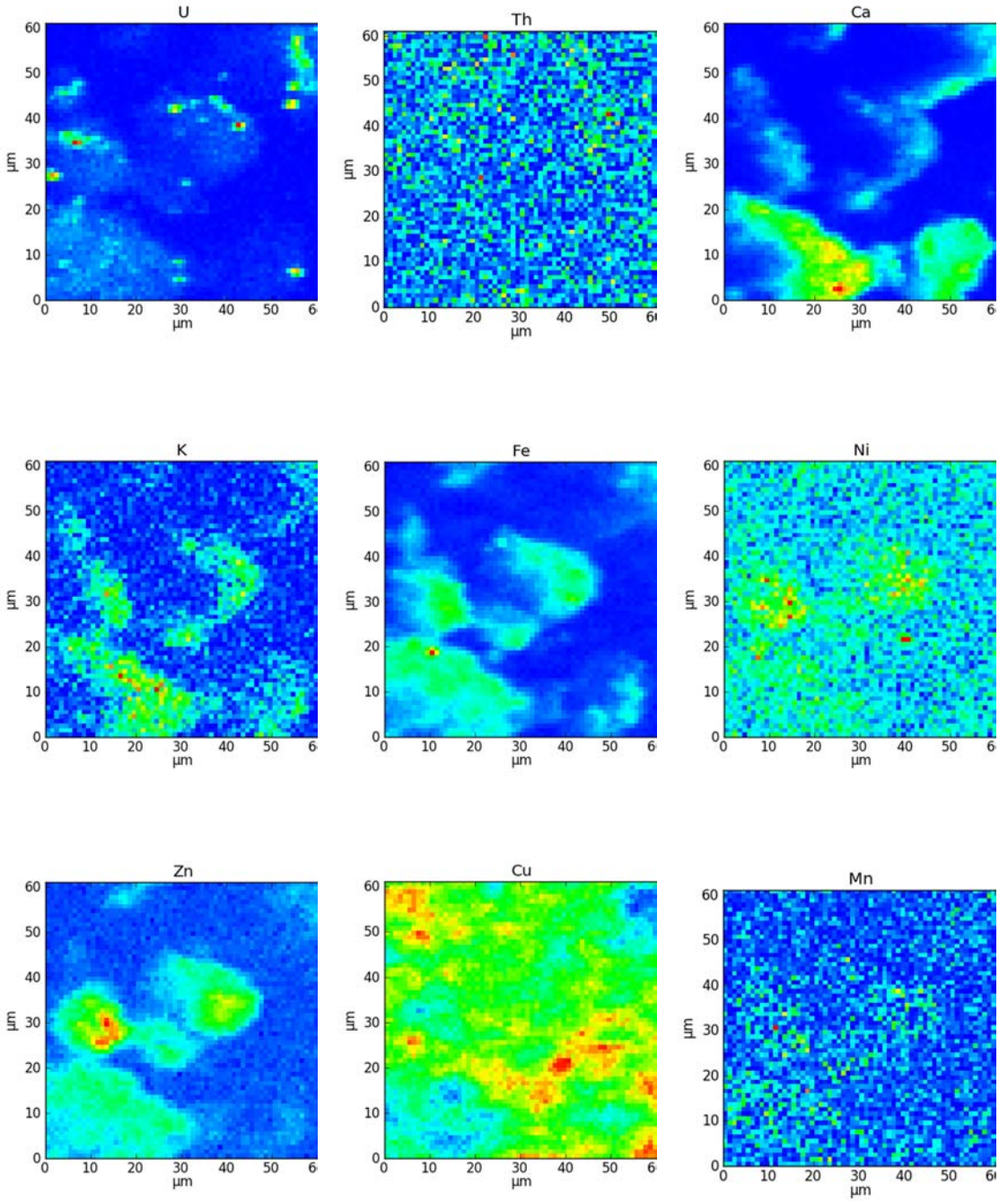

Figure 6.20: Fluorescence maps for nine selected elements in spots aa, sample of sludge at 8.1m depth. The maps are obtained by peak fitting (PyMca program package) of full MCA spectra recorded at each pixel. The colour intensity indicates the qualitative concentration of the element, where blue indicates the lowest relative concentration (background) and red the highest relative concentration. The full scale for each element is: U: 0-776 cts/p, Th: 0-123 cts/p, Ca: 0-2050 cts/p, K: 0-45 cts/p, Fe: 37-3393 cts/p, Ni: 0-53 cts/p, Zn: 122-1155 cts/p, Cu: 2245-3932 cts/p, Mn: 0-152 cts/p.

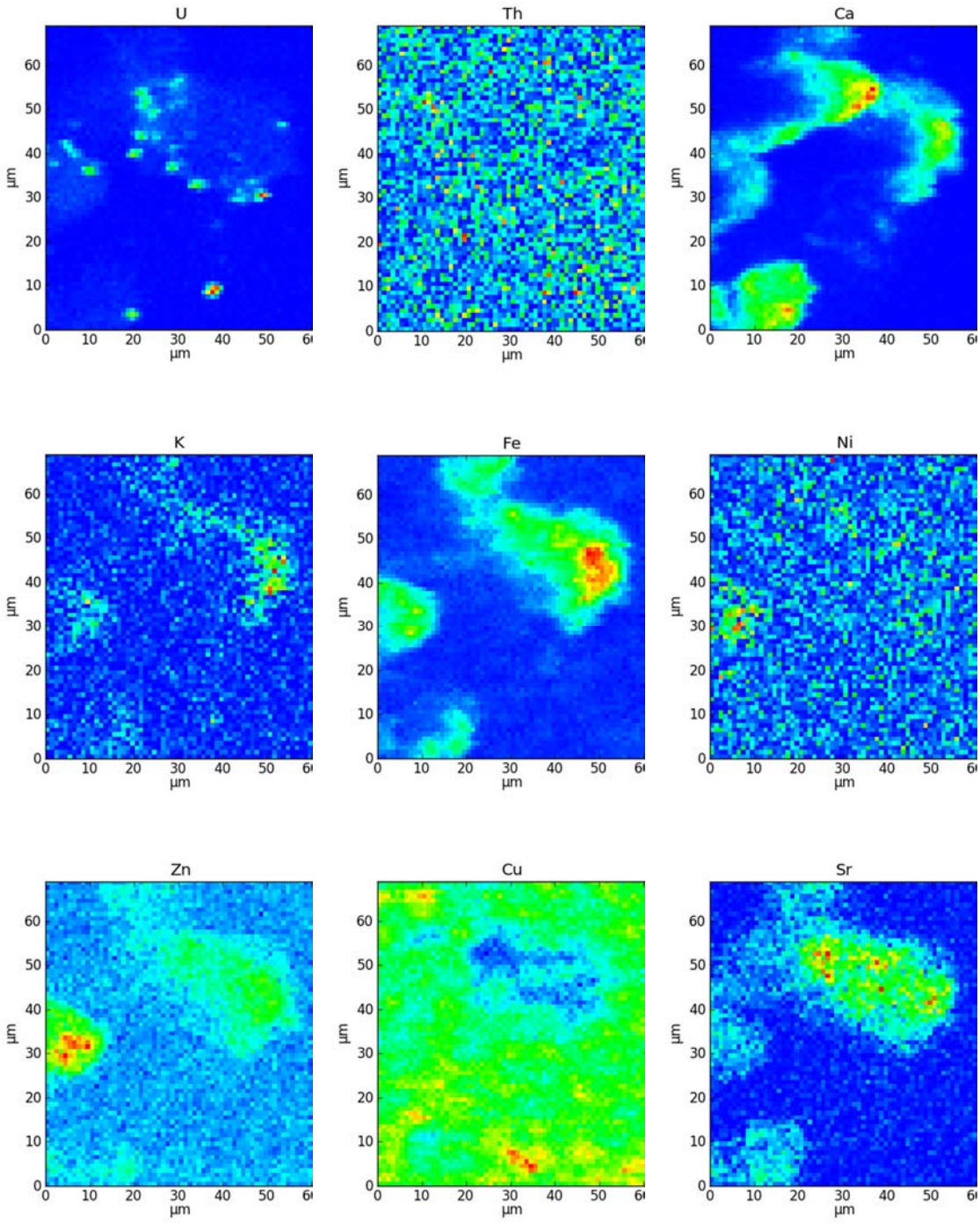

Figure 6.21: Fluorescence maps for nine selected elements in spot a, sample of sludge at 8.1m depth. The maps are obtained by peak fitting (PyMca program package) of full MCA spectra recorded at each pixel. The colour intensity indicates the qualitative concentration of the element, where blue indicates the lowest relative concentration (background) and red the highest relative concentration. The full scale for each element is: U: 0-423 cts/p, Th: 0-49 cts/p, Ca: 0-790 cts/p, K: 0-22 cts/p, Fe: 4-1113 cts/p, Ni: 0-14 cts/p, Zn: 28-359 cts/p, Cu: 892-1933 cts/p.

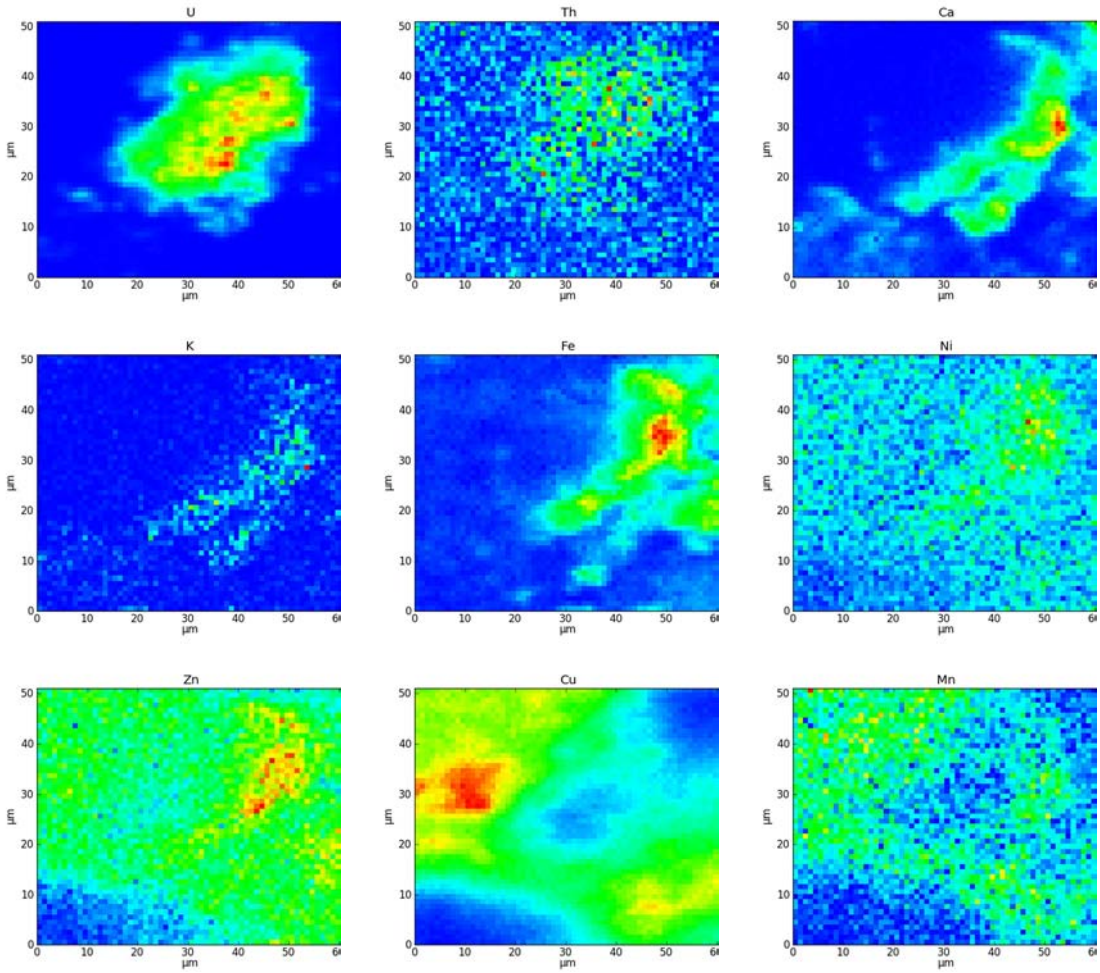

Figure 6.22: Fluorescence maps for nine selected elements in spot b, sample of sludge at 8.1m depth. The maps are obtained by peak fitting (PyMca program package) of full MCA spectra recorded at each pixel. The colour intensity indicates the qualitative concentration of the element, where blue indicates the lowest relative concentration (background) and red the highest relative concentration. The full scale for each element is: U: 0-7298 cts/p, Th: 0-111 cts/p, Ca: 0-1133 cts/p, K: 0-289 cts/p, Fe: 8-1329 cts/p, Ni: 0-54 cts/p, Zn: 17-209 cts/p, Cu: 201-3047 cts/p, Mn: 0-81 cts/p.

6.5 Composition and geochemistry of water samples

6.5.1 Overview

Groundwater samples were collected from the existing monitoring wells located in the B1/B2 basins as described in Section 5.3. The samples were filtered through a 0.22 µm nitrocellulose membrane Millipore filter prior to analysis as detailed in Section 4.2.4.

Samples of pore water were extracted from the core samples of soil collected from location SC429. The samples were collected at depths of 3.2 m (mixture of soil and sludge), 6.8 m (sludge) and 8.8 m (tailings). The methodology for extraction and analysis of the samples is described in Section 4.2.3. Due to the method of extraction used, which

comprises centrifuging the soil samples to obtain a liquid sample is carried out in air, the redox behaviour of the samples (including redox measurement and analysis of redox pairs Fe(II)/Fe(III) and NO_2^-/NO_3^-) was not carried out.

6.5.2 pH and Eh

The pH of the groundwater samples was neutral, ranging from pH ≈ 6.0 in the samples of tailings and mixture of soil and sludge and up to pH = 8.1 in the sample of sludge (Table 6.5). Redox conditions were oxic (in the Alluvium) to oxidising in all the other strata of waste, indicating that uranium will likely be present in the U(VI) form. The 2009 analysis (Bary *et al.*, 2010a) indicated similar values of pH, although lower redox values were measured.

Table 6.5: pH and Eh values of groundwater samples.

BH ID	Strata	pH	pH (2009*)	Eh (mV)	Eh (mV) (2009*)
SC417a	Sludge	8.1 ± 0.1	8.4	357 ± 20	273
SC417b	Tailings	5.7 ± 0.1	6.02	399 ± 20	310
SC417c	Alluvium	6.7 ± 0.1	6.3	225 ± 20	53
SC416a	Mixture of Soil and Sludge	5.8 ± 0.1	6.0	433 ± 20	360
SC416b	Tailings	5.6 ± 0.1	6.0	441 ± 20	-50
SC416c	Alluvium	6.8 ± 0.1	6.7	184 ± 20	117
SC429	Mixture of Soil and Sludge	6.9 ± 0.1	-	-	-
SC429	Sludge	7.2 ± 0.1	-	-	-
SC429	Tailings	6.3 ± 0.1	-	-	-

Iron(III) concentrations were within typical range for oxidising environmental conditions, of between ≈ 10^{-6} mol/l in the samples of sludge and alluvium and ≈ 10^{-7} mol/l in the samples of tailings and mixture of soil and sludge (Table 6.5). Iron(II) was generally below the detection limit of $7.1 \cdot 10^{-8}$ mol/l except in the samples of alluvium.

Table 6.6: Fe^{2+}, Fe^{3+} and total Fe measured in the samples of groundwater.

BH ID	Strata	Fe total (mol/l)	Fe^{2+} (mol/l)	Fe^{3+} (mol/l)
SC417a	Sludge	$1.2(\pm0.1) \cdot 10^{-6}$	$< 7.1 \cdot 10^{-8}$	$1.2(\pm0.1) \cdot 10^{-6}$
SC417b	Tailings	$2.3(\pm1.4) \cdot 10^{-7}$	$< 7.1 \cdot 10^{-8}$	$2.3(\pm1.4) \cdot 10^{-7}$
SC417c	Alluvium	$3.9(\pm0.3) \cdot 10^{-6}$	$3.5(\pm0.3) \cdot 10^{-6}$	$4.0(\pm3.9) \cdot 10^{-7}$
SC416a	Mixture of Soil and Sludge	$5.4(\pm2.7) \cdot 10^{-7}$	-	$5.4(\pm2.7) \cdot 10^{-7}$
SC416b	Tailings	$< 7.1 \cdot 10^{-8}$	$< 7.1 \cdot 10^{-8}$	$< 7.1 \cdot 10^{-8}$
SC416c	Alluvium	$2.9(\pm0.1) \cdot 10^{-6}$	$2.2(\pm0.1) \cdot 10^{-6}$	$7.5(\pm1.9) \cdot 10^{-7}$

Nitrate concentrations in the groundwater of the waste (≈ 10^{-1} mol/l) result from the disposal of effluents rich in nitrates, including ammonium nitrates, nitric acid and ammonium fluoride (Perez, 1980) to the B1/B2 basins over the operation of the plant. The low concentrations of nitrate measured in the two samples of alluvium, $1.83(\pm0.04)\cdot10^{-4}$ mol/l in SC416c and $2.26(\pm0.06)\cdot10^{-4}$ mol/l in SC417c, suggest that migration of nitrate to this stratum is limited (Table 6.7). Nitrate reduction into nitrite and ammonium, and eventually gaseous nitrogen by bacterial activity, was seen occur in the waste strata, as discussed in Section 6.1.2. Concentrations of nitrite varied from a minimum of ≈ 10^{-6} mol/l in the alluvium to a maximum of 10^{-3} mol/l in the sludge. Sulphate concentrations were in the order of 10^{-3} mol/l and did not vary much between the different strata (Table 6.7).

Table 6.7: NO_3^-, NO_2^- and SO_4^{2-} measured in the samples of groundwater.

BH ID	Strata	NO_3^- (mol/l)	NO_2^- (mol/l)	SO_4^{2-} (mol/l)
SC417a	Sludge	$4.05(\pm0.02)\cdot10^{-1}$	$6.87(\pm0.01)\cdot10^{-3}$	$2.08(\pm0.01)\cdot10^{-3}$
SC417b	Tailings	$4.39(\pm0.08)\cdot10^{-1}$	$1.78(\pm0.06)\cdot10^{-5}$	$2.39(\pm0.10)\cdot10^{-3}$
SC417c	Alluvium	$2.26(\pm0.06)\cdot10^{-4}$	$2.25(\pm0.03)\cdot10^{-5}$	$6.18(\pm0.01)\cdot10^{-3}$
SC416a	Mixture of Soil and Sludge	$1.85(\pm0.05)\cdot10^{-1}$	$1.33(\pm0.01)\cdot10^{-4}$	$2.75(\pm0.10)\cdot10^{-3}$
SC416b	Tailings	$4.24(\pm0.26)\cdot10^{-1}$	$1.23(\pm0.04)\cdot10^{-5}$	$2.35(\pm0.42)\cdot10^{-3}$
SC416c	Alluvium	$1.83(\pm0.04)\cdot10^{-4}$	$3.97(\pm0.30)\cdot10^{-6}$	$7.54(\pm0.03)\cdot10^{-3}$

The redox potential distribution of three redox pairs (Fe(II)/Fe(III), NO_2^-/NO_3^- and HS^-/SO_4^{2-}) was calculated using Phreeqc. A comparison of the theoretical redox potential obtained for each pair with the redox potential of the samples is shown in Figure 6.23. The Eh of the samples of alluvium is very similar to the Eh of the iron pair (Eh_{meas} = -0.02 mV, $Eh_{calFe2+/Fe3+}$ = 0.09 mV in SC416 and Eh_{meas} = 0.02 mV, $Eh_{calFe2+/Fe3+}$ = 0.08 mV in SC417). The redox conditions of the alluvium are likely dominated by the Fe pair, as expected for a stratum of natural soil.

The Eh measured in the samples of mixture of soil and sludge and tailings is lower than the redox potential given by the Fe pair but higher than that given by the nitrate/nitrite pair. It is likely that more than one redox pair predominates in these two systems. Nitrate reduction is likely to be significant in the tailings, as discussed in Section 0, particularly with depth. The HS^-/SO_4^{2-} is also likely to have an influence in the redox conditions due to the origin of the tailings from the former sulphur mine. However, this redox pair cannot be quantified as the only sulphur compound analysed in the samples was sulphate. Hydrogen sulphide was tested in the samples collected in 2009 (Bary *et al.*, 2010a), but it was found to be below the limit of detection of $5.9\cdot10^{-7}$ mol/l in all the samples

(uncertainty not given in the original results). The Eh of the sample of sludge is likely controlled by a mixture of the redox pairs of Fe^{2+}/Fe^{3+} and NO_2^-/NO_3^-.

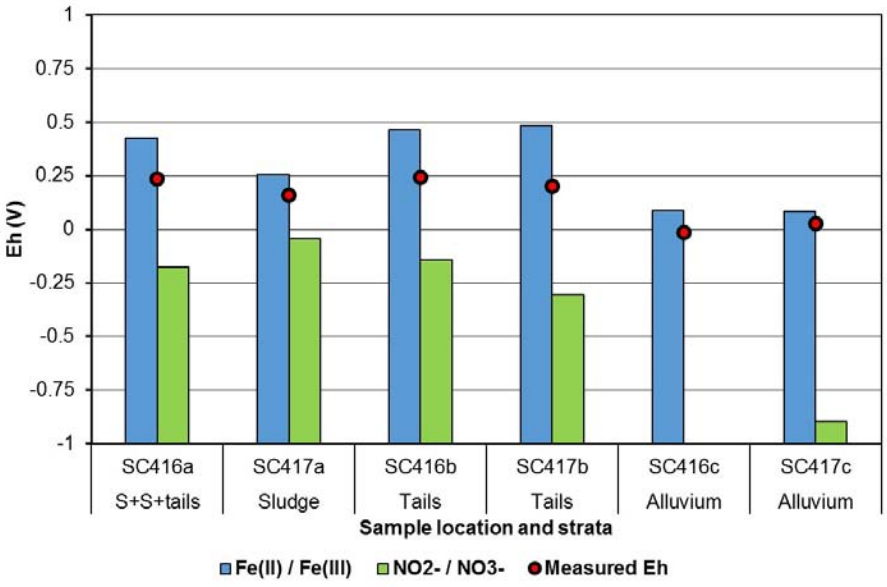

Figure 6.23: Measured Eh and the redox couples of Fe^{2+}/Fe^{3+} and NO_2^-/NO_3^-.

6.5.3 Major ion composition

Calcium and nitrate dominate the major ion composition of the samples of waste (Figure 6.24), a direct result of the neutralisation of the uranium conversion nitrate-rich effluents with calcium oxide. The groundwater in the alluvium is characterised by the Na^+ - Mg^+ - SO_4^{2-} ions. The chemical composition of the groundwater and pore water samples is presented in Table 1 in Appendix 2.

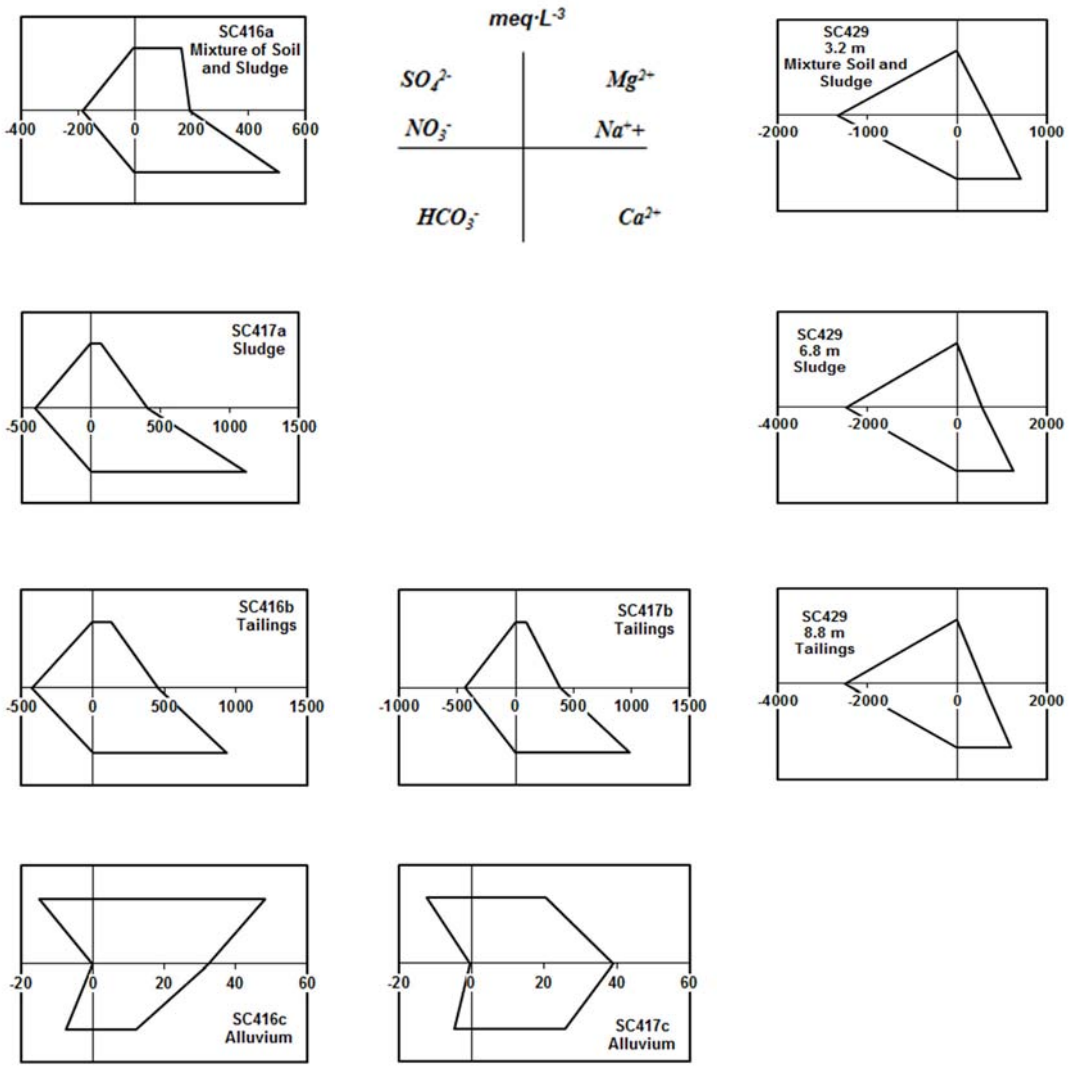

Figure 6.24: Stiff diagrams of the samples of groundwater (SC416 and SC417) and pore water (SC429).

6.5.4 Depth profile of the main elements

The results of analysis of the groundwater and pore water samples were compared with the results of groundwater monitoring at locations SC416 and SC417, carried out in 2009 by AREVA NC (Bary *et al.*, 2010a). The results of the analysis carried out in 2011 are within the same order of magnitude of the results of the previous monitoring for most determinands, except for the concentrations of iron which were lower by two orders of magnitude in 2011 (Figure 6.26 and Figure 6.27). However, this may be an artefact of sample preparation as iron is known to form colloids under environmental conditions and unfiltered samples may result in elevated measurements.

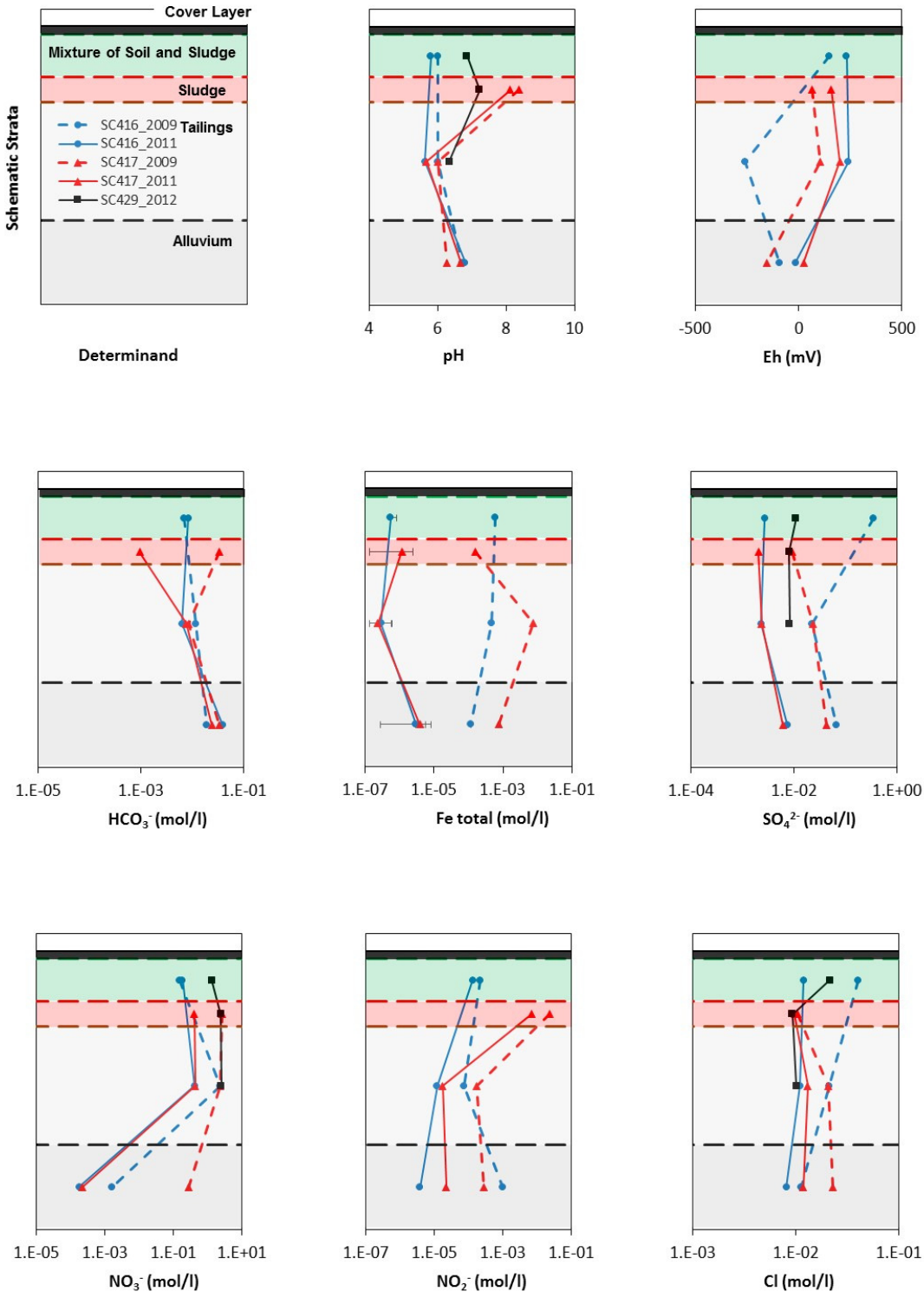

Figure 6.25: Depth profile of the main parameters in groundwater and pore water samples.

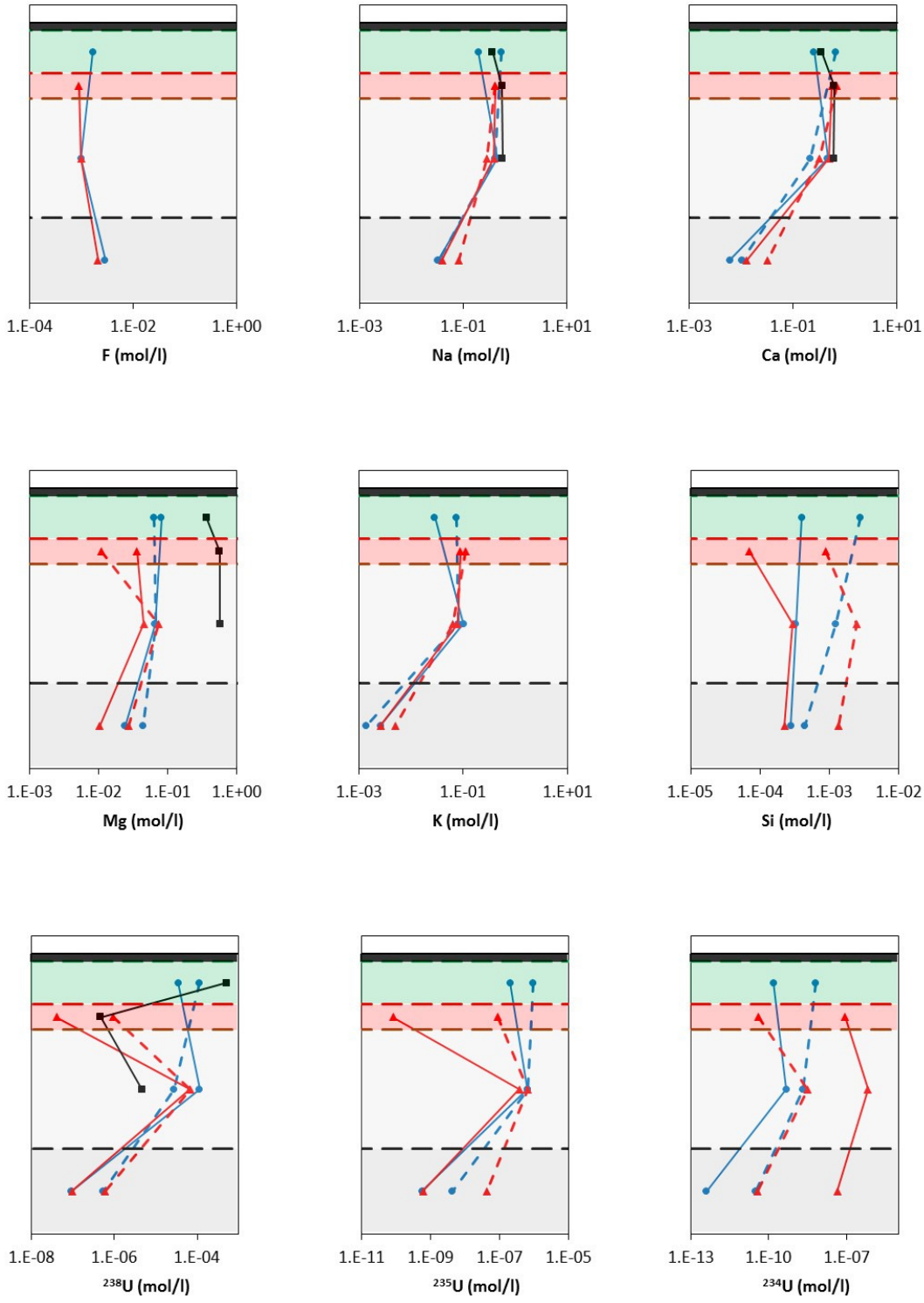

Figure 6.26: Depth profile of the main parameters in groundwater and pore water samples.

6.5.5 Geochemical speciation of uranium and thorium

The aqueous speciation of uranium and thorium was calculated with Phreeqc using the Thermochimie database (version 9a), as described in Chapter 4. Where there was no analysis of carbon or Si (samples of pore water), these elements were assumed to be in equilibrium with calcite and SiO_2(am) respectively. The assumption is based on the XRD analysis which indicated that these two minerals predominate in all the strata.

The results of the modelling indicate the aqueous uranium speciation to be consistently dominated by the calcium-uranyl-carbonate complexes, $Ca_2UO_2(CO_3)_3$ and $CaUO_2(CO_3)_3^{2-}$ (Figure 6.27). These two complexes represent over 99% of the speciation in the samples of sludge and alluvium and over 88% in one sample of mixture of soil and sludge. The aqueous speciation in the tailings is varied and includes uranyl-fluoride (UO_2F_2) and uranyl-phosphate ($UO_2[PO_4]^-$ and $UO_2[HPO_4]$) complexes.

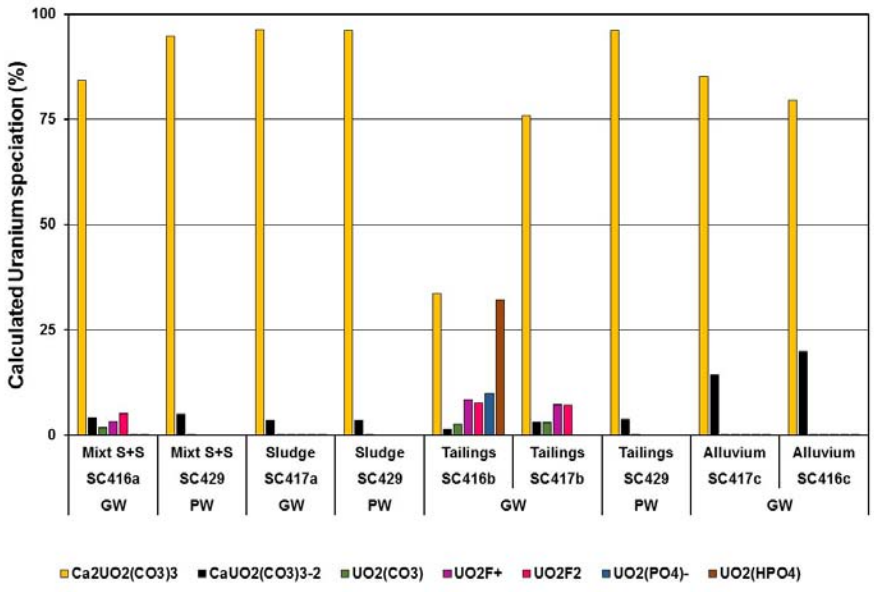

Figure 6.27: Calculated aqueous complexation of uranium in the samples of groundwater (GW) and pore water (PW). Mixt S+S: Mixture of Soil and Sludge.

The Th concentrations were below detection level in all samples except in the pore water collected from the sample of sludge. The measured Th concentration of $1.1 \cdot 10^{-6}$ mol/l was, however, considered elevated to correspond to truly dissolved thorium. It could have resulted from an analytical error or the possible presence of colloidal thorium that returned to solution after centrifugation.

According to the geochemical speciation results, the main carbonate minerals calcite ($CaCO_3$), aragonite ($CaCO_3$), dolomite ($CaMg(CO_3)_2$) and magnesite ($MgCO_3$) were

near equilibrium in the sludge and alluvium but slightly undersaturated in the mixture of soil and sludge (SI < -1) and in the tailings (SI < -1) (Table 6.8). Gypsum and quartz were close to equilibrium in all the strata. The iron minerals were generally over saturated with the exception of ferrihydrite ($Fe(OH)_3$), which was close to equilibrium in all the strata except in the sludge where it was oversaturated.

Table 6.8: Saturation indices of mineral phases near equilibrium.

Sample	Strata	Calcite	Aragonite	Dolomite	Magnesite	Gypsum	SiO2(am)	Quartz	Ferrihydrite
SC416a	Mixt. S.S.	-1.06	-1.23	-2.48	-1.15	**-0.58**	**-0.67**	**0.36**	**0.15**
SC429	Mixt. S.S.	**0.0***	**-0.17**	**-0.14**	**0.13**	**-0.04**	0.0*	1.03	NA
SC417a	Sludge	**0.76**	**0.59**	**0.44**	**-0.05**	**-0.62**	-1.42	-0.39	3.39
SC429	Sludge	**0.0***	**-0.17**	-1.16	**-0.89**	**-0.05**	**0.0***	1.03	NA
SC416b	Tailings	-1.35	-1.52	-3.45	-1.83	**-0.61**	**-0.74**	**0.29**	**-0.64**
SC417b	Tailings	-1.20	-1.37	-3.32	-1.86	**-0.58**	**-0.78**	**0.25**	**-0.18**
SC429	Tailings	**0.0***	**-0.17**	**-0.59**	**-0.32**	**-0.08**	**0.0***	1.03	NA
SC416c	Alluvium	**0.09**	**-0.08**	**0.71**	**0.89**	**-0.67**	**-0.84**	**0.19**	**0.08**
SC417c	Alluvium	**-0.13**	**-0.30**	**-0.20**	**0.20**	**-0.55**	**-0.93**	**0.10**	**-0.09**

0.0* Assumed in equilibrium, NA: Fe not analysed; Samples near equilibrium, i.e. -1 < SI < 1, are highlighted in bold

Uranium mineral phases were undersaturated in the samples of sludge and alluvium. Clarkeite [$Na(UO_2)O(OH)$] and soddyite [$(UO_2)_2SiO_4{:}2H_2O$] were near equilibrium in the samples of mixture of soil and sludge and tailings. Additionally, rutherfordine [$(UO_2)(CO_3)$], $UO_2(OH)_2$(beta), schoepite [$UO_3{:}2H_2O$] and compreignacite [$K_2(UO_2)_6O_4(OH)_6.7H_2O$] were in equilibrium in the samples of tailings. Thorium oxyhydroxides phases were oversaturated in the only sample where Th was above the detection limit. Table 6.9 summarises the saturation indeces of selected uranium minerals.

Table 6.9: Saturation indices of selected uranium phases.

Sample	Strata	Uranophane	Clarkeite	Rutherfordine	$UO_2(OH)_2$(beta)	Schoepite(des)	Becquerelite	Coffinite	Compreignacite	Soddyite
SC416a	Mixt. S.S.	1.13	**-0.92**	-1.38	-1.36	-1.43	2.58	-2.46	-6.27	**-0.13**
SC429	Mixt. S.S.	5.09	**0.56**	-2.28	-1.12	-1.19	6.15	-11.95	-	1.00
SC417a	Sludge	-2.52	-1.78	-7.88	-4.84	-4.91	-13.48	-8.74	-21.56	-7.85
SC429	Sludge	1.85	-1.01	-5.28	-3.19	-3.26	-5.39	-10.74	-	-3.14
SC416b	Tailings	2.33	**0.05**	**-0.67**	**-0.57**	**-0.64**	7.07	-1.65	**-0.83**	1.37
SC417b	Tailings	1.86	**-0.23**	**-0.86**	**-0.81**	**-0.88**	5.71	**-0.60**	-2.43	**0.84**
SC429	Tailings	-1.54	-2.69	-4.29	-3.99	-4.06	-11.99	-14.56	-	-4.74
SC416c	Alluvium	-8.49	-5.74	-6.28	-6.47	-6.54	-27.12	-1.31	-36.82	-10.53
SC417c	Alluvium	-7.66	-5.21	-5.81	-5.90	-5.97	-23.85	-1.95	-33.68	-9.49

Samples near equilibrium, i.e. -1 < SI < 1, are highlighted in bold

6.6 Implications

The solid characterisation of the samples has highlighted the importance of the use of a multi-technique approach in the characterisation of the speciation of uranium and thorium. The various techniques used in this study provided complimentary information that either supported each other or allowed identification of a different speciation.

The stratum of mixture of soil and sludge is characterised by quartz, calcite, muscovite, and low contents of gypsum. The tailings are characterised by gypsum, dolomite and muscovite, with variable contents of quartz and calcite. Mineral fractions that could play a role in the retention of both U and Th, such as clays and iron oxi-hydroxides, were not identified by XRD.

Each stratum has characteristic geochemical conditions that affect differently the retention of uranium. The upper stratum of the waste, comprising the unsaturated sludge, is oxic and rich in amorphous and clay minerals of Al, Si and Fe that provide high surface area and sorption capacity. This stratum is chemically highly heterogeneous with variable concentrations of F, Ca, Mg, Si, Fe and U, reflecting the variability of the uranium ore and evolution of the chemical processes used at the plant over time. The sludge contains variable concentrations of uranium, of between 60 and 4,190 mg/kg, and the uranium speciation is varied. It is found in its majority associated with the carbonate minerals or sorbed (between 50 and 70%), and present as secondary uranium minerals or incorporated within amorphous iron phases, such as ferrihydrite (up to 40%). Thorium

concentrations also decrease considerably with depth, from up to 90 mg/kg in the sludge to less than 10 mg/kg in the tailings, and it is predominantly associated with the crstalline iron oxides, hydroxides and oxyhydroxides, as well as with amorphous minerals of Fe, Al and Si. Thorium only has one valence state and would not, therefore, be affected by increasing reductive conditions with depth along the basins. Similarly to what is observed for the uranium, the concentrations of thorium decrease with depth, from up to 90 mg/kg in the sludge to less than 10 mg/kg in the tailings.

These results suggest that 90-95% of the uranium contained in the sludge may be labile or easily available for groundwater transport under natural conditions. Uranium-bearing particles are heterogeneously distributed and are likely to consist mostly of uranyl-silicates of the uranophane group of minerals. Nonetheless, due to the chemical heterogeneity of the sludge, other phases not identified by this study may also be present.

The underlying stratum of tailings becomes less oxic with depth, reducing contaminant mobility. Uranium is present mostly sorbed (56%) and associated with the amorphous iron minerals or present as secondary uranium phases (17%). Uranium concentration was too low (<50 mg/kg) to allow further spectroscopic identification.

7. Batch Experiments

7.1 Overview and experimental design

Evaluating the geochemical behaviour of uranium and thorium in the B1/B2 basins requires an understanding of the mechanisms responsible for controlling the retention and release of these contaminants in this specific environment. This chapter presents the results of laboratory batch studies that were set up to assess the release behaviour of uranium and thorium under simulated static conditions. Data generated from the studies was used in conjunction with field measurements (Chapter 5) and the results of solid characterisation (Chapter 6) to model the processes controlling contaminant mobility within the system.

Specific subjects that have been investigated in detail are as follows:

- Formation of U- and Th-colloids during release of these elements into solution;
- Role of carbonates in controlling the system's pH; and
- Effect of the aging of the sample after collection from the basins and the effect of sample conditioning and treatment on the release of uranium and thorium.

The number of batch experiments, samples used and experimental conditions is described in Section 4.6.2. The initial content of U and Th in the samples is summarised in

Table 7.1 below.

Table 7.1: Initial concentration of uranium and thorium in samples used in the batch experiments (in dry mass).

Group	Year of Sampling	Sample / Depth	Strata	Initial [U] (mg/kg)	Initial [Th] (mg/kg)	S:L ratio
Dry	2009	SC30 / 0-2.15m	Mixt. of soil and sludge	484 ± 88	9.0 ± 2.7	1:10
		SC19 / 2.5-3.8m	Sludge	3,390 ± 327	47.2 ± 133.6	1:10; 1:5
		SC417b / 8.2-10.2m	Tailings	14 ± 1	3.7 ± 1.5	1:10; 1:5
		SC417a / 1.5-3.0 m <0.5mm	Sludge	2,151 ± 105	117.0 ± 24.0	1:10
		SC417a / 1.5-3.0 m 0.5-1.0mm	Sludge	1,636 ± 151	73.8 ± 17.8	1:10
	2012	SC429 / 3.2m	Mixt. of soil and sludge	1,426 ± 21	38.4 ± 0.7	1:10
		SC429 / 6.8m	Sludge	58 ± 2	10.3 ± 1.0	1:10
		SC429 / 8.8m	Tailings	22 ± 1	7.7 ± 0.8	1:10
Wet		SC429 / 3.2m	Mixt. of soil and sludge	1,426 ± 21	38.4 ± 0.7	1:10
		SC429 / 6.8m	Sludge	58 ± 2	10.3 ± 1.0	1:10
		SC429 / 8.8m	Tailings	22 ± 1	7.7 ± 0.8	1:10

S:L – solid to liquid ratio

7.2 Investigation of the presence of uranium and thorium in the colloidal form

7.2.1 Overview

The potential for increased mobility of uranium and thorium in the B1/B2 basins was investigated by separating the colloidal fraction of selected aliquots of the batch and

column experiments. The objective was to investigate whether U and Th were correlated with particle size. The investigation comprised two separate experiments, described in Section 4.7.2, the ultracentrifugation experiment and the ultrafiltration experiment. In the ultracentrifugation experiment, selected aliquots of the wet batch experiment were collected at 1 and 7 days of contact time, and divided in two sub-aliquots. One sub-aliquot of each sample was centrifuged at 18,000 rpm for 1 hour whilst the other was ultra-centrifuged at 90,000 rpm for 1 hour. In the ultrafiltration experiment, selected aliquots of the batch and column experiments were centrifuged in centrifugal filters of 3kD, 10 kD, 30 kD, 100 kD 0.2 µm and 0.45 µm for between 5 and 20 minutes.

7.2.2 Ultracentrifugation experiment

The concentration of uranium in solution obtained after one hour of centrifugation at either 18,000 rpm or 90,000 rpm was within the same order of magnitude for the same strata and contact time (Table 7.2). The comparable concentrations of uranium obtained indicate that the particle fraction present in the samples can be removed by applying a centrifugation speed of 18,000 rpm.

The concentrations of thorium in the aliquots of sludge and mixture of soil and sludge decreased from 10^{-9} mol/l when ultra-centrifuged at rotation velocities of 18,000 rpm to below the detection limit of $1.7x10^{-10}$ mol/l when ultra-centrifuged at 90,000 rpm. Rotation velocities of 50,000 rpm (centrifugal speed of about $1.5x10^{5}$ g) are sufficient to remove Th(IV) eigencolloids (Altmaier, Neck and Fanghänel, 2004) and the decreased concentration of Th after ultra-centrifugation at 90,000 rpm may indicate the presence of colloidal thorium in these aliquots. Ultracentrifugation of the samples of tailings did not confirm the presence of Th-colloids as dissolved thorium was found to be below the detection limit after centrifugation at both 18,000 and 90,000 rpm.

Table 7.2: Concentrations of U and Th in the aliquots of batch samples collected at 1 day and 7 days contact time after ultracentrifugation.

Strata	Contact time (days)	U (mol/l) 18,000 rpm	U (mol/l) 90,000 rpm	Th (mol/l) 18,000 rpm	Th (mol/l) 90,000 rpm
Mixt. Soil and Sludge	1	$3.00(0.04)\cdot10^{-5}$	$3.10(0.04)\cdot10^{-5}$	$4.31(0.51)\cdot10^{-9}$	<DL
	7	$4.76(0.09)\cdot10^{-5}$	$4.90(0.07)\cdot10^{-5}$	$4.31(1.29)\cdot10^{-9}$	<DL
Sludge	1	$1.43(0.03)\cdot10^{-7}$	$1.30(0.03)\cdot10^{-7}$	$4.31(0.74)\cdot10^{-9}$	<DL
	7	$3.11(0.06)\cdot10^{-7}$	$2.98(0.08)\cdot10^{-7}$	$8.62(1.32)\cdot10^{-9}$	<DL

Strata	Contact time (days)	U (mol/l) 18,000 rpm	U (mol/l) 90,000 rpm	Th (mol/l) 18,000 rpm	Th (mol/l) 90,000 rpm
Tailings	1	$3.36(0.03)\cdot10^{-7}$	$2.86(0.05)\cdot10^{-7}$	<DL	$4.31(1.06)\cdot10^{-9}$
	7	$6.60(0.17)\cdot10^{-7}$	$5.76(0.10)\cdot10^{-7}$	<DL	<DL

*<DL – below detection limit of $1.7\cdot10^{-10}$ mol/l

7.2.3 Ultrafiltration experiment

The concentrations of uranium measured in aliquots of dry samples of sludge after filtration with various filter sizes remained above 96% of the total uranium measured at the smaller filter size of 3 kD (Figure 7.1). These results suggest there was no release of colloidal particles of uranium in these samples. The particle size of the solid samples (smaller than 0.5 mm and between 0.5 and 1.0 mm) did not affect the distribution of colloids in the aliquots. The aliquot of fresh wet sample of sludge, however, showed that 40% of the total uranium was retained in the 0.2 µm filter, indicating the presence of uranium particles of dimensions between 0.2 and 0.45 µm.

There was no release of particulate uranium from the aliquot of mixture of soil and sludge (Figure 7.2). No uranium fractionation between filter sizes was measured in the aliquots of samples of tailings (Figure 7.3). The concentration of uranium passing the 0.45 µm filter in the wet batch of tailings was half the concentration passing the other filters, indicating a possible laboratory error as it is unlikely that there would be more uranium passing a smaller filter than the uranium passing a larger filter.

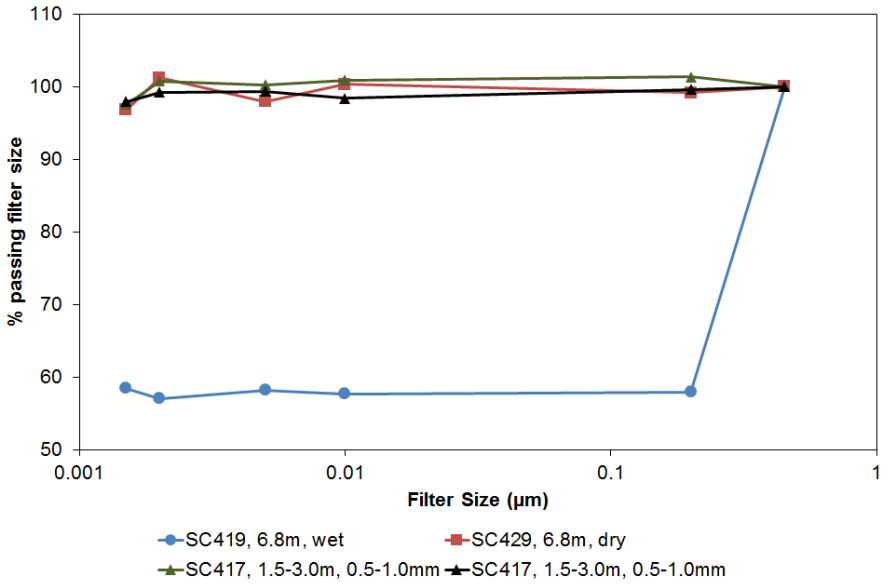

Figure 7.1: Distribution of normalised concentration of uranium by filter size – samples of sludge.

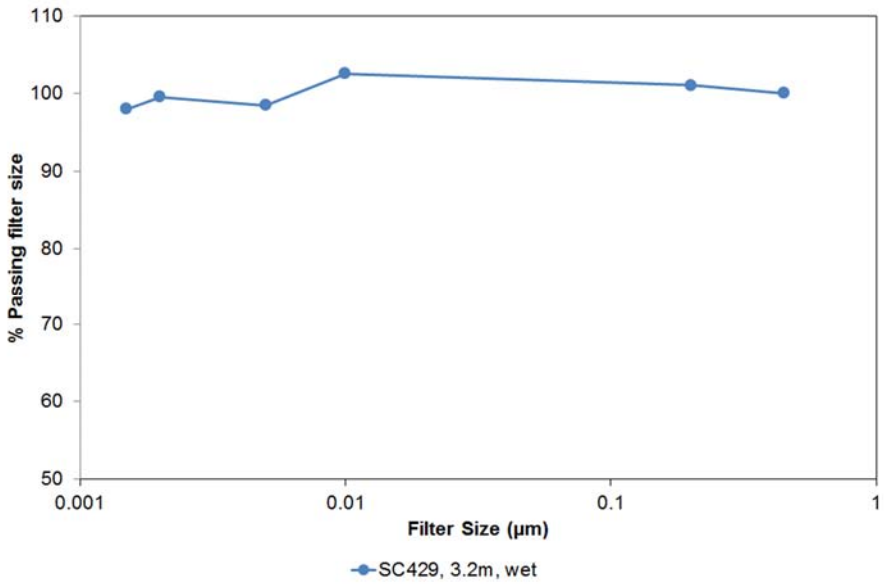

Figure 7.2: Distribution of normalised concentration of uranium by filter size – sample of mixture of soil and sludge.

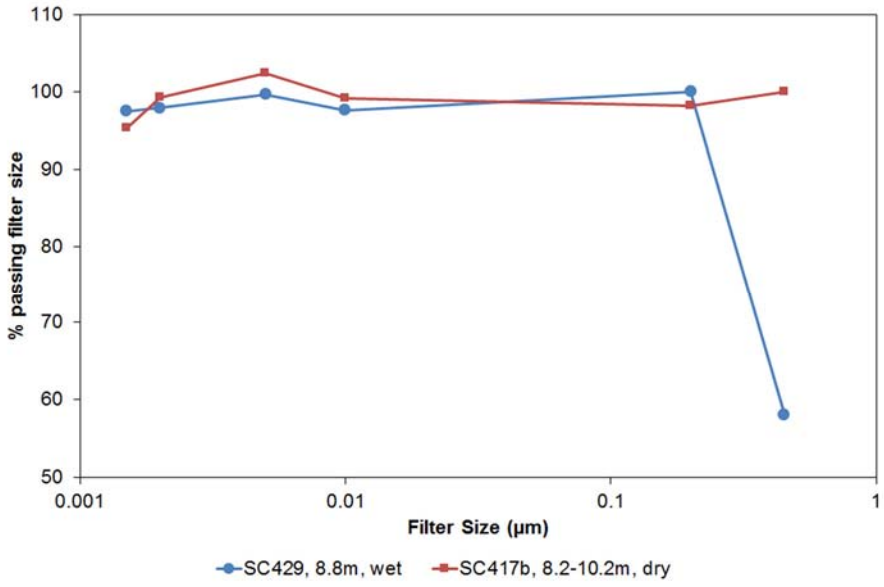

Figure 7.3: Distribution of normalised concentration of uranium by filter size – samples of tailings. The point "wet batch" at higher filter size is probably the result of an experimental error. For details see text.

7.2.4 Interpretation

The formation of uranium and thorium colloids has been widely documented due to their effect on the increased mobility of U and Th in the aqueous environment (Neck and Kim,

2001; Zänker and Hennig, 2014). Thorium, in particular, can be absorbed on carrier particles or occur as intrinsic colloids when its solubility limit is exceeded (Kersting et al, 1999; Opel et al, 2007; Utsunomiya et al, 2009; Geckeis et al, 2011).

Under the experimental conditions, both the ultracentrifugation and the ultrafiltration experiments showed no evidence of a colloidal fraction of uranium that could be separated at 90,000 rpm or by filter sizes as small as 3 kD. Uranium is, therefore, likely to be present as true dissolved species in the aliquots of the batch experiments for all the strata. Uranium was found as true dissolved species in other natural environments, such as the Osamu Utsumi (Miekeley *et al.*, 1992) and the Koongarra sites (Short, 1988). The only aliquot where the presence of uranium particles of between 0.2 and 0.45 µm was measured, was in the wet sample of sludge. This could indicate the presence of low stability colloids in the sludge that breakdown after drying of the samples.

Field studies have found thorium associated with mobile colloids composed principally of iron and silicon species, probably ferrihydrite associated with silicate and discrete colloidal silica, at the Koongarra uranium deposit, Australia (Short, 1988; Payne *et al.*, 1992). At the Osamu Utsumi uranium mine, Miekeley and co-workers (1992) found transport by colloids, predominantly composed of hydrous ferric oxides and sorbed organics, to control the mobility of thorium in groundwater. Other types of colloids formed by tetravalent actinides include oxyhydroxides, aluminosilicates and clusters of actinides associated with low molecular mass organic acids. In this study, thorium particles appeared to be retained by higher centrifugation speeds, of 90,000 rpm compared to 18,000 rpm. However, this could not be confirmed by the ultrafiltration experiment as the measured concentrations were below the detection limit. The concentration of iron measured in this investigation was always below the detection limit of $7 \cdot 10^{-7}$ mol/l, confirming the unlikely formation of colloids.

7.3 Evolution of pH in the batch experiments

The evolution of the pH in the batch experiments is presented in Figure 7.4. The samples of mixture of soil and sludge (black symbols) had initial pH values of 8-8.2, which decreased with time, stabilising, after 30 to 40 days, at pH values of between 6.6 and 7.7. The initial pH values ranged from 7.6 to 8.4 in the experiments with samples of sludge. With the exception of the wet sample, where a slight increase in pH was observed during the initial 30 days, all the experiments showed a decrease of pH with time. After approximately 30 days, the pH stabilised at values of between 7.1 and 7.9. The initial pH

in the samples of tailings (green symbols), of between 7.1 and 7.4, decreased with time, stabilising at values of between 6.4 and 7.3.

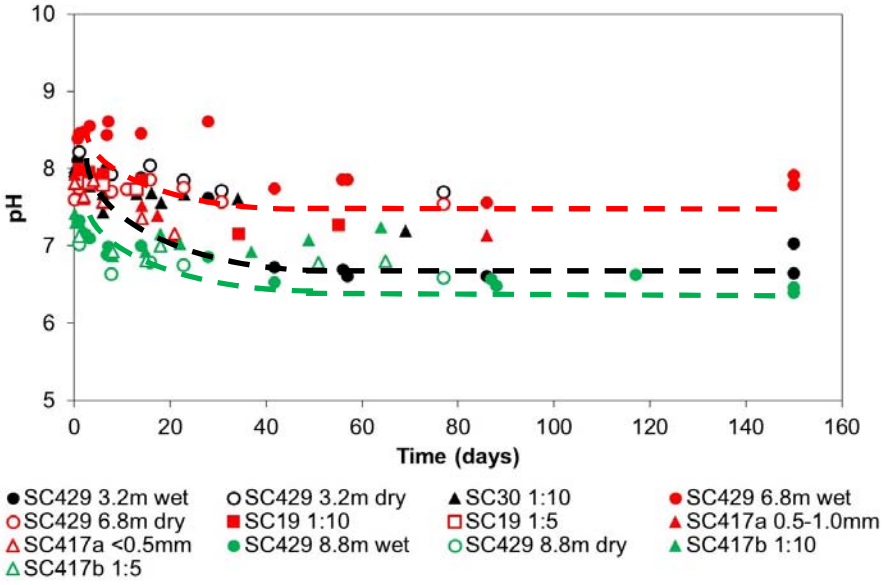

Figure 7.4: Experimentally measured pH values in the batch aliquots (symbols in black represent samples of mixture of soil and sludge, symbols in red represent samples of sludge, symbols in green represent samples of tailings). Dashed lines schematically represent the general evolution of pH with time.

7.3.1 Investigation of the pH buffer capacity of the samples

Solid characterisation of the samples provided evidence of the presence of both calcite and dolomite in all the strata of waste (Chapter 6). The modelling of the pore water and groundwater geochemistry (Chapter 6) further indicated the potential role of carbonates as pH buffers in aqueous samples.

The stabilisation of the pH at neutral values, as observed by the evolution of pH behaviour with contact times (Figure 7.4), indicated the possible presence of a mineral phase controlling the pH of the batch aliquots. A separate experiment was therefore envisaged to investigate and characterise the buffer mineral. Samples of fresh wet sample (two of each strata of mixture of soil and sludge, sludge and tailings) were prepared following the same method used in the batch experiments. After contact times of 60 to 70 days, the pH of the aliquots was measured and the pH buffer capacity experiment started. At the beginning of the experiment, concentrated nitric acid was added to the batch sample to set the pH value between 5.5 and 6 (approximately 10^{-2} mol/l HNO_3^- was added). The pH of the aliquots was then measured periodically.

The results show the pH of the acidified samples of mixture of soil and sludge and of tailings to increase rapidly during the first 3 days of experiment (Figure 7.5 and Figure 7.7). After 10 days, the pH had returned to its initial (pre-acidification) value (pH ≈ 6.7 in the mixture of soil and sludge and pH ≈ 6.5 in the tailings). The pH of the sample of sludge increased during the first 3 days and stabilised at a value of 7.2 after 17 days of experiment, although it never recovered to its original pH value of approximately 7.8 (Figure 7.6). This may have been a result of a loss of $pCO_2(g)$ during acidification resulting in a lower equilibrium pH.

As calcite was observed in the samples analysed by XRD (Chapter 6), it is reasonable to assume that calcite may be controlling the pH under experimental conditions. In the presence of acid, calcite would dissolve to produce calcium and bicarbonate, raising the pH of the solution, according to equation (7.1):

$$CaCO_3 + H^+ \rightarrow Ca^{2+} + HCO_3^- \quad \textbf{(7.1)}$$

The pH behaviour in the experiments was modelled by allowing calcite to dissolve or precipitate to reach equilibrium. The dissolution kinetics suggested by Plummer and co-workers (1978) and the geochemical code Phreeqc (Parkhurst and Appelo, 2015) were used. According to Plummer and co-workers (1978), calcite dissolution can be described by an expression of the form (7.2):

$$R = k_1 \cdot a_{H^+}^n + k_2 \cdot a_{H_2CO_3^*}^p + k_3 \cdot a_{H_2O} - k_4 \cdot a_{Ca^{2+}} \cdot a_{CO_3^{2-}} \quad \textbf{(7.2)}$$

Where R is the dissolution rate in mmol/cm^2.s, k_1, k_2 and k_3 are the forward rate constants (in cm/s) dependent on temperature, k_4 is the backward rate constant (a function of temperature and pCO_2), $H_2CO_3^*$ represents the sum of $CO_{2(aq)} + H_2CO_3^0$ species, and a denotes the activity (unitless) of the indicated constituent. The exponents n and p are equal to 1 (Plummer et al, 1978; Busenberg and Plummer, 1982).

This rate expression accounts for the solid surface protonation at pH ≤ 5/6 (first term), surface carbonation at 4 ≤ pH ≤ 6 (second term), surface hydration at pH ≥ 6 (third term) and the precipitation reaction (fourth term).

The rate constants derived by Plummer and co-workers (1978) were used:

$$\log k_1 = 0.198 - 444/T$$

$\log k_2 = 2.84 - 2177/T$

$\log k_3 = -5.86 - 317/T \; for \; T \leq 298$

$\log k_4 = -1.1 - 1737/T \; for \; T > 298$

The modelled dissolution of calcite is presented in Figure 7.5 to Figure 7.7. Following addition of nitric acid, the presence of calcite immediately buffered the pH to a value of approximately 5, as observed in the first experimental point measured (within 5 minutes) of addition of acid (Table 7.3). The calculated concentration of calcite in the system ranged from 0.2 mmol/l in the samples of sludge to 0.8 mmol/l in the sample of tailings (Table 7.3). The model provided a good representation of the observed pH behaviour and final modelled pH values stabilised within 0.2 pH units of the final experimentally measured pH value.

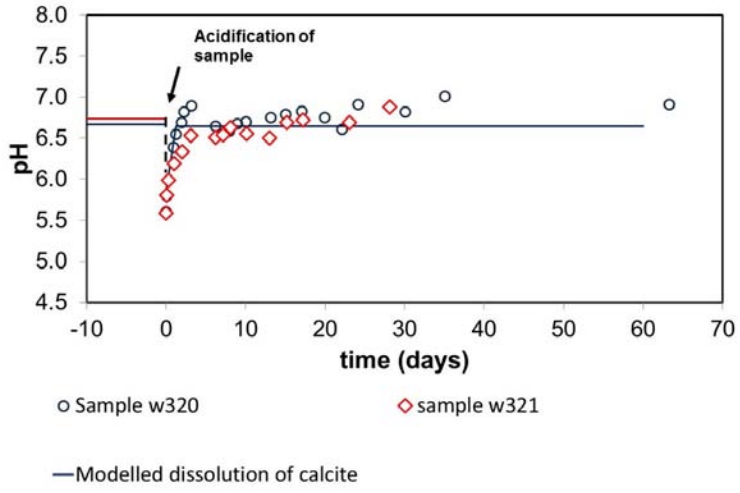

Figure 7.5: Evolution of pH in two samples of mixture of soil and sludge.

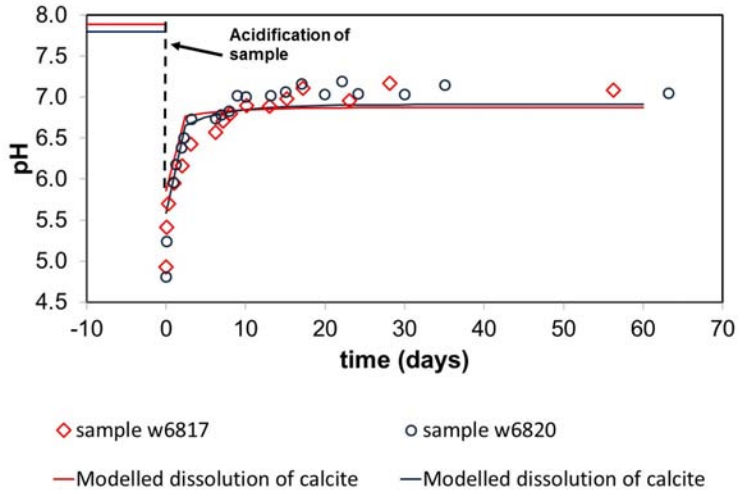

Figure 7.6: Evolution of pH in two samples of sludge.

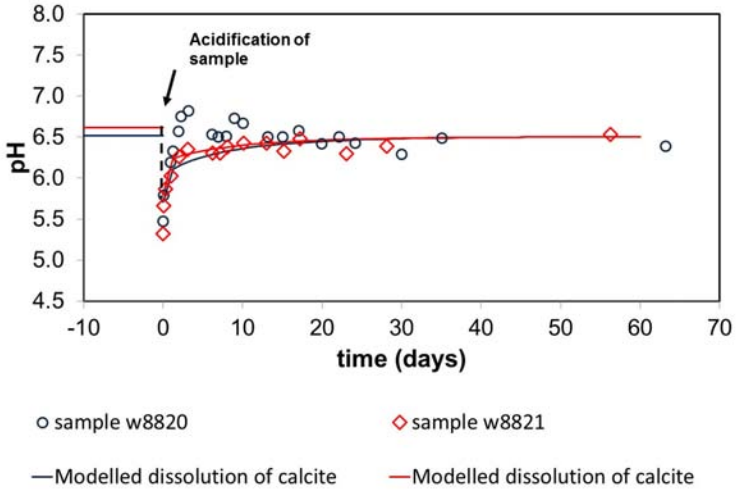

Figure 7.7: Evolution of pH in two samples of tailings.

Table 7.3: Evolution of the experimental and modelled pH values obtained in the pH buffer capacity experiment.

Sample	Strata	Initial pH	pH after addition of HNO_3		Final pH		Amount of calcite (mmol/l)
			Measured	Modelled	Measured	Modelled	Calculated
W320	Mixt S+S	6.7	5.6	5.6	6.9	6.7	0.56
W6817	Sludge	7.9	4.9	5.9	7.1	6.9	0.18
W6820	Sludge	7.8	4.8	5.6	7.1	6.9	0.32
W8820	Tailings	6.5	5.5	5.7	6.4	6.5	0.81
W8821	Tailings	6.6	5.3	5.8	6.5	6.5	0.64

*The sample w321, presented in Figure 7.5, was not modelled as the solution composition, including alkalinity and calcium, was not analysed.

7.4 Evolution of Eh in the batch experiments

The Eh behaviour was characterised by increasing Eh values with contact time, in particular during the initial 30 days of experimental conditions (Figure 7.8). Initial values ranged from 300 to 415 mV in the experiments with samples of mixture of soil and sludge, 330 to 415 mV (sludge) and 330 to 450 mV (tailings). The Eh stabilised at values ranging between 340 mV (sample of sludge) and 460 mV (sample of tailings). The systems remained oxidising throughout the experimental conditions.

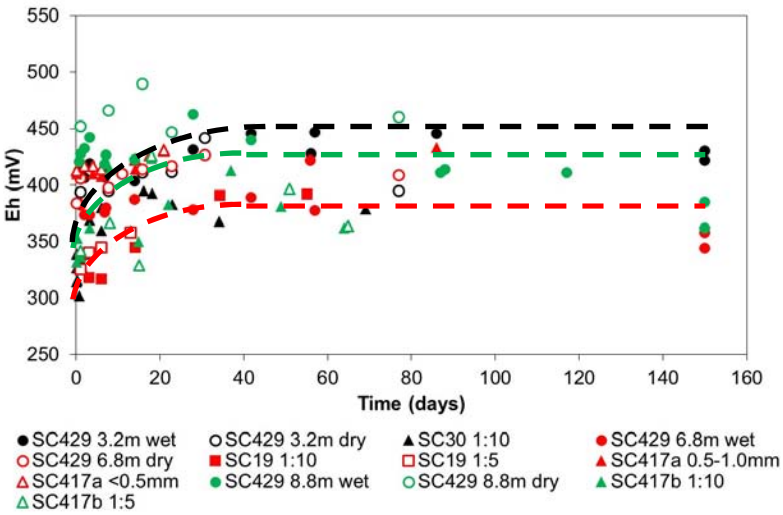

Figure 7.8: Experimentally measured Eh values in the batch aliquots (symbols in black represent samples of mixture of soil and sludge, symbols in red represent samples of sludge, symbols in green represent samples of tailings) and dashed lines schematically representing the evolution of the Eh.

7.5 Evolution of alkalinity in the batch experiments

The alkalinity in the batch experiments was measured with the method of Gran titration as described in section 4.7. Initial alkalinity values ranged between 0.5 and 1.0 mmol/l (Figure 7.9) and increased with increasing contact times.

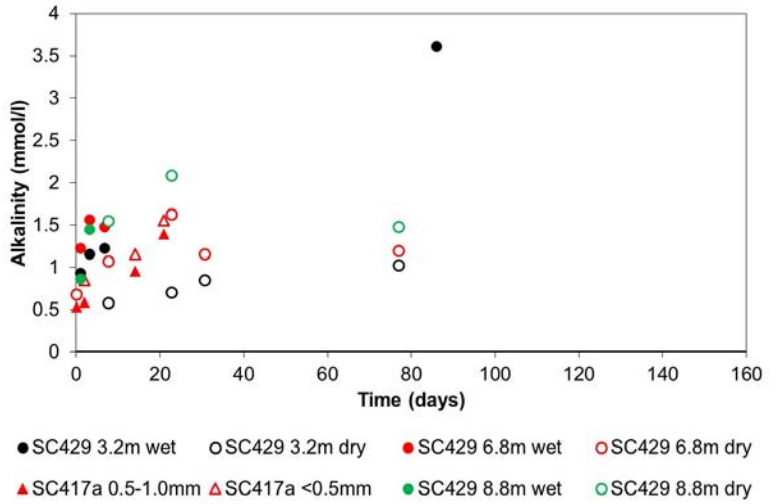

Figure 7.9: Evolution of alkalinity in the batch aliquots (symbols in black represent samples of mixture of soil and sludge, samples in red represent samples of sludge, symbols in green represent samples of tailings).

The carbon dioxide partial pressure ($pCO_{2(g)}$) in solution can be estimated from the measured pH and alkalinity values. The calculated $pCO_{2(g)}$ was close to atmospheric pressure (0.03% or $pCO_{2(g)} = 10^{-3.5}$) at the start of the experiments and stabilised at

concentrations of generally 3% ($pCO_{2(g)} = 10^{-1.5}$) in the mixture of soil and sludge and tailings and 0.1% ($pCO_{2(g)} = 10^{-3.0}$) in the sludge (Figure 7.10). These values lie within normal pressures of CO_2 content in soil gas ($10^{-3.5}$ atm) and groundwater ($10^{-1.5}$ atm).

Although the batch vials were not hermetically closed to atmosphere, it is reasonable to assume that only minor transfer of air occurred with the atmosphere. Modelling the CO_2 evolution considering a closed system, i.e. where no transfers of CO_2 occur with the atmosphere, the source of carbon dioxide will be a result of reactions occurring within the closed system. The most likely sources of CO_2 in soil are root respiration and decay of organic matter. Unfortunately, the concentrations of organic carbon in solution were not analysed so the origin of carbon dioxide in the aliquots cannot be confirmed. Nonetheless, the pH behaviour in solution was modelled assuming that there was a source of organic carbon in the samples which, when degraded provided carbon into solution as $CO_{2(g)}$.

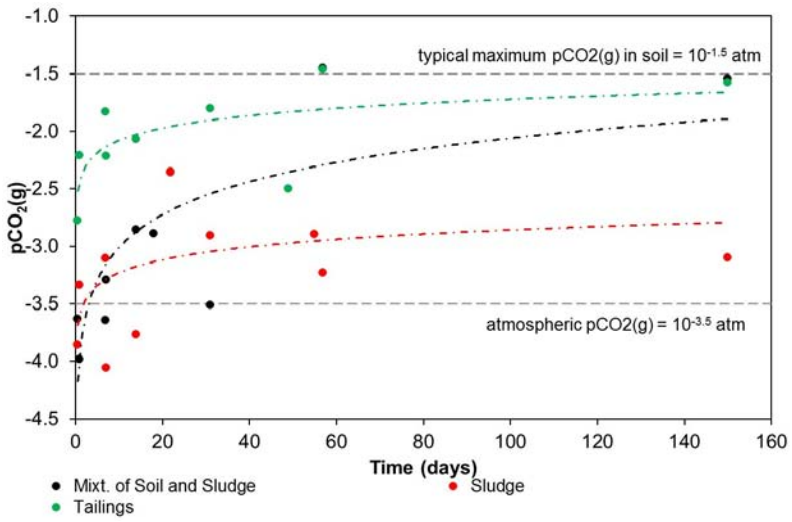

Figure 7.10: Evolution of the pressure of CO_2 (gas) ($pCO_{2(g)}$) in the batch aliquots (symbols in black represent samples of mixture of soil and sludge, samples in red represent samples of sludge, symbols in green represent samples of tailings) (calculated with experimentally measured pH and alkalinity values).

The oxidation of organic matter was calculated with the first order reaction:

$$\frac{dCO_{2(gas)}}{dt} = k * CO_{2(gas)} = k * \left(CO_{2(gas)final} - SR\left(CO_{2(gas)}\right)\right) \quad (7.3)$$

Where:

$\frac{dCO_{2(gas)}}{dt}$ is the change in $CO_{2(gas)}$ concentration with time;

k is the rate of $CO_{2(gas)}$ increase in solution (sec^{-1}), obtained by fitting the experimental results;

$CO_{2(gas)final}$ is the final $pCO_{2(gas)}$ in the system, obtained from the experimental results;

$SR(CO_{2(gas)})$ is the saturation state of $CO_{2(gas)}$.

The rate of organic matter degradation was obtained from fitting the $pCO_{2(gas)}$ during the initial 30 days of experimental conditions (Table 7.4). The rates for the three strata were within the same order of magnitude, ranging between 0.02 and 0.07 day^{-1}. However, the $pCO_{2(gas)}$ measured at the end of the experiments was lower in the case of the stratum of sludge (10^{-3} atm), when compared with the other two strata ($10^{-1.6}$ to $10^{-1.5}$ atm). This indicates less organic matter present in the sludge when compared with the other strata. The lower concentration of organic carbon available for degradation was not sufficient to raise the $pCO_{2(gas)}$ to the normal soil gas content of $10^{-1.5}$ atm.

Table 7.4: Rates of organic matter oxidation (fitted) and average final pCO_2(g) for each strata (measured).

Strata	Rate (sec^{-1})	Rate (day^{-1})	$CO_{2(g)final}$ (atm)
Mixture of soil and sludge	$8.1 \cdot 10^{-7}$	0.07	$10^{-1.5}$
Sludge	$4.6 \cdot 10^{-7}$	0.04	$10^{-3.0}$
Tailings	$2.4 \cdot 10^{-7}$	0.02	$10^{-1.6}$

The modelled degradation of organic matter in the samples using the CO_2 rates derived from the experimental measurements (Table 7.4) is presented in Figure 7.11 and Figure 7.12. The model showed a good fit with both increasing pCO_2 and decreasing pH values.

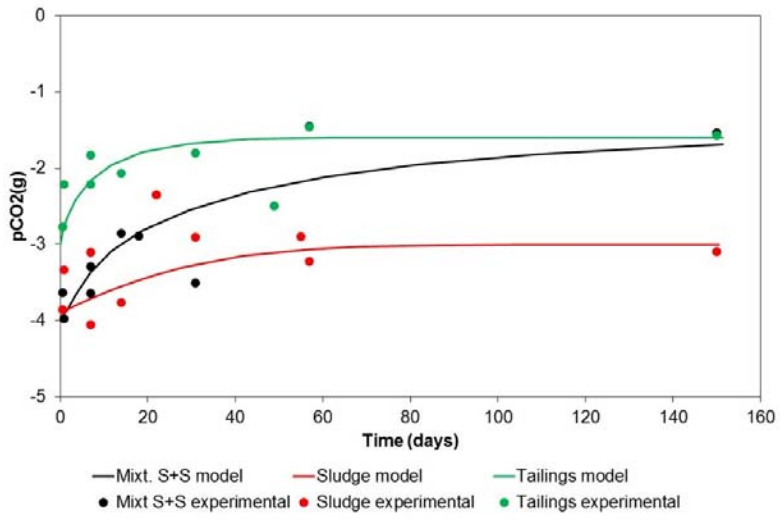

Figure 7.11: Experimental and modelled evolution of $pCO_{2(g)}$ with time resulting from oxidation of organic matter.

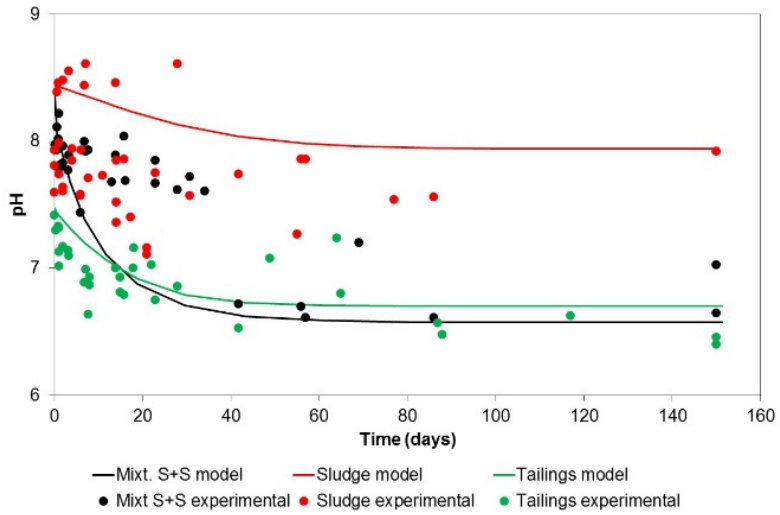

Figure 7.12: Experimental and modelled evolution of pH with time resulting from oxidation of organic matter.

7.6 Evolution of the major chemistry in the batch experiments

In addition to the pH, Eh and alkalinity, selected batch aliquots were analysed for the major cations, anions, the Fe(II)/Fe(III) and NO_2/NO_3 pairs as described in Section 4.7. Geochemical speciation modelling of the batch aliquots was carried out to investigate the behaviour of the main phases in solution. The geochemical speciation was computed with the Thermochimie database (Giffaut *et al.*, 2014) and the solubility reactions therein as described in Chapter 4.

The geochemical modelling predicted gypsum, fluorite and the carbonate minerals calcite, dolomite and magnesite to be near equilibrium, i.e. with saturation indices close to zero (Figure 7.13). Moreover, these phases remained at or close to equilibrium throughout the experimental conditions. Rhodochrosite was generally undersaturated, except in the tailings (both wet and dry samples) where it was found to be in equilibrium. Although not identified by XRD analysis, rhodochrosite in the tailings may result from replacement of magnesium in one of the main mineral phases present in this stratum, dolomite.

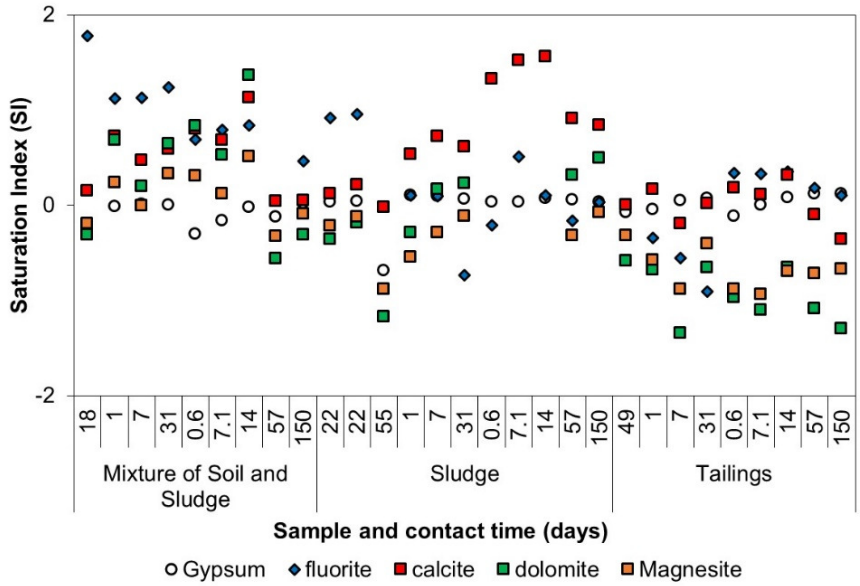

Figure 7.13: Main phases predicted to be near equilibrium at the end of the batch experiments.

The iron minerals ferrihydrite, goethite and lepidocrocite were predicted to be oversaturated, with saturation indices generally above 2. The exception was in the batch experiment with the wet sample of mixture of soil and sludge where, at long contact times (57 and 150 days), ferrihydrite was in equilibrium. Barite was generally between equilibrium and slight oversaturation with saturation indices of between 0 and 1. Barite was observed in the samples of sludge analysed by SEM (Chapter 6).

7.7 Evolution of dissolved concentrations of uranium

The analysis of uranium was carried out by ICP-MS. Three isotopes of U were analysed (^{234}U, ^{235}U and ^{238}U). The total concentration of uranium (mass sum of the three isotopes) released under batch experimental conditions is presented in Figure 7.14 to Figure 7.16 for the samples of mixture of soil and sludge, samples of sludge and samples of tailings, respectively.

7.7.1 Mixture of Soil and Sludge

Two stages of uranium release were present in the samples of mixture of soil and sludge (Figure 7.14). Rapid release occurred within the first week, followed by a slower release during the remainder of the experiment. At 70 days, the concentration of uranium in the aqueous phase continued to increase in sample SC30 indicating that equilibrium had not yet been attained. Aqueous uranium concentrations for sample SC429 reached an

apparent steady state equilibrium after approximately 30 days, both in the dry and wet samples. At the beginning of the experiment, the aqueous uranium concentrations in the wet sample were approximately one order of magnitude higher, $(2.3\pm0.1)\cdot10^{-5}$ mol/l at 0.6 days, than in the dry samples: $(3.1\pm0.1)\cdot10^{-6}$ mol/l at 0.01 days in SC30 and $(7.2\pm0.1)\cdot10^{-6}$ mol/l at 1 day in SC429 (dry). The wet sample produced the higher concentrations of aqueous uranium throughout the experiment. Nonetheless, even at steady state, at concentrations of approximately $(1.1\pm0.1)\cdot10^{-4}$ mol/l, the experimental aqueous concentrations remained lower than the uranium concentration measured in the pore water $(5.1\pm1.0)\cdot10^{-4}$ mol/l of the mixture of soil and sludge in SC429.

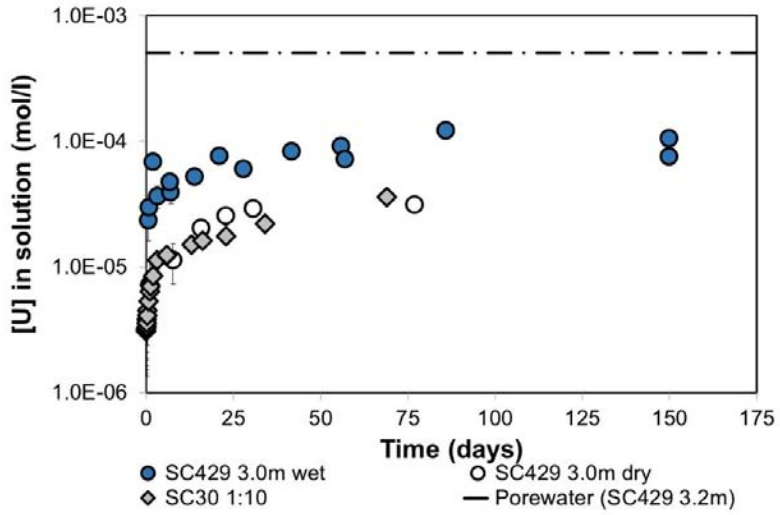

Figure 7.14: Uranium release under batch conditions from samples of mixture of soil and sludge.

7.7.2 Sludge

The batch experiments with samples of sludge (Figure 7.15) also exhibited two rates of uranium release. A fast rate was observed during the first 15 days, followed by a slow rate, similar to what was observed in the second phase of release from samples of mixture of soil and sludge. Uranium release behaviour was similar for both S:L ratios (1:5 and 1:10) used in sample SC19 and for both particle sizes (<0.5 mm and 0.5-1.0 mm) used in sample SC417, with similar concentrations of aqueous uranium for the same contact time. These two variables have not affected uranium release. Drying of a sample resulted in a minor effect on the release behaviour of uranium, in particular after 10-15 days of contact time, as observed with sample SC429 at 6.8 m depth. The experiments carried out with this sample reached an apparent steady state at $8.1(\pm0.1)\cdot10^{-7}$ mol/l for the dry sample and $7.6(\pm0.1)\cdot10^{-7}$ mol/l for the wet sample, within the same order of

magnitude as the uranium aqueous concentration measured in the pore water ($4.8(\pm0.1)\cdot10^{-7}$ mol/l).

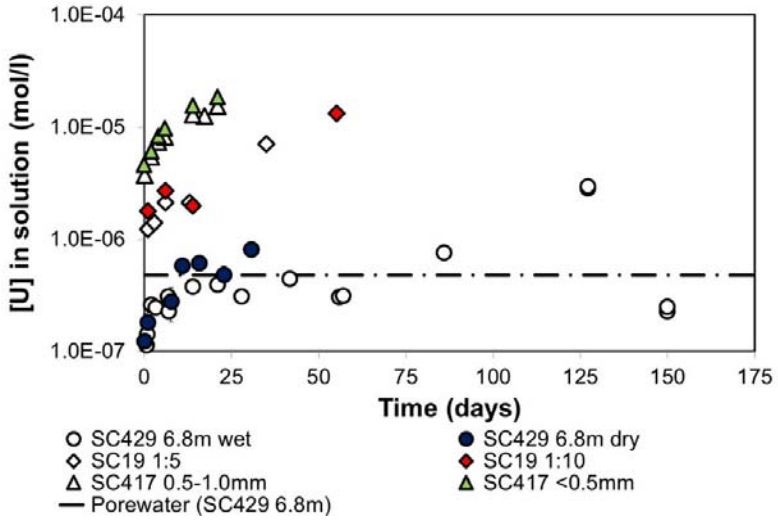

Figure 7.15: Uranium release under batch conditions from samples of sludge.

7.7.3 Tailings

The batch experiments with samples of tailings (Figure 7.16) indicated rapid release to occur during the first 7 to 15 days. The aqueous uranium then stabilised at apparent steady state concentrations of between $4.7(\pm0.1)\cdot10^{-7}$ mol/l (SC429 8.8m dry) and $1.8(\pm0.1)\cdot10^{-6}$ mol/l (SC417b 1:10), one order of magnitude lower than the pore water concentration ($4.7(\pm0.1)\cdot10^{-6}$ mol/l). As observed with samples of other strata, the solid to liquid ratio did not affect the behaviour of uranium release (see sample SC417b). Drying of sample SC429 resulted in higher aqueous uranium concentrations.

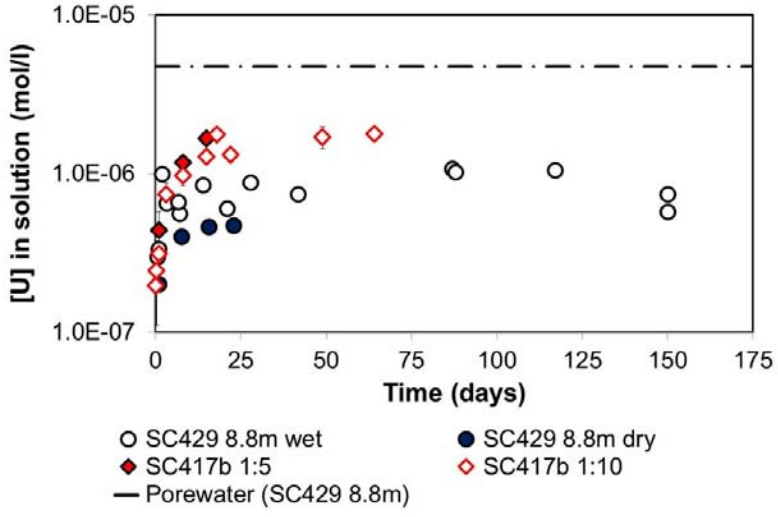

Figure 7.16: Uranium release under batch conditions from samples of tailings

7.7.4 Fraction of uranium released

The total fraction of uranium released from each stratum varied from less than 4.1% for the sludge, between 5.2% and 19.7% for the mixture of soil and sludge and between 4.6% and 30.5% for the tailings (Table 7.5). An increase in the solid to liquid ratio of 1:5 to 1:10 resulted in at least double the fraction of uranium released, increasing from 0.3% to 1.1% in the sample of sludge (SC19) and from 14.1% to 30.5% in the sample of tailings (SC417b). Drying of the samples resulted in an increase of aqueous uranium in the sample of sludge and tailings, however, the opposite effect was observed in the sample of mixture of soil and sludge. The fraction of uranium released from each stratum was noticeably lower than the results obtained by sequential extraction, which indicated at least a 50% release associated with the easily labile fraction, i.e. as adsorbed phase and carbonate minerals.

The uranium release resulted in a partition coefficient, (K_D), at the end of the experiments, of as low as 30 l/kg in the sample of aged tailings (SC417b) and as high as 2,015 l/kg in the sample of aged sludge (SC19). However, initially, the K_D was up to one order of magnitude higher and ranged between 110 l/kg in the sample of aged tailings (SC417b) and 11,600 l/kg in the sample of sludge (SC19). In addition to variation with the experimental contact time, the K_D also varied with pH and alkalinity, which were found to decrease by approximately 1 pH unit and increase by up to 1 mmol/l, respectively, see section 7.3. The partition coefficient was found to vary with the solid to liquid ratio, almost doubling with a decrease in ratio from 1:10 to 1:5. Comparison of the two S:L ratios used indicated similar uranium concentrations in solution at the end of the experiments: $1.33(\pm0.02)\cdot10^{-5}$ and $1.41(\pm0.03)\cdot10^{-5}$ mol/l with the sample of sludge at 1:10 and 1:5, respectively, and $1.78(\pm0.13)\cdot10^{-6}$ and $1.67(\pm0.13)\cdot10^{-6}$ mol/ in the sample of tailings at 1:10 and 1:5, respectively.

7.7.5 Uranium aqueous speciation

The aqueous speciation of uranium in the batch experiments was computed using the Thermochimie database (Giffaut *et al.*, 2014) and the solubility reactions therein as described in Chapter 4.

The geochemical modelling indicated uranium aqueous speciation at the end of the experimental time to be consistently dominated by the calcium-carbonate complexes, $Ca_2UO_2(CO_3)_3$ and $CaUO_2(CO_3)_3^{2-}$ (Figure 7.17). All the samples, regardless of the strata they represented, contained more than 75% of total uranium speciated as $Ca_2UO_2(CO_3)_3$

with the remaining uranium complexed as $CaUO_2(CO_3)_3^{2-}$. Speciation modelling of additional aliquots sampled at other times during the experiments (data not included in Figure 7.17) predicted the same calcium-carbonate complexes. The only exception to this was the sample of dry sludge collected in 2009 where the uranium aqueous speciation comprised uranium-fluoride complexes. The concentration of F measured in the aliquot of this experiment was of $2.8 \cdot 10^{-1}$ mol/l.

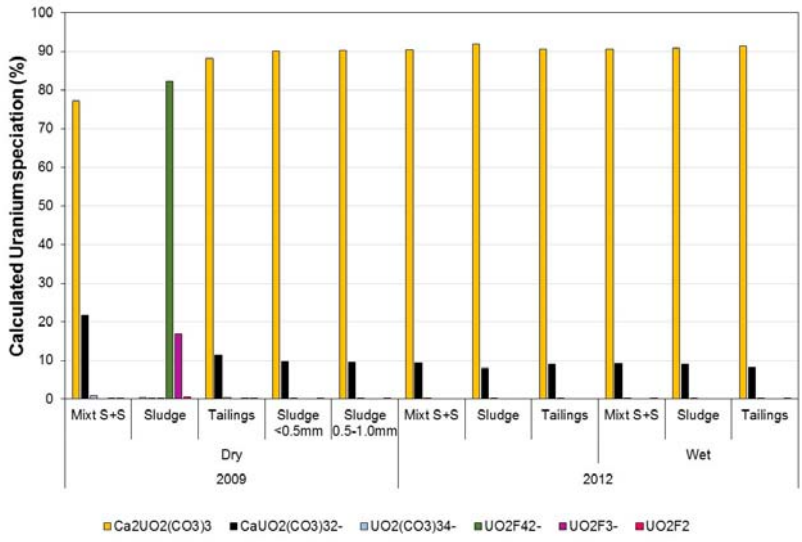

Figure 7.17: Aqueous speciation of uranium in the batch experiments at equilibrium.

7.7.6 Uranium solid speciation

The saturation state of uranium with respect to the main uranium phases found in nature and the uranium phases identified in the characterisation of the samples (Chapter 6) was computed using the Thermochimie database (Giffaut *et al.*, 2014) and the solubility reactions therein. Predicted uranium phases were: uranophane $[Ca(UO_2)2(SiO_3OH)_2.5H_2O]$, $UO_2(OH)_2$(beta), clarkeite $[Na(UO_2)O(OH)]$, schoepite $[UO_3.2H_2O]$, dehydrated schoepite $[UO_3.0.9H_2O]$, becquerelite(nat) $[Ca(UO_2)_6O_4(OH)_6.8H_2O]$, rutherfordine $[UO_2CO_3]$ and soddyite $[(UO_2)_2SiO_4.2H_2O]$. The calculations assumed that uranium was limited by the solubility of one of these phases and were performed using the solution compositions at steady state.

The calculation indicated the solutions to be undersaturated with respect to most uranium minerals (Table 7.6). Uranophane was the uranium mineral closer to equilibrium in most aliquots, including all the samples of sludge and all the samples of tailings. The saturation index of uranophane with respect to the samples of sludge and tailings ranged from -3.1 to +0.6 and from -3.7 to -2.1, respectively. The samples of mixture of soil and sludge

were close to equilibrium with different phases: although the fresh wet sample (SC429 3.0m wet) was closer to equilibrium with uranophane, the same sample when dried (SC429 3.0m dry) appeared to be closer to equilibrium with becquerelite. The aged sample of mixture of soil and sludge (SC30), in turn, was closer to equilibrium with dehydrated schoepite (SI=-0.5) and with $UO_2(OH_2)$(beta) (SI=-0.4).

A comparison of the experimentally determined aqueous concentration of uranium with the predicted concentrations of uranium in equilibrium with uranophane, dehydrated schoepite and becquerelite, under the experimental conditions at steady state, is presented in Figure 7.18. The figure shows the concentration of uranium in the dry sample SC429 3.0m ($2.9 \cdot 10^{-5}$ mol/l) to be very close to the equilibrium concentration with becquerelite ($3.3 \cdot 10^{-5}$ mol/l), while the aqueous concentration of uranium in sample SC30 ($2.4 \cdot 10^{-5}$ mol/l) was closer to the calculated concentration in equilibrium with dehydrated schoepite ($3.9 \cdot 10^{-5}$ mol/l). The remaining samples indicated aqueous concentrations close to the calculated equilibrium with uranophane.

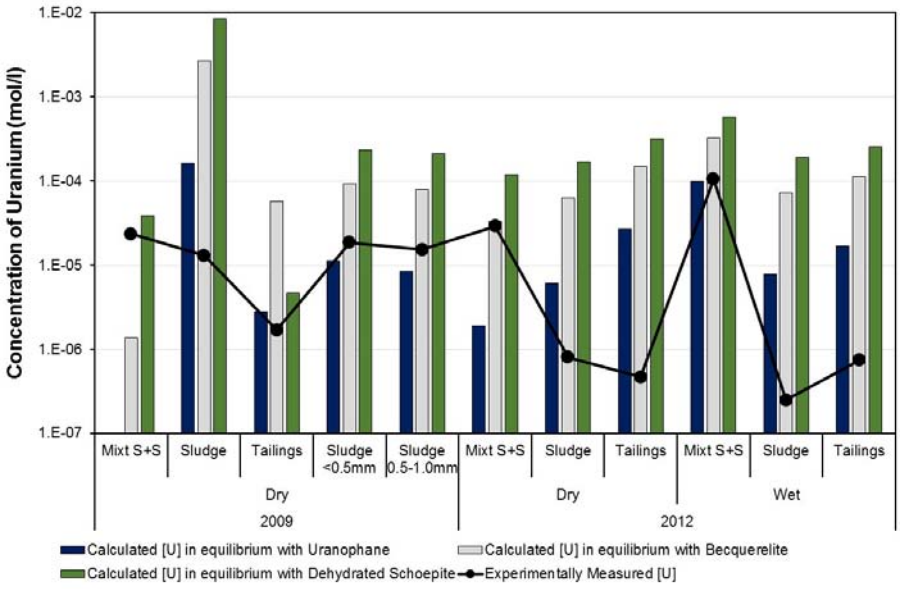

Figure 7.18: Experimentally measured concentration of uranium and uranium concentration calculated to be in equilibrium with uranophane, becquerelite and dehydrated schoepite.

Table 7.5: Fraction of uranium released from batch experiments.

Group		Sample	Strata	S:L Ratio	[U] in sample (mg/kg)	U in solution (mol/l)	Total U release (%)	Partition coefficient, K_D(l/kg)	
								Min	Max
2009	Dry	SC30 0-2.15m	Mix. S + S	1:10	484 ± 88.4	$3.60\ (\pm0.03)\cdot10^{-5}$	17.9	46	647
	Dry	SC19 2.5-3.8m	Sludge	1:10	3390.4 ± 326.9	$1.33\ (\pm0.02)\cdot10^{-5}$	1.1	1060	7998
	Dry	SC19 2.5-3.8m	Sludge	1:5	3390.4 ± 326.9	$1.41\ (\pm0.03)\cdot10^{-5}$	0.3	2015	11600
	Dry	SC417b 8.2-10.2m	Tailings	1:10	14.1 ± 0.5	$1.78\ (\pm0.13)\cdot10^{-6}$	30.5	23	315
	Dry	SC417b 8.2-10.2m	Tailings	1:5	14.1 ± 0.5	$1.67\ (\pm0.13)\cdot10^{-6}$	14.1	30	129
	Dry	SC417a <0.5 mm	Sludge	1:10	2150.1 ± 104.5	$1.86\ (\pm0.03)\cdot10^{-5}$	2.1	475	1956
	Dry	SC417a 0.5 – 1.0 mm	Sludge	1:10	1636.2 ± 150.8	$1.54\ (\pm0.03)\cdot10^{-5}$	2.2	437	1841
2012	Dry	SC429 3.0 m	Mix. S + S	1:10	1425.1 ± 20.6	$2.91\ (\pm0.02)\cdot10^{-5}$	5.2	181	826
	Dry	SC429 6.8 m	Sludge	1:10	58.0 ± 1.8	$8.06\ (\pm0.07)\cdot10^{-7}$	4.1	236	1962
	Dry	SC429 8.8 m	Tailings	1:10	21.6 ± 1.2	$4.72\ (\pm0.05)\cdot10^{-7}$	4.6	182	443
	Wet	SC429 3.0 m	Mix. S + S	1:10	1425.1 ± 20.6	$1.06\ (\pm0.11)\cdot10^{-4}$	19.7	38	245
	Wet	SC429 6.8 m	Sludge	1:10	58.0 ± 1.8	$2.29\ (\pm0.02)\cdot10^{-7}$	1.8	307	2134
	Wet	SC429 8.8 m	Tailings	1:10	21.6 ± 1.2	$7.44\ (\pm0.07)\cdot10^{-7}$	9.9	74	292

Table 7.6: Saturation indices of uranium phases at steady state.

Group		Sample	Strata	Solid : Liquid Ratio	Uranophane	$UO_2(OH)_2$(beta)	Clarkeite	Schoepite	Schoepite (des)	Becquerelite	Rutherfordine	Soddyite (synt 1)
2009	Dry	SC30 0-2.15m	Mix. S + S	1:10	6.6	-0.4	1.9	-1.6	**-0.5**	10.8	-2.6	2.2
	Dry	SC19 2.5-3.8m	Sludge	1:10	**-2.2**	-4.7	-2.7	-5.9	-4.8	-15.3	-6.1	-6.5
	Dry	SC417b 8.2-10.2m	Tailings	1:10	**-2.1**	-3.6	-1.7	-4.8	-3.7	-9.1	-4.7	-5.2
	Dry	SC417a <0.5 mm	Sludge	1:10	**0.5**	-3.2	-2.7	-4.2	-3.2	-6.6	-3.8	-3.1
	Dry	SC417a 0.5 – 1.0 mm	Sludge	1:10	**0.6**	-3.2	-2.6	-4.2	-3.2	-6.4	-3.8	-3.1
2012	Dry	SC429 3.0 m	Mix. S + S	1:10	3.0	-2.3	-1.5	-3.3	-2.4	**-0.6**	-3.6	-1.3
	Dry	SC429 6.8 m	Sludge	1:10	**-1.8**	-4.4	-3.8	-5.4	-4.5	-13.9	-5.1	-5.5
	Dry	SC429 8.8 m	Tailings	1:10	**-3.7**	-5.1	-4.7	-6.1	-5.2	-18.6	-5.3	-7.0
	Wet	SC429 3.0 m	Mix. S + S	1:10	**0.1**	-3.1	-2.9	-4.1	-3.1	-6.5	-3.0	-2.8
	Wet	SC429 6.8 m	Sludge	1:10	**-3.1**	-5.0	-4.3	-6.0	-5.0	-17.4	-5.6	-6.7
	Wet	SC429 8.8 m	Tailings	1:10	**-2.9**	-4.8	-4.3	-5.8	-4.8	-16.3	-5.1	-6.2

Uranium phases closer to equilibrium (ie with a saturation index of zero), are highlighted in bold and red

7.7.7 Mineral dissolution

The pH and Eh conditions measured in the batch experiments, as well as the calculation of the uranium aqueous complexation, pointed to an aqueous uranium speciation in the oxidised form, U(VI). Considering that dissolution of a uranium mineral is occurring in the batch experiments, the dissolution of a uranium phase to aqueous U(VI) can be described as:

$$Umineral + H_2O \underset{k_{-1}}{\overset{k_1}{\rightleftharpoons}} U(VI) \quad \textbf{(7.4)}$$

Where $Umineral$ is the uranium solid phase, $U(VI)$ represents total dissolved uranium and k_1 and k_{-1} are the equilibrium constants for the forward and backward reactions, respectively. The rate equation can be written as:

$$\frac{dU(VI)}{dt} = k_1 - k_{-1}[U(VI)] \quad \textbf{(7.5)}$$

By derivation, the evolution of the concentration of aqueous uranium with time, $[U(VI)]_{(t)}$, is given by:

$$[U(VI)]_{(t)} = (e^{-k_{-1}t})[U(VI)_0] + \frac{k_1}{k_{-1}}(1 - e^{-k_{-1}t}) \quad \textbf{(7.6)}$$

Where $[U(VI)_0]$ is the initial concentration of uranium in solution and can be conceptualised as the uranium release corresponding to surface sorbed uranium being released within the first minutes or hours of batch elution.

The parameters k_1, k_{-1} and $[U(VI)_0]$ were obtained by fitting expression (7.6) to the uranium concentrations measured in the experiments, as shown in Figure 7.19 to Figure 7.21, and the parameters obtained are presented in Table 7.7. The value of the forward rate constant, k_1, was normalised to the total surface area of the sample (refer to Chapter 6 for the results of surface area analysis). Unfortunately, the surface area of some of the dry samples was not measured as these samples were not available in the laboratory where the EGME sorption experiments were carried out. These were samples SC30 (mixture of soil and sludge), SC19 (sludge) and SC417b (tailings). Due to the

heterogeneity of all the strata of waste, it was not considered appropriate to make any assumption with regards to the surface area of these samples and the rate constants were not normalised for these samples.

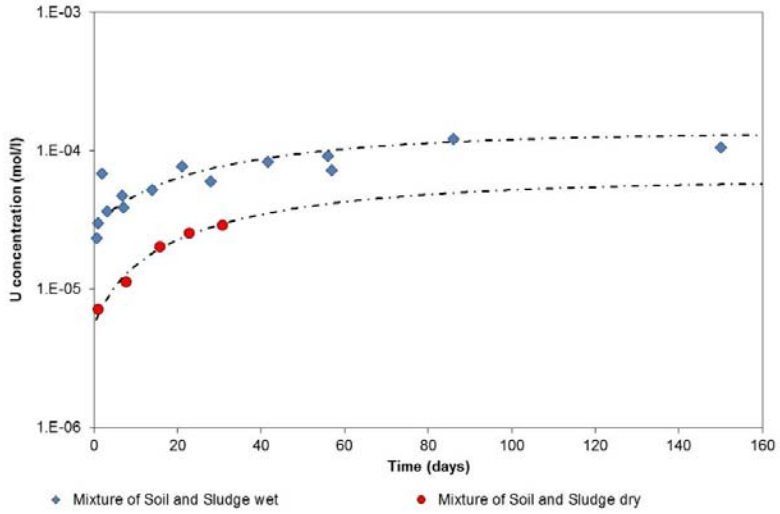

Figure 7.19: Experimental results (points) for the samples of mixture of soil and sludge and fitting with expression (7.6) (dashed lines).

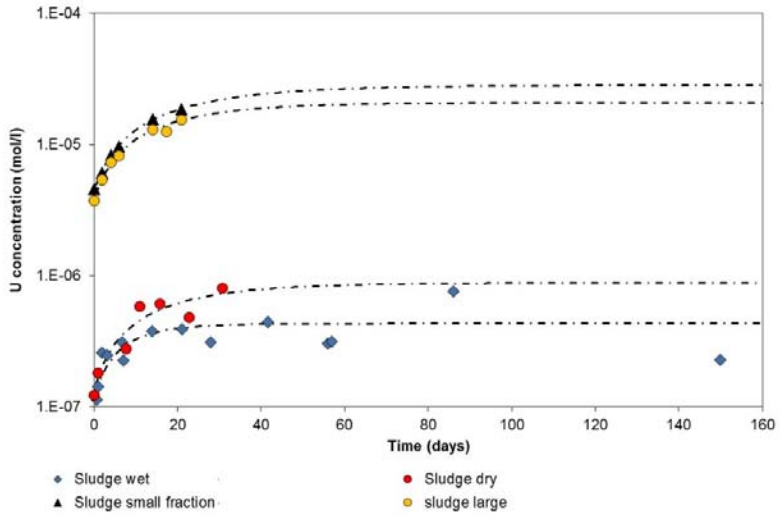

Figure 7.20: Experimental results (points) for the samples of sludge and fitting with expression (7.6) (dashed lines).

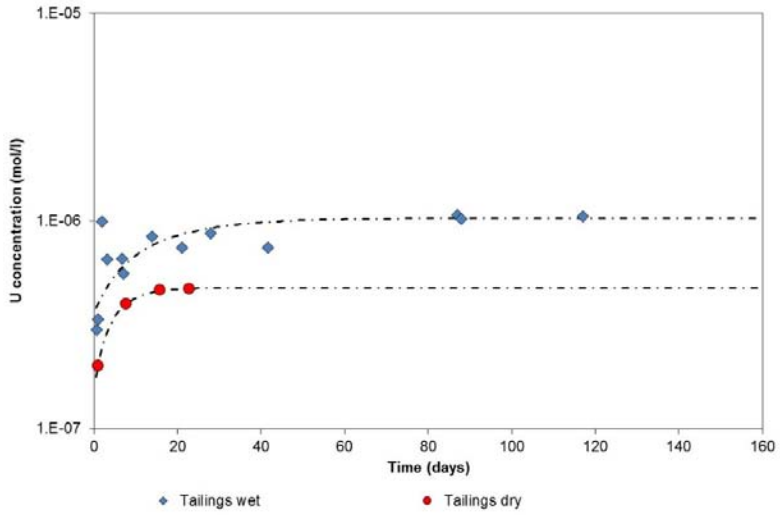

Figure 7.21: Experimental results (points) for the samples of tailings and fitting with expression (7.6) (dashed lines).

The fitted forward rate constant was faster, by at least one order of magnitude, in the fresh samples of mixture of soil and sludge and in the aged samples of sludge (10^{-10} – 10^{-11} mol/m^2.day). The forward rate constant was approximately 10^{-12} mol/m^2.day in the fresh samples of sludge and tailings. Drying of a sample did not affect the value of k_1, within the measured uncertainty. The apparent rate constant (k_1 in mol/l.day) appeared to be similar for both the small (<0.5 mm) and large (0.5 – 1.0 mm) particle sizes of sample SC417a. However, once normalized (k_1 in mol/m^2.day), the forward rate constant was one order of magnitude faster in the sample with small particle size.

Table 7.7: Fitted initial concentration of uranium ($U(VI)_0$), forward (k_1) and backward (k_{-1}) rates for uranium phase dissolution, and the goodness of fit (adjusted r^2).

Strata	Sample / Experimental conditions	$U(VI)_0$ (fitted) (mol/l)	$U(VI)_0$ measured* (mol/l)	k_1 (mol/l.day)	k_1 (mol/m².day)	k_{-1} (day^{-1})	r^2
Mixt. Soil and Sludge	**SC429 3.0 m** Fresh (2012) - Wet	$2.8(\pm0.6)\cdot10^{-5}$	$2.3(\pm0.4)\cdot10^{-5}$	$2.3\ (\pm1.0)\cdot10^{-6}$	$1.5\ (\pm0.6)\cdot10^{-10}$	$2.4\ (\pm0.9)\cdot10^{-2}$	0.8711
	SC429 3.0 m Fresh (2012) - Dry	$5.4(\pm1.6)\cdot10^{-6}$	$7.2(\pm0.1)\cdot10^{-6}$	$1.1\ (\pm1.4)\cdot10^{-6}$	$6.3\ (\pm7.5)\cdot10^{-11}$	$1.9\ (\pm1.9)\cdot10^{-2}$	0.9752
Sludge	**SC429 6.8 m** Fresh (2012) - Wet	$1.1(\pm0.3)\cdot10^{-7}$	$1.1(\pm0.3)\cdot10^{-7}$	$4.8\ (\pm2.2)\cdot10^{-8}$	$2.4\ (\pm1.1)\cdot10^{-12}$	$1.1\ (\pm0.5)\cdot10^{-1}$	0.8423
	SC429 6.8 m Fresh (2012) - Dry	$1.3(\pm1.0)\cdot10^{-7}$	$1.2(\pm0.1)\cdot10^{-7}$	$4.6\ (\pm5.4)\cdot10^{-8}$	$2.3\ (\pm2.7)\cdot10^{-12}$	$5.2\ (\pm5.7)\cdot10^{-2}$	0.7425
	SC417a <0.5 mm Aged (2009) - Dry	$4.4(\pm0.2)\cdot10^{-6}$	$4.6(\pm0.1)\cdot10^{-6}$	$1.2\ (\pm0.3)\cdot10^{-6}$	$1.6\ (\pm0.6)\cdot10^{-10}$	$5.4\ (\pm0.9)\cdot10^{-2}$	0.9977
	SC417a 0.5 – 1.0 mm Aged (2009) - Dry	$3.7(\pm0.2)\cdot10^{-6}$	$3.7(\pm0.1)\cdot10^{-6}$	$1.1\ (\pm0.2)\cdot10^{-6}$	$2.3\ (\pm0.5)\cdot10^{-11}$	$4.4\ (\pm0.9)\cdot10^{-2}$	0.9993
Tailings	**SC429 8.8 m** Fresh (2012) - Wet	$3.5(\pm0.7)\cdot10^{-7}$	$3.0(\pm0.1)\cdot10^{-7}$	$6.8\ (\pm2.1)\cdot10^{-8}$	$7.1\ (\pm2.4)\cdot10^{-12}$	$1.9\ (\pm0.1)\cdot10^{-1}$	0.9993
	SC429 8.8 m Fresh (2012) - Dry	$1.4(\pm0.1)\cdot10^{-7}$	$2.0(\pm0.1)\cdot10^{-7}$	$8.6\ (\pm0.9)\cdot10^{-8}$	$9.4\ (\pm1.5)\cdot10^{-12}$	$6.6\ (\pm2.0)\cdot10^{-2}$	0.9752

$U(VI)_0$ experimental concentration < 1 day contact time. All experiments carried out at S:L of 1:10

7.7.7.1 Dependency of forward rate constant with uranium content

The value of k_1 was found to be higher for higher concentrations of uranium in the solid (Figure 7.22). In the case of the samples analysed, the fresh samples of mixture of soil and sludge contained elevated concentrations of uranium (1,420 mg/kg), resulting in a fast forward rate, while the fresh samples of sludge had a relatively low content of uranium (60 mg/kg) and slower forward rate. Given the heterogeneity of the waste, it would be expected that the release of uranium under field conditions could range by at least two orders of magnitude (between 10^{-10} and 10^{-12} mol/m^2.day) within these two strata, under conditions similar to the experimental conditions. The concentration of uranium in the sample of tailings in the experiments (22 mg/kg) was slightly lower than the average concentration in the strata of tailings measured by Bary and co-workers (2010) (134 mg/kg). It is possible that the release rates of uranium in the tailings under field conditions are higher than the rates observed in the experiments.

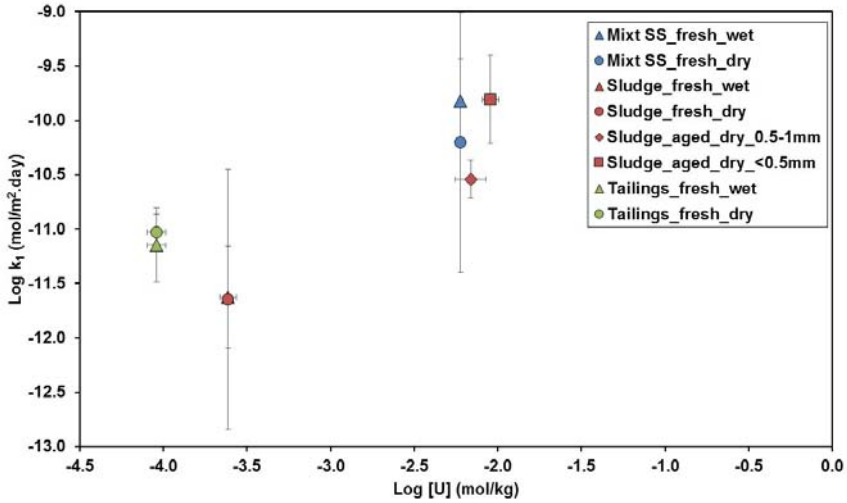

Figure 7.22: Dependency of the log forward rate constant (k_1) and the log concentration of uranium in the solid sample at the start of the experiments (error bar in uranium concentrations represent analytical error; error bar in k_1 represents 95% confidence as calculated from fitting of expression (7.6). All experiments carried out at 1:10 solid to liquid ratio.

7.7.7.2 Dependency of rate constants with dissolved calcium concentrations

The initial concentration of dissolved calcium appeared to affect the release of uranium from the samples. Figure 7.23 presents the calculated forward rate constants and the concentration of dissolved calcium measured in the first experimental point, collected at 1 day of contact time. Decreasing values of forward rate constants were obtained for increasing concentrations of dissolved calcium, in agreement with the process of dissolution of a calcium containing uranium phase, such as uranophane [$Ca(UO_2)_2(SiO_3OH)_2.5H_2O$], which would dissolve faster for lower concentrations of calcium in solution.

The experimental concentrations of aqueous calcium are expected to result from a multitude of dissolution and ion exchange processes of the various solid phases contained in the samples. Although not all calcium in solution would arise from dissolution of a uranium phase, aqueous calcium concentrations could be applied to the dissolution rate model of uranium under the experimental conditions.

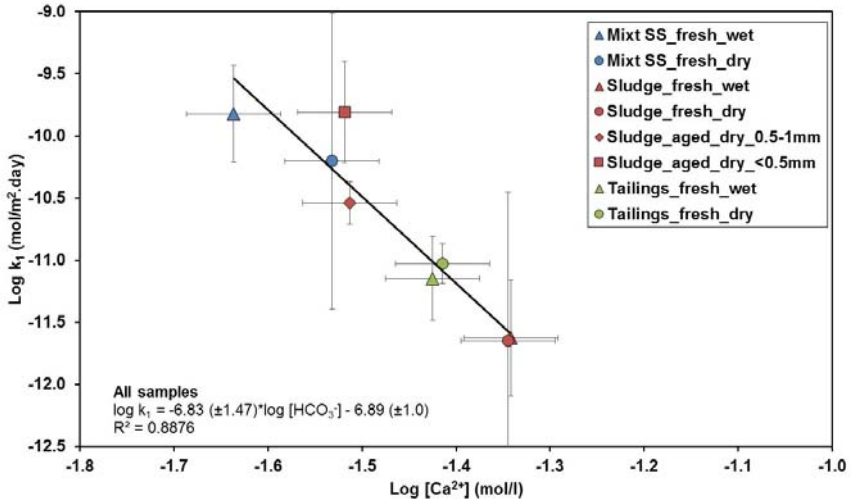

Figure 7.23: Dependency of the log forward rate constant (k_1) and log dissolved calcium concentration (error bar in calcium concentrations calculated as 5% of the analytical measurement; error bar in k_1 represents 95% confidence as calculated from fitting of expression (7.6). All experiments carried out at 1:10 solid to liquid ratio.

7.7.7.3 Dependency of rate constants with dissolved bicarbonate concentrations

The increase in uranyl mineral dissolution rate with increasing bicarbonate concentrations has been observed for uranophane (Pérez *et al.*, 2000); soddyite (Pérez *et al.*, 1997); uranyl oxyhydroxides, including metaschoepite and becquerelite (Sowder, Clark and Fjeld, 2001); and $UO_3.H_2O$ and U_3O_8 (Steward and Mones, 1996). The kinetics of dissolution of uranium minerals in bicarbonate solutions have been described as first order. Pérez and co-workers (2000) derived a rate expression proportional to carbonate concentration ($[HCO_3^-]^{0.7}$) for uranophane dissolution in batch and stirred flow systems. Steward and Mones (1996) obtained a rate order of 0.65 with respect to total carbonate concentration from a regression analysis of the measured rates of uranyl oxyhydroxides dissolution in bicarbonate solutions. Liu and co-workers (2004) observed a 15 time increase in the dissolution rate of U(VI) from Hanford sediments when the bicarbonate activity increased by 17-20 times.

In general, the forward rate constant appeared to be independent of the initial concentration of bicarbonate in solution (Figure 7.24). However, in the case of the samples of fresh sludge and tailings, increasing concentrations of bicarbonate resulted in increasing forward rates. The forward rate for these samples can be expressed proportionally to bicarbonate concentrations, as $[HCO_3^-]^{1.5}$.

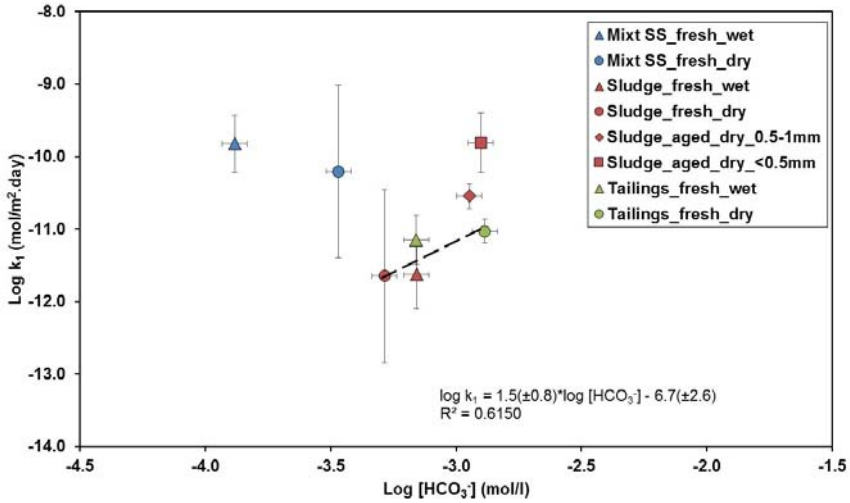

Figure 7.24: Dependency of the log forward rate constant (k_1) and the log dissolved bicarbonate concentration (error bar in bicarbonate concentrations represent analytical error; error bar in k_1 represents 95% confidence as calculated from fitting of expression (7.6). All experiments carried out at 1:10 solid to liquid ratio.

7.7.7.4 Dependency of rate constants with pH

Proton-promoted dissolution of oxide and silicate minerals is extensively described in the literature (Wieland, Wehrli and Stumm, 1988). However, no relationship between pH and either the forward (Figure 7.25) or the backward (Figure 7.26) rates was observed in the experimental results.

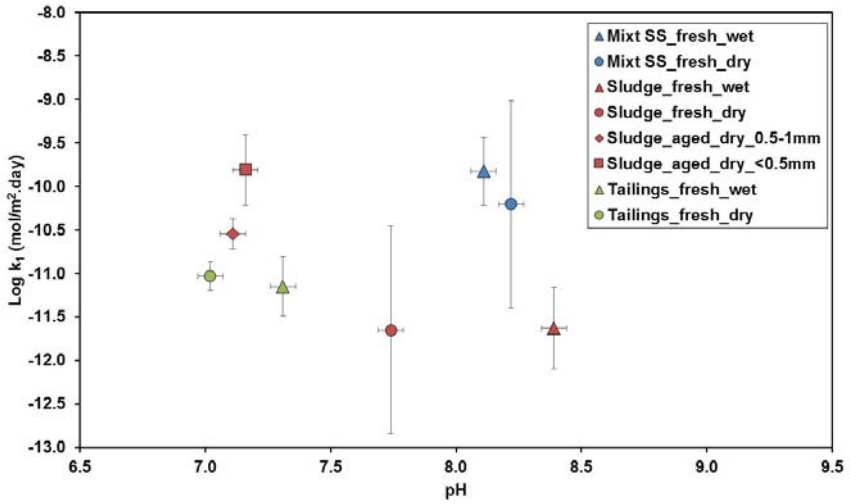

Figure 7.25: Dependency of the log forward rate constant (k_1) and pH (error bar in calcium concentrations calculated as 5% of the analytical measurement; error bar in k_1 represents 95% confidence as calculated from fitting of expression (7.6)). All experiments carried out at 1:10 solid to liquid ratio.

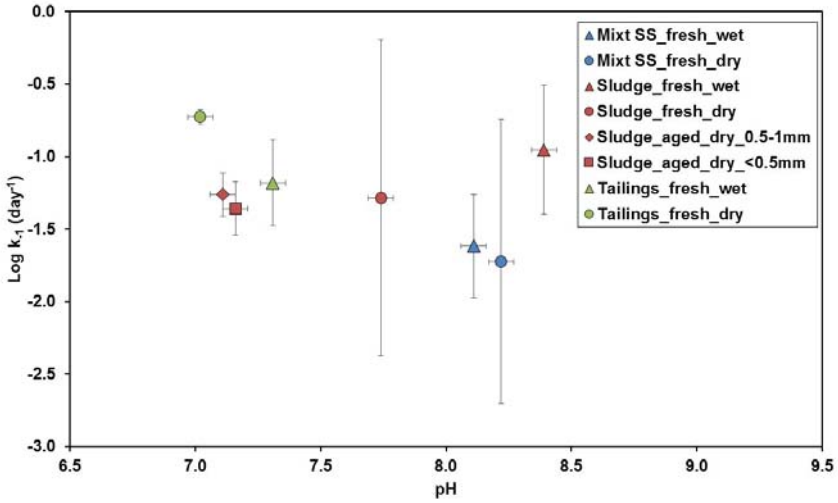

Figure 7.26: Dependency of the log backward rate constant (k_{-1}) and pH (error bar in calcium concentrations calculated as 5% of the analytical measurement; error bar in k_{-1} represents 95% confidence as calculated from fitting of expression (7.6)). All experiments carried out at 1:10 solid to liquid ratio.

7.7.7.5 Dependency of rate constants with other parameters

A relation between the dissolved concentrations of silicon and the rate constants could not be considered. This element was not quantified in most of the experiments (as it was below the equipment detection limit operated in semi-quantitative mode). Dissolved silicon concentrations used in speciation modelling were based in equilibrium with amorphous SiO_2.

7.7.7.6 Predicted equilibrium of dissolved uranium concentrations

The aqueous concentrations of uranium at steady state (for time tending to ∞) are given by the ratio of forward and backward rates of reaction, resulting from substituting for infinite time in equation 7.6:

$$[U]_{\infty} = \frac{k_1}{k_{-1}} \left(\frac{mol}{l}\right) \qquad \textbf{(7.7)}$$

The calculated steady state concentrations vary between $\log[U]_{\infty} = -3.5$ and $\log[U]_{\infty} = -5$ in the samples of mixture of soil and sludge and between $\log[U]_{\infty} = -6.5$ and $\log[U]_{\infty} = -5$ in the samples of sludge and in the samples of tailings (Table 7.8). These values, which can be taken as experimentally derived equilibrium constants are within the values for solubility constants of uranium oxides and silicates reported in the literature. Log K

values have been reported as 6.2±0.5 (Moll et al, 1992) and 5.7±0.2 (Nguyen et al, 1992) for soddyite and 5.38 (Gustafsson, 2007) for schoepite. The solubility constant for uranophane has been reported as 7.8±0.8 (Casas et al, 1994), 9.4±0.5 (Nguyen et al, 1992), 11.0±0.1 (Prikryl, 2008) and log K = 11.7±0.6 (Perez et l, 2000). The experimental values are likely to represent the equilibrium reached by various uranium phases simultaneously rather than represent one single phase.

Table 7.8: Calculated Log K value and uranium concentration at steady state.

Strata	Sample / Experimental conditions		$K = k_1/k_{-1}$ (mol/l)	Log K
Mixture of Soil and Sludge	**SC429 3.0 m**	Fresh (2012) - Wet	$1.1 (\pm 0.6) \cdot 10^{-4}$	-4.0 (±0.5)
	SC429 3.0 m	Fresh (2012) - Dry	$6.1 (\pm 9.3) \cdot 10^{-5}$	-4.2 (±1.5)
	SC30	Aged (2009) - Dry	$1.3 (\pm 0.2) \cdot 10^{-5}$	-4.9 (±0.1)
Sludge	**SC429 6.8 m**	Fresh (2012) - Wet	$4.3 (\pm 2.8) \cdot 10^{-7}$	-6.4 (±0.6)
	SC429 6.8 m	Fresh (2012) - Dry	$8.8 (\pm 14.3) \cdot 10^{-7}$	-6.1 (±1.6)
	SC417a <0.5 mm	Aged (2009) - Dry	$2.8 (\pm 0.8) \cdot 10^{-5}$	-4.6 (±0.3)
	SC417a 0.5 – 1.0 mm	Aged (2009) - Dry	$2.1 (\pm 0.5) \cdot 10^{-5}$	-4.7 (±0.2)
Tailings	**SC429 8.8 m**	Fresh (2012) - Wet	$1.0 (\pm 0.4) \cdot 10^{-6}$	-6.0 (±0.4)
	SC429 8.8 m	Fresh (2012) - Dry	$4.8 (\pm 0.3) \cdot 10^{-7}$	-6.3 (±0.1)
	SC417b	Aged (2009) - Dry	$1.2 (\pm 0.8) \cdot 10^{-6}$	-5.9 (±0.6)

7.8 Thorium release under batch conditions

The liquid aliquots of the batch experiments were analysed for Th by ICP-MS. The isotope analysed was ^{232}Th, which has a natural abundance of more than 99%. The analysis of ^{230}Th by alpha-spectrometry was considered. However, preliminary calculations indicated that the required measuring times for each aliquot would be between 1 and 2 months, ruling this methodology out based on timescale constraints. Thorium was below the detection limit of $1.7 \cdot 10^{-10}$ mol/l on a large fraction of the aliquots. Where the thorium concentrations were above the detection limit, these are presented in Figure 7.27.

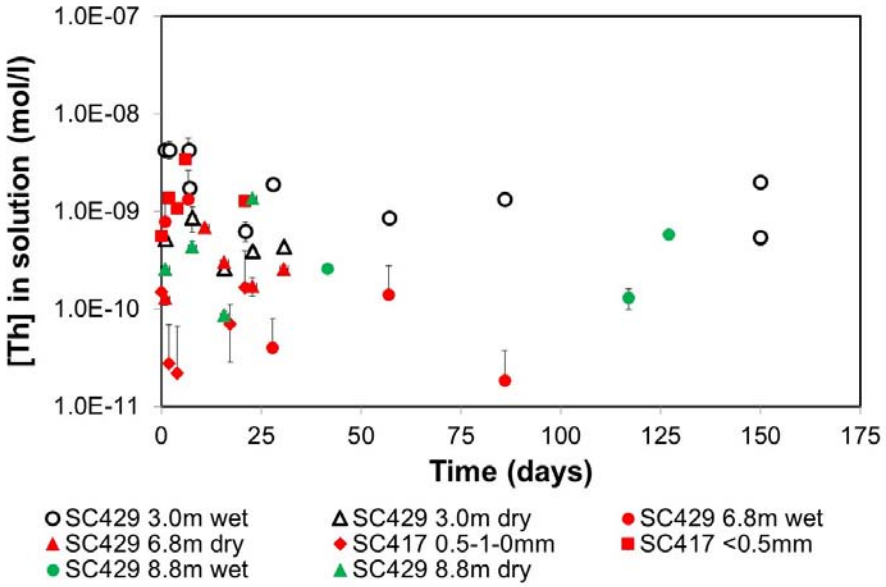

Figure 7.27: Thorium release under batch conditions.

The release of thorium appeared to be slightly higher at the start of the experiments, with aqueous concentrations rapidly decreasing within 7-15 days to remain at or below the detection limit. The behaviour observed, with negative rates, indicated an instantaneous release of thorium from the sample to the liquid phase, followed by retention of thorium back onto the solid fraction. The strong particle-activity of thorium, described by many authors (Santschi et al., 2006 and references therein), was likely responsible for this behaviour. Drying of the sample resulted in lower aqueous concentrations at the end of the experiments for the sample of mixture of soil and sludge ($2.01(\pm0.15)\cdot10^{-9}$ mol/l was reduced to $4.31(\pm0.13)\cdot10^{-10}$ mol/l) but had almost no effect in the sample of sludge ($4.31(\pm0.19)\cdot10^{-10}$ mol/l was reduced to $2.59(\pm0.18)\cdot10^{-10}$ mol/l). However, it resulted in an increase in aqueous concentrations in the sample of tailings ($1.29\ (\pm0.31)\cdot10^{-10}$ mol/l was increased to $1.38(\pm0.07)\cdot10^{-9}$ mol/l). Final aqueous concentrations were similar for both particle sizes of the sample of sludge ($1.29(\pm0.23)\cdot10^{-9}$ mol/l for the fraction <0.5 mm and $1.72(\pm0.17)\cdot10^{-9}$ mol/l for the fraction 0.5-1.0 mm).

7.8.1 Fraction of thorium release

The total fraction of thorium released from each strata was less than 1% with the higher fraction (0.041%) released from the dry sample of tailings (Table 7.9). The results contrast with the sequential extraction experiments where between 20 and 30% total thorium was easily labile as surface sorbed and carbonate complexes. The elevated

partition coefficient values calculated, of between 51,640 and 2,924,006 l/kg, indicate thorium to be essentially immobile under the experimental conditions.

7.8.2 Thorium aqueous speciation

Thorium aqueous speciation in the batch experiments comprised predominantly of thorium carbonates and oxyhydroxides in the fresh wet and fresh dry samples (Figure 7.28). The thorium carbonate complexes, $Th(OH)_3(CO_3)^-$ and $Th(OH)_2(CO_3)_2^{2-}$, comprised more than 50% of total thorium in solution, with thorium hydroxides $Th(OH)_4$, $Th(OH)^{3+}$ and $Th(OH)_2^{2+}$ comprising the remaining speciation. Thorium fluorides, mainly ThF_4, comprised between 10 and 20% of aqueous speciation in the fresh wet samples of mixture of soil and sludge and tailings and 3-4% of total thorium in solution in the two particle sizes of the aged sample of sludge.

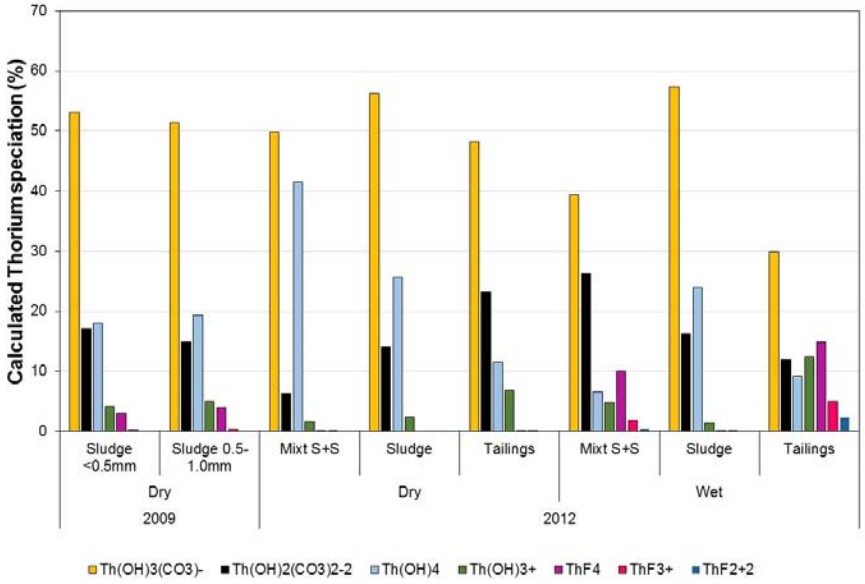

Figure 7.28: Aqueous speciation of thorium in the batch experiments at equilibrium.

7.8.3 Thorium solid speciation

Calculation of the saturation for the main thorium phases found in nature, i.e. the thorium oxyhydroxides $ThO_{2(aged)}$ and $ThO_{2(fresh)}$, indicated thorium phases to remain generally undersaturated (Table 7.10 and Figure 7.29). $ThO_{2(aged)}$ was predicted to be near equilibrium in the fresh dry and fresh wet samples of mixture of soil and sludge as well as in the aged samples of sludge. $ThO_{2(fresh)}$ was near equilibrium in the aged samples of mixture of soil and sludge.

Table 7.9: Fraction of Th released from batch experiments.

Group		Sample	Strata	S:L Ratio	[Th] in sample (mg/kg)	Th in solution (mol/l)	Total Th release (%)	Partition coefficient, K_D (l/kg)	
								Min	Max
2009	Dry	SC30 0-2.15m	Mix. S + S	1:10	9.0 ± 2.7	<DL	<DL	-	-
	Dry	SC19 2.5-3.8m	Sludge	1:10	47.2 ± 133.6	<DL	<DL	-	-
	Dry	SC19 2.5-3.8m	Sludge	1:5	47.2 ± 133.6	<DL	<DL	-	-
	Dry	SC417b 8.2-10.2m	Tailings	1:10	3.7 ± 1.5	<DL	<DL	-	-
	Dry	SC417b 8.2-10.2m	Tailings	1:5	3.7 ± 1.5	<DL	<DL	-	-
	Dry	SC417a <0.5 mm	Sludge	1:10	117.0 ± 24.0	$1.29\ (\pm 0.23)\cdot 10^{-9}$	0.003	389,859	2,924,006
	Dry	SC417a 0.5 – 1.0 mm	Sludge	1:10	73.8 ± 17.8	$1.72\ (\pm 0.17)\cdot 10^{-9}$	0.005	184,538	1,230,307
2012	Dry	SC429 3.0 m	Mix. S + S	1:10	38.4 ± 0.7	$4.31\ (\pm 0.13)\cdot 10^{-10}$	0.003	192,078	640,283
	Dry	SC429 6.8 m	Sludge	1:10	10.3 ± 1.0	$2.59\ (\pm 0.18)\cdot 10^{-10}$	0.006	64,556	344,343
	Dry	SC429 8.8 m	Tailings	1:10	7.7 ± 0.8	$1.38\ (\pm 0.07)\cdot 10^{-9}$	0.041	24,132	386,269
	Wet	SC429 3.0 m	Mix. S + S	1:10	38.4 ± 0.7	$2.01\ (\pm 0.15)\cdot 10^{-9}$	0.014	82,253	960,428
	Wet	SC429 6.8 m	Sludge	1:10	10.3 ± 1.0	$4.31\ (\pm 0.19)\cdot 10^{-10}$	0.007	51,640	258,246
	Wet	SC429 8.8 m	Tailings	1:10	7.7 ± 0.8	$1.29\ (\pm 0.31)\cdot 10^{-10}$	0.006	193,127	386,266

Table 7.10: Saturation indices of thorium phases at steady state.

Group		Sample	Strata	Solid : Liquid Ratio	$ThO_{2(aged)}$	$ThO_{2(fresh)}$	$ThO_{2(coll)}$
2009	Dry	SC30 0-2.15m	Mix. S + S	1:10	1.22	0.42	-1.38
	Dry	SC19 2.5-3.8m	Sludge	1:10	-6.47	-7.27	-9.07
	Dry	SC417b 8.2-10.2m	Tailings	1:10	-1.74	-2.54	-4.34
	Dry	SC417a <0.5 mm	Sludge	1:10	-0.91	-1.71	-3.51
	Dry	SC417a 0.5 – 1.0 mm	Sludge	1:10	-0.58	-1.38	-3.18
2012	Dry	SC429 3.0 m	Mix. S + S	1:10	-0.85	-1.65	-3.45
	Dry	SC429 6.8 m	Sludge	1:10	-1.28	-2.08	-3.88
	Dry	SC429 8.8 m	Tailings	1:10	-0.90	-1.70	-3.50
	Wet	SC429 3.0 m	Mix. S + S	1:10	-0.98	-1.78	-3.58
	Wet	SC429 6.8 m	Sludge	1:10	-1.76	-2.56	-4.36
	Wet	SC429 8.8 m	Tailings	1:10	-1.90	-2.70	-4.50

Thorium concentrations in the aliquots of samples of sludge and mixture of soil and sludge were generally within the region for the onset of colloid formation (Altmaier, Neck and Fanghänel, 2004). Concentrations in the samples of tailings were below the onset of colloid formation (Figure 7.29). These results are in agreement with Section 7.2.2, which indicated the possible presence of colloids in the samples of sludge and mixture of soil and sludge but not in the samples of tailings.

It is likely that thorium in solution is controlled by equilibrium between the solid phase (a Th-oxyhydroxide phase), truly dissolved aqueous phases (Th-carbonate and Th-oxyhydroxide complexes) and Th-colloids.

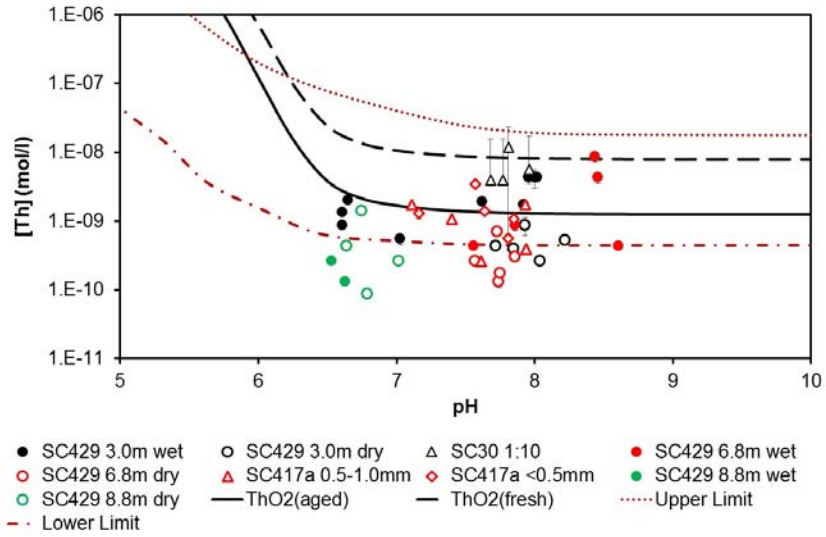

Figure 7.29: Thorium release under batch conditions from the strata of mixture of soil and sludge (black symbols), sludge (red symbols) and tailings (green symbols). The stability limit of ThO_2(aged) and ThO_2(fresh) is shown as calculated for the aliquot composition at the end of the batch experiment with fresh wet sludge. Lower and Upper Limit represent the limits for onset of colloid formation (Altmaier, Neck and Fanghänel, 2004).

7.9 Conclusions relating to the batch experimental results

7.9.1 Uranium

The release of uranium under experimental conditions indicated that a small fraction of uranium is adsorbed to the sample matrix. This fraction is released to solution within the first hour of experimental time and is followed by the slow dissolution of a uranium mineral, which contributes to the remaining of the aqueous uranium in solution. In addition, the steady state concentrations of uranium in solution appear to be controlled by the solubility of a uranium mineral. The solid phases controlling uranium release are likely uranium-oxides and uranium-silicates.

The rate of release of uranium was found to increase with increasing concentrations of bicarbonate in solution and decrease with increasing aqueous concentrations of calcium. No dependence of the rate on the solution pH was observed, nonetheless, the pH will have an indirect effect on uranium dissolution via bicarbonate concentrations. The values of pH under the experimental conditions, pH 6 to pH 8.5, are expected to remain similar under field conditions due to calcite buffering.

There was no evidence of colloidal particles contributing to uranium mobility in the samples analysed, with exception of the sample of wet fresh sludge. As this was the only sample of sludge that was not dried prior to use in the batch experiments, the presence of uranium colloids in the basins cannot be dismissed or confirmed.

7.9.2 Thorium

The concentrations of thorium in solution within the initial 7 to 15 days of experimental conditions can be interpreted as the fast release of sorbed thorium into solution. As the samples reach equilibrium with solution, the solubility control of ThO_2 becomes apparent, setting thorium concentration to approximately 10^{-9} mol/l.

Thorium in colloidal form is likely to contribute to dissolved thorium concentrations in the samples of sludge and mixture of soil and sludge but unlikely to be present in samples of tailings, as observed in Sections 7.2.2 and 7.8.3.Thorium colloids could have formed by complexation of organic matter. Nonetheless, under the experimental conditions, the formation of colloids does not appear to increase substantially the aqueous concentrations of thorium.

Both the groundwater and pore water samples collected from site (Chapter 6) contained thorium concentrations of less than the analytical detection limit of $1.7 \cdot 10^{-10}$ mol/l, within the range of the solubility of ThO_2. Thorium oxide is an insoluble phase, which will prevent thorium's migration in the long term.

8. Column Experiments

8.1 Overview

The release of contaminants can vary depending on the experimental conditions. Batch experiments are in some cases affected by saturation effects, as the solution in contact with the solid changes its composition as the solid dissolves. It is also common practice to set batch experiments with a too low solid to liquid ratio when compared with real field situations. This may lead to difficult interpretation of data or, at least, to a lower degree of representability of the actual *in situ* setting. To avoid these experimental artefacts, flow-through experiments can be used. This Chapter presents a series of flow-through experiments prepared with solid samples collected from the B1/B2 basins (mixture of soil and sludge, sludge and tailings). This type of experimental configurations allows increasing the solid to liquid ratio, given by the porosity of the column. It also avoids saturation effects, as the solution, once interacted with the solid, leaves the system. This helps in the understanding of the behaviour of the contaminants under conditions resembling real situations, where there is a continuous flow of groundwater.

8.2 Experimental Design

The experimental design is detailed in section 4.6.2.

A total of four packed and two undisturbed column experiments were carried out, as follows:

Packed column of aged sludge

This column was prepared with sample of sludge SC417a 1.5-3.0 m depth, collected in 2009. The sample was dried and the size fraction 0.5-1.0mm was used to pack the column. The experiment was run at three different flow rates during 2012, following which the experiment was ceased for 9 months, between 29 August 2012 and 27 May 2013. In 2013, the column was re-run at a different flow rate.

Packed column of fresh sludge

This column was prepared with the fresh (dried and sieved to 0.5-1.0mm) sample of sludge SC429 at 8.1m depth. The column was run at one flow rate.

Undisturbed column of fresh sludge

This column was prepared as detailed in Section 4.6.2 with sample of sludge SC429 at 8.1 m depth. The sample core was left undisturbed and used in the column experiment.

Packed column of aged tailings

Column prepared with sample of tailings SC416b at 5.8-7.3 m depth. The sample was dried and the size fraction 0.5-1.0mm was used. The column was run at three flow rates during 2012.

Packed column of fresh tailings

Column prepared with the fresh sample of tailings SC429 at 11.75-11.85m depth, dried and sieved to 0.5-1.0mm. The column was run at one flow rate.

Undisturbed column of fresh tailings

This column was prepared as detailed in Section 4.6.2 with sample of tailings SC429 at 8.35-8.45 m depth. The sample core was left undisturbed and used in the column experiment.

Elution conditions

All columns were eluted with artificial rainwater except the column of fresh tailings, which was eluted with artificial sludge effluent and a pulse injection of ^{233}U (refer to section 4.6.2 for preparation of rainwater and sludge effluent). The elution with artificial rainwater simulated the effect of elution of the B1/B2 basins with uncontaminated water and allowed investigation of the release behaviour of U and Th. The sludge effluent simulated the water leached from the strata of sludge and was prepared to obtain the average composition of the effluent obtained from leaching the packed column of aged sludge at the slowest flow rate. The injection of ^{233}U was carried out to evaluate the retention characteristics of the tailings under simulated field conditions. The compositions of the artificial rainwater and the artificial sludge effluent are given in Table 8.1

Table 8.1: Composition of artificial rainwater used in the column experiments.

Parameters	Rainwater average concentration in France (G. Miquel, 2003)	Artificial rainwater*	Artificial Sludge Effluent*
Mg (mg/l)	0.05 – 0.9	0.151 – 0166	175.2 – 177.7

Parameters	Rainwater average concentration in France (G. Miquel, 2003)	Artificial rainwater*	Artificial Sludge Effluent*
Na (mg/l)	0.2 – 6	0.225 – 0.275	132.0 – 132.3
K (mg/l)	-	<0.1	108.2 – 123.0
Ca (mg/l)	-	<0.1	276.0 – 292.2
Cl (mg/l)	0.2 – 10	0.346 – 0.421	<0.1
NO_3 (mg/l)	0.3	0.425 – 0.581	240.6 – 261.1
SO_4 (mg/l)	0.5	0.488 – 0.539	660.0 – 790.5
^{233}U (mol/kg)	-	-	$4.87 \cdot 10^{-8}$**
pH (pH units)	5	5.07 – 5.14	7.9 – 8.2

*minimum and maximum concentrations measured in the solutions prepared,

**^{233}U injected during the sorption experiment

According to historical weather data (Appendix 4), the average rainfall at the site was of 390 mm, between 2009 and 2015, ranging from 280 to 680 mm. Eighty percent of the precipitation events consisted of less than 2 mm per day. Three percent of the events were characterised by more than 10 mm/day. The daily flow rates in the basins can then be assumed to average 0.77 ml/min, for an annual precipitation of 390 mm, and 1.39 ml/min during a typical rainfall event of 2 mm/day.

For the experimental set-up, flow rates were selected so that a tracer test could be completed in less than 24 hours, but at slow enough velocities that the effluent would not create preferential pathways and lead to erosion of the sample contained in the columns. In addition, where more than one flow rate was used, their range was selected to vary by at least one order of magnitude. Final flow rates varied between 0.036 ml/min and 0.859 ml/min (Table 8.2) and can be assumed to be characteristic of the average field conditions in basins B1/B2. The experimental leaching periods, when normalised against the average annual rainfall of 390 mm (vol. eluted/annual rainfall of 390 mm), were equivalent to between 1 and 50 years of leaching Table 8.2.

Table 8.2: Comparison of flow rates applied in each column and the average annual rainfall at the site of 390 mm.

Column	Q, flow rate, (ml/min)	Q, flow rate, (mm/year)	Time eluted (years)	Total volume eluted (mm)	Vol. eluted / annual rainfall of 390 mm
Aged sludge	0.036	60,301	0.062	3714	9.5
	0.146	244,555	0.011	2697	6.9
	0.357	597,986	0.005	2953	7.6
	0.129	216,079	0.055	11881	30.5
Fresh sludge	0.156	261,305	0.037	9721	24.9
Undisturbed fresh sludge	0.065	43,830	0.082	3591	9.2
	0.859	578,912	0.019	10,715	27.5
Aged tailings	0.037	61,976	0.055	279	0.7
	0.126	211,054	0.003	589	1.5
	0.331	554,436	0.006	3465	8.9
	0.396	503,092	0.005	2371	6.1
Fresh tailings	0.154	257,955	0.077	19988	51.3

8.3 Column Hydrodynamics

8.3.1 Methodology

The hydrodynamics of the columns were characterised by carrying out tracer tests with tritiated water (HTO) and modelling the elution results with the CXTFIT computer code (Toride, Leij and Van Genuchten, 1995). The program was used to solve the inverse problem by fitting mathematical solutions of theoretical transport models, such as the conventional convection-dispersion equation (CDE) and the chemical and physical non-equilibrium CDE (MIM) models, to experimental results (Toride, Leij and Van Genuchten, 1995). The application provided an estimation of the values of the dispersivity (λ), effective water content (θ), time of pulse injection (t_0) and, additionally, mobile water fraction (β) and mass transfer coefficient (ω) in the case of physical non-equilibrium. Although the experimental conditions were controlled, the time of pulse injection was not known as the tracer experiments were set to run overnight and the input flow rate injected in the column was compounded by the non-tritiated water and the HTO pumped by the peristaltic and

syringe pumps, respectively. Nonetheless, the volume of HTO being injected in each experiment was controlled, to allow mass recovery calculations. The average linear pore water velocity (cm/min) was defined as the time required for the HTO $C/C_0 = 1$. The permeability was calculated by derivation of Darcy's Law, using the measured pressure difference at the inlet and outlet of the columns and the viscosity of water. The HTO recovery was calculated by integration of the area of the breakthrough curves (BTCs) of the normalised concentration of HTO (C/C_0) versus the pore volumes eluted. HTO recovery was generally above 90%.

The experimental conditions are presented in Table 8.3.

Table 8.3: Experimentally controlled parameters in the tracer column experiments.

Column	Column dimensions (length, cm / diameter, cm)	Θ, calculated volumetric water content (%)	Q, flow rate (ml/min)*	V_d, average linear pore water velocity (cm/min)	Time of pulse injection (min)	k, permeability (m^2)	HTO recovery (%)
Packed – Aged sludge	8.4 / 2.0	53.4 ± 0.1	0.036 ± 0.002 (12)	0.006	1300.0	$5.80 \cdot 10^{-14}$	95.8±8.3
			0.146 ± 0.003 (11)	0.027	536.0	NM	96.5±5.5
			0.357 ± 0.005 (8)	0.052	468.8	5.34·10-13	98.6±5.2
			0.129 ± 0.010 (11)	0.013	594.2	$3.45 \cdot 10^{-13}$	104.5±10.0
Packed – Fresh sludge	8.4 / 2.0	57.9 ± 0.1	0.156 ± 0.018 (25)	0.027	588.6	NM	102.5±6.0
Undisturbed – Fresh sludge	11.0 / 7.8	35.4 ± 1.0	Test 1	0.00076	6491.6	$1.1–6.4 \cdot 10^{-15}$	95.9 ± 5.5
Packed – Aged tailings	8.4 / 2.0	35.5 ± 0.1	0.037 ± 0.003 (3)	0.008	878.8	$4.94 \cdot 10^{-14}$	103.3±10.1
			0.126 ± 0.009 (9)	0.029	410.7	$1.58 \cdot 10^{-13}$	103.6±8.8
			0.331 ± 0.006 (6)	0.088	509.2	NM	102.9±5.6
			0.396 ± 0.081 (6)	0.075	176.4	NM	109.4±23.3
Packed – Fresh tailings	8.4 / 2.0	53.7 ± 0.1	0.154 ± 0.020 (31)	0.019	6169.0		102.8±14.3

*figure in parentheses are the number of experimental measurements of the flow rate. NM – permeability not measured

8.3.2 Packed columns

The dimensionless breakthrough curves (BTCs) of HTO were determined by plotting the value of the normalised concentration (C/C0) versus the number of pore volumes eluted, where a column pore volume is the total amount of aqueous phase in the column, expressed in volume.

The visual observation of the BTC provides a preliminary indication of whether the system is in equilibrium or whether there may be two-region flow. If a system is in equilibrium, then the BTC will be symmetrical. Spreading of the arrival edge and the elution edge of the curve will give an indication of the amount of dispersion present in the column.

The application of the CDE model provided an excellent fit to most of the BTC curves, with $r^2 > 0.99$ (Table 8.3, Figure 8.1 and Figure 8.2), indicating the applicability of the CDE model to transport in the packed columns of sludge and tailings. The last tracer test applied in the packed column of aged sludge could not be described by the CDE model and is discussed further below. The effective porosities fitted with the CDE model are very similar to the volumetric water content calculated independently from the column packing (Table 8.4). As the columns were homogeneously packed, no double porosity, i.e. zones of mobile and immobile water content, was expected.

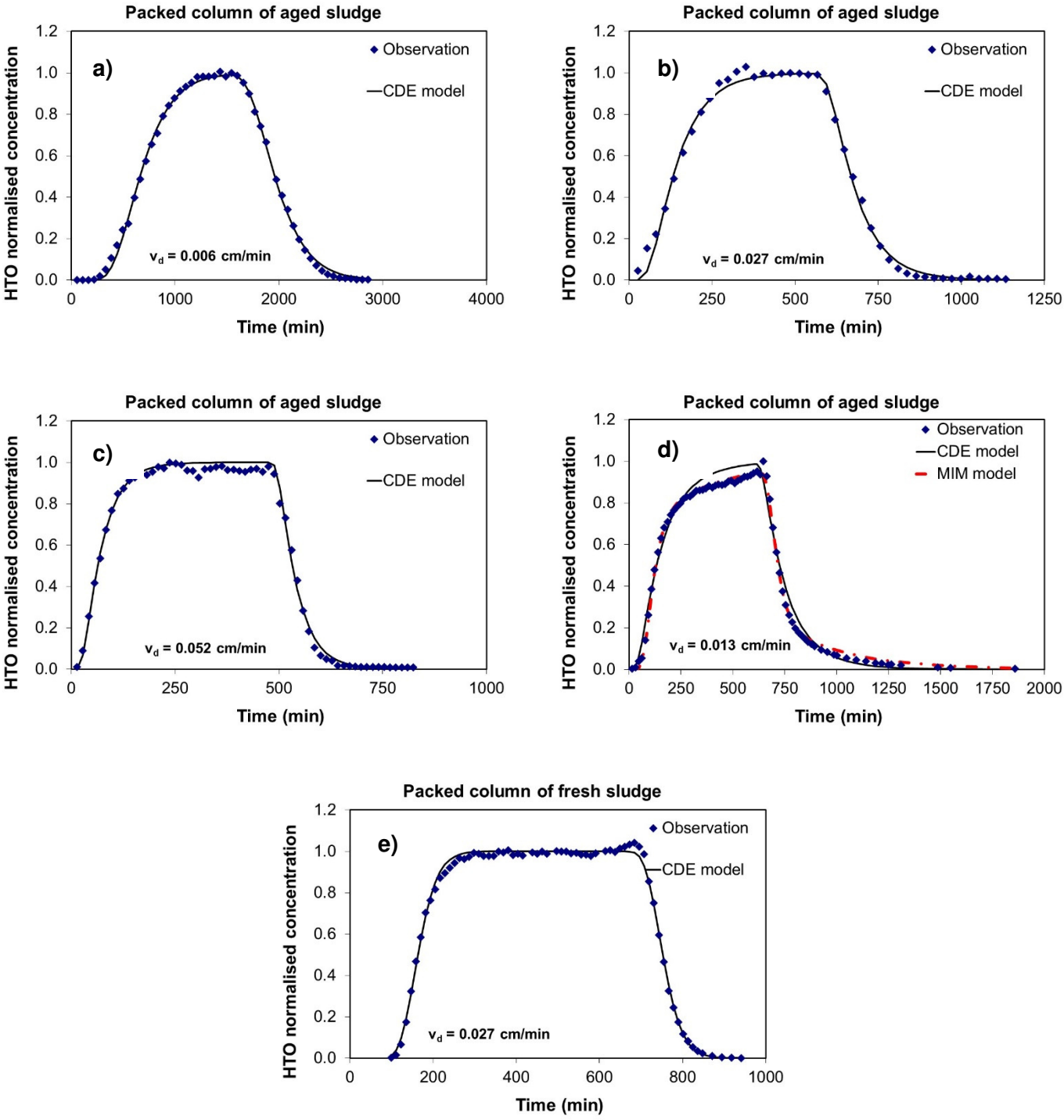

Figure 8.1: Results of the HTO tracer tests in the packed column of aged sludge at flow velocities of 0.006 cm/min (a), 0.027 cm/min (b), 0.052 cm/min (c) and 0.013 cm/min (d), and in the packed column of fresh sludge at a flow velocity of 0.027 cm/min (d). Experimental observations and fitting with the CXTFIT code using the conventional CDE equation (CDE Model) and the MIM equation (MIM Model) shown.

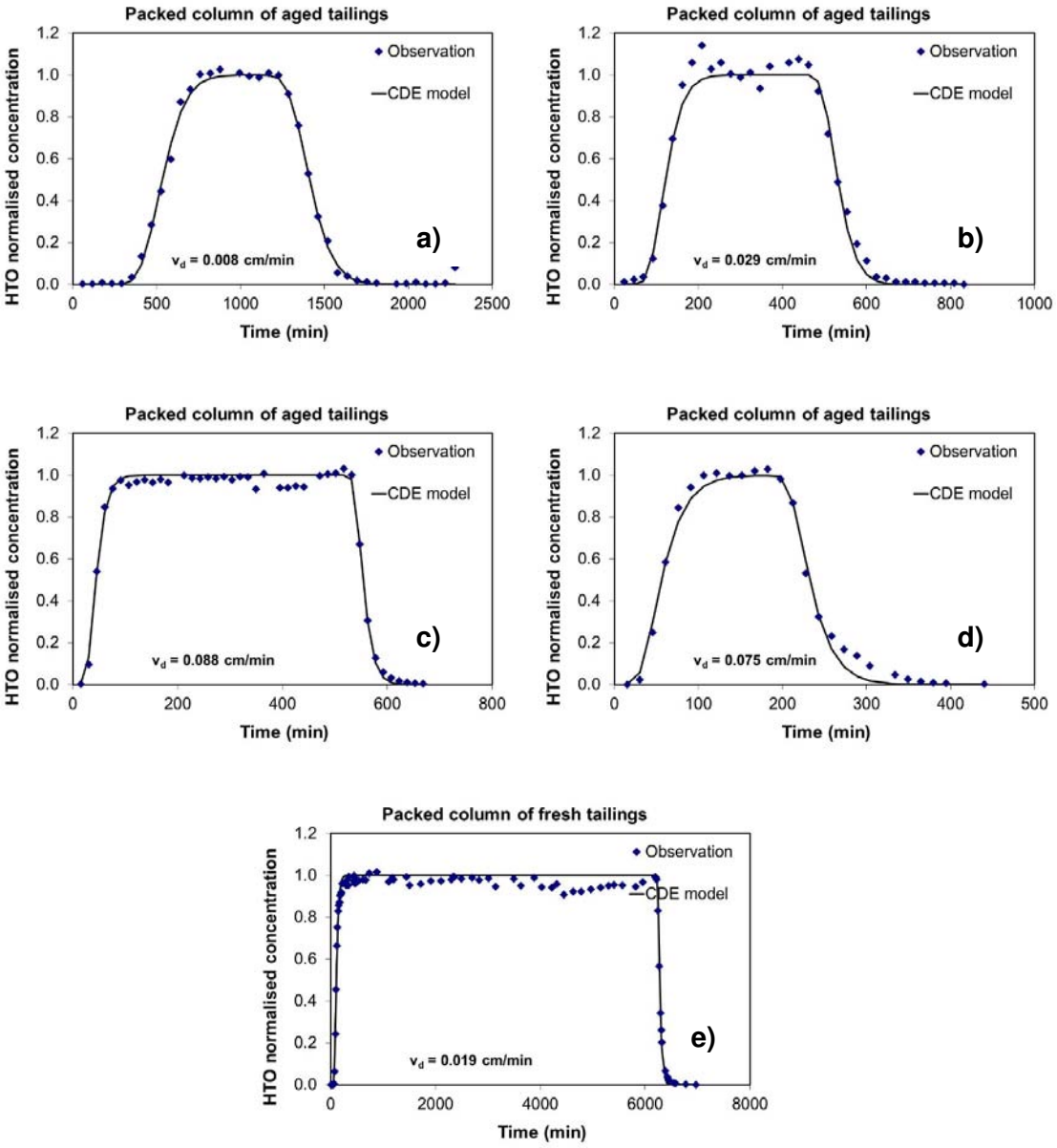

Figure 8.2: Results of the HTO tracer tests in the packed column of aged tailings at flow velocities of 0.008 cm/min (a), 0.029 cm/min (b), 0.088 cm.min (c) and 0.075 cm/min (d) and in the packed column of fresh tailings at a flow velocity of 0.019 cm/min (d). Experimental observations and fitting with the CXTFIT code using the conventional CDE equation (CDE Model) and the MIM equation (MIM Model) shown.

The BTC on the column of aged sludge at a flow velocity of 0.013 cm/min was not well described by the CDE model (Figure 8.1, d)), especially in the vicinity of the $C/C_0 = 1$. This could be a result of an increase in the tortuosity and/or an increase in dispersion within the column. The tortuosity is a measure of the effect of the shape of the flowpath followed by water molecules in a porous media. The flowpath is longer in a poorly sorted

sediment in which the smaller grains are filling the voids between the larger grains than in a well-sorted sediment. Dispersion also affects the movement of the fluid particles causing them to move faster or slower depending on the flow path taken. This would be reflected in the low slope of the breakthrough curve observed at concentrations of HTO of C/C_0 between 0.8 and 1. The comparison of the tracer test with the previous test carried out at 0.146 ml/min (Figure 8.3) shows a low slope in the breakthrough arrival and a long tailing in the elution of the tracer. There is an additional 15-20% of dispersion in the column compared with the previous test.

It is likely that the additional dispersion resulted from dissolution of the sample material and of the finer fraction adsorbed to it during the previous elutions. The results of the surface area discussed previously in Chapter 7, indicated the potential for a finer fraction of material being contained within the 0.5-1.0mm size fraction. The finer material fills the space between the larger pores increasing the tortuosity and dispersion. This leads to the creation of inhomogeneous flow conditions with water flowing in certain parts of the medium and being stagnant in other parts, such as particle aggregates.

The transport of a solute between the mobile zones and the stagnant regions will be carried out by diffusion. In this case, only the mobile water fraction participates in the flow of a solute. The mobile fraction of the porosity, β, is defined as θ_m/θ_w, where θ_w is the total water filled porosity and θ_m is the mobile water filled porosity. The fitting of the observed HTO concentrations using the physical non-equilibrium equation (MIM model), Figure 8.3 is better able to describe the breakthrough curve, both in the arrival and in the tailing. The parameters obtained are presented in Table 8.4. The mobile water fraction is 62% of the total porosity and the effective water content is 31%. This gives a total porosity (mobile plus immobile fractions) of 51% which is very close to the effective water contents estimated with the previous tracer tests (51%, 49% and 47%).

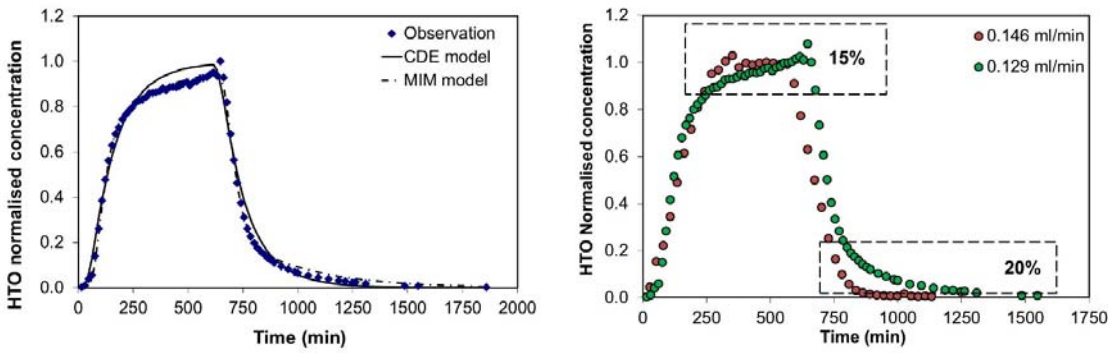

Figure 8.3: HTO tracer tests in the packed column of aged sludge, at 0.146 ml/min and 0.129 ml/min. The lower slope in the breakthrough arrival and the long elution tailing in the new tracer test (at 0.129 ml/min) can be clearly seen when compared with the results of the tracer test at 0.147 ml/min. The place where the curves' slope diverge is at approximately 85% C/C_0 and 20% C/C_0.

Between application of the first three flow rates (0.036, 0.146 and 0.357 ml/min) and the fourth flow rate (0.129 ml/min) where double porocity characteristics were observed, no experimental work was carried out with the packed column of sludge. During the period of no flow conditions (of approximately 9 months) dissolution of finer materials may have occurred resulting in thean increase in tortuosity and dispersion as discussed above.

Table 8.4: CXTFIT estimated parameters in the tracer column experiments.

Column	θ, estimated volumetric water content (%)	Λ, dispersivity (cm)	β, mobile water fraction (%)	ω, mass transfer coefficient (-)	r^2
	51.1±0.3	0.55±0.02	-	-	0.9981
	48.8±1.0	1.31±0.11	-	-	0.9948
Aged Sludge	46.7±1.0	1.56±0.11	-	-	0.9958
	26.3±0.6	2.47±0.23	-	-	0.9840
	31.2±0.5	0.62±0.05	61.5±1.1	0.29±0.02	0.9978
Fresh Sludge	53.5±0.3	0.20±0.01	-	-	0.9973
Aged Tailings	52.2±0.4	0.17±0.01	-	-	0.9962
	43.2±1.0	0.31±0.06	-	-	0.9862
	49.4±1.0	0.51±0.06	-	-	0.9949
	54.5±1.5	0.70±0.11	-	-	0.9896
Fresh Tailings	25.5±0.4	0.50±0.05	-	-	0.9890

*Figures in parentheses represent the number of flow rate experimental measurements. Goodness of fit is represented by r^2.

8.3.3 Undisturbed column of fresh sludge

8.3.3.1 Results of HTO

The undisturbed column of fresh sludge was eluted on two separate occasions with artificial rainwater. It was first eluted at 0.065 ml/min and then at 0.953 ml/min.

To confirm that there was no preferential flow along the column, for example, along the PVC core liner, the conductivity of the eluate was measured periodically during the first flow experiment. The results are presented in Figure 8.4. The conductivity is high at the start of the experiment (116 mS/cm) confirming that the eluted liquid corresponds to the initial pore water in the column. It then decreases with time, a result of the mix of artificial

rainwater being injected and the column pore water. As a comparison, the conductivity of the water being injected is 0.0072 mS/cm.

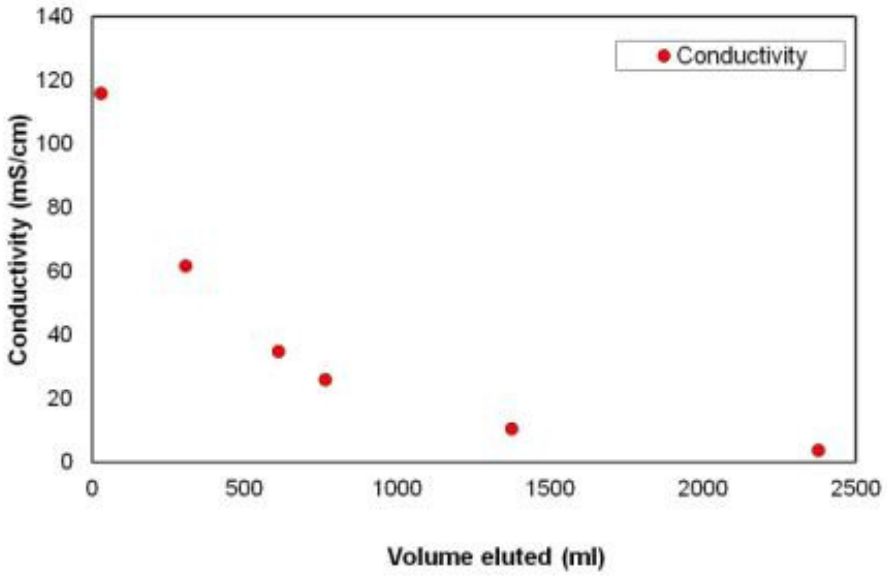

Figure 8.4: Effluent conductivity with volume eluted.

8.3.3.2 Fitting of the First Tracer Test

The one-site equilibrium model failed to reproduce the experimental tracer test in the undisturbed column at both the breakthrough and the elution portions (Figure 8.5). The physical non-equilibrium, which arises from the presence of dual porosity in the medium, i.e. two distinct mobile (flowing) and immobile (stagnant) liquid regions, also failed to reproduce the long tailing of the elution curve although the total normalised HTO concentration is closer to the values observed. The column may be a partly saturated system.

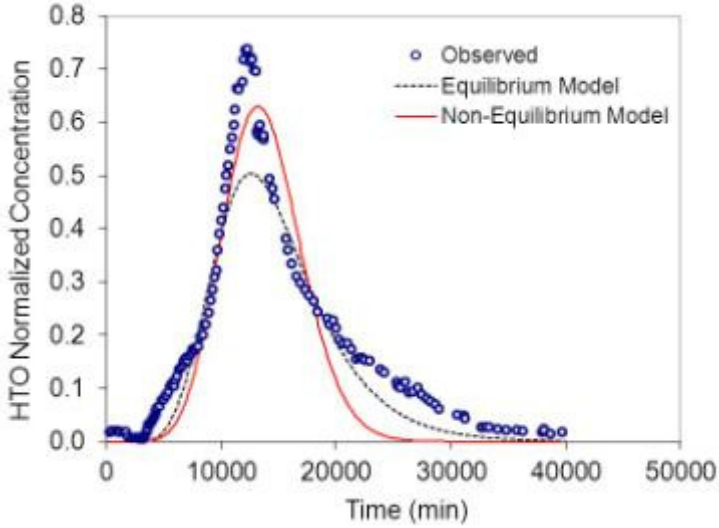

Figure 8.5: HTO breakthrough curve and model fittings in the undisturbed column of sludge.

8.3.3.3 Fitting of the second tracer test

The second injection of HTO indicated early breakthrough of the non-reactive tracer (Figure 8.6). Visual observation of the column showed the formation of new pockets of water in the column, formed in the space between the material and the PVC core liner. It was therefore possible that preferential flow was occurring in the column during the second rainwater elution. This possibility was verified by injection of a fluorescent tracer, uranine. The test showed uranine in the walls of the column after approximately 1 minute (Figure 8.7) confirming this hypothesis. These pockets of water were not observed during the first rainwater elution. The experiment was stopped and the results of the second flow experiment were not analysed further.

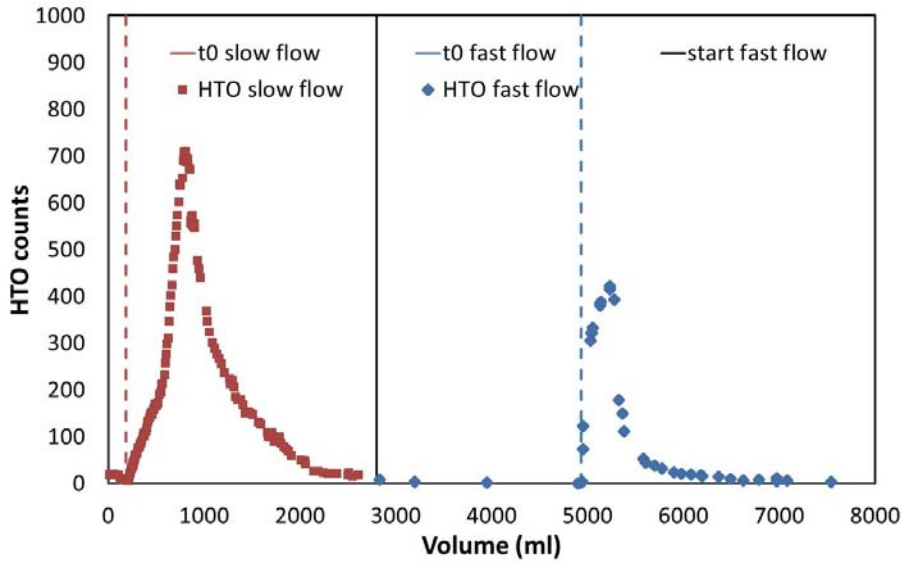

Figure 8.6: Breakthrough curves of HTO at slow flow rate (0.065 ml/min in red) and at fast flow rate (0.953 ml/min in blue) showing the fast breakthrough of HTO at 0.953 ml/min. t0 - start of HTO injection.

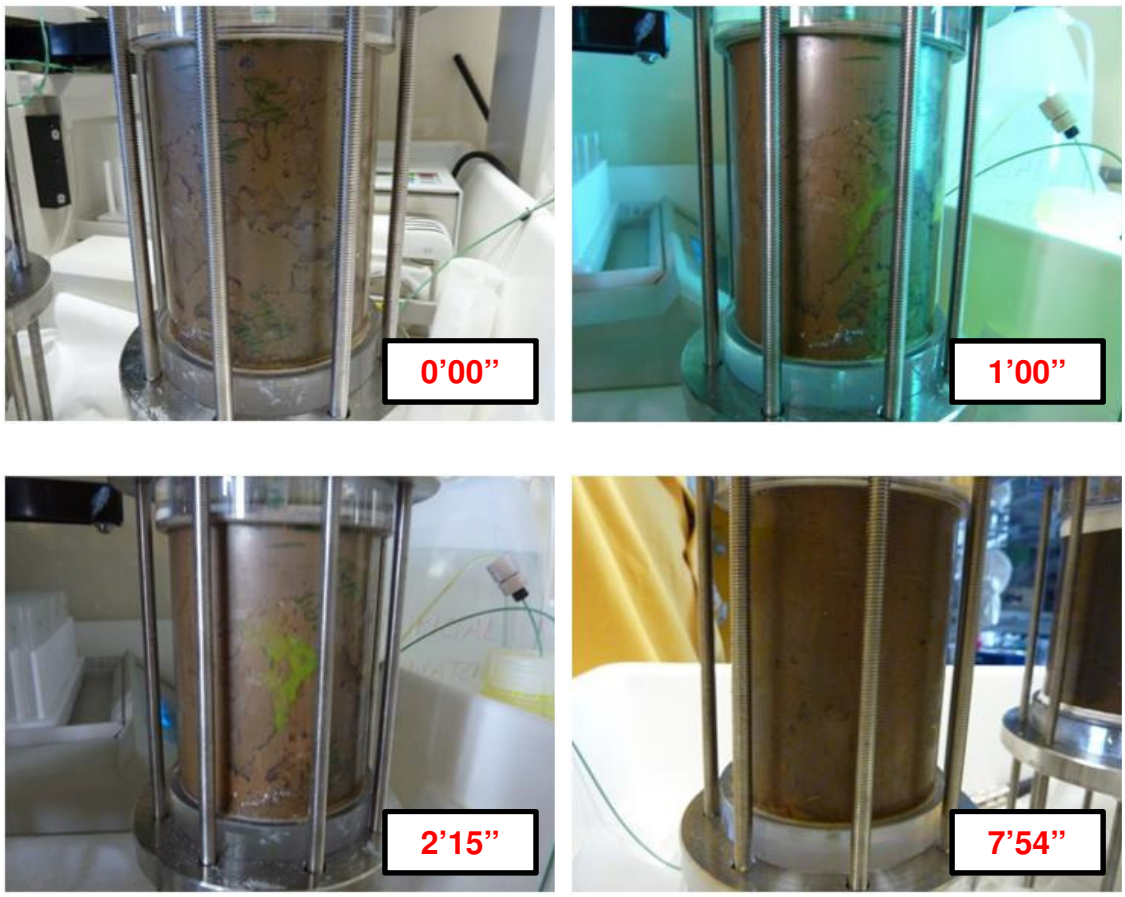

Figure 8.7: Uranine test on the undisturbed column of sludge. a) before injection of uranine; b) after 1' of injection, uranine can be seen on the wall of the column; c) after

2'15'', uranine can be seen on the wall of the column; d) after 7'54'', no preferential flow is seen on the opposite side of the column.

8.3.4 Undisturbed column of fresh tailings

8.3.4.1 Results of HTO

An undisturbed column of fresh tailings was prepared and eluted with artificial rainwater at 0.205 ml/min. The HTO breakthrough, shown in Figure 8.8, was very fast, as seen from the sharp slope of the curve and from the first appearance of HTO in the effluent after elution with only 4 ml of artificial rainwater. The breakthrough curve provided an estimated pore volume of only 20 ml, less than 5% of the total volume of the core of 480 ml. This result could be due to preferential flow within the tailings.

During the preparation of the column, it was noticed that the material had formed irregularities in the top side of the column and a fracture was apparent at the base of the column (Figure 8.9). The fracture was closed at the surface by applying water and pressing the sides with a spatula, however, as seen from the breakthrough curve, this was not sufficient. It was considered that this column would not provide reliable results and no further work was carried out. To replace it, the packed column of fresh tailings was prepared.

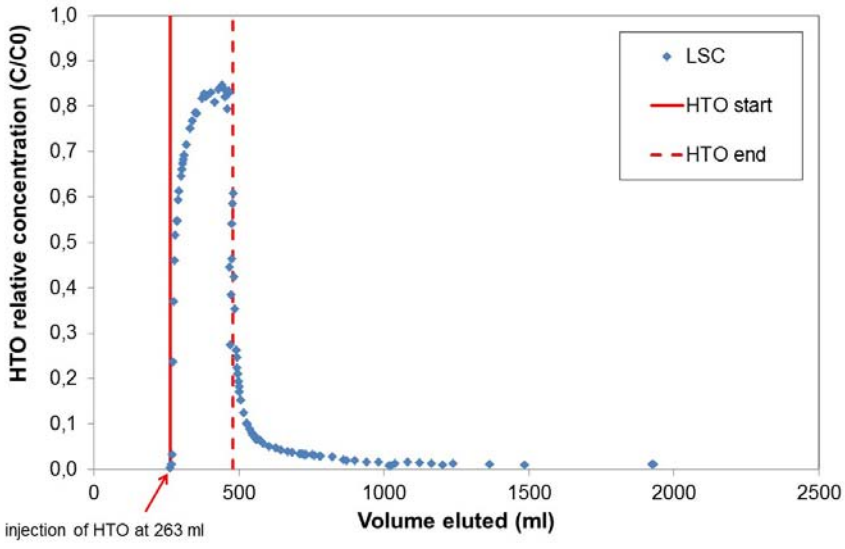

Figure 8.8: Breakthrough curve of HTO in the column of undisturbed tailings, Core B, with time (expressed as pore volume).

Figure 8.9: Base (on the left) and top (on the right) of the undisturbed column of tailings, Core B, showing irregularities and a fracture in the material.

8.4 Major chemistry of the column effluents

8.4.1 Evolution of pH, Eh and Alkalinity

The evolution of the pH with time in the effluents of the columns is represented in Figure 8.10.

In the columns of packed fresh sludge, undisturbed sludge and packed aged and fresh columns of tailings, the pH shows little variation between values of 7 and 8.5 during the first 100 to 200 pore volumes, stabilising at average values of 7.5 in all the columns thereafter.

The measured pH in the column of aged sludge increased to a value of up to 9.5 in the initial 200 pore volumes of elution. The flow was then interrupted for approximately 9 months and at re-start the pH was back at neutral values of between 7 and 8. The increase in pH values appears to be inconsistent with the decreasing alkalinity and with the fact that calcite is buffering the pH in the system. Speciation calculations support the alkalinity behaviour and indicate that, according to the measured parameters and chemical analysis, the likely pH in the system was neutral. The cause for the erroneous pH values could not be ascertained.

The redox value of the eluates ranged between 350 and 500 mV within the initial 200 pore volumes, stabilising at average values of 400-450 mV (Figure 8.11). The values of alkalinity measured decreased rapidly within the first 20 pore volumes of effluent from as high as 10 mmol/l, stabilising afterwards in average values of between 0.5 and 1 mmol/l (Figure 8.12).

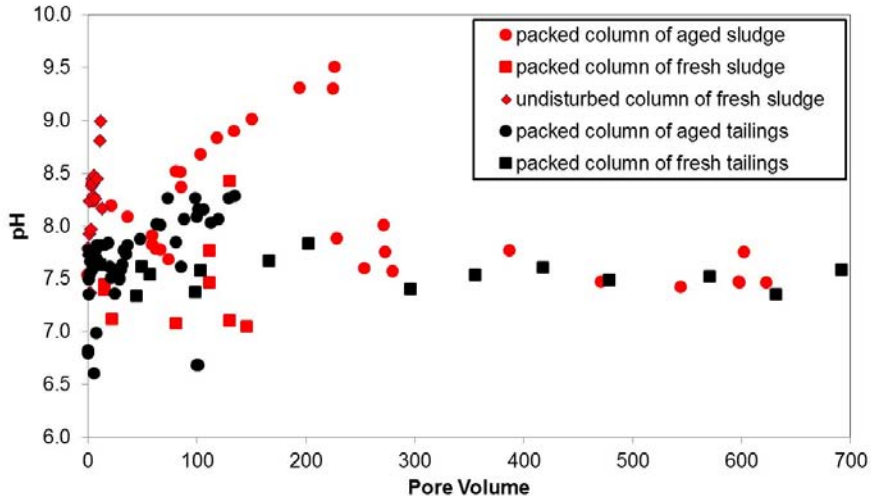

Figure 8.10: Evolution of the pH with time (expressed as pore volumes) in the columns of aged and fresh sludge, aged and fresh tailings and undisturbed column of sludge.

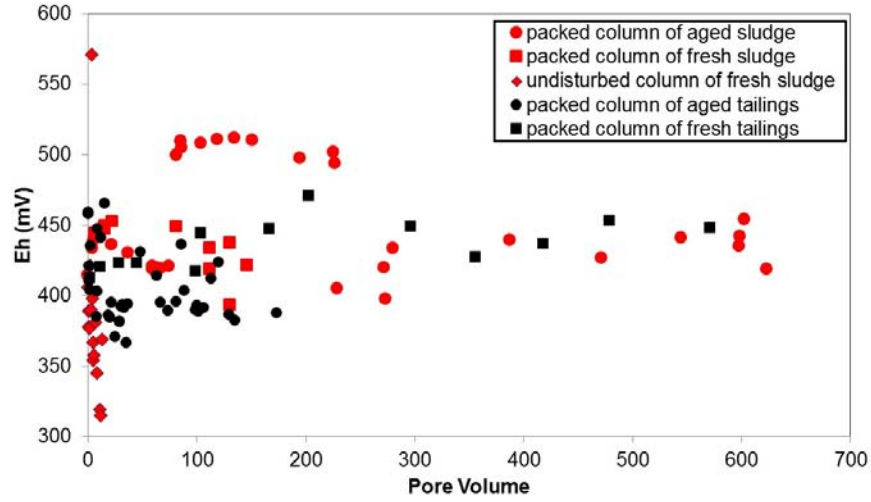

Figure 8.11: Evolution of the Eh with time (expressed as pore volumes) in the columns of aged and fresh sludge, aged and fresh tailings and undisturbed column of sludge.

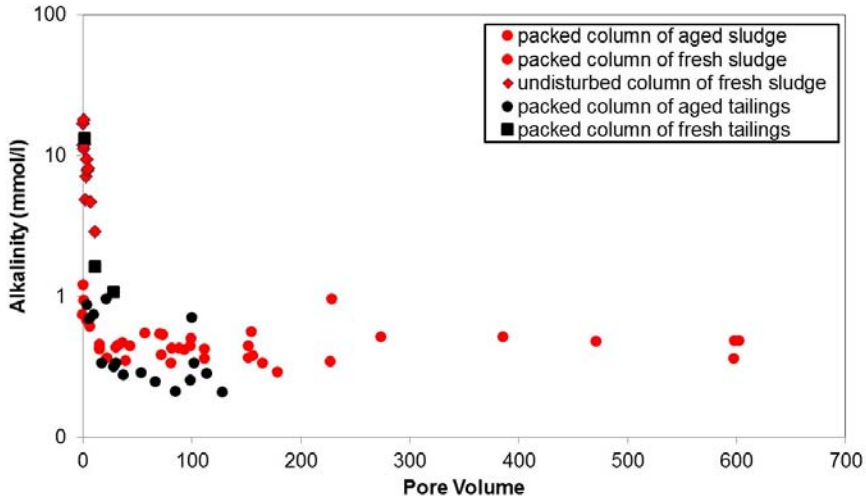

Figure 8.12: Evolution of the alkalinity with time (expressed as pore volumes) in the columns of aged and fresh sludge, aged and fresh tailings and undisturbed column of sludge. Packed columns of fresh sludge and fresh tailings eluted for 600 pore volumes. No alkalinity analysis carried out in the eluate of fresh tailings after 30 pore volumes. All other columns eluted with less than 200 pore volumes.

8.4.2 Equilibrium Phases

The results of chemical speciation of the eluate with time are presented in Appendix 6.

Sludge

The aliquots collected from the packed column of aged sludge were slightly oversaturated with calcite and fluorite and in equilibrium with barite. Magnesite and rhodochrosite were undersaturated throughout the experimental conditions whilst gypsum, dolomite and celestite, initially in equilibrium, became depleted with continuous elution.

During PV<3 in the column of fresh sludge, the eluate was oversaturated in calcite, dolomite, fluorite and barite. Continuous elution of the column with artificial rainwater decreased these phases' saturation to equilibrium and finally, by the end of the experiment at PV=80, to undersaturation. Fluorite was the only phase that kept constantly above saturation limit.

In the undisturbed column of sludge, gypsum and barite were in equilibrium. Calcite, dolomite, fluorite and magnesite were oversaturated throughout the experiment whilst rhodochrosite and celestite remained undersaturated.

Tailings

The eluates collected from the packed column of tailings were not charge balanced until pore volume 25. This was likely due to the aliquots collected not having sufficient volume to carry out all the chemical analyses. The analyses were divided among different aliquots, which could be spread by more than two pore volumes.

After 25 pore volumes, calcite, gypsum and barite were calculated to be in equilibrium. Dolomite, magnesite, rhodochrosite and celestite were undersaturated. Fluorite was initially in equilibrium, however, it became undersaturated with time. Gypsum, celestite and MnO_2 were in equilibrium throughout the elution of the column of fresh tailings. Manganite and barite were undersaturated.

8.5 Uranium Release under Dynamic Conditions

The stopflow technique (SF) has been extensively used in the investigation of non-equilibrium adsorption and desorption in column experiments (Brusseau *et al.*, 1989; Liu *et al.*, 2008). As the solute will tend to equilibrium between the aqueous and solid phases, the SF event allows evaluating the mass transfer between the two phases in the column. If, during a SF event, the solute concentration decreases in the aqueous phase, then the solute tends to adsorb to the solid phase. Otherwise, a rise in solute concentrations after a SF event will indicate continuous release into the aqueous phase.

Stop-flow events of various durations were employed throughout the elution of the columns to evaluate whether the uranium release from the samples is controlled by equilibrium or kinetics. All the stop-flow events (in sludge and tailings) led to an increase in the effluent concentrations of uranium followed by gradual decrease in concentrations with time as the flow was re-established.

8.5.1 Packed column of aged sludge

The packed column of aged sludge was eluted for a total of 657 pore volumes (PV) at four flow rates: 0.036, 0.146, 0.357 and 0.129 ml/min with artificial rainwater.

The effluent concentration of uranium at the slowest flow rate (0.036 ml/min) was initially $5.5 \cdot 10^{-6}$ mol/l and decreased gently to a concentration of $3.4 \cdot 10^{-6}$ mol/l by the end of the flushing (Figure 8.13). Under these conditions, the release of uranium was in apparent near equilibrium, with a distribution coefficient (K_d) of 2030 ± 30 l/kg and at

concentrations close to the solubility limit of uranophane ($3.6 \cdot 10^{-6}$ mol/l). However, after application of a SF event at PV=70, the concentration of uranium increased immediately to $6.1 \cdot 10^{-6}$ mol/l, indicating that uranyl release was primarily kinetically controlled.

At 0.146 and 0.357 ml/min, the effluent concentration of uranium decreased rapidly to 50% of its initial value within the first 10 PVs (Figure 8.13). It was then followed by a slower decrease in effluent concentrations. The flushing at these flow rates was stopped before equilibrium between the aqueous and the liquid phases was achieved. At the end of the two flushings, the concentrations of uranium were $1.1 \cdot 10^{-6}$ and $4.1 \cdot 10^{-7}$ mol/l.

At a flow rate of 0.129 ml/min, the column was flushed for a longer period (approximately 450 pore volumes), and an apparent steady state of uranium release was observed. Uranium concentrations at this apparent steady state decreased slowly from $5.3 \cdot 10^{-7}$ mol/l at PV=386 to $3.9 \cdot 10^{-7}$ mol/l at PV=657. This range was within the magnitude of U concentrations measured in the pore water of the sludge ($4.8 \cdot 10^{-7}$ mol/l) (refer to Chapter 1).

All the SF events indicated kinetic behaviour in the release of U. The SF applied at PV=228 had a duration of 6510 hours (271 days or 9 months) and, therefore, the U concentration measured immediately after re-start of flushing is assumed to correspond to equilibrium. It was also comparable to the value obtained after the SF of the first flow rate (the slowest one) ($6.2 \cdot 10^{-6}$ and $6.1 \cdot 10^{-6}$ mol/l respectively).

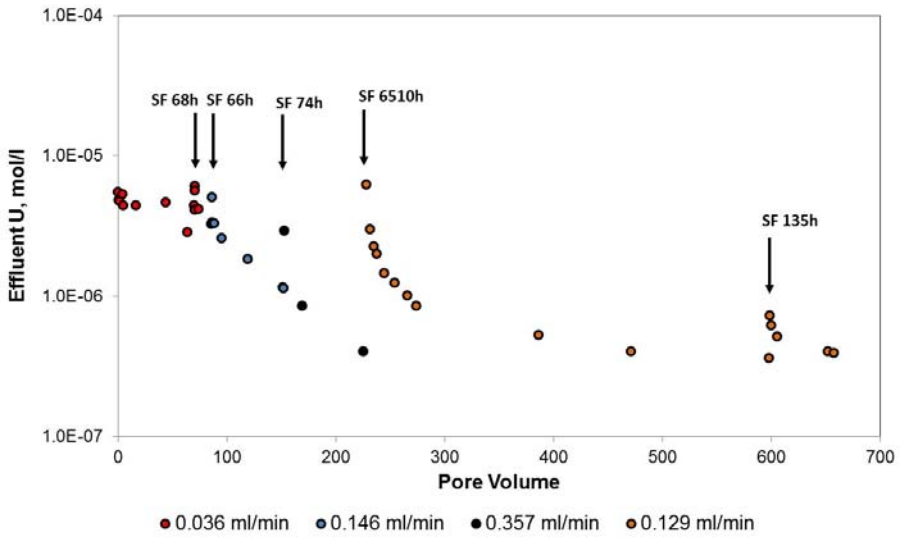

Figure 8.13: Release of U from the packed column of aged sludge, with time (expressed as pore volume). Error bars smaller than the symbols. Spikes in the elution profiles

result from stop flow events (SF) where advection was stopped for the noted time periods.

The rate of uranium release at near steady state ranged between $1.03(\pm0.02)\cdot10^{-10}$ at a flow rate of 0.129 ml/min and $2.16(\pm0.04)\cdot10^{-10}$ mol/l.sec at 0.146 ml/min. The linear correlation of the uranium steady-state concentrations at the four flow rates results in an average rate of uranium release of $1.51(\pm0.10)\cdot10^{-10}$ mol/l.sec for the experimental conditions (Figure 8.14).

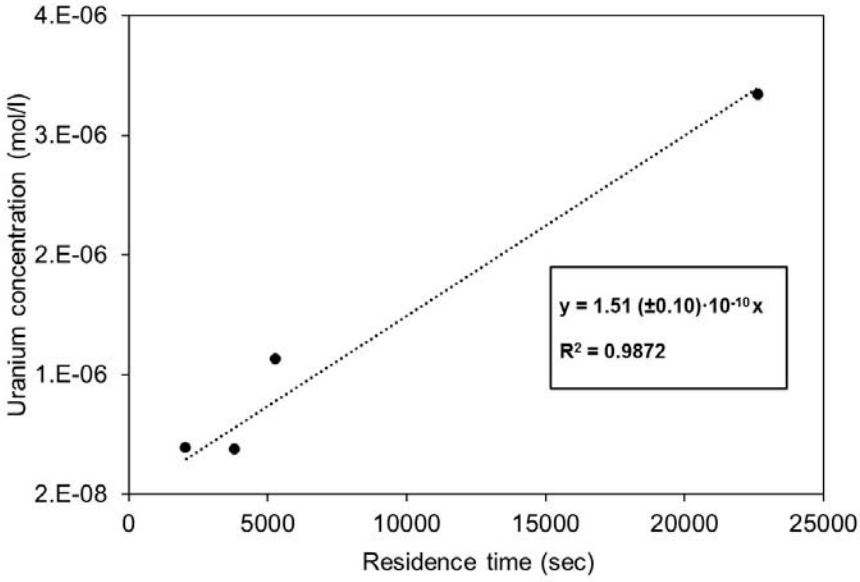

Figure 8.14: Uranium concentration near steady state vs residence time at each of the four flow rates applied in the column of aged sludge. Error lines for the experimental points are smaller than the symbols.

8.5.2 Packed column of fresh sludge

The packed column of fresh sludge was eluted for a total of 216 pore volumes at a flow rate of 0.156 ml/min with artificial rainwater.

The effluent U concentration was highest in the first pore volume ($1.77\cdot10^{-5}$ mol/l) but decreased fast to 20% of this value by PV=3. The curve of the elution of uranium suggested the existence of two rates of release, a fast rate of $3.7\cdot10^{-10}$ mol/l.sec up to PV=50, followed by a slower release rate of $5.2\cdot10^{-11}$ mol/l.sec to the end of the experiment. This would suggest that uranium was sorbed to a population of sites with different kinetic and/or thermodynamic properties. The SF event at PV=130 confirmed the kinetic behaviour of the uranium release. After elution of 216 pore volumes, the concentration of uranium in the eluate was $1.40\cdot10^{-7}$ mol/l.

The behaviour of the release of U from the fresh sludge and from the aged sludge were similar at PV<100, with uranium concentrations within the same range for the same pore volume (Figure 8.15) and release rates within the same order of magnitude ($1.1 \cdot 10^{-10}$ mol/l.sec for the fresh sludge and $1.5 \cdot 10^{-10}$ mol/l.sec for the aged sludge). Aging of the sample does not, therefore, appear to affect uranium release within the first 100 pore volumes. Initially, uranium concentrations also do not appear to be controlled by the uranium concentration in the sample (1,636 mg/kg in the aged sludge and 12,802 mg/kg in the fresh sludge). For PV>100, the concentration of effluent uranium in the fresh sludge is slightly lower than in the aged sludge although within the same order of magnitude ($1.4 \cdot 10^{-7}$ mol/l at PV=216 in the fresh sludge and $3.9 \cdot 10^{-7}$ mol/l at PV=430 in the aged sludge).

8.5.3 Undisturbed column of sludge

The undisturbed column of sludge was eluted for 15 pore volumes at a flow rate of 0.065 ml/min. This column experiment provides the closest simulation to field conditions, with the sample left undisturbed and application of slow flow rates. Uranium concentrations in PV=1 averaged $3.5 \cdot 10^{-7}$ mol/l, close to the concentration of uranium measured in the pore water ($4.8 \cdot 10^{-7}$ mol/l, refer to Table 6.5). By the end of the experiment, the concentration of uranium had decreased slightly to $1.7 \cdot 10^{-7}$ mol/l (Figure 8.16).

The effluent uranium concentrations decreased slowly when compared with the packed columns. The average rate of release throughout the experimental time, was of $1.5(\pm 0.5) \cdot 10^{-12}$ mol/l.sec. Similarly to what was observed in the packed column of fresh sludge, this could indicate the existence of populations of sites with different kinetic properties. The SF events confirm the kinetic behaviour of this release, although at a very small scale.

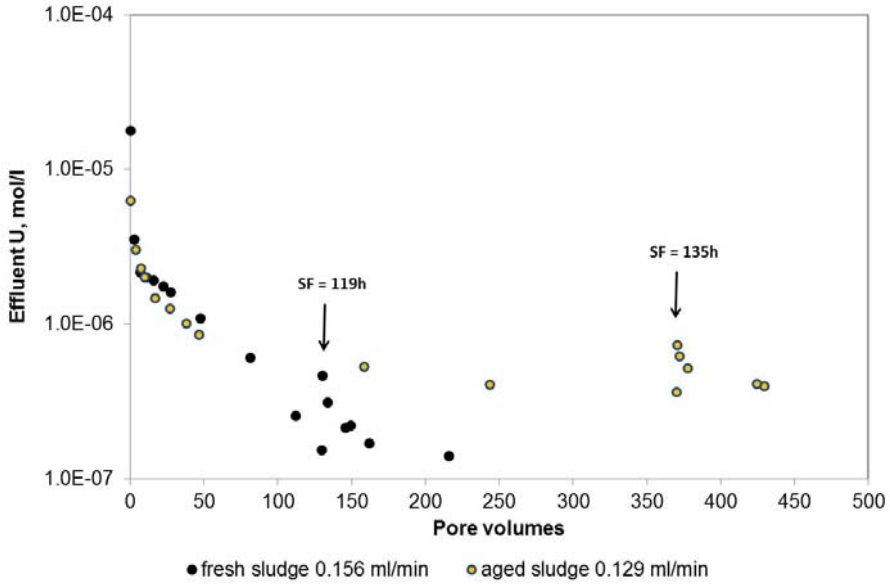

Figure 8.15: Release of U from the packed fresh column of sludge with time (expressed as pore volume). Comparison with the last flow rate applied to the packed aged column of sludge. Packed column of aged sludge, Q = 0.129 ml/m, residence time = 64 min. Packed column of fresh sludge, Q = 0.156 ml/min, residence time = 90 min. Error bars shown but smaller than the symbols. Spikes in the elution profiles result from stop flow events (SF) where advection was stopped for the noted time periods.

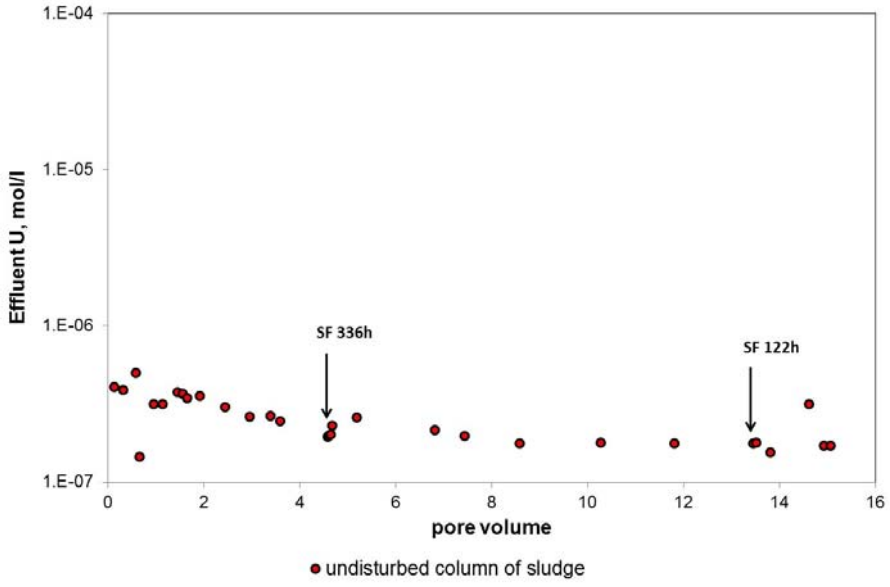

Figure 8.16: Release of U from the undisturbed column of sludge with time (expressed as pore volume). Error bars smaller than the symbols. Spikes in the elution profiles result from stop flow events (SF) where advection was stopped for the noted time periods.

8.5.4 Packed column of aged tailings

The packed column of aged tailings was eluted for a total of 171 pore volumes at four flow rates: 0.037 ml/min, 0.126 ml/min, 0.331 ml/min and 0.396 ml/min. Concentrations of uranium were highest at the start of each flow rate and decreased rapidly during the first 10 pore volumes (Figure 8.17). A state of apparent equilibrium was reached at 0.331 ml/min and 0.396 ml/min at concentrations of approximately $2.0 \cdot 10^{-7}$ mol/l.

All the SF events applied resulted in an increase in aqueous uranium concentrations, indicating kinetic release. The rate of uranium release ranged between $8.74(\pm 0.30) \cdot 10^{-11}$ mol/l.sec at a flow rate of 0.396 ml/min and $2.55(\pm 0.04) \cdot 10^{-10}$ mol/l.sec at 0.126 ml/min. Linear correlation of these values results in an average rate of uranium release of $2.16(\pm 0.11) \cdot 10^{-10}$ mol/l.sec for the experimental conditions (Figure 8.18). A similar rate of release from the sludge ($1.51(\pm 0.10) \cdot 10^{-10}$ mol/l.sec) and from the tailings ($2.16(\pm 0.11) \cdot 10^{-10}$ mol/l.sec) was therefore observed.

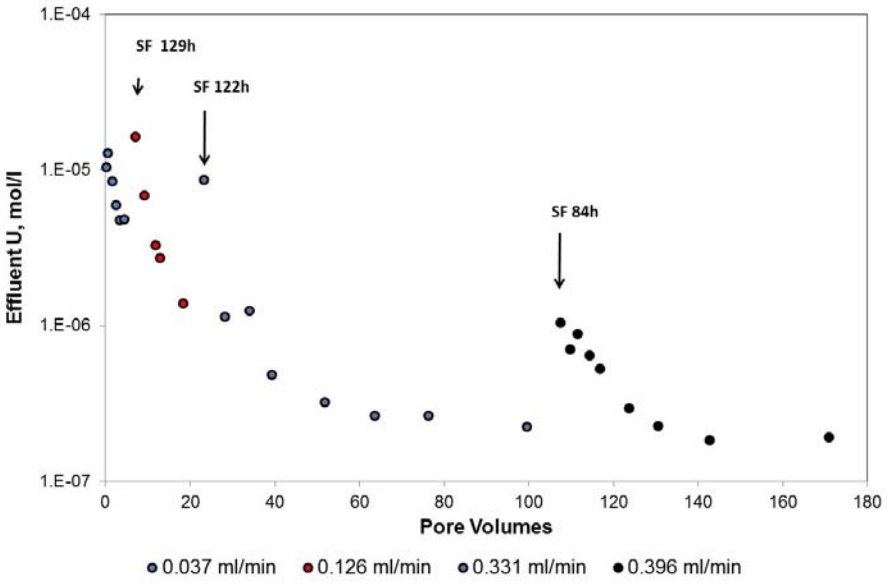

Figure 8.17: U elution from the column of aged tailings. Error bars smaller than the symbols. Spikes in the elution profiles result from stop flow events (SF) where advection was stopped for the noted time periods.

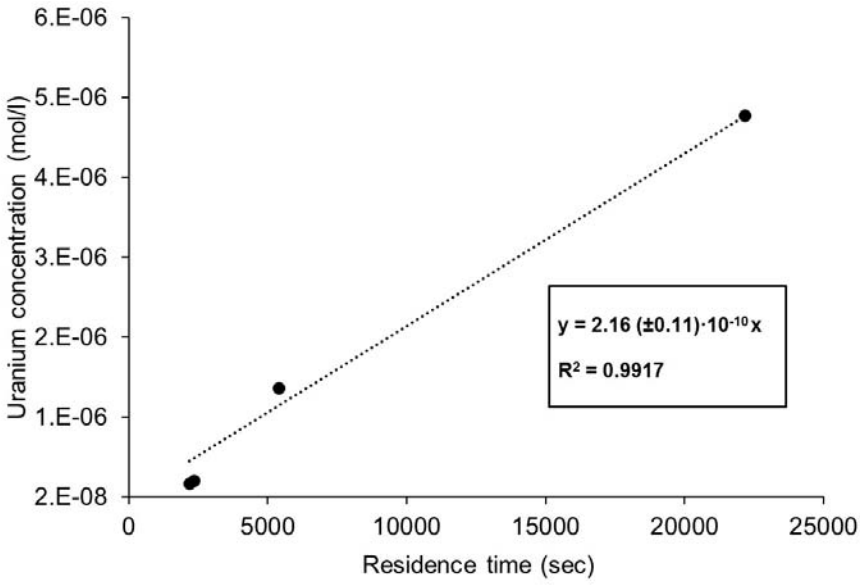

Figure 8.18: Uranium concentration near steady state vs residence time at each of the four flow rates applied in the column of aged tailings. Error lines for the experimental points are smaller than the symbols.

8.5.5 Packed column of fresh tailings

The fresh column of tailings was eluted for 900 pore volumes at a flow rate of 154 ml/min with artificial sludge effluent. The effluent reproduced the eluate obtained from the column of sludge and had a [^{233}U] = 0 M (Table 8.1). Uranium concentrations decreased by over one order of magnitude during the first five pore volumes, from $2.4 \cdot 10^{-5}$ mol/l to $1.5 \cdot 10^{-6}$ mol/l (Figure 8.19). Uranium concentration continued to decrease rapidly up to PV≈550, when an apparent steady-state was attained. The SF event at PV=192 resulted in an increase in aqueous uranium, confirming kinetic behaviour. The rate of uranium release was $1.0 \cdot 10^{-11}$ mol/l.sec.

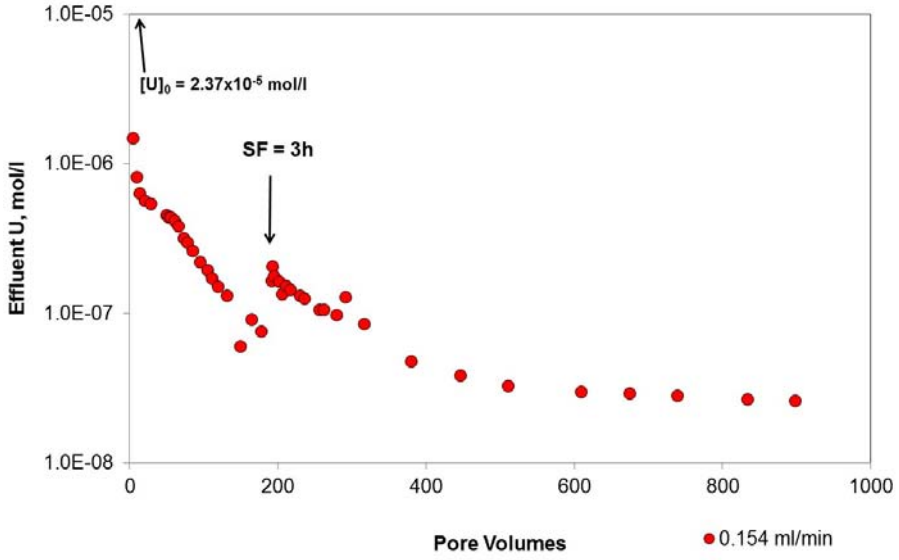

Figure 8.19: U elution from the column of fresh tailings. Error bars smaller than the symbols. Spikes in the elution profiles result from stop flow events (SF) where advection was stopped for the noted time periods.

8.6 Uranium retention under dynamic conditions

The sorption of uranium was studied in the column of fresh tailings by injection of artificial sludge effluent labelled with [^{233}U] = $4.9 \cdot 10^{-8}$ M. This sample of tailings contained an initial uranium concentration of 45 mg/kg. The objective was to reproduce the environmental conditions of the B1/B2 basins where the contaminated effluent migrates downwards from the strata of sludge to the “clean” strata of tailings. Uranium-labelled artificial sludge effluent was flushed during 32 pore volumes, between PV=48 and PV=180.

The late arrival of the breakthrough curve compared with the breakthrough of the tracer shows the retardation of ^{233}U (Figure 8.20). There was a delay of 21 pore volumes, between the start of ^{233}U injection and the first appearance of ^{233}U in the column effluent. During this time, all the ^{233}U is being retained by the tailings. After the first appearance of ^{233}U, the concentrations rise slowly and continue to increase even after ceasing the injection of ^{233}U (Figure 8.21). The SF event applied at the end of ^{233}U injection, at PV=180, resulted in no change in ^{233}U aqueous concentrations suggesting sorption equilibrium. However, it is likely that the duration of the SF event (3 hours) was not sufficient to confirm this. Once the concentrations of ^{233}U started to decrease, the long elution tailing indicated slow release. At the end of the experiment, 22% of the ^{233}U

injected had been recovered from the column, with the remaining 78% remaining adsorbed to the tailings.

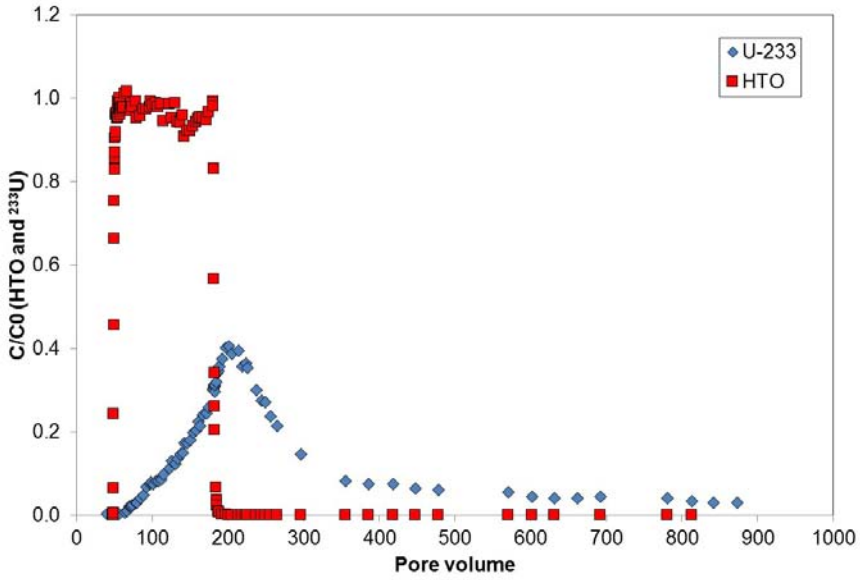

Figure 8.20: Breakthrough curves of HTO and ^{233}U in the column of fresh tailings with time (expressed as pore volume).

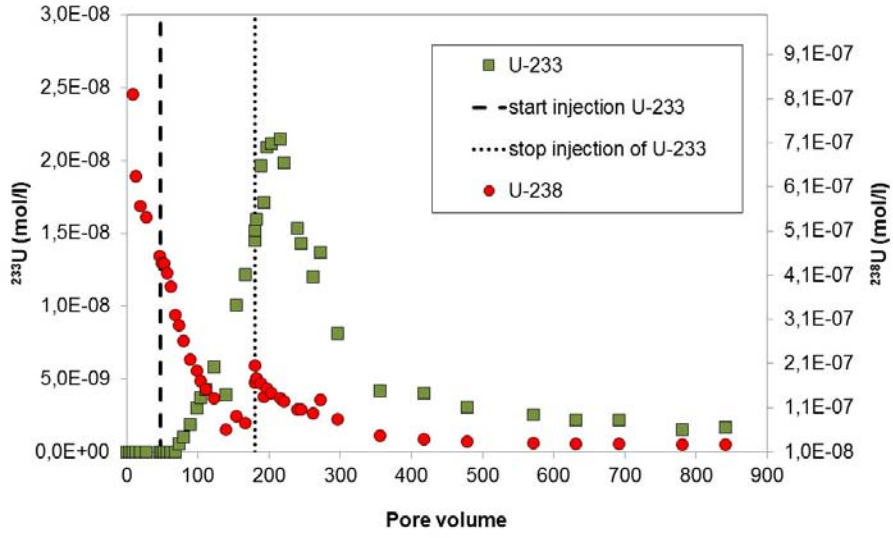

Figure 8.21: Release of U from the column of fresh tailings with time (expressed as pore volume).

8.7 Uranium speciation under dynamic conditions

The aqueous and solid speciation of uranium in the column experiments was computed using the Thermochimie database (Giffaut *et al.*, 2014) and the solubility reactions

therein as described in Chapter 4. The results of effluent speciation are presented in Appendix 6.

8.7.1 Uranium aqueous speciation

Uranium aqueous speciation comprised of predominantly the uranyl-calcium-carbonate complexes $Ca_2UO_2(CO_3)_3$ and $CaUO_2(CO_3)_3^{2-}$ (Figure 8.22 to Figure 8.26). These complexes form readily in the presence of elevated concentrations of calcium and bicarbonate, which are released into solution by dissolution of major constituents, such as calcite, dolomite and gypsum. As the concentrations of aqueous calcium decrease with time, uranium speciation evolved to predominantly uranyl-carbonate speciation. Absence of uranyl-calcium-carbonate complexes was only observed when aqueous calcium concentrations were below the limit of detection, as observed in the packed columns of aged sludge (Figure 8.22) and fresh tailings (Figure 8.26). However, it should be noted that the experimental determination of calcium in solution was carried out semi-quantitatively, resulting in a high limit of detection (of approximately $1 \cdot 10^{-6}$ mol/l).

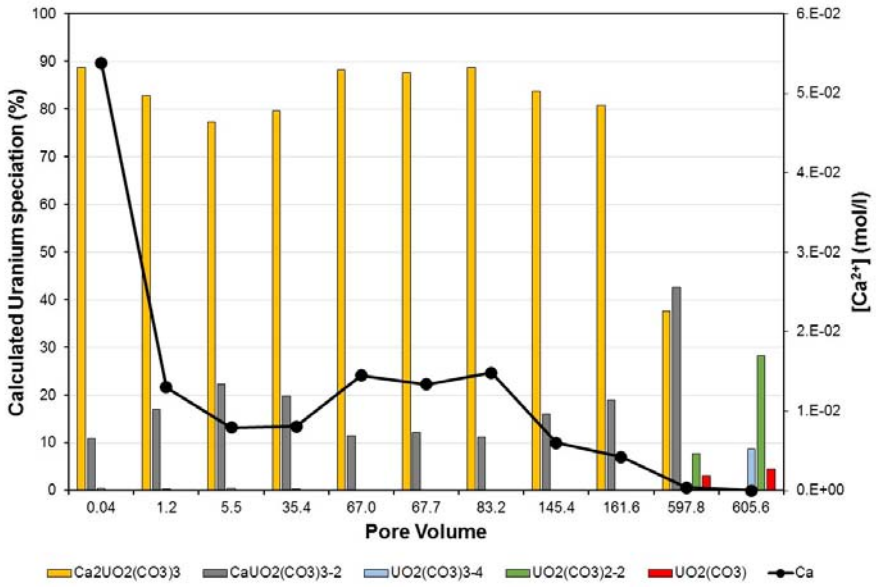

Figure 8.22: Aqueous speciation of uranium in the effluent of the packed column of aged sludge with experimental time expressed as pore volumes.

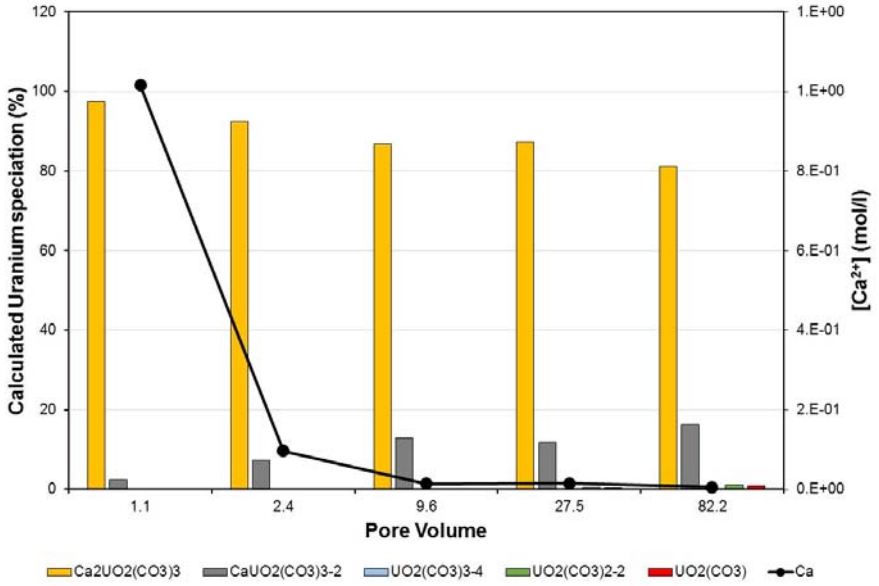

Figure 8.23: Aqueous speciation of uranium in the effluent of the packed column of fresh sludge with experimental time expressed as pore volumes.

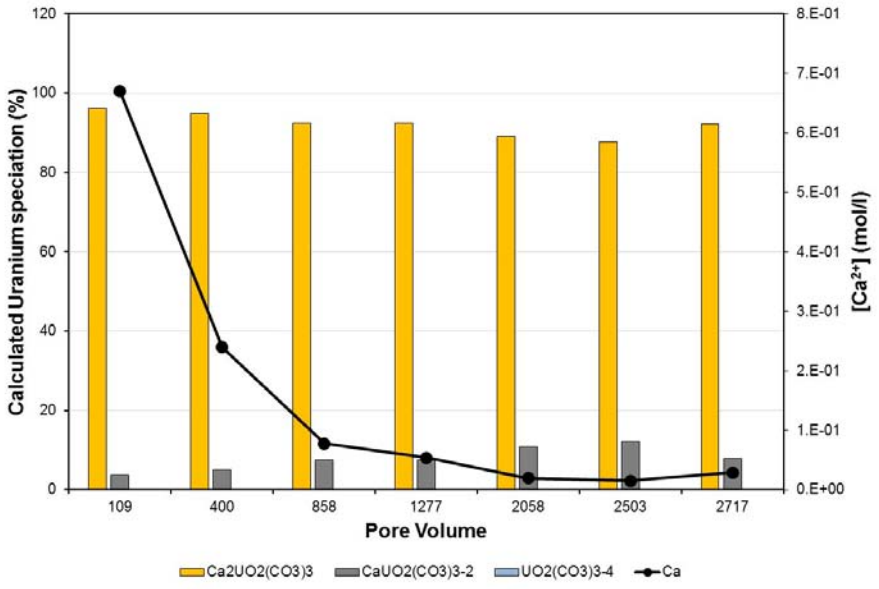

Figure 8.24: Aqueous speciation of uranium in the effluent of the undisturbed column of fresh sludge with experimental time expressed as pore volumes.

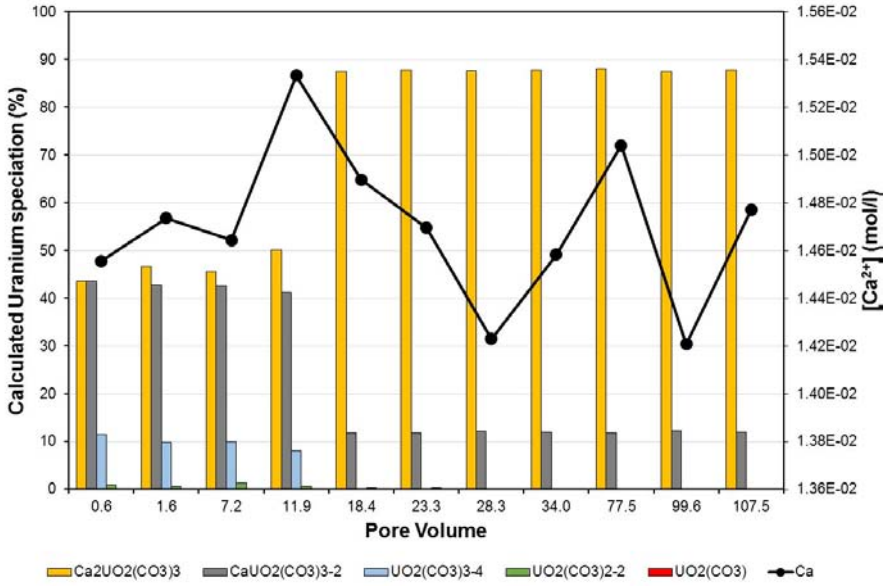

Figure 8.25: Aqueous speciation of uranium in the effluent of the packed column of aged tailings with experimental time expressed as pore volumes.

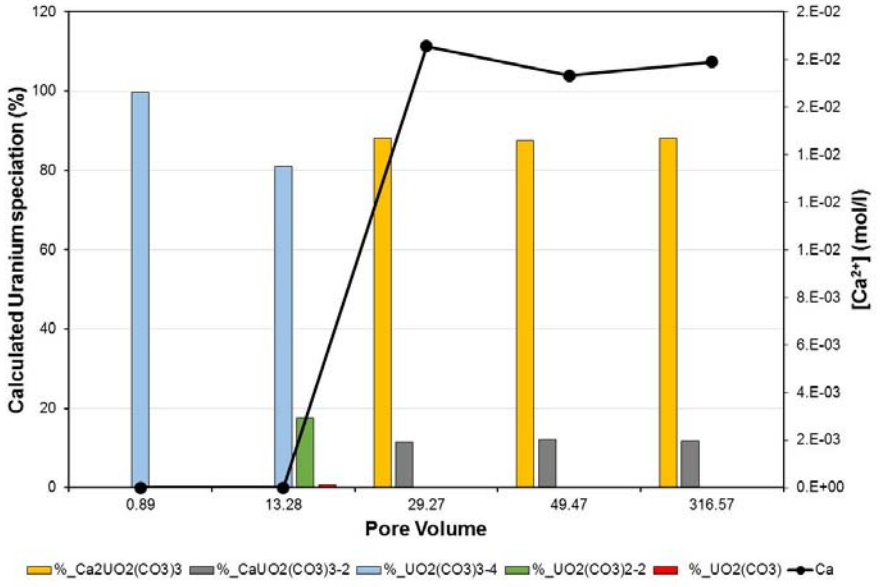

Figure 8.26: Aqueous speciation of uranium in the effluent of the packed column of fresh tailings with experimental time expressed as pore volumes.

Uranyl-calcium-carbonate have been observed to predominate under environmentally relevant conditions, i.e. neutral pH, low ionic strength, under equilibrium with atmospheric CO_2 (Dong and Brooks, 2006). For elevated concentrations of dissolved calcium, the $Ca_2UO_2(CO_3)_3$ complex will predominate while for concentrations of dissolved calcium

below 2.2 mmol/l, the $CaUO_2(CO_3)_3^{2-}$ complex will gain relevance. These species have also been found to predominate in uranium-contaminated sediments collected from the Hanford, USA (Liu *et al.*, 2004) and Ittevile, France (Phrommavanh, 2008) sites. The dominance of these species under *in situ* conditions in the B1/B2 basins, which is supported by the findings of the batch (Chapter 7) and column studies, as well as from the results of analysis of groundwater samples (Chapter 6), will increase the mobility of uranium in the basins. Aqueous uranyl-carbonate species, however, adsorb to varying degrees on hydroxylated mineral surfaces (Duff and Amrhein, 1996) and the overall mobility of uranium will be controlled by competition between aqueous and surface complexation.

8.7.2 Uranium solid speciation

Dissolved uranium in the columns' effluent was calculated to be undersaturated with regards to the most common uranium phases found in nature, including the two shoepite phases, schoepite and dehydrated schoepite (Appendix 6). Other silicate (soddyite, Na-boltwoodite and Na-weeksite) and non-silicate (clarkeite, becquerelite) phases were occasionally near equilibrium although no relation could be established between equilibrium and flow rate or experimental time elapsed.

Under batch conditions (Chapter 7), and particularly at apparent steady-state, equilibrium of uranium phases, such as uranophane and schoepite, was observed. Under column conditions, dissolved concentrations of uranium are a function of the rate of uranium release (desorption, dissolution or a combination of both) and flow rate. Undersaturation of the uranium phases indicate that the flow rates applied did not permit sufficient contact time to reach equilibrium between the solid and aqueous phases.

8.8 Percentage of uranium release

The total uranium mass released from each column can be calculated as a percentage of its initial concentration in the sample. At the end of the experiments, the three columns of sludge had released less than 3% of the initial mass of uranium each (Table 8.5). The two columns of tailings released approximately 30% of the initial uranium content.

The low release of uranium from the packed columns of sludge (2.1% and 0.2% for the aged and fresh sludge, respectively) was observed despite the large volume of artificial rainwater flushed through the columns, 660 and 220 pore volumes, respectively.

Similarly, the hundreds of hours of stop-flow conditions applied did not result in increased release of uranium as would have been expected given the extended contact times. The fraction of uranium released from the undisturbed column of fresh sludge was negligible at <0.001%, partly due to the short experimental time, only 15 pore volumes eluted, partly due to the slow kinetics of release. The low release of uranium from the samples of sludge under dynamic conditions is identical to that observed under batch conditions where the maximum percentage released was 4% (fresh dried sludge) and appear to indicate uranium to be present as a relatively insoluble and immobile phase.

These results contrast with the results of sequential extraction where more than 90% uranium was found to be easily labile. These phases are operationally defined by the extractants used to remove them (NaOAc at pH 5 and a solution of oxalic acid and ammonium oxalate). The results of the column experimental conditions are more likely to mimic uranium release and migration under field conditions.

With regards to the tailings, 26% of the total uranium was released from the column of aged tailings, which was eluted with more than 150 pore volumes, and 33% was released from the column of fresh tailings, eluted with 930 pore volumes. These values are, once again, similar to those observed under batch conditions where the release of uranium ranged from 5% to 30% of the initial solid uranium. The fraction of uranium eluted was low when compared with the fraction of easily labile uranium measured by sequential extraction (≈75%) probably as a result of the less aggressive extraction conditions and solutions used in the batch experiments (no mixing or shaking, extraction with low ionic strength artificial rainwater).

Table 8.5: Amount of ^{238}U and ^{233}U released from column experiments.

Column	Pore volumes eluted	[^{238}U] in the sample (mg/kg)	Total ^{238}U in column (mg)	^{238}U released (%)	[^{233}U] injected (mol/l)	Total ^{233}U injected (mol)	^{233}U released (%)
Aged sludge	681	1640 ± 150	54 ± 5	**2.1 ± 0.2**	-	-	**-**
Fresh sludge	216	12800 ± 1120	280 ± 25	**0.2 ± 0.1**	-	-	**-**
Undisturbed sludge	15	4200 ± 20	2820 ± 12	**< 0.001**	-	-	**-**
Aged tailings	175	60 ± 1	2.30 ± 0.04	**33 ± 1**	-	-	**-**
Fresh tailings	932	45 ± 1	1.15 ± 0.01	**26 ± 1**	$49(\pm2)\cdot10^{-9}$	$46(\pm2)\cdot10^{-9}$	**22 ± 11**

8.9 Main findings on uranium release under dynamic conditions

The sequential extraction results discussed in Chapter 6, indicated the majority of the uranium solid speciation in the samples of sludge and tailings to comprise association with carbonate minerals, amorphous minerals of Fe, Al and Si, as adsorbed phase and as secondary uranium phases. The spectroscopic analysis corroborated these findings for the samples of sludge although the concentrations of uranium in the samples of tailings were below detection limits. Although the contribution of each phase to aqueous concentrations of uranium cannot be quantified solely on the results of the kinetic experiments, the initial fast release observed during the first 15 days of the batch experiments is likely to correspond to a mechanism of desorption. This in turn, is followed by the slow continuous dissolution of a uranium phase. In the case of the dynamic experiments, the predominant mechanism contributing to uranium release will be a function of the flow rate. If the flow rate is sufficiently slow, equilibrium conditions are established. An increase of the flow rate will not allow equilibration of the system, and the release will be dominated by kinetics. As observed with the experimental adsorption of ^{233}U, uranium can be sorbed and desorbed in parallel (Figure 8.21Figure 8.21: Release of U from the column of fresh tailings with time (expressed as pore volume)), so it is likely that aqueous uranium migrating along the column will be subject to re-sorption before being eluted.

In the case of the tailings, apparent steady state of uranium release given by phase dissolution was not observed in the columns, even at very slow flow rates (0.037 ml/min).

The dissolution rates of uranium were found to be within the same order of magnitude regardless of the experimental set-up (Table 8.6). The dissolution rates varied between 10^{-10} and 10^{-11} mol/m^2.day in the experiments carried out with the aged sample of sludge (SC417a 1.5-3.0m) and between 10^{-12} and 10^{-13} mol/m^2.day for the fresh sample of sludge (SC429 6.8m) The dissolution rate of uranium in the samples of tailings indicated less variance between the samples and ranged between $7 \cdot 10^{-12}$ and $2 \cdot 10^{-11}$ mol/m^2.day.

Table 8.6: Rates of uranium phase dissolution in sample of sludge and tailings under batch and column conditions.

Strata	Sample	Experiment	Preparation	U mass in sample (mg/kg)	Surface area (m^2/g)	Dissolution Rate ($mol/m^2.day$)
Sludge	SC417a 1.5-3.0m	Packed column of aged sludge	0.5-1.0mm	1,640 ± 150	400 ± 20	$3.3\ (\pm 0.3) \cdot 10^{-11}$
	SC417a 1.5-3.0m	Batch, aged sludge	0.5-1.0mm Dry			$2.3\ (\pm 0.5) \cdot 10^{-11}$
	SC417a 1.5-3.0m	Batch, aged sludge	<0.5 mm Dry	2,150 ± 100	80 ± 30	$1.6\ (\pm 0.6) \cdot 10^{-10}$
	SC429 6.8m	Batch, fresh wet sample of sludge	Wet	60 ± 2	200 ± 10	$2.4\ (\pm 1.1) \cdot 10^{-12}$
	SC429 6.8m	Batch, fresh wet sample of sludge	Dry			$2.3\ (\pm 2.7) \cdot 10^{-12}$
	SC429 8.1m	Packed column of fresh sludge	0.5-1.0mm	12,800 ± 1,100	500 ± 15	$8.8\ (\pm 4.9) \cdot 10^{-12}$
	SC429 8.1m	Undisturbed column of sludge	unsieved	4,200 ± 20	480 ± 80	$2.7\ (\pm 0.1) \cdot 10^{-13}$
Tailings	SC416B 5.8-7.3m	Packed column of aged tailings	0.5-1.0mm	10 ± 1	1,100 ± 25	$1.7\ (\pm 0.1) \cdot 10^{-11}$
	SC429 11.75-11.85m	Packed column of fresh tailings	0.5-1.0mm	45 ± 1	50 ± 15	$1.8\ (\pm 0.1) \cdot 10^{-11}$
	SC429 8.8m	Batch, fresh wet sample of sludge	Wet	20 ± 1	100 ± 15	$7.1\ (\pm 2.4) \cdot 10^{-12}$
	SC429 8.8m	Batch, fresh wet sample of sludge	Dry	20 ± 1	100 ± 15	$9.4\ (\pm 1.5) \cdot 10^{-12}$

8.10 Kinetics of Thorium Release

8.10.1 Packed column of aged sludge

The concentrations of thorium were below the detection limit of $4.3 \cdot 10^{-11}$ mol/l in all the eluates from the first three tests run in the packed column of aged sludge. However, in the fourth flow rate (0.129 ml/min), thorium concentrations were above detection limit (Figure 8.24). The appearance of thorium concentrations above detection limit during the last flow rate may have resulted from the SF event of long duration (271 days) applied before elution, which allowed a slow release of thorium into the aqueous phase prior to the start of flushing. Thorium eluted slowly at a rate of $1.1 \cdot 10^{-13}$ mol/l.sec. The stop flow of 135 hour duration led to an increase in Th concentrations, confirming kinetic release.

8.10.2 Packed column of fresh sludge

The release of thorium from the packed column of fresh sludge was highest in the first pore volume ($3.45 \cdot 10^{-9}$ mol/l) and then decreased rapidly during the following 30 pore volumes to $1.34 \cdot 10^{-9}$ mol/l. (Figure 8.24). A slower decrease in concentrations was observed until the end of the experiment. The rate of thorium release was $1.4 \cdot 10^{-13}$ mol/l.sec, two orders of magnitude lower than the rate of uranium release.

8.10.3 Undisturbed column of sludge

The concentration of thorium in the eluate of the undisturbed column of sludge were always below the detection limit of $4.3 \cdot 10^{-10}$ mol/l.

8.10.4 Packed column of aged tailings

Thorium concentrations above detection limit were measured only during the flushing at 0.037 ml/min, where the residence time of the aqueous phase was 456 min (Figure 8.27). Thorium concentrations were also measured in two aliquots where the residence time was 114 min, although it dropped again below the limit of detection in the subsequent aliquots. Thorium concentrations decreased from $3.9 \cdot 10^{-10}$ mol/l in the first pore volume

to $4.9 \cdot 10^{-11}$ mol/l at 8.6 pore volumes, at a rate of $2.3 \cdot 10^{-15}$ mol/l.sec. The stopflow of 129 hours did not appear to change the concentrations of aqueous thorium.

8.10.5 Packed column of fresh tailings

The concentration of thorium in the eluate of the packed column of fresh tailings was not analysed due to the low concentrations of this element in the initial sample of tailings (6.88 mg per kg of dry soil).

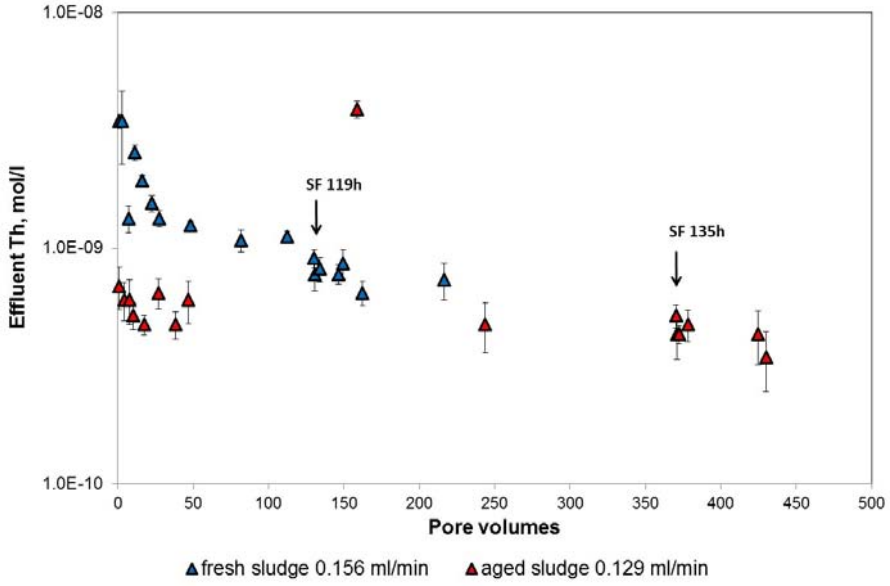

Figure 8.27: Release of Th from the two packed columns of sludge, aged and fresh, with time (expressed as pore volume). Packed column of aged sludge, Q = 0.129 ml/m, residence time = 64 min. Packed column of fresh sludge, Q = 0.156 ml/min, residence time = 90 min. Spikes in the elution profiles result from stop flow events (SF) where advection was stopped for the noted time periods.

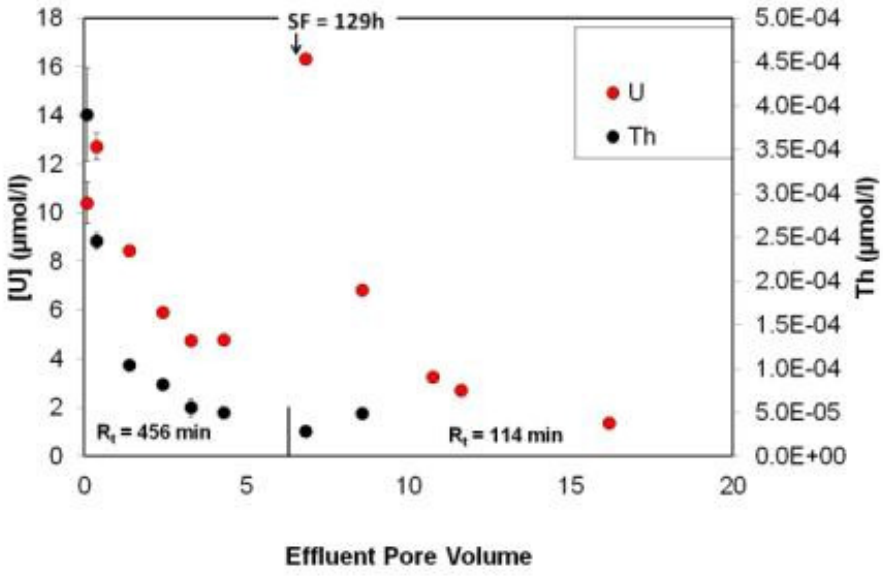

Figure 8.28: Elution of Th and U from the column of aged tailings during the first 20 pore volumes eluted (R_t – transit time). Detection limit of Th = $4.3 \cdot 10^{-5}$ µmol/l. Spikes in the elution profiles result from stop flow events (SF) where advection was stopped for the noted time periods.

8.11 Thorium speciation under dynamic conditions

The aqueous and solid speciation of uranium in the column experiments was computed using the Thermochimie database (Giffaut *et al.*, 2014). The results of effluent speciation are presented in Appendix 6.

8.11.1 Thorium aqueous speciation

Thorium aqueous speciation (Figure 8.30 to Figure 8.32) comprised mostly of mixed carbonate-hydroxide ($Th(OH)_3(CO_3)^-$ and $Th(OH)_2(CO_3)_2^{2-}$) and hydroxide ($Th(OH)_4$ and $Th(OH)_3^+$) complexes. The mixed carbonate-hydroxide species represented more than 50% of the total thorium speciation, particularly at the beginning of the experimental time coinciding with the maximum concentrations of dissolved bicarbonate. With column elution, and the gradual decrease in bicarbonate concentrations, carbonate-hydroxide species are replaced by fluoride complexes (ThF_4 and ThF_3^+). Throughout the experimental time, thorium-hydroxide complexes remained an important fraction of total thorium representing between 30% and 50%.

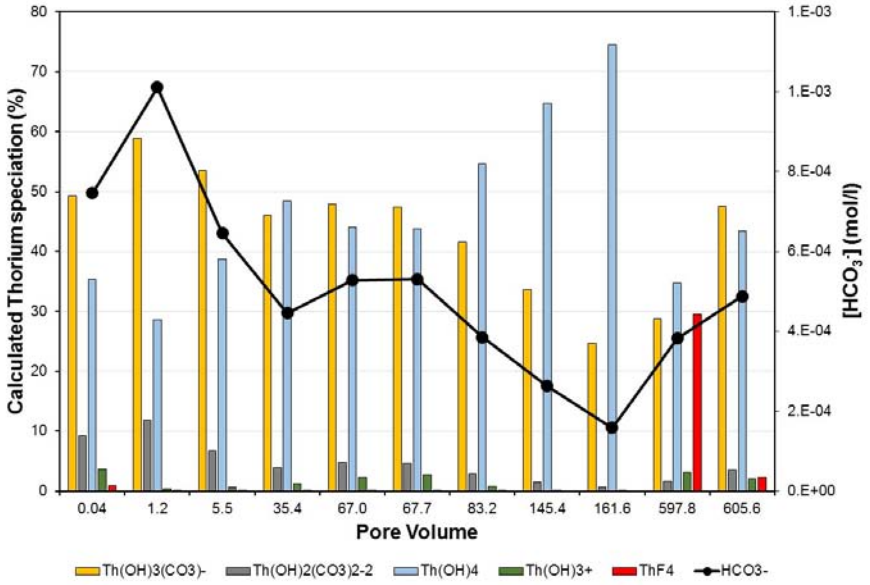

Figure 8.29: Aqueous speciation of thorium in the effluent of the packed column of aged sludge with experimental time expressed as pore volumes.

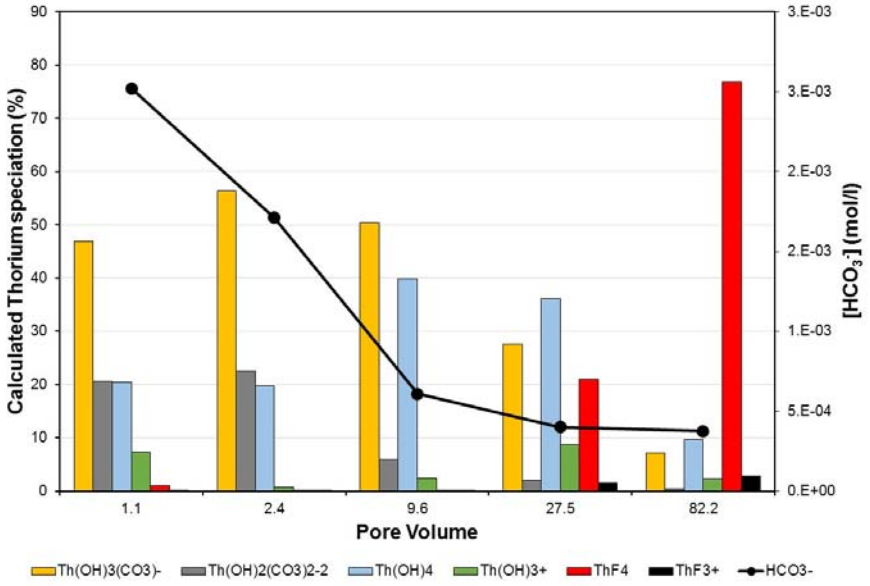

Figure 8.30: Aqueous speciation of thorium in the effluent of the packed column of fresh sludge with experimental time expressed as pore volumes.

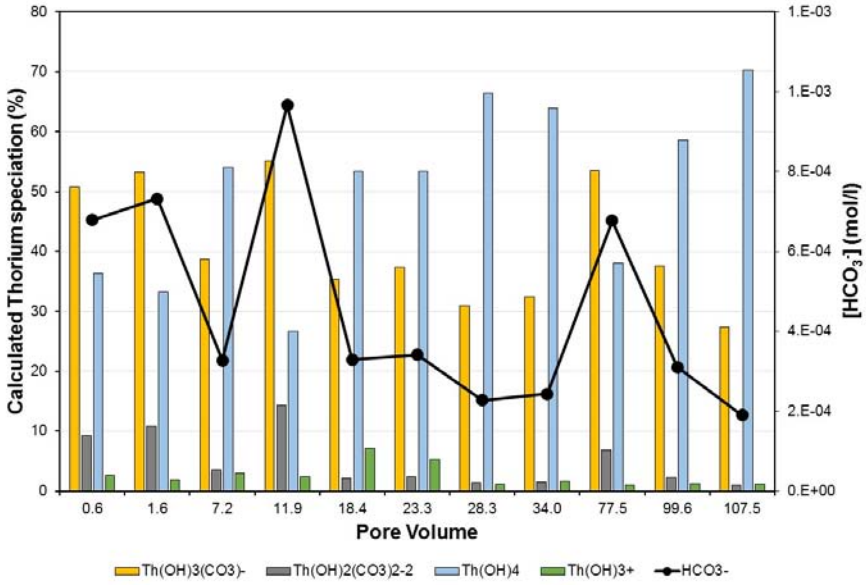

Figure 8.31: Aqueous speciation of thorium in the effluent of the packed column of aged tailings with experimental time expressed as pore volumes.

Although the concentrations of thorium were below detection limit in the samples of groundwater and porewater (Chapter 6), both batch (Chapter 7) and column experiments indicate the hydroxide and mixed carbonate-hydroxide species to be the most stable complexes in solution. Under field conditions, in the B1/B2 basins, carbonate complexation will affect thorium mobility by reducing its adsorption to solid surfaces (Osthols, Bruno and Grenthe, 1994; Neck *et al.*, 2002; M. Altmaier *et al.*, 2005).

8.11.2 Thorium solid speciation

Thorium phases were consistently undersaturated in the eluates of all the columns of sludge (Appendix 6). ThO_2 was near equilibrium at the beginning of the experimental time, and up to pore volume 30, in the column of fresh sludge but became undersaturated with continuous elution.

8.12 Percentage of thorium release

Total thorium eluted was less than 1% in all the column experiments, both sludge and tailings (Table 8.6), confirming the highly refractile behaviour of this element. Between 20 and 30% of total thorium contained in the samples of sludge is potentially easily labile (as discussed in Chapter 6), with the majority of thorium associated with the crystalline

Fe oxides, hydroxides and oxyhydroxides. The smaller fraction of thorium released in the batch and column experiments (maximum of 0.04% and 0.01% respectively) suggests that, under field conditions, thorium is essentially immobile.

Table 8.7: Amount of ^{232}Th released from column experiments.

Column	Pore volumes eluted	[^{232}Th] in the sample (mg/kg)	Total ^{232}Th in column (mg)	^{232}Th released (%)
Aged sludge	681	74 ± 18	2.43 ± 0.59	**0.08 ± 0.02**
Fresh sludge	216	3 ± 1	0.11 ± 0.01	**< 0.002**
Undisturbed sludge	15	373 ± 46	8.15 ± 1.02	**< 0.003**
Aged tailings	175	7 ± 1	0.18 ± 0.01	**Not Measured**
Fresh tailings	932	86 ± 6	57.60 ± 3.76	**0**

8.13 Main findings on thorium release under dynamic conditions

Aqueous concentrations of thorium in the column effluents is controlled by dissolution of ThO_2. The slow kinetic of release was of the order of 10^{-13} mol/l.sec from the sludge and 10^{-15} mol/l.sec from the tailings. Under field conditions, dissolved thorium is likely to be controlled by the low solubility ThO_2 phase and aqueous complexation with carbonates which enhance thorium mobility by reducing surface sorption.

Thorium release into solution was inversely related with its initial solid concentration in the sample (Figure 8.32). In addition, drying of the sample resulted in a higher fraction of thorium being released which may be related with the pre-treatment making a higher fraction of solid available for contact with solution. It is possible that thorium is present in sites of difficult accessibility to groundwater flow

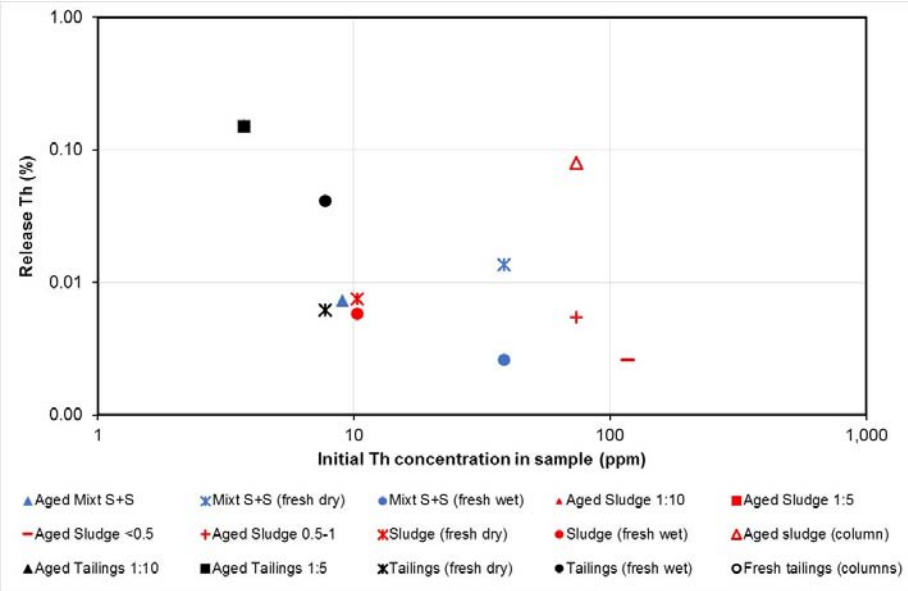

Figure 8.32: Percentage thorium release vs initial thorium concentration in the sample under both batch and column conditions.

9. Conclusions and Implications

9.1 Conclusions

The process of uranium conversion used in the nuclear fuel cycle results in the production of high quantities of liquid effluent. In the case of the AREVA NC Malvési facility, these effluents are currently temporarily stored on site, in decantation basins. Uranium (as ^{234}U and ^{238}U) and thorium (as ^{230}Th) are the main alpha emitters in the waste, representing 30% and 50% of total alpha activity, respectively.

The waste contained in basins B1/B2 was characterised to investigate the geochemical speciation of U and Th in this specific environment. In addition, elution experiments were carried out to study the processes likely to control the mobility of these two elements.

The data reported in this thesis have elucidated the geochemical mechanisms that control the migration of these elements and how this migration can be affected in the long term. The waste in the decantation basins B1/B2 is comprised of various strata, each of different origin and chemical composition. The strata of sludge, with concentrations of up to 4,200 mg/kg of U and 100 mg/kg of Th, acts as a source of these elements. Whilst the strata of tailings control their migration to the underlying aquifer by acting as a sink. Evidence in support of this tenet is derived from the examination of solid samples and pore waters (Chapter 6), batch experiments and geochemical modelling (Chapter 7) and column experiments (Chapter 8). The conclusions drawn from these complementary studies demonstrate that the solid speciation and mobility of these elements are governed by the geochemical environment of each strata.

9.1.1 Th B1/B2 Basins

This study characterised the three main strata of waste contained in the basins B1/B2, the top stratum of mixture of soil and sludge, the middle stratum of sludge and the former sulphur mine tailings present in the base of the basins. Although the samples analysed were collected from a single borehole location, the depth profile in density and moisture content, as well as the elemental composition and mineralogy of the samples were within the range of values obtained in previous investigations (Bary *et al.*, 2010a) which

comprised characterisation of a set of samples distributed horixontally and vertically across the basins.

The upper stratum of waste comprises the mixture of soil and sludge which is characterised by quartz, calcite, muscovite, and low contents of gypsum. The sludge has oxidising conditions and high moisture content which increases with depth. This stratum is rich in amorphous and clay minerals of Al, Si and Fe that provide high surface area and sorption capacity. The amorphous nature of many of the minerals precluded their identification by the X-ray techniques employed in this study. However, the main crystalline phases present were found to be quartz, calcite, dolomite and gypsum, in various relative proportions. The sludge is chemically highly heterogeneous with variable concnetrations of F, Ca, Mg, Si, Fe and U, reflecting the variability of the U ore received, and the evolution of the chemical processes used at the Malvési plant.

The underlying stratum of tailings results from the former sulphur mine tailings and flotation waste and is, as expected charcaterised by gypsum, dolomite and muscovite, with variable contents of quartz and calcite. Throughout the depth of the unsaturated zone, this stratum is characterised by increasing anaerobic decomposition of organic material and increasing nitrate reduction, resulting in decreasing oxidising conditions with depth.

9.1.2 Uranium

This study found that, in the strata of sludge, uranium can be present in more than one solid speciation, as observed by other authors in uranium contaminated sites elsewhere (Catalano *et al.*, 2006; Stubbs *et al.*, 2009). The co-presence of various uranium phases may relate to an immobilisation process, as observed by Brown et al (2010), of initial sorption onto mineral grains and then precipitation as coatings or intergrowths with non-uranium bearing phases, or as discrete uranium-particles. In the sludge, uranium is present as surface sorbed complexes on major crystalline phases, such as calcite and gypsum, as surface sorbed complexes of Fe oxyhydroxide and as uranium mineral phases, such as uranophane and uranyl-oxide. Uranophane, or a similar uranyl-silicate phase, represents the main mineral phase. The release of U into solution and its aqueous transport in the oxidising strata of sludge is compounded by two mechanisms: a fast, initial release, likely uranium release from Fe and carbonate surface complexes; and a slow, continuous release, resulting from dissolution of uranium phases and that becomes dominant in the long term. Ultimately, the concentrations of dissolved uranium under

experimental conditions are controlled by equilibrium with a uranium hydroxide phase, such as dehydrated schoepite. Two possible mechanisms may be taking place during dissolution of uranium, one being the transformation of uranophane into schoepite during elution, the other being dissolution of a surface sorbed layer of uranophane in an existing schoepite phase. At the field scale, and due to the heterogeneous nature of the sludge, it is possible that, locally, other uranium phases may control dissolved uranium concentrations.

Elevated concentrations of calcium, arising from neutralisation of the effluent with lime (CaO), and bicarbonate in the pore water of the sludge results in the formation of strong anionic aqueous calcium-carbonate-uranyl complexes that dominate uranium aqueous complexation and increase uranium solubility. This finding is in agreement with observations made elsewhere at the laboratory (Waite *et al.*, 1994; Um *et al.*, 2007) and field (Zhou and Gu, 2005) scales. Enhanced aqueous mobility of uranium due to colloid formation does not appear to take place in the mixture of soil and sludge nor in the tailings, although it could not be disproved in the samples of sludge.

Dissolved uranium present in the pore water of the strata of sludge percolates downwards to the strata of tailings. Aqueous uranium is readily retained in the strata of tailings, which has an average U content of 100 mg/kg (Bary *et al.*, 2010a). The mechanism of uranium retention in the tailings is primarily by surface sorption, as indicated by the results of sequential extraction which indicated that approximately 70% of the uranium present in this stratum is associated with carbonate and amorphous Fe minerals. Formation of uranium mineral phases may also be occurring in the tailings, however, efforts to characterise the uranium speciation in the tailings were unsuccessful due to the low concentrations of solid uranium in the samples analysed. Decreasing redox conditions with depth in the tailings are likely to further reduce uranium mobility towards the base of the tailings. However, saturated samples of tailings were not characterised or investigated.

9.1.3 Thorium

Thorium was found, by µ-XRF analysis, to be homogeneously distributed in the samples of sludge, and occasionally correlated with uranium, pointing to the presence of a mixed U-Th oxide. In addition, geochemical calculations indicated the ThO_2 phase to govern dissolved Th concentrations (of the order of 10^{-9} mol/l) in all the strata of waste. No kinetic mechanisms were observed in the various experiments, nonetheless, it should be noted

that the low experimental concentrations, coupled with the low analytical limit of detection (of the order of 10^{-10} mol/l), precludes firm conclusions. *In situ* enhanced thorium migration via colloid formation could not, likewise be excluded. Thorium oxide is an insoluble phase and mobility of Th in the basins is expected to be limited.

9.2 Implications and Future Work

This study provided information to characterise the long term behaviour of U and Th in the B1/B2 basins and to support selection of a final disposal option for the waste. Acquisition of such knowledge will assist in the development of appropriate closure criteria, engineering controls and contingency measures, to ensure the waste is managed in the long term in a safe and secure manner.

Rates of release of U and Th into solution were obtained under a set of experimental conditions which elucidated the main macroscale mechanisms. Characterisation of the solid samples during sample elution would provide additional insight into the various mechanisms contributing to U release.

The degradation of organic matter was found to play an important role in controlling dissolved carbonate concentrations and, therefore, uranium mobility in the waste. Future investigations of the mobility of uranium would benefit from characterisation of the nature and content of organic matter as well as the role of microbial activity in the waste.

This study supports the findings by others (Catalano et al, 2006) of the potential association of uranium with calcite in contaminated environments. However, the mechanism of association could not be established. Further work should comprise an investigation of the mechanism of association between uranium and calcite.

Prior to the start of this thesis, there was limited information available relating to the speciation of U and Th in the waste. The methodology adopted in this thesis was therefore to analyse both solid and liquid samples for a range of chemical elements in an analytical semi-quantitative mode, as a balance was required between a need to characterise the chemical composition of the samples and time-budget constraints. This resulted in observations of the correlation of U with elements which could not be fully quantified, such as Ca and Si, therefore increasing the uncertainty relating to the role of calcium-uranyl-silicates in the waste. Further work should aim to quantify Ca and Si and the relation between these elements and U.

Colloids were not found to affect the mobility of either uranium nor thorium in the samples of mixture of soil and sludge and tailings. However, the study was inconclusive with regards to the samples of sludge and future investigations into the role of colloid formation in the aqueous mobility of uranium should be carried out.

This work has put in evidence the importance of an approach comprising complementary techniques in the characterisation of the solid speciation of uranium and thorium in a heterogeneous material. The use of multiple techniques is required to identify different phases and in order to establish multiple lines of evidence for the presence of a certain physical form. Future choice of analytical techniques for both the solid and liquid phases should take into consideration the low concentrations of solid phase uranium in the tailings and low solid and aqueous concentrations of Th throughout the basins. Analysis of Th in solution should attempt to achieve detection limits below the solubility limit of ThO_2.

This study has been laboratory-based experimentation and direct application of the results to the field scale should be preceded by field-scale investigations/trials.

List of References

Ahonen, L., Kaija, J., Paananen, M., Hakkarainen, V. and Ruskeeniemi, T. (2004) *Palmottu natural analogue: A summary of the studies*. Espoo.

Altmaier, B. M., Neck, V. and Fanghänel, T. (2004) 'Solubility and colloid formation of Th (IV) in concentrated NaCl and MgCl2 solution', *Radiochimica Acta*, 92, pp. 537–543.

Altmaier, M., Neck, V., Müller, R. and Fanghänel, T. (2005) 'Solubility of ThO2.xH2O(am) in carbonate solution and the formation of ternary Th(IV) hydroxide-carbonate complexes', *Radiochimica Acta*, 93(2–2005), pp. 83–92. doi: 10.1524/ract.93.2.83.59420.

Altmaier, M., Neck, V., Müller, R. and Fanghänel, T. (2005) 'Solubility of ThO2·xH2O (am) in carbonate solution and the formation of ternary Th (IV) hydroxide-carbonate complexes', *Radiochimica Acta*, 93, pp. 83–92.

Altmaier, M. and Vercouter, T. (2012) 'Aquatic chemistry of the actinides: aspects relevant to their environmental behavior', in *Radionuclide Behaviour in the Natural Environment*, pp. 44–69.

AREVA NC - Comurhex (2010) 'Comurhex Geographic Information System Database'.

AREVA NC Malvési (2013) *Rapport d'information sur la sûreté nucléaire et la radioprotection de l'INB ECRIN, Édition 2013*.

Arnold, T., Zorn, T., Bernhard, G. and Nitsche, H. (1998) 'Sorption of uranium(VI) onto phyllite', *Chemical Geology*, 151(1–4), pp. 129–141. doi: 10.1016/S0009-2541(98)00075-8.

ASN (2013) *Plan National de Gestion des Matières et des Déchets Radioactifs 2013 - 2015*.

ATSDR (1990a) *Toxicological Profile for Radium*.

ATSDR (1990b) *Toxicological Profile for Thorium*.

ATSDR (2013) *Toxicological Profile for Uranium*.

Bary, F., Loriquer, A., Poncet, S. and Delos, A. (2009) *Note Intermédiaire 1.1. Synthèse Documentaire. AREVA-Comurhex-Site de Malvesi (11). Exploitation de l'Entreposage. Lot 1 - Inventaire Detaille des Déchets en Place.*

Bary, F., Loriquer, A., Poncet, S. and Delos, A. (2010a) *Note Intermédiaire 1.2. Compte-rendu factuel des reconnaissances de sols, des essais et analyses. AREVA-Comurhex-Site de Malvesi (11). Exploitation de l'Entreposage. Lot 1 - Inventaire Detaille des Déchets en Place.*

Bary, F., Loriquer, A., Poncet, S. and Delos, A. (2010b) *Note Intermédiaire 1.3. Inventaire des Déchets et des Materiaux en Place. AREVA-Comurhex-Site de Malvesi (11). Exploitation de l'Entreposage. Lot 1 - Inventaire Detaille des Déchets en Place.*

Bernhard, G., Geipel, G., Reich, T., Brendler, V., Amayri, S. and Nitsche, H. (2001) 'Uranyl(VI) carbonate complex formation: Validation of the Ca2UO2(CO3)3(aq.) species', *Radiochimica Acta*, 89, pp. 511–518. doi: 10.1524/ract.2001.89.8.511.

Bitea, C., Müller, R., Neck, V., Walther, C. and Kim, J. I. (2003) 'Study of the generation and stability of thorium(IV) colloids by LIBD combined with ultrafiltration', *Colloids and Surfaces A: Physicochemical and Engineering Aspects*, 217, pp. 63–70. doi: 10.1016/S0927-7757(02)00559-9.

British Standard (1996) 'Method of test for Soils for civil engineering purposes - Part 2: Classification tests. BS 1377-2:1990', p. 72.

Brown, C. F., Serne, R. J., Catalano, J. G., Krupka, K. M. and Icenhower, J. P. (2010) 'Mineralization of contaminant uranium and leach rates in sediments from Hanford, Washington', *Applied Geochemistry*. Elsevier Ltd, 25(1), pp. 97–104. doi: 10.1016/j.apgeochem.2009.10.005.

Bruno, J., Cera, E., Pablo, J. de, Duro, L., Jordana, S. and Savage, D. (1997) *Determination of radionuclide solubility limits to be used in SR 97– Uncertainties associated to calculated solubilities*.

Bruno, J., de Pablo, J., Duro, L. and Figuerola, E. (1995) 'Experimental study and modeling of the U(VI)-Fe(OH)3 surface precipitation/coprecipitation equilibria', *Geochimica et Cosmochimica Acta*, 59(20), pp. 4113–4123.

Brusseau, M. L., Rao, P. S. C., Jessup, R. E. and Davidson, J. M. (1989) 'Flow interruption: A method for investigating sorption nonequilibrium', *Journal of Contaminant Hydrology*, 4(3), pp. 223–240. doi: 10.1016/0169-7722(89)90010-7.

Burgeap (2009a) *Chimie et comportement migratoire des radionucléides d'intérêt*.

Burgeap (2009b) *Comurhex Usine de Malvési-Narbonne (11) Etude Hydrogéologique. Synthèse des Données Existantes*.

Burgeap (2010) *COMURHEX Usine de Malvési – Narbonne (11) Travaux de confortement environnemental. Etude hydrogéologique. Résultats de la modélisation*.

Cantrell, K. J., Serne, R. J. and Last, G. V. (2002) *Hanford Contaminant Distribution Coefficient Database and Users Guide*, *Distribution*.

Casacuberta, N., Christl, M., Lachner, J., Rutgers Van Der Loeff, M., Masqué, P. and Synal, H.-A. (2014) 'A first transect of 236U in the North Atlantic Ocean', *Geochimica et Cosmochimica Acta*, 133, pp. 34–46. doi: 10.1016/j.gca.2014.02.012.

Catalano, J. G. and Brown, G. E. (2005) 'Uranyl adsorption onto montmorillonite: Evaluation of binding sites and carbonate complexation', *Geochimica et Cosmochimica Acta*, 69(12), pp. 2995–3005. doi: 10.1016/j.gca.2005.01.025.

Catalano, J. G., McKinley, J. P., Zachara, J. M., Heald, S. M., Smith, S. C. and Brown, G. E. (2006) 'Changes in uranium speciation through a depth sequence of contaminated Hanford sediments', *Environmental Science & Technology*, 40(8), pp. 2517–2524. doi: 10.1021/es0520969.

Cera, E., Ahonen, L., Rollin, C., Bruno, J., Kaija, J. and Blomqvist, R. (2002) 'Redox Processes at the Palmottu uranium deposit', in von Maravic, H. and Alexander, R. (eds) *Eight EC NAWG Meeting*. Strasbourg, France, pp. 183–200.

Cera, E., Bruno, J. and Duro, L. (1999) 'Redox buffering effect on iron and uranium minerals in Palmottu, Finland', in Ármmansson, H. (ed.) *Geochemistry of the Earth's Surface: Proceedings of the 5th International Symposium on Geochemistry of the Earth's Surface*. Reykjavik, Iceland, pp. 441–444.

Cerato, A. B. and Lutenegger, A. J. (2002) 'Determination of surface area of fine-grained soils by the ethylene glycol monoethyl ether (EGME) method', *Geotechnical Testing Journal*, 25(3), pp. 315–321. doi: 10.1520/GTJ11087J.

Chabaux, F., Riotte, J. and Dequincey, O. (1992) 'U-Th-Ra Fractionation During Weathering and River Transport', in, p. 44.

Chen, C. L. and Wang, X. K. (2007) 'Influence of pH, soil humic/fulvic acid, ionic strength and foreign ions on sorption of thorium(IV) onto γ-Al2O3', *Applied Geochemistry*, 22(2), pp. 436–445. doi: 10.1016/j.apgeochem.2006.11.010.

Chen, C. and Wang, X. (2007) 'Sorption of Th (IV) to silica as a function of pH, humic/fulvic acid, ionic strength, electrolyte type', *Applied Radiation and Isotopes*, 65(2), pp. 155–163. doi: 10.1016/j.apradiso.2006.07.003.

Constantin, H. and Fick, M. (1997) 'Influence of C-sources on the denitrification rate of a high-nitrate concentrated industrial wastewater', *Water Research*, 31(3), pp. 583–589.

Constantin, H., Raoult, S., Montigny, W. and Fick, M. (1996) 'Denitrification of concentrated industrial wastewater: Microorganism selection and kinetic studies', *Environmental Technology*, 17, pp. 831–840.

Dong, W. and Brooks, S. C. (2006) 'Determination of the formation constants of ternary complexes of uranyl and carbonate with alkaline earth metals (Mg2+, Ca2+, Sr2+, and Ba2+) using anion exchange method.', *Environmental Science & Technology*, 40(15), pp. 4689–95.

Duff, M. and Amrhein, C. (1996) 'Uranium(VI) Adsorption on Goethite and Soil in Carbonate Solutions', *Soil Science Society of America Journal*, 60, pp. 1393–1400.

Duff, M. C., Morris, D. E., Hunter, D. B. and Bertsch, P. M. (2000) 'Spectroscopic characterization of uranium in evaporation basin sediments', *Geochimica et Cosmochimica Acta*, 64(9), pp. 1535–1550. doi: 10.1016/S0016-7037(99)00410-X.

Dzombak, D. A. and Morel, F. M. M. (1990) *Surface Complexation Modeling: Hydrous Ferric Oxide*. John Wiley & Sons. doi: 10.1016/B978-0-12-409548-9.05311-2.

Fanghänel, T. and Neck, V. (2002) 'Aquatic chemistry and solubility phenomena of actinide oxides/hydroxides', *Pure and Applied Chemistry*, 74(10), pp. 1895–1907. doi: 10.1351/pac200274101895.

Felmy, A. R., Dhanpat, R. and Mason, M. J. (1991) 'The Solubility of Hydrous Thorium(IV) Oxide in Chloride Media: Development of an Aqueous Ion-Interaction Model', *Radiochimica Acta*, 55, pp. 177–185.

Fox, P., Davis, J. A., Hay, M. B., Conrad, M. E., Campbell, K. M., Williams, K. H. and Long, P. E. (2012) 'Rate-Limited U(VI) Desorption during a Small-Scale Tracer Test in a Heterogeneous Uranium Contaminated Aquifer', *Water Resources Research*.

Fox, P. M., Davis, J. a. and Zachara, J. M. (2006) 'The effect of calcium on aqueous uranium(VI) speciation and adsorption to ferrihydrite and quartz', *Geochimica et Cosmochimica Acta*, 70(6), pp. 1379–1387. doi: 10.1016/j.gca.2005.11.027.

Frost, R. L., Čejka, J., Weier, M. L. and Martens, W. N. (2006) 'Raman spectroscopy study of selected uranophanes', *Journal of Molecular Structure*, 788(1–3), pp. 115–125. doi: 10.1016/j.molstruc.2005.11.025.

Gavrilescu, M., Pavel, L. V. and Cretescu, I. (2009) 'Characterization and remediation of soils contaminated

with uranium', *Journal of Hazardous Materials*, 163, pp. 475–510. doi: 10.1016/j.jhazmat.2008.07.103.

Gieré, R., Kaltenmeier, R. and Pourcelot, L. (2012) 'Uranium oxide and other airborne particles deposited on cypress leaves close to a nuclear facility', *Journal of Environmental Monitoring*, 14, p. 1264. doi: 10.1039/c2em11000h.

Giffaut, E., Grivé, M., Blanc, P., Vieillard, P., Colàs, E., Gailhanou, H., Gaboreau, S., Marty, N., Madé, B. and Duro, L. (2014) 'Andra thermodynamic database for performance assessment: ThermoChimie', *Applied Geochemistry*. Elsevier Ltd, 49, pp. 225–236. doi: 10.1016/j.apgeochem.2014.05.007.

Glaus, M., Hummel, W. and Van Loon, L. R. (1997) *Experimental determination and modelling of trace metal-humate interactions: A pragmatic approach for applications in groundwater*, *Nagra Technischer Bericht*.

Grenthe, I., Drozdzynski, J., Fujino, T., Buck, E. C., Albrecht-Schmitt, T. E. and Wolf, S. F. (2006) 'Uranium', in *The chemistry of the actinide and transactinide elements*.

Guillaumont, R. (2003) *Update on the Chemical Thermodynamics of Uranium, Neptunium, Plutonium, Americium and Technetium*. Elsevier B.V.

Van Hecke, W., Chabran, J. M., Barandas, C. and Ligney, J. . (2009) *COMURHEX - Malvési Etablissement. Dossier d'Options de Surete Bassins d'Entreposage B1 et B2*.

Hennig, C., Weiss, S., Banerjee, D., Brendler, E., Honkimäki, V., Cuello, G., Ikeda-Ohno, A., Scheinost, A. C. and Zänker, H. (2013) 'Solid-state properties and colloidal stability of thorium(IV)–silica nanoparticles', *Geochimica et Cosmochimica Acta*, 103, pp. 197–212. doi: 10.1016/j.gca.2012.10.051.

Herring, J. S. (2004) 'Uranium and Thorium Resource Assessment', *Encyclopedia of Energy*.

Hongxia, Z., Zheng, D. and Zuyi, T. (2006) 'Sorption of thorium(IV) ions on gibbsite: Effects of contact time, pH, ionic strength, concentration, phosphate and fulvic acid', *Colloids and Surfaces A: Physicochemical and Engineering Aspects*, 278(1–3), pp. 46–52. doi: 10.1016/j.colsurfa.2005.11.078.

Hsi, C.-K. D. and Langmuir, D. (1985) 'Adsorption of uranyl onto ferric oxyhydroxides. Application of the surface complexation site-binding model', *Geochimica et Cosmochimica Acta*, 49, pp. 1931–1941.

IAEA (1999) *Minimization of waste from uranium purification, enrichment and fuel fabrication*. Vienna.

IAEA (2014) *Nuclear Technology Review 2014*, *Nuclear technology review*.

IAEA (2016) 'Nuclear Technology Review 2016', *International Atomic Energy Agency General Conference*, (June), p. 58.

Jakobsson, A. (1999) 'Measurement and Modeling of Th Sorption onto TiO(2).', *Journal of colloid and interface science*, 220(2), pp. 367–373. doi: 10.1006/jcis.1999.6535.

Jang, J.-H., Dempsey, B. A. and Burgos, W. D. (2007) 'A Model-Based Evaluation of Sorptive Reactivities of Hydrous Ferric Oxide and Hematite for U(VI)', *Environmental Science & Technology*, 41(12), pp. 4305–4310. doi: 10.1021/es070068f.

Jernstrom, J., Vuorinen, U. and Hakanen, M. (2002) *Solubility of thorium in 0.1 M NaCl solution and in saline and fresh anoxic reference groundwater*.

Kabata-Pendias, A. and Pendias, H. (1985) *Trace elements in soils and plants*. Boca Raton.

Kalmykov, S. N. and Choppin, G. R. (2000) 'Mixed Ca2+/UO22+/CO32-complex formation at different ionic

strengths', *Radiochimica Acta*, 88(9–11_2000), pp. 603–606. doi: 10.1524/ract.2000.88.9-11.603.

Kaplan, D. I. and Serkiz, S. M. (2001) 'Quantification of thorium and uranium sorption to contaminated sediments', *Journal of Radioanalytical and Nuclear Chemistry*, 248(3), pp. 529–535. doi: 10.1023/A:1010606325979.

Keith, S. and Wohlers, D. W. (2014) *Addendum to the Toxicological Profile for Thorium Agency for Toxic Substances and Disease Registry*. Atlanta.

Kelly, S. D., Newville, M. G., Cheng, L., Kemner, K. M., Sutton, S. R., Fenter, P., Sturchio, N. C. and Spötl, C. (2003) 'Uranyl incorporation in natural calcite', *Environmental Science & Technology*, 37(7), pp. 1284–1287. doi: 10.1021/es025962f.

Krauskopf, K. B. and Bird, D. K. (1995) *Introduction to Geochemistry*. Singapure: McGraw-Hill Inc.

Krupka, K. M. and Serne, R. J. (2002) *Geochemical Factors Affecting the Behavior of Antimony, Cobalt, Europium, Technetium, and Uranium in Vadose Sediments*.

LaFlamme, B. D. and Murray, J. W. (1987) 'Solid/Solution interaction: The effect of carbonate alkalinity on adsorbed thorium', *Geochimica et Cosmochimica Acta*, 51(2), pp. 243–250. doi: 10.1016/0016-7037(87)90235-3.

Landa, E. (1980) *Geological Survey Circular 814. Isolation of Uranium Mill Tailings and Their Component Radionuclides From the Biosphere-Some Earth Science Perspectives*.

Landa, E., Cravotta, C., Naftz, D., Verplanck, P., Nordstrom, D. and Zielinski, R. (2000) 'Geochemical Investigations by the U.S. Geological Survey on Uranium Mining, Milling, and Environmental Restoration', *Technology*, 7, pp. 381–396.

Landa, E. R. (2004) 'Uranium mill tailings: Nuclear waste and natural laboratory for geochemical and radioecological investigations', *Journal of Environmental Radioactivity*, 77, pp. 1–27. doi: 10.1016/j.jenvrad.2004.01.030.

Langmuir, D. (1978) 'Uranium solution-mineral equilibria at low temperatures with applications to sedimentary ore deposits', *Geochimica et Cosmochimica Acta*, 42, pp. 547–569. doi: 10.1016/0016-7037(79)90011-5.

Langmuir, D. (1997) *Aqueous Environmental Geochemistry*. Prentice Hall. doi: 10.1029/97EO00355.

Langmuir, D. and Herman, J. S. (1980) 'The mobility of thorium in natural waters at low temperatures', *Geochimica et Cosmochimica Acta*, 44, pp. 1753–1766.

Liu, C., Zachara, J. M., Qafoku, N. P. and Wang, Z. (2008) 'Scale-dependent desorption of uranium from contaminated subsurface sediments', *Water Resources Research*, 44, pp. 1–13. doi: 10.1029/2007WR006478.

Liu, C., Zachara, J. M., Qafoku, O., McKinley, J. P., Heald, S. M. and Wang, Z. (2004) 'Dissolution of uranyl microprecipitates in subsurface sediments at Hanford Site, USA', *Geochimica et Cosmochimica Acta*, 68(22), pp. 4519–4537. doi: 10.1016/j.gca.2004.04.017.

MacKenzie, A., Scott, R., Linsalata, P. and Miekeley, N. (1992) 'Natural decay series studies of the redox front system in the Poços de Caldas uranium mineralization', *Journal of Geochemical Exploration*, 45(1–3), pp. 289–322.

Massey, M. S., Lezama-Pacheco, J. S., Nelson, J. M., Fendorf, S. and Maher, K. (2014) 'Uranium incorporation into amorphous silica', *Environmental Science & Technology*, 48(15), pp. 8636–8644. doi: 10.1021/es501064m.

McKinley, J. P., Zachara, J. M., Liu, C., Heald, S. C., Prenitzer, B. I. and Kempshall, B. W. (2006) 'Microscale controls on the fate of contaminant uranium in the vadose zone, Hanford Site, Washington', *Geochimica et Cosmochimica Acta*, 70, pp. 1873–1887. doi: 10.1016/j.gca.2005.10.037.

Miekeley, N., Coutinho de Jesus, H., Porto da Silveira, C. and Degueldre, C. (1992) 'Chemical and physical characterization of suspended particles and colloids in waters from the Osamu Utsumi mine and Morro do Ferro analogue study sites, Poços de Caldas, Brazil', *Journal of Geochemical Exploration*, 45(1–3), pp. 409–437.

Miekeley, N. and Küchler, I. L. (1987) 'Interactions between thorium and humic compounds in surface waters', *Inorganica Chimica Acta*, 140, pp. 315–319. doi: 10.1016/S0020-1693(00)81113-5.

Moon, H. (1989) 'Equilibrium Ultrafiltration of Hydrolyzed Thorium(IV) Solutions', *Bull. Korean Chem. Soc.*, 10(3).

Murakami, T., Sato, T., Ohnuki, T. and Isobe, H. (2005) 'Field evidence for uranium nanocrystallization and its implications for uranium transport', *Chemical Geology*, 221, pp. 117–126. doi: 10.1016/j.chemgeo.2005.04.004.

Neck, V., Altmaier, M., Müller, R., Bauer, A., Fanghänel, T. and Kim, J. I. (2003) 'Solubility of crystalline thorium dioxide', *Radiochimica Acta*, 91(5), pp. 253–262. doi: 10.1524/ract.91.5.253.20306.

Neck, V. and Kim, J. I. (2001) 'Solubility and hydrolysis of tetravalent actinides', *Radiochimica Acta*, 89, pp. 1–16. doi: 10.1524/ract.2001.89.1.001.

Neck, V., Müller, R., Bouby, M., Altmaier, M., Rothe, J., Denecke, M. a. and Kim, J. I. (2002) 'Solubility of amorphous Th(IV) hydroxide - Application of LIBD to determine the solubility product and EXAFS for aqueous speciation', *Radiochimica Acta*, 90(9–11), pp. 485–494. doi: 10.1524/ract.2002.90.9-11_2002.485.

Nico, P. S., Stewart, B. D. and Fendorf, S. (2009) 'Incorporation of Oxidized Uranium into Fe (Hydr)oxides during Fe(II) Catalyzed Remineralization', *Environmental Science & Technology*, 43(19), pp. 7391–7396. doi: 10.1021/es900515q.

Nordberg, G. F., Fowler, B. A., Nordberg, M. and Friberg, L. (2008) *Handbook of The Toxicology of Metal*. Third Edit, *Academic Press, Inc*. Third Edit.

Östhols, E. (1995) 'Thorium sorption on amorphous silica', *Geochimica et Cosmochimica Acta*, 59(7), pp. 1235–1249. doi: 10.1016/0016-7037(95)00040-7.

Osthols, E., Bruno, J. and Grenthe, I. (1994) 'On the influence of carbonate on mineral dissolution: III. The solubility of microcrystalline ThO2 in CO-H2O media', *Geochimica et Cosmochimica Acta*, 58(2), pp. 613–623.

Parkhurst, D. L. and Appelo, C. (1999) *User's Guide To PHREEQC (version 2) — a computer program for speciation, batch-reaction, one-dimensional transport and inverse geochemical calculations*, *Water-Resources Investigations Report 99-4259*. doi: Rep. 99-4259.

Parkhurst, D. L. and Appelo, C. A. J. (2015) 'PHREEQC Version 3--A Computer Program for Speciation,

Batch-Reaction, One-Dimensional Transport, and Inverse Geochemical Calculations'.

Payne, T. (1999) *Uranium (VI) interactions with mineral surfaces: controlling factors and surface complexation modelling*. University of New South Wales.

Payne, T. E., Brendler, V., Comarmond, M. J. and Nebelung, C. (2011) 'Assessment of surface area normalisation for interpreting distribution coefficients (K(d)) for uranium sorption.', *Journal of environmental radioactivity*. Elsevier Ltd, 102(10), pp. 888–895. doi: 10.1016/j.jenvrad.2010.04.005.

Payne, T., Edis, R., Herczeg, A., Sekine, K., Seo, Y., Waite, T. and Yanase, N. (1992) *Groundwater chemistry. Alligator Riv- ers Analogue Project Final Report, Volume 7*. Sydney, Australia.

Perez, A. (1980) 'Du Concentré d'Uranium a l'Hexafluorure', in *Proceedings of an Advisory Group Meeting, Paris, 5-8 June 1979*. Paris: IAEA, International Atomic Energy Agency, pp. 201–228.

Pérez, I., Casas, I., Martín, M. and Bruno, J. (2000) 'The thermodynamics and kinetics of uranophane dissolution in bicarbonate test solutions', *Geochimica et Cosmochimica Acta*, 64(4), pp. 603–608. doi: 10.1016/S0016-7037(99)00337-3.

Pérez, I., Casas, I., Torrero, M., Cera, E., Duro, L. and Bruno, J. (1997) 'Dissolution Studies of Soddyite as a Long-Term Analogue of the Oxidative Alteration of the Spent Nuclear Fuel Matrix', in *MRS Proceedings*, p. 465.

Peterson, J., MacDonell, M., Haroun, L. and Monette, F. (2007) *Radiological and chemical fact sheets to support health risk analyses for contaminated areas*.

Phrommavanh, V. (2008) *Etude de la migration de l'uranium en milieu naturel: Approche experimentale et modelisation geochimique*. Universite Joseph Fourier - Grenoble I.

Plummer, L., Wigley, T. and Parkhurst, D. (1978) 'The kinetics of calcite dissolution in CO2-water systems at 5º to 60ºC and 0.0 to 1.0 atm CO2', *American Journal of Science*, 278, pp. 179–216.

Pourcelot, L. (2008) *Bilan radioécologique de l'environnement du site de Malvési. Etude complémentaire menée en 2008*.

Pourcelot, L., Boulet, B., Le Corre, C., Loyen, J., Fayolle, C., Tournieux, D., Van Hecke, W., Martinez, B. and Petit, J. (2011) 'Isotopic evidence of natural uranium and spent fuel uranium releases into the environment.', *Journal of Environmental Monitoring*, 13, pp. 355–361. doi: 10.1039/c0em00407c.

Pourcelot, L. and Le Roux, G. (2008) *Etude radioécologique de l'environnement du site de Malvési (société COMURHEX)*.

Puigdomenech, I. (2010) 'MEDUSA: Making Equilibrium Diagrams Using Sophisticated Algorithms'. Stockholm: Royal Institute of Technology, Stockholm, Sweden.

Qafoku, N. P., Zachara, J. M., Liu, C., Gassman, P. L., Qafoku, O. S. and Smith, S. C. (2005) 'Kinetic desorption and sorption of U(VI) during reactive transport in a contaminated Hanford sediment', *Environmental Science & Technology*, 39(9), pp. 3157–3165. doi: 10.1021/es048462q.

Quigley, M. S., Honeyman, B. D. and Santschi, P. H. (1996) 'Throium sorption in the marine environment: equilibrium partitioning at the hematite/water interface, sorption/desorption kinetics and particle tracing', *Aquatic Geochemistry*, 1, pp. 277–301.

Raffo-Caiado, A. C., Begovich, J. M., Ferrada, J. J., Ladd-lively, J., Antonio, M., Marzo, S., Grund, M. S., Saraiva Marzo, M. A., Crissiuma Palhares, L., Cordeiro Diaz, F. and Grund, M. S. (2009) *Model of a Generic Natural Uranium Conversion Plant — Suggested Measures to Strengthen International Safeguards*. Oak Ridge National Laboratory / Brazilian Nuclear Energy Commission.

Rautman, C., McGraw, M., Istok, J., Sigda, J. and Kaplan, P. (1994) 'Probabilistic Comparison of Alternative Characterization Technologies at the Fernald Uranium-in-Soils Integrated Demonstration Project', p. 11.

Reiller, P., Moulin, V., Casanova, F. and Dautel, C. (2002) 'Retention behaviour of humic substances onto mineral surfaces and consequences upon thorium (IV) mobility: Case of iron oxides', *Applied Geochemistry*, 17(12), pp. 1551–1562. doi: 10.1016/S0883-2927(02)00045-8.

Righetto, L., Bidoglio, G., Azimonti, G. and Bellobono, I. R. (1991) 'Competitive actinide interactions in colloidal humic acid-mineral oxide systems', *Environmental Science & Technology*, 25(11), pp. 1913–1919. doi: 10.1021/es00023a012.

Rojo, I., Seco, F., Rovira, M., Giménez, J., Cervantes, G., Martí, V. and de Pablo, J. (2009) 'Thorium sorption onto magnetite and ferrihydrite in acidic conditions', *Journal of Nuclear Materials*. Elsevier B.V., 385(2), pp. 474–478. doi: 10.1016/j.jnucmat.2008.12.014.

Rothe, J., Denecke, M. A., Neck, V., Müller, R. and Kim, J. I. (2002) 'XAFS investigation of the structure of aqueous thorium(IV) species, colloids, and solid thorium(IV) oxide/hydroxide', *Inorganic chemistry*, 41(2), pp. 249–258.

Ryan, J. L. and Rai, D. (1987) 'Thorium(IV) Hydrous Oxide Solubility', *Inorganic chemistry*, 26, pp. 4140–4142.

Saito, T., Koopal, L., Nagasaki, S. and Tanaka, S. (2004) 'Application of the NICA-Donnan model for proton, copper and uranyl binding to humic acid', *Radiochimica Acta*, 92, pp. 567–574.

Santschi, P. H., Murray, J. W., Baskaran, M., Benitez-Nelson, C. R., Guo, L. D., Hung, C. C., Lamborg, C., Moran, S. B., Passow, U. and Roy-Barman, M. (2006) 'Thorium speciation in seawater', *Marine Chemistry*, 100(3–4 SPEC. ISS.), pp. 250–268. doi: 10.1016/j.marchem.2005.10.024.

Sato, T., Murakami, T., Yanase, N., Isobe, H., Payne, T. E. and Airey, P. L. (1997) 'Iron nodules scavenging uranium from groundwater', *Environmental Science and Technology*, 31(10), pp. 2854–2858. doi: 10.1021/es970058m.

Schindler, P. (1967) 'Heterogeneous equilibria involving oxides, hydroxides, carbonates, and hydroxide carbonates', in Stumm, W. (ed.) *Equilibrium concepts in natural water systems*. American Chemical Society, pp. 196–221.

Schmidt, M., Lee, S. S., Wilson, R. E., Soderholm, L. and Fenter, P. (2012) 'Sorption of tetravalent thorium on muscovite', *Geochimica et Cosmochimica Acta*. Elsevier Ltd, 88, pp. 66–76. doi: 10.1016/j.gca.2012.04.001.

Schmitt, J. M. (1998) *Caractérisation lithologique, minéralogique et géochimique du substratum des bassin B1/B2*.

Schneider, E., Carlsen, B. W. and Tavrides, E. (2010) *Measures of the Environmental Footprint of the Front End of the Nuclear Fuel Cycle*.

Seah, M. P., Gilmore, I. S. and Beamson, G. (1998) 'XPS: binding energy calibration of electron spectrometers 5—re-evaluation of the reference energies', *Surface and Interface Analysis*, 26, pp. 642–649. doi: 10.1002/(SICI)1096-9918(199808)26:9<642::AID-SIA408>3.0.CO;2-3.

Seeley, F. and Kelmers, A. (1985) *Geochemical information for sites contaminated with low-level radioactive wastes: III - Weldon Spring Storage Site*.

Serkiz, S. M., Johnson, W. H., Wile, L. M. J. and Clark, S. B. (2007) 'Environmental Availability of Uranium in an Acidic Plume at the Savannah River Site', *Vadose Zone Journal*, 6(2), pp. 354–362. doi: 10.2136/vzj2006.0072.

Short, S. A. (1988) *Chemical transport of uranium and thorium in the Alligator Rivers Uranium Province , Northern Territory , Australia*.

Singer, D. M., Zachara, J. M. and Brown, G. E. (2009) 'Uranium speciation as a function of depth in contaminated Hanford sediments - A micro-XRF, micro-XRD, and micro- and bulk-XAFS study', *Environmental Science & Technology*, 43(3), pp. 630–636. doi: 10.1021/es8021045.

SLREM, S. L. de R. et d'Exploitations M. (1952) *La Production Française de Soufre Natif*. Paris.

Sowder, A. G., Clark, S. B. and Fjeld, R. A. (2001) 'The impact of mineralogy in the U(VI)–Ca–PO4 system on the environmental availability of uranium', *Journal of Radioanalytical and Nuclear Chemistry*, 248(3), pp. 517–524.

Steier, P., Bichler, M., Fifield, L. K., Golser, R., Kutschera, W., Priller, A., Quinto, F., Richter, S., Srncik, M., Terrasi, P., Wacker, L., Wallner, A., Wallner, G., Wilcken, K. M. and Wild, E. M. (2008) 'Natural and anthropogenic 236U in environemntal samples', *Nuclear Instruments and Methods in Physics Research B*, 266, pp. 2246–2250. doi: 10.1016/j.nimb.2008.03.002.

Steward, S. A. and Mones, E. T. (1996) 'Comparison and Modeling of Aqueous Dissolution Rates of Various Uranium Oxides', in *Materials Research Society Fall Meeting*, p. 12.

Stubbs, J. E., Veblen, L. a., Elbert, D. C., Zachara, J. M., Davis, J. a. and Veblen, D. R. (2009) 'Newly recognized hosts for uranium in the Hanford Site vadose zone', *Geochimica et Cosmochimica Acta*. Elsevier Ltd, 73(6), pp. 1563–1576. doi: 10.1016/j.gca.2008.12.004.

Sylwester, E. ., Hudson, E. . and Allen, P. . (2000) 'The structure of uranium (VI) sorption complexes on silica, alumina, and montmorillonite', *Geochimica et Cosmochimica Acta*, 64(14), pp. 2431–2438. doi: 10.1016/S0016-7037(00)00376-8.

Tan, X., Wang, X., Chen, C. and Sun, A. (2007) 'Effect of soil humic and fulvic acids, pH and ionic strength on Th(IV) sorption to TiO2 nanoparticles', *Applied Radiation and Isotopes*, 65(4), pp. 375–381. doi: 10.1016/j.apradiso.2006.10.014.

Taylor, S. (1964) 'Abundance of chemical elements in the continental crust: a new table', *Geochimica et Cosmochimica Acta*, 28, pp. 1273–1285.

Tessier, a, Campbell, P. G. C. and Bisson, M. (1979) 'Sequential Extraction Procedure for the Speciation of Particulate Trace Metals', *Analytical Chemistry*, 51(7), pp. 844–851. doi: 10.1021/ac50043a017.

Toride, N., Leij, F. and Van Genuchten, Mt. (1995) *The CXTFIT code for estimating transport parameters from laboratory or field tracer experiments. Version 2.0*.

Tripathi, V. S. (1984) *URANIUM (VI) TRANSPORT MODELING : GEOCHEMICAL DATA AND SUBMODELS ADSORPTION*. Stanford University.

Um, W., Icenhower, J. P., Brown, C. F., Serne, R. J., Wang, Z., Dodge, C. J. and Francis, A. J. (2010) 'Characterization of uranium-contaminated sediments from beneath a nuclear waste storage tank from Hanford, Washington: Implications for contaminant transport and fate', *Geochimica et Cosmochimica Acta*, 74(4), pp. 1363–1380. doi: 10.1016/j.gca.2009.11.014.

Um, W., Serne, R. J., Brown, C. F. and Last, G. V. (2007) 'U(VI) adsorption on aquifer sediments at the Hanford Site', *Journal of Contaminant Hydrology*, 93(1–4), pp. 255–269. doi: 10.1016/j.jconhyd.2007.03.002.

Um, W., Serne, R. J., Brown, C. F. and Rod, K. a. (2008) 'Uranium(VI) sorption on iron oxides in Hanford Site sediment: Application of a surface complexation model', *Applied Geochemistry*, 23(9), pp. 2649–2657. doi: 10.1016/j.apgeochem.2008.05.013.

Waite, T., Davis, J., Payne, T., Waychunas, G. and Xu, N. (1994) 'Uranium(VI) adsorption to ferrihydrite: Application of a surface complexation model', *Geochimica et Cosmochimica Acta*, 58(24), pp. 5465–5478.

Wang, Z., Zachara, J. M., Gassman, P. L., Liu, C., Qafoku, O., Yantasee, W. and Catalano, J. G. (2005) 'Fluorescence spectroscopy of U(VI)-silicates and U(VI)-contaminated Hanford sediment', *Geochimica et Cosmochimica Acta*, 69(6), pp. 1391–1403. doi: 10.1016/j.gca.2004.08.028.

Wazne, M., Korfiatis, G. P. and Meng, X. (2003) 'Carbonate effects on hexavalent uranium adsorption by iron oxyhydroxide', *Environmental Science and Technology*, 37(16), pp. 3619–3624. doi: 10.1021/es034166m.

White, J. L., McCowan, O. J., Laughter, M. D., Garcia, F., Vanhooser, B. and Hunt, A. (2010) *Stakeholders in Global Monitoring of UF6 Cylinders*.

Whitfield, M. and Turner, D. R. (1987) 'The role of particles in regulating the composition of seawater', in *Aquatic Surface Chemistry: Chemicla Processes at the Particle-Water Interface*. New York: John Wiley and Sons, pp. 457–493.

Wieland, E., Wehrli, B. and Stumm, W. (1988) 'The coordination chemistry of weathering: III. A generalization on the dissolution rates of minerals', *Geochimica et Cosmochimica Acta*, 52, pp. 1969–1981.

Wu, W., Fan, Q., Xu, J., Niu, Z. and Lu, S. (2007) 'Sorption–desorption of Th(IV) on attapulgite: Effects of pH, ionic strength and temperature', *Applied Radiation and Isotopes*, 65(10), pp. 1108–1114. doi: 10.1016/j.apradiso.2007.05.009.

Xu, D., Chen, C., Tan, X., Hu, J. and Wang, X. (2007) 'Sorption of Th(IV) on Na-rectorite: Effect of HA, ionic strength, foreign ions and temperature', *Applied Geochemistry*, 22(12), pp. 2892–2906. doi: 10.1016/j.apgeochem.2007.08.003.

Yanase, N. (1991) 'Uranium distribution in mineral phases of rock by sequential extraction procedure', *Radiochimica Acta*, 52/53, pp. 387–393.

Yu, S. M., Chen, C. L., Chang, P. P., Wang, T. T., Lu, S. S. and Wang, X. K. (2008) 'Adsorption of Th(IV) onto Al-pillared rectorite: Effect of pH, ionic strength, temperature, soil humic acid and fulvic acid', *Applied Clay Science*, 38(3–4), pp. 219–226. doi: 10.1016/j.clay.2007.03.008.

Zachara, J. M., Long, P. E., Bargar, J., Davis, J. A., Fox, P., Fredrickson, J. K., Freshley, M. D., Konopka, A. E., Liu, C., McKinley, J. P., Rockhold, M. L., Williams, K. H. and Yabusaki, S. B. (2013) 'Persistence of uranium groundwater plumes: contrasting mechanisms at two DOE sites in the groundwater-river interaction zone.', *Journal of contaminant hydrology*. Elsevier B.V., 147, pp. 45–72. doi: 10.1016/j.jconhyd.2013.02.001.

Zänker, H. and Hennig, C. (2014) 'Colloid-borne forms of tetravalent actinides: A brief review', *Journal of Contaminant Hydrology*. Elsevier B.V., 157, pp. 87–105. doi: 10.1016/j.jconhyd.2013.11.004.

Zhao, D. and Ewing, R. C. (2000) 'Alteration products of uraninite from the Colorado Plateau', *Radiochimica Acta*. doi: 10.1016/S0003-2670(00)87274-8.

Zhou, P. and Gu, B. (2005) 'Extraction of oxidized and reduced forms of uranium from contaminated soils: Effects of carbonate concentration and pH', *Environmental Science & Technology*, 39(865), pp. 4435–4440. doi: 10.1021/es0483443.

Ahonen, L., Kaija, J., Paananen, M., Hakkarainen, V. and Ruskeeniemi, T. (2004) *Palmottu natural analogue: A summary of the studies*. Espoo.

Altmaier, B. M., Neck, V. and Fanghänel, T. (2004) 'Solubility and colloid formation of Th (IV) in concentrated NaCl and MgCl2 solution', *Radiochimica Acta*, 92, pp. 537–543.

Altmaier, M., Neck, V., Müller, R. and Fanghänel, T. (2005) 'Solubility of ThO2.xH2O(am) in carbonate solution and the formation of ternary Th(IV) hydroxide-carbonate complexes', *Radiochimica Acta*, 93(2–2005), pp. 83–92. doi: 10.1524/ract.93.2.83.59420.

Altmaier, M., Neck, V., Müller, R. and Fanghänel, T. (2005) 'Solubility of ThO2·xH2O (am) in carbonate solution and the formation of ternary Th (IV) hydroxide-carbonate complexes', *Radiochimica Acta*, 93, pp. 83–92.

Altmaier, M. and Vercouter, T. (2012) 'Aquatic chemistry of the actinides: aspects relevant to their environmental behavior', in *Radionuclide Behaviour in the Natural Environment*, pp. 44–69.

AREVA NC - Comurhex (2010) 'Comurhex Geographic Information System Database'.

AREVA NC Malvési (2013) *Rapport d'information sur la sûreté nucléaire et la radioprotection de l'INB ECRIN, Édition 2013*.

Arnold, T., Zorn, T., Bernhard, G. and Nitsche, H. (1998) 'Sorption of uranium(VI) onto phyllite', *Chemical Geology*, 151(1–4), pp. 129–141. doi: 10.1016/S0009-2541(98)00075-8.

ASN (2013) *Plan National de Gestion des Matières et des Déchets Radioactifs 2013 - 2015*.

ATSDR (1990a) *Toxicological Profile for Radium*.

ATSDR (1990b) *Toxicological Profile for Thorium*.

ATSDR (2013) *Toxicological Profile for Uranium*.

Bary, F., Loriquer, A., Poncet, S. and Delos, A. (2009) *Note Intermédiaire 1.1. Synthèse Documentaire. AREVA-Comurhex-Site de Malvesi (11). Exploitation de l'Entreposage. Lot 1 - Inventaire Detaille des Déchets en Place.*

Bary, F., Loriquer, A., Poncet, S. and Delos, A. (2010a) *Note Intermédiaire 1.2. Compte-rendu factuel des reconnaissances de sols, des essais et analyses. AREVA-Comurhex-Site de Malvesi (11). Exploitation de*

l'Entreposage. Lot 1 - Inventaire Detaille des Déchets en Place.

Bary, F., Loriquer, A., Poncet, S. and Delos, A. (2010b) *Note Intermédiaire 1.3. Inventaire des Déchets et des Materiaux en Place. AREVA-Comurhex-Site de Malvesi (11). Exploitation de l'Entreposage. Lot 1 - Inventaire Detaille des Déchets en Place*.

Bernhard, G., Geipel, G., Reich, T., Brendler, V., Amayri, S. and Nitsche, H. (2001) 'Uranyl(VI) carbonate complex formation: Validation of the Ca2UO2(CO3)3(aq.) species', *Radiochimica Acta*, 89, pp. 511–518. doi: 10.1524/ract.2001.89.8.511.

Bitea, C., Müller, R., Neck, V., Walther, C. and Kim, J. I. (2003) 'Study of the generation and stability of thorium(IV) colloids by LIBD combined with ultrafiltration', *Colloids and Surfaces A: Physicochemical and Engineering Aspects*, 217, pp. 63–70. doi: 10.1016/S0927-7757(02)00559-9.

British Standard (1996) 'Method of test for Soils for civil engineering purposes - Part 2: Classification tests. BS 1377-2:1990', p. 72.

Brown, C. F., Serne, R. J., Catalano, J. G., Krupka, K. M. and Icenhower, J. P. (2010) 'Mineralization of contaminant uranium and leach rates in sediments from Hanford, Washington', *Applied Geochemistry*. Elsevier Ltd, 25(1), pp. 97–104. doi: 10.1016/j.apgeochem.2009.10.005.

Bruno, J., Cera, E., Pablo, J. de, Duro, L., Jordana, S. and Savage, D. (1997) *Determination of radionuclide solubility limits to be used in SR 97– Uncertainties associated to calculated solubilities*.

Bruno, J., de Pablo, J., Duro, L. and Figuerola, E. (1995) 'Experimental study and modeling of the U(VI)-Fe(OH)3 surface precipitation/coprecipitation equilibria', *Geochimica et Cosmochimica Acta*, 59(20), pp. 4113–4123.

Brusseau, M. L., Rao, P. S. C., Jessup, R. E. and Davidson, J. M. (1989) 'Flow interruption: A method for investigating sorption nonequilibrium', *Journal of Contaminant Hydrology*, 4(3), pp. 223–240. doi: 10.1016/0169-7722(89)90010-7.

Burgeap (2009a) *Chimie et comportement migratoire des radionucléides d'intérêt*.

Burgeap (2009b) *Comurhex Usine de Malvési-Narbonne (11) Etude Hydrogéologique. Synthèse des Données Existantes*.

Burgeap (2010) *COMURHEX Usine de Malvési – Narbonne (11) Travaux de confortement environnemental. Etude hydrogéologique. Résultats de la modélisation*.

Cantrell, K. J., Serne, R. J. and Last, G. V. (2002) *Hanford Contaminant Distribution Coefficient Database and Users Guide*, *Distribution*.

Casacuberta, N., Christl, M., Lachner, J., Rutgers Van Der Loeff, M., Masqué, P. and Synal, H.-A. (2014) 'A first transect of 236U in the North Atlantic Ocean', *Geochimica et Cosmochimica Acta*, 133, pp. 34–46. doi: 10.1016/j.gca.2014.02.012.

Catalano, J. G. and Brown, G. E. (2005) 'Uranyl adsorption onto montmorillonite: Evaluation of binding sites and carbonate complexation', *Geochimica et Cosmochimica Acta*, 69(12), pp. 2995–3005. doi: 10.1016/j.gca.2005.01.025.

Catalano, J. G., McKinley, J. P., Zachara, J. M., Heald, S. M., Smith, S. C. and Brown, G. E. (2006) 'Changes in uranium speciation through a depth sequence of contaminated Hanford sediments', *Environmental*

Science & Technology, 40(8), pp. 2517–2524. doi: 10.1021/es0520969.

Cera, E., Ahonen, L., Rollin, C., Bruno, J., Kaija, J. and Blomqvist, R. (2002) 'Redox Processes at the Palmottu uranium deposit', in von Maravic, H. and Alexander, R. (eds) *Eight EC NAWG Meeting*. Strasbourg, France, pp. 183–200.

Cera, E., Bruno, J. and Duro, L. (1999) 'Redox buffering effect on iron and uranium minerals in Palmottu, Finland', in Ármmansson, H. (ed.) *Geochemistry of the Earth's Surface: Proceedings of the 5th International Symposium on Geochemistry of the Earth's Surface*. Reykjavik, Iceland, pp. 441–444.

Cerato, A. B. and Lutenegger, A. J. (2002) 'Determination of surface area of fine-grained soils by the ethylene glycol monoethyl ether (EGME) method', *Geotechnical Testing Journal*, 25(3), pp. 315–321. doi: 10.1520/GTJ11087J.

Chabaux, F., Riotte, J. and Dequincey, O. (1992) 'U-Th-Ra Fractionation During Weathering and River Transport', in, p. 44.

Chen, C. L. and Wang, X. K. (2007) 'Influence of pH, soil humic/fulvic acid, ionic strength and foreign ions on sorption of thorium(IV) onto γ-Al2O3', *Applied Geochemistry*, 22(2), pp. 436–445. doi: 10.1016/j.apgeochem.2006.11.010.

Chen, C. and Wang, X. (2007) 'Sorption of Th (IV) to silica as a function of pH, humic/fulvic acid, ionic strength, electrolyte type', *Applied Radiation and Isotopes*, 65(2), pp. 155–163. doi: 10.1016/j.apradiso.2006.07.003.

Constantin, H. and Fick, M. (1997) 'Influence of C-sources on the denitrification rate of a high-nitrate concentrated industrial wastewater', *Water Research*, 31(3), pp. 583–589.

Constantin, H., Raoult, S., Montigny, W. and Fick, M. (1996) 'Denitrification of concentrated industrial wastewater: Microorganism selection and kinetic studies', *Environmental Technology*, 17, pp. 831–840.

Dong, W. and Brooks, S. C. (2006) 'Determination of the formation constants of ternary complexes of uranyl and carbonate with alkaline earth metals (Mg2+, Ca2+, Sr2+, and Ba2+) using anion exchange method.', *Environmental Science & Technology*, 40(15), pp. 4689–95.

Duff, M. and Amrhein, C. (1996) 'Uranium(VI) Adsorption on Goethite and Soil in Carbonate Solutions', *Soil Science Society of America Journal*, 60, pp. 1393–1400.

Duff, M. C., Morris, D. E., Hunter, D. B. and Bertsch, P. M. (2000) 'Spectroscopic characterization of uranium in evaporation basin sediments', *Geochimica et Cosmochimica Acta*, 64(9), pp. 1535–1550. doi: 10.1016/S0016-7037(99)00410-X.

Dzombak, D. A. and Morel, F. M. M. (1990) *Surface Complexation Modeling: Hydrous Ferric Oxide*. John Wiley & Sons. doi: 10.1016/B978-0-12-409548-9.05311-2.

Fanghänel, T. and Neck, V. (2002) 'Aquatic chemistry and solubility phenomena of actinide oxides/hydroxides', *Pure and Applied Chemistry*, 74(10), pp. 1895–1907. doi: 10.1351/pac200274101895.

Felmy, A. R., Dhanpat, R. and Mason, M. J. (1991) 'The Solubility of Hydrous Thorium(IV) Oxide in Chloride Media: Development of an Aqueous Ion-Interaction Model', *Radiochimica Acta*, 55, pp. 177–185.

Fox, P., Davis, J. A., Hay, M. B., Conrad, M. E., Campbell, K. M., Williams, K. H. and Long, P. E. (2012) 'Rate-Limited U(VI) Desorption during a Small-Scale Tracer Test in a Heterogeneous Uranium Contaminated

Aquifer', *Water Resources Research*.

Fox, P. M., Davis, J. a. and Zachara, J. M. (2006) 'The effect of calcium on aqueous uranium(VI) speciation and adsorption to ferrihydrite and quartz', *Geochimica et Cosmochimica Acta*, 70(6), pp. 1379–1387. doi: 10.1016/j.gca.2005.11.027.

Frost, R. L., Čejka, J., Weier, M. L. and Martens, W. N. (2006) 'Raman spectroscopy study of selected uranophanes', *Journal of Molecular Structure*, 788(1–3), pp. 115–125. doi: 10.1016/j.molstruc.2005.11.025.

Gavrilescu, M., Pavel, L. V. and Cretescu, I. (2009) 'Characterization and remediation of soils contaminated with uranium', *Journal of Hazardous Materials*, 163, pp. 475–510. doi: 10.1016/j.jhazmat.2008.07.103.

Gieré, R., Kaltenmeier, R. and Pourcelot, L. (2012) 'Uranium oxide and other airborne particles deposited on cypress leaves close to a nuclear facility', *Journal of Environmental Monitoring*, 14, p. 1264. doi: 10.1039/c2em11000h.

Giffaut, E., Grivé, M., Blanc, P., Vieillard, P., Colàs, E., Gailhanou, H., Gaboreau, S., Marty, N., Madé, B. and Duro, L. (2014) 'Andra thermodynamic database for performance assessment: ThermoChimie', *Applied Geochemistry*. Elsevier Ltd, 49, pp. 225–236. doi: 10.1016/j.apgeochem.2014.05.007.

Glaus, M., Hummel, W. and Van Loon, L. R. (1997) *Experimental determination and modelling of trace metal-humate interactions: A pragmatic approach for applications in groundwater*, *Nagra Technischer Bericht*.

Grenthe, I., Drozdzynski, J., Fujino, T., Buck, E. C., Albrecht-Schmitt, T. E. and Wolf, S. F. (2006) 'Uranium', in *The chemistry of the actinide and transactinide elements*.

Guillaumont, R. (2003) *Update on the Chemical Thermodynamics of Uranium, Neptunium, Plutonium, Americium and Technetium*. Elsevier B.V.

Van Hecke, W., Chabran, J. M., Barandas, C. and Ligney, J. . (2009) *COMURHEX - Malvési Etablissement. Dossier d'Options de Surete Bassins d'Entreposage B1 et B2*.

Hennig, C., Weiss, S., Banerjee, D., Brendler, E., Honkimäki, V., Cuello, G., Ikeda-Ohno, A., Scheinost, A. C. and Zänker, H. (2013) 'Solid-state properties and colloidal stability of thorium(IV)–silica nanoparticles', *Geochimica et Cosmochimica Acta*, 103, pp. 197–212. doi: 10.1016/j.gca.2012.10.051.

Herring, J. S. (2004) 'Uranium and Thorium Resource Assessment', *Encyclopedia of Energy*.

Hongxia, Z., Zheng, D. and Zuyi, T. (2006) 'Sorption of thorium(IV) ions on gibbsite: Effects of contact time, pH, ionic strength, concentration, phosphate and fulvic acid', *Colloids and Surfaces A: Physicochemical and Engineering Aspects*, 278(1–3), pp. 46–52. doi: 10.1016/j.colsurfa.2005.11.078.

Hsi, C.-K. D. and Langmuir, D. (1985) 'Adsorption of uranyl onto ferric oxyhydroxides. Application of the surface complexation site-binding model', *Geochimica et Cosmochimica Acta*, 49, pp. 1931–1941.

IAEA (1999) *Minimization of waste from uranium purification, enrichment and fuel fabrication*. Vienna.

IAEA (2014) *Nuclear Technology Review 2014*, *Nuclear technology review*.

IAEA (2016) 'Nuclear Technology Review 2016', *International Atomic Energy Agency General Conference*, (June), p. 58.

Jakobsson, A. (1999) 'Measurement and Modeling of Th Sorption onto TiO(2).', *Journal of colloid and interface science*, 220(2), pp. 367–373. doi: 10.1006/jcis.1999.6535.

Jang, J.-H., Dempsey, B. A. and Burgos, W. D. (2007) 'A Model-Based Evaluation of Sorptive Reactivities of Hydrous Ferric Oxide and Hematite for U(VI)', *Environmental Science & Technology*, 41(12), pp. 4305–4310. doi: 10.1021/es070068f.

Jernstrom, J., Vuorinen, U. and Hakanen, M. (2002) *Solubility of thorium in 0.1 M NaCl solution and in saline and fresh anoxic reference groundwater*.

Kabata-Pendias, A. and Pendias, H. (1985) *Trace elements in soils and plants*. Boca Raton.

Kalmykov, S. N. and Choppin, G. R. (2000) 'Mixed Ca2+/UO22+/CO32-complex formation at different ionic strengths', *Radiochimica Acta*, 88(9–11_2000), pp. 603–606. doi: 10.1524/ract.2000.88.9-11.603.

Kaplan, D. I. and Serkiz, S. M. (2001) 'Quantification of thorium and uranium sorption to contaminated sediments', *Journal of Radioanalytical and Nuclear Chemistry*, 248(3), pp. 529–535. doi: 10.1023/A:1010606325979.

Keith, S. and Wohlers, D. W. (2014) *Addendum to the Toxicological Profile for Thorium Agency for Toxic Substances and Disease Registry*. Atlanta.

Kelly, S. D., Newville, M. G., Cheng, L., Kemner, K. M., Sutton, S. R., Fenter, P., Sturchio, N. C. and Spötl, C. (2003) 'Uranyl incorporation in natural calcite', *Environmental Science & Technology*, 37(7), pp. 1284–1287. doi: 10.1021/es025962f.

Krauskopf, K. B. and Bird, D. K. (1995) *Introduction to Geochemistry*. Singapure: McGraw-Hill Inc.

Krupka, K. M. and Serne, R. J. (2002) *Geochemical Factors Affecting the Behavior of Antimony, Cobalt, Europium, Technetium, and Uranium in Vadose Sediments*.

LaFlamme, B. D. and Murray, J. W. (1987) 'Solid/Solution interaction: The effect of carbonate alkalinity on adsorbed thorium', *Geochimica et Cosmochimica Acta*, 51(2), pp. 243–250. doi: 10.1016/0016-7037(87)90235-3.

Landa, E. (1980) *Geological Survey Circular 814. Isolation of Uranium Mill Tailings and Their Component Radionuclides From the Biosphere-Some Earth Science Perspectives*.

Landa, E., Cravotta, C., Naftz, D., Verplanck, P., Nordstrom, D. and Zielinski, R. (2000) 'Geochemical Investigations by the U.S. Geological Survey on Uranium Mining, Milling, and Environmental Restoration', *Technology*, 7, pp. 381–396.

Landa, E. R. (2004) 'Uranium mill tailings: Nuclear waste and natural laboratory for geochemical and radioecological investigations', *Journal of Environmental Radioactivity*, 77, pp. 1–27. doi: 10.1016/j.jenvrad.2004.01.030.

Langmuir, D. (1978) 'Uranium solution-mineral equilibria at low temperatures with applications to sedimentary ore deposits', *Geochimica et Cosmochimica Acta*, 42, pp. 547–569. doi: 10.1016/0016-7037(79)90011-5.

Langmuir, D. (1997) *Aqueous Environmental Geochemistry*. Prentice Hall. doi: 10.1029/97EO00355.

Langmuir, D. and Herman, J. S. (1980) 'The mobility of thorium in natural waters at low temperatures', *Geochimica et Cosmochimica Acta*, 44, pp. 1753–1766.

Liu, C., Zachara, J. M., Qafoku, N. P. and Wang, Z. (2008) 'Scale-dependent desorption of uranium from

contaminated subsurface sediments', *Water Resources Research*, 44, pp. 1–13. doi: 10.1029/2007WR006478.

Liu, C., Zachara, J. M., Qafoku, O., McKinley, J. P., Heald, S. M. and Wang, Z. (2004) 'Dissolution of uranyl microprecipitates in subsurface sediments at Hanford Site, USA', *Geochimica et Cosmochimica Acta*, 68(22), pp. 4519–4537. doi: 10.1016/j.gca.2004.04.017.

MacKenzie, A., Scott, R., Linsalata, P. and Miekeley, N. (1992) 'Natural decay series studies of the redox front system in the Poços de Caldas uranium mineralization', *Journal of Geochemical Exploration*, 45(1–3), pp. 289–322.

Massey, M. S., Lezama-Pacheco, J. S., Nelson, J. M., Fendorf, S. and Maher, K. (2014) 'Uranium incorporation into amorphous silica', *Environmental Science & Technology*, 48(15), pp. 8636–8644. doi: 10.1021/es501064m.

McKinley, J. P., Zachara, J. M., Liu, C., Heald, S. C., Prenitzer, B. I. and Kempshall, B. W. (2006) 'Microscale controls on the fate of contaminant uranium in the vadose zone, Hanford Site, Washington', *Geochimica et Cosmochimica Acta*, 70, pp. 1873–1887. doi: 10.1016/j.gca.2005.10.037.

Miekeley, N., Coutinho de Jesus, H., Porto da Silveira, C. and Degueldre, C. (1992) 'Chemical and physical characterization of suspended particles and colloids in waters from the Osamu Utsumi mine and Morro do Ferro analogue study sites, Poços de Caldas, Brazil', *Journal of Geochemical Exploration*, 45(1–3), pp. 409–437.

Miekeley, N. and Küchler, I. L. (1987) 'Interactions between thorium and humic compounds in surface waters', *Inorganica Chimica Acta*, 140, pp. 315–319. doi: 10.1016/S0020-1693(00)81113-5.

Moon, H. (1989) 'Equilibrium Ultrafiltration of Hydrolyzed Thorium(IV) Solutions', *Bull. Korean Chem. Soc.*, 10(3).

Murakami, T., Sato, T., Ohnuki, T. and Isobe, H. (2005) 'Field evidence for uranium nanocrystallization and its implications for uranium transport', *Chemical Geology*, 221, pp. 117–126. doi: 10.1016/j.chemgeo.2005.04.004.

Neck, V., Altmaier, M., Müller, R., Bauer, A., Fanghänel, T. and Kim, J. I. (2003) 'Solubility of crystalline thorium dioxide', *Radiochimica Acta*, 91(5), pp. 253–262. doi: 10.1524/ract.91.5.253.20306.

Neck, V. and Kim, J. I. (2001) 'Solubility and hydrolysis of tetravalent actinides', *Radiochimica Acta*, 89, pp. 1–16. doi: 10.1524/ract.2001.89.1.001.

Neck, V., Müller, R., Bouby, M., Altmaier, M., Rothe, J., Denecke, M. a. and Kim, J. I. (2002) 'Solubility of amorphous Th(IV) hydroxide - Application of LIBD to determine the solubility product and EXAFS for aqueous speciation', *Radiochimica Acta*, 90(9–11), pp. 485–494. doi: 10.1524/ract.2002.90.9-11_2002.485.

Nico, P. S., Stewart, B. D. and Fendorf, S. (2009) 'Incorporation of Oxidized Uranium into Fe (Hydr)oxides during Fe(II) Catalyzed Remineralization', *Environmental Science & Technology*, 43(19), pp. 7391–7396. doi: 10.1021/es900515q.

Nordberg, G. F., Fowler, B. A., Nordberg, M. and Friberg, L. (2008) *Handbook of The Toxicology of Metal*. Third Edit, *Academic Press, Inc*. Third Edit.

Östhols, E. (1995) 'Thorium sorption on amorphous silica', *Geochimica et Cosmochimica Acta*, 59(7), pp.

1235–1249. doi: 10.1016/0016-7037(95)00040-7.

Osthols, E., Bruno, J. and Grenthe, I. (1994) 'On the influence of carbonate on mineral dissolution: III. The solubility of microcrystalline ThO2 in CO-H2O media', *Geochimica et Cosmochimica Acta*, 58(2), pp. 613–623.

Parkhurst, D. L. and Appelo, C. (1999) *User's Guide To PHREEQC (version 2) — a computer program for speciation, batch-reaction, one-dimensional transport and inverse geochemical calculations*, *Water-Resources Investigations Report 99-4259*. doi: Rep. 99-4259.

Parkhurst, D. L. and Appelo, C. A. J. (2015) 'PHREEQC Version 3--A Computer Program for Speciation, Batch-Reaction, One-Dimensional Transport, and Inverse Geochemical Calculations'.

Payne, T. (1999) *Uranium (VI) interactions with mineral surfaces: controlling factors and surface complexation modelling*. University of New South Wales.

Payne, T. E., Brendler, V., Comarmond, M. J. and Nebelung, C. (2011) 'Assessment of surface area normalisation for interpreting distribution coefficients (K(d)) for uranium sorption.', *Journal of environmental radioactivity*. Elsevier Ltd, 102(10), pp. 888–895. doi: 10.1016/j.jenvrad.2010.04.005.

Payne, T., Edis, R., Herczeg, A., Sekine, K., Seo, Y., Waite, T. and Yanase, N. (1992) *Groundwater chemistry. Alligator Riv- ers Analogue Project Final Report, Volume 7*. Sydney, Australia.

Perez, A. (1980) 'Du Concentré d'Uranium a l'Hexafluorure', in *Proceedings of an Advisory Group Meeting, Paris, 5-8 June 1979*. Paris: IAEA, International Atomic Energy Agency, pp. 201–228.

Pérez, I., Casas, I., Martín, M. and Bruno, J. (2000) 'The thermodynamics and kinetics of uranophane dissolution in bicarbonate test solutions', *Geochimica et Cosmochimica Acta*, 64(4), pp. 603–608. doi: 10.1016/S0016-7037(99)00337-3.

Pérez, I., Casas, I., Torrero, M., Cera, E., Duro, L. and Bruno, J. (1997) 'Dissolution Studies of Soddyite as a Long-Term Analogue of the Oxidative Alteration of the Spent Nuclear Fuel Matrix', in *MRS Proceedings*, p. 465.

Peterson, J., MacDonell, M., Haroun, L. and Monette, F. (2007) *Radiological and chemical fact sheets to support health risk analyses for contaminated areas*.

Phrommavanh, V. (2008) *Etude de la migration de l'uranium en milieu naturel: Approche experimentale et modelisation geochimique*. Universite Joseph Fourier - Grenoble I.

Plummer, L., Wigley, T. and Parkhurst, D. (1978) 'The kinetics of calcite dissolution in CO2-water systems at 5º to 60ºC and 0.0 to 1.0 atm CO2', *American Journal of Science*, 278, pp. 179–216.

Pourcelot, L. (2008) *Bilan radioécologique de l'environnement du site de Malvési. Etude complémentaire menée en 2008*.

Pourcelot, L., Boulet, B., Le Corre, C., Loyen, J., Fayolle, C., Tournieux, D., Van Hecke, W., Martinez, B. and Petit, J. (2011) 'Isotopic evidence of natural uranium and spent fuel uranium releases into the environment.', *Journal of Environmental Monitoring*, 13, pp. 355–361. doi: 10.1039/c0em00407c.

Pourcelot, L. and Le Roux, G. (2008) *Etude radioécologique de l'environnement du site de Malvési (société COMURHEX)*.

Puigdomenech, I. (2010) 'MEDUSA: Making Equilibrium Diagrams Using Sophisticated Algorithms'. Stockholm: Royal Institute of Technology, Stockholm, Sweden.

Qafoku, N. P., Zachara, J. M., Liu, C., Gassman, P. L., Qafoku, O. S. and Smith, S. C. (2005) 'Kinetic desorption and sorption of U(VI) during reactive transport in a contaminated Hanford sediment', *Environmental Science & Technology*, 39(9), pp. 3157–3165. doi: 10.1021/es048462q.

Quigley, M. S., Honeyman, B. D. and Santschi, P. H. (1996) 'Throium sorption in the marine environment: equilibrium partitioning at the hematite/water interface, sorption/desorption kinetics and particle tracing', *Aquatic Geochemistry*, 1, pp. 277–301.

Raffo-Caiado, A. C., Begovich, J. M., Ferrada, J. J., Ladd-lively, J., Antonio, M., Marzo, S., Grund, M. S., Saraiva Marzo, M. A., Crissiuma Palhares, L., Cordeiro Diaz, F. and Grund, M. S. (2009) *Model of a Generic Natural Uranium Conversion Plant — Suggested Measures to Strengthen International Safeguards*. Oak Ridge National Laboratory / Brazilian Nuclear Energy Commission.

Rautman, C., McGraw, M., Istok, J., Sigda, J. and Kaplan, P. (1994) 'Probabilistic Comparison of Alternative Characterization Technologies at the Fernald Uranium-in-Soils Integrated Demonstration Project', p. 11.

Reiller, P., Moulin, V., Casanova, F. and Dautel, C. (2002) 'Retention behaviour of humic substances onto mineral surfaces and consequences upon thorium (IV) mobility: Case of iron oxides', *Applied Geochemistry*, 17(12), pp. 1551–1562. doi: 10.1016/S0883-2927(02)00045-8.

Righetto, L., Bidoglio, G., Azimonti, G. and Bellobono, I. R. (1991) 'Competitive actinide interactions in colloidal humic acid-mineral oxide systems', *Environmental Science & Technology*, 25(11), pp. 1913–1919. doi: 10.1021/es00023a012.

Rojo, I., Seco, F., Rovira, M., Giménez, J., Cervantes, G., Martí, V. and de Pablo, J. (2009) 'Thorium sorption onto magnetite and ferrihydrite in acidic conditions', *Journal of Nuclear Materials*. Elsevier B.V., 385(2), pp. 474–478. doi: 10.1016/j.jnucmat.2008.12.014.

Rothe, J., Denecke, M. A., Neck, V., Müller, R. and Kim, J. I. (2002) 'XAFS investigation of the structure of aqueous thorium(IV) species, colloids, and solid thorium(IV) oxide/hydroxide', *Inorganic chemistry*, 41(2), pp. 249–258.

Ryan, J. L. and Rai, D. (1987) 'Thorium(IV) Hydrous Oxide Solubility', *Inorganic chemistry*, 26, pp. 4140–4142.

Saito, T., Koopal, L., Nagasaki, S. and Tanaka, S. (2004) 'Application of the NICA-Donnan model for proton, copper and uranyl binding to humic acid', *Radiochimica Acta*, 92, pp. 567–574.

Santschi, P. H., Murray, J. W., Baskaran, M., Benitez-Nelson, C. R., Guo, L. D., Hung, C. C., Lamborg, C., Moran, S. B., Passow, U. and Roy-Barman, M. (2006) 'Thorium speciation in seawater', *Marine Chemistry*, 100(3–4 SPEC. ISS.), pp. 250–268. doi: 10.1016/j.marchem.2005.10.024.

Sato, T., Murakami, T., Yanase, N., Isobe, H., Payne, T. E. and Airey, P. L. (1997) 'Iron nodules scavenging uranium from groundwater', *Environmental Science and Technology*, 31(10), pp. 2854–2858. doi: 10.1021/es970058m.

Schindler, P. (1967) 'Heterogeneous equilibria involving oxides, hydroxides, carbonates, and hydroxide carbonates', in Stumm, W. (ed.) *Equilibrium concepts in natural water systems*. American Chemical Society, pp. 196–221.

Schmidt, M., Lee, S. S., Wilson, R. E., Soderholm, L. and Fenter, P. (2012) 'Sorption of tetravalent thorium on muscovite', *Geochimica et Cosmochimica Acta*. Elsevier Ltd, 88, pp. 66–76. doi: 10.1016/j.gca.2012.04.001.

Schmitt, J. M. (1998) *Caractérisation lithologique, minéralogique et géochimique du substratum des bassin B1/B2*.

Schneider, E., Carlsen, B. W. and Tavrides, E. (2010) *Measures of the Environmental Footprint of the Front End of the Nuclear Fuel Cycle*.

Seah, M. P., Gilmore, I. S. and Beamson, G. (1998) 'XPS: binding energy calibration of electron spectrometers 5—re-evaluation of the reference energies', *Surface and Interface Analysis*, 26, pp. 642–649. doi: 10.1002/(SICI)1096-9918(199808)26:9<642::AID-SIA408>3.0.CO;2-3.

Seeley, F. and Kelmers, A. (1985) *Geochemical information for sites contaminated with low-level radioactive wastes: III - Weldon Spring Storage Site*.

Serkiz, S. M., Johnson, W. H., Wile, L. M. J. and Clark, S. B. (2007) 'Environmental Availability of Uranium in an Acidic Plume at the Savannah River Site', *Vadose Zone Journal*, 6(2), pp. 354–362. doi: 10.2136/vzj2006.0072.

Short, S. A. (1988) *Chemical transport of uranium and thorium in the Alligator Rivers Uranium Province , Northern Territory , Australia*.

Singer, D. M., Zachara, J. M. and Brown, G. E. (2009) 'Uranium speciation as a function of depth in contaminated Hanford sediments - A micro-XRF, micro-XRD, and micro- and bulk-XAFS study', *Environmental Science & Technology*, 43(3), pp. 630–636. doi: 10.1021/es8021045.

SLREM, S. L. de R. et d'Exploitations M. (1952) *La Production Française de Soufre Natif*. Paris.

Sowder, A. G., Clark, S. B. and Fjeld, R. A. (2001) 'The impact of mineralogy in the U(VI)–Ca–PO4 system on the environmental availability of uranium', *Journal of Radioanalytical and Nuclear Chemistry*, 248(3), pp. 517–524.

Steier, P., Bichler, M., Fifield, L. K., Golser, R., Kutschera, W., Priller, A., Quinto, F., Richter, S., Srncik, M., Terrasi, P., Wacker, L., Wallner, A., Wallner, G., Wilcken, K. M. and Wild, E. M. (2008) 'Natural and anthropogenic 236U in environemntal samples', *Nuclear Instruments and Methods in Physics Research B*, 266, pp. 2246–2250. doi: 10.1016/j.nimb.2008.03.002.

Steward, S. A. and Mones, E. T. (1996) 'Comparison and Modeling of Aqueous Dissolution Rates of Various Uranium Oxides', in *Materials Research Society Fall Meeting*, p. 12.

Stubbs, J. E., Veblen, L. a., Elbert, D. C., Zachara, J. M., Davis, J. a. and Veblen, D. R. (2009) 'Newly recognized hosts for uranium in the Hanford Site vadose zone', *Geochimica et Cosmochimica Acta*. Elsevier Ltd, 73(6), pp. 1563–1576. doi: 10.1016/j.gca.2008.12.004.

Sylwester, E. ., Hudson, E. . and Allen, P. . (2000) 'The structure of uranium (VI) sorption complexes on silica, alumina, and montmorillonite', *Geochimica et Cosmochimica Acta*, 64(14), pp. 2431–2438. doi: 10.1016/S0016-7037(00)00376-8.

Tan, X., Wang, X., Chen, C. and Sun, A. (2007) 'Effect of soil humic and fulvic acids, pH and ionic strength on Th(IV) sorption to TiO2 nanoparticles', *Applied Radiation and Isotopes*, 65(4), pp. 375–381. doi:

10.1016/j.apradiso.2006.10.014.

Taylor, S. (1964) 'Abundance of chemical elements in the continental crust: a new table', *Geochimica et Cosmochimica Acta*, 28, pp. 1273–1285.

Tessier, a, Campbell, P. G. C. and Bisson, M. (1979) 'Sequential Extraction Procedure for the Speciation of Particulate Trace Metals', *Analytical Chemistry*, 51(7), pp. 844–851. doi: 10.1021/ac50043a017.

Toride, N., Leij, F. and Van Genuchten, Mt. (1995) *The CXTFIT code for estimating transport parameters from laboratory or field tracer experiments. Version 2.0*.

Tripathi, V. S. (1984) *URANIUM (VI) TRANSPORT MODELING : GEOCHEMICAL DATA AND SUBMODELS ADSORPTION*. Stanford University.

Um, W., Icenhower, J. P., Brown, C. F., Serne, R. J., Wang, Z., Dodge, C. J. and Francis, A. J. (2010) 'Characterization of uranium-contaminated sediments from beneath a nuclear waste storage tank from Hanford, Washington: Implications for contaminant transport and fate', *Geochimica et Cosmochimica Acta*, 74(4), pp. 1363–1380. doi: 10.1016/j.gca.2009.11.014.

Um, W., Serne, R. J., Brown, C. F. and Last, G. V. (2007) 'U(VI) adsorption on aquifer sediments at the Hanford Site', *Journal of Contaminant Hydrology*, 93(1–4), pp. 255–269. doi: 10.1016/j.jconhyd.2007.03.002.

Um, W., Serne, R. J., Brown, C. F. and Rod, K. a. (2008) 'Uranium(VI) sorption on iron oxides in Hanford Site sediment: Application of a surface complexation model', *Applied Geochemistry*, 23(9), pp. 2649–2657. doi: 10.1016/j.apgeochem.2008.05.013.

Waite, T., Davis, J., Payne, T., Waychunas, G. and Xu, N. (1994) 'Uranium(VI) adsorption to ferrihydrite: Application of a surface complexation model', *Geochimica et Cosmochimica Acta*, 58(24), pp. 5465–5478.

Wang, Z., Zachara, J. M., Gassman, P. L., Liu, C., Qafoku, O., Yantasee, W. and Catalano, J. G. (2005) 'Fluorescence spectroscopy of U(VI)-silicates and U(VI)-contaminated Hanford sediment', *Geochimica et Cosmochimica Acta*, 69(6), pp. 1391–1403. doi: 10.1016/j.gca.2004.08.028.

Wazne, M., Korfiatis, G. P. and Meng, X. (2003) 'Carbonate effects on hexavalent uranium adsorption by iron oxyhydroxide', *Environmental Science and Technology*, 37(16), pp. 3619–3624. doi: 10.1021/es034166m.

White, J. L., McCowan, O. J., Laughter, M. D., Garcia, F., Vanhooser, B. and Hunt, A. (2010) *Stakeholders in Global Monitoring of UF6 Cylinders*.

Whitfield, M. and Turner, D. R. (1987) 'The role of particles in regulating the composition of seawater', in *Aquatic Surface Chemistry: Chemicla Processes at the Particle-Water Interface*. New York: John Wiley and Sons, pp. 457–493.

Wieland, E., Wehrli, B. and Stumm, W. (1988) 'The coordination chemistry of weathering: III. A generalization on the dissolution rates of minerals', *Geochimica et Cosmochimica Acta*, 52, pp. 1969–1981.

Wu, W., Fan, Q., Xu, J., Niu, Z. and Lu, S. (2007) 'Sorption–desorption of Th(IV) on attapulgite: Effects of pH, ionic strength and temperature', *Applied Radiation and Isotopes*, 65(10), pp. 1108–1114. doi: 10.1016/j.apradiso.2007.05.009.

Xu, D., Chen, C., Tan, X., Hu, J. and Wang, X. (2007) 'Sorption of Th(IV) on Na-rectorite: Effect of HA, ionic

strength, foreign ions and temperature', *Applied Geochemistry*, 22(12), pp. 2892–2906. doi: 10.1016/j.apgeochem.2007.08.003.

Yanase, N. (1991) 'Uranium distribution in mineral phases of rock by sequential extraction procedure', *Radiochimica Acta*, 52/53, pp. 387–393.

Yu, S. M., Chen, C. L., Chang, P. P., Wang, T. T., Lu, S. S. and Wang, X. K. (2008) 'Adsorption of Th(IV) onto Al-pillared rectorite: Effect of pH, ionic strength, temperature, soil humic acid and fulvic acid', *Applied Clay Science*, 38(3–4), pp. 219–226. doi: 10.1016/j.clay.2007.03.008.

Zachara, J. M., Long, P. E., Bargar, J., Davis, J. A., Fox, P., Fredrickson, J. K., Freshley, M. D., Konopka, A. E., Liu, C., McKinley, J. P., Rockhold, M. L., Williams, K. H. and Yabusaki, S. B. (2013) 'Persistence of uranium groundwater plumes: contrasting mechanisms at two DOE sites in the groundwater-river interaction zone.', *Journal of contaminant hydrology*. Elsevier B.V., 147, pp. 45–72. doi: 10.1016/j.jconhyd.2013.02.001.

Zänker, H. and Hennig, C. (2014) 'Colloid-borne forms of tetravalent actinides: A brief review', *Journal of Contaminant Hydrology*. Elsevier B.V., 157, pp. 87–105. doi: 10.1016/j.jconhyd.2013.11.004.

Zhao, D. and Ewing, R. C. (2000) 'Alteration products of uraninite from the Colorado Plateau', *Radiochimica Acta*. doi: 10.1016/S0003-2670(00)87274-8.

Zhou, P. and Gu, B. (2005) 'Extraction of oxidized and reduced forms of uranium from contaminated soils: Effects of carbonate concentration and pH', *Environmental Science & Technology*, 39(865), pp. 4435–4440. doi: 10.1021/es0483443.

APPENDICES

Appendix 1

Borehole Log SC429

Site: AREVA NC -Malvési, Decantation Basin B1

Borehole ID **SC429**

Location x: 652466.277 (± 5m)
y: 101666.885 (± 5m)
z: approximately 22m but GPS measurement did not stabilise

Start date: 23/02/2012
End date: 24/02/2012

Depth (m bgl)	Description* *based on observation at the PVC liner ends (every meter) – all liners left unopened	Strata	Approximate core recovery (%)	Observations / Samples selected for transport to the INE
0 – 1	Light brown SAND	COVER LAYER	95	
1 – 5.2	Brown slightly sandy CLAY very cohesive between 3 and 4m depth very loose between 4 and 5m depth	MIXTURE OF SOIL AND SLUDGE	85 (1-2m)	
			70 (2-3m)	Sample @ 3-3.5m
			100 (3-4m)	
			20 (4-5m)	
5.2 – 6	Light brown yellow clayey SILT Very humid	SLUDGE	65 (5-6m)	
6 – 7	Light brown yellow mottled orange and light grey CLAY Very wet		95-100	Sample @ 6-6.5m Sample @ 6.5-7m
7 – 8	Brown to light brown orange mottled CLAY Humid to wet		80	
8 – 8.3	Yellow mottled orange CLAY		100 (8-9m)	Sample@ 8-8.5m
8.3 – 13.20	Dark grey SAND with pockets of grey CLAY Water on core at about 11.5-12m Sludge at about 12 to 12.5m (probably fell from above during drilling) From 13m depth – very dense sand - very difficult to core	TAILINGS		Sample @ 8.5-9m
			100 (9-10m)	
			100 (10-11m)	
			100 (12-13m)	Sample @ 11.5-12m
			20 (13-14m)	Water level @ 13m depth

Site investigation carried out by COURTOIS SONDAGES. Drilling rig Comacchio GEO 305. Corer: ext diam 87mm, int diam 81mm. Liner: ext diam 80mm; int diam 78mm

Borehole SC429 - Photographs

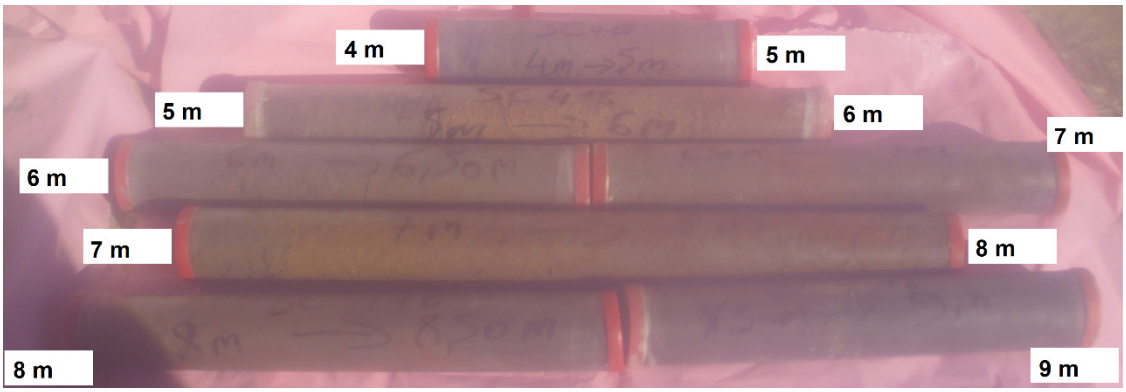

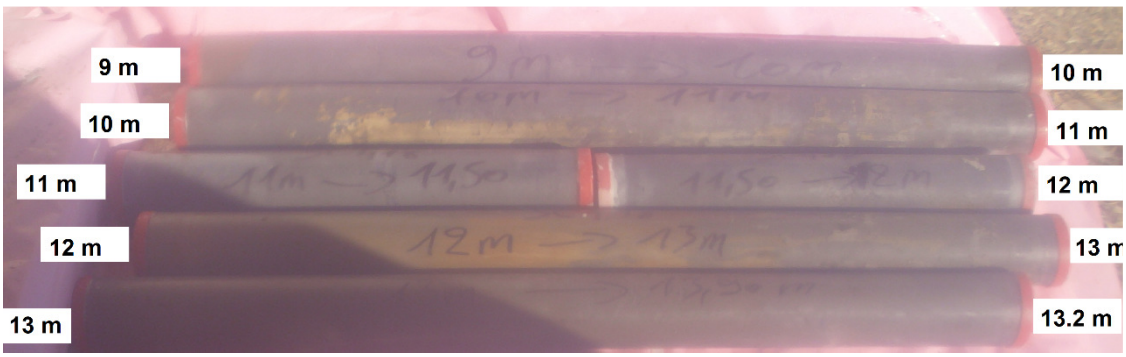

Appendix 2

Solids and Pore Waters

Table A2.1: Elemental composition of the samples used in the experiments.

	Fresh Samples (collected 2012)							Aged Samples (collected 2009)		
Sample	**Mixture Soil and Sludge 3.2m**	**Sludge 6.8m**	**Sludge 8.1m**	**Sludge 8.1m (0.5-1.0mm)**	**Tailings 8.5m**	**Tailings 8.8m**	**Fresh Tailings 11.8m (0.5-1.0mm)**	**Aged Tailings 0.5-1.0mm**	**Aged Sludge <0.5mm**	**Aged Sludge 0.5-1.0mm**
Experiment	**Batch**	**Batch**	**Column**	**Column**	**Column**	**Batch**	**Column**	**Column**	**Batch**	**Batch/ Column**
Na (g/kg)	8.6 (0.5)	11.7(1.1)	17.2(1.7)	33.7(2.3)	18.4(0.5)	8.8(0.6)	7.2(0.1)	3.2(0.1)	9.2(0.9)	8.5(1.8)
Mg (g/kg)	21.5(1.0)	72.0(10.7)	46.5(8.3)	33.5(2.1)	68.7(4.1)	29.7(4.5)	129.1(1.0)	64.8(2.4)	28.2(4.1)	30.5(5.0)
Al (g/kg)	99.2(0.5)	70.1(9.3)	56.9(11.2)	46.6(3.1)	69.6(3.8)	27.0(3.2)	36.4(1.4)	17.2(0.2)	62.2(8.7)	67.1(17.8)
K (g/kg)	29.6(1.2)	26.3(1.1)	24.0(1.4)	22.1(1.5)	27.0(1.0)	24.3(0.1)	10.6(0.2)	4.6(0.3)	22.0(0.5)	24.5(2.3)
Ca (g/kg)	297(20)	287(15)	285(36)	397(23)	241(13)	145(2)	352(1)	203(3)	277(30)	256(43)
Fe (g/kg)	53.2(1.1)	42.0(4.4)	43.1(3.0)	93.8(3.5)	36.6(1.5)	23.5(2.0)	21.8(0.4)	7.4(0.3)	46.2(3.5)	43.6(9.7)
Ti (g/kg)	3.31(0.13)	3.45(0.11)	2.61(0.09)	1.41(0.13)	2.76(0.04)	3.08(0.03)	1.41(0.02)	0.44(0.02)	3.17(0.05)	3.38(0.20)
V (mg/kg)	267(11)	118(4)	211(12)	372(26)	106(4)	115(1)	57(2)	23.4(0.3)	279.6(18.5)	293.2(27.6)
Mn (mg/kg)	806(45)	277(15)	655(43)	1680(79)	328(24)	251(4)	371(2)	101(3)	777(34)	742(137)
Co (mg/kg)	57(2)	40(4)	312(2)	527(70)	19(2)	16(0.4)	12(0.1)	7(0.02)	41(1)	52(7)
Ni (mg/kg)	180(22)	75	378(13)	737(93)	614(874)	-	-	6(0.5)	183(5)	171(17)
Cu (mg/kg)	179(21)	345(43)	323(8)	1615(61)	319(500)	37(8)	26(2)	20(1)	150(7)	173(22)
Zn (mg/kg)	463(143)	396(66)	906(28)	5343(474)	429(421)	350(49)	789(300)	65(46)	302(23)	295(48)
As (mg/kg)	72(6)	14(2)		298(13)	13(1)	8(-)	8(-)	3(0.2)	230(22)	165(24)
Rb (mg/kg)	171(0.3)	116(14)	90(17)	49(3)	117(8)	61(2)	58(2)	22(0.4)	99(10)	115(23)
Sr (mg/kg)	584(27)	762(46)	502(51)	426(24)	467(58)	582(8)	2447(145)	839(40)	881(142)	943(244)
Zr (mg/kg)	1338(129)	133(15)	1561(185)	5183(510)	104(12)	82(3)	71(2)	37(2)	2987(306)	2408(550)
Mo (mg/kg)	396(44)	44(5)	488(31)	1178(73)	39(13)	10(2)	16(2)	10(0.2)	1017(26)	821(165)
Ba (mg/kg)	566(23)	314(15)	456(55)	1429(151)	265(23)	271(2)	201(6)	98(7)	550(34)	490(136)
Pb (mg/kg)	65(8)	29(1)	135(5)	574(30)	24(8)	26(1)	16(1)	15(2)	75(11)	65(19)
U (mg/kg)	1425.1(20.6)	58.0(1.8)	4189.7(18.4)	12802(1123)	50.4(17.0)	21.6(1.2)	45.0(0.5)	8.6(0.6)	2150.1(104.5)	1636.2(150.8)
Th (mg/kg)	38.4(0.7)	10.3(1.0)	85.7(5.6)	372.7(46.5)	9.7(1.6)	7.7(0.8)	6.9(0.1)	0.45(0.04)	117.0(24.0)	73.8(17.8)

Table A2.2: Total Al, Si, Fe, Mg, Ti, Mn, Th and U extracted by sequential extraction of samples of mixture of soil and sludge, sludge and tailings (mg/g or µg/g of dry sample).

Sample	Element extracted	Reagent					Sum extracted Al, Si and Fe (mg/g) and Th and U (µg/g)
		Morgan's Solution	TAO	CDB	6M HCl	Digestion and fusion	
SC416b 0.45-4.3m Mixt. of soil and sludge	Al (mg/g soil)	<0.004	1.15±0.16	1.17±0.48	4.64±0.34	22.19±0.37	29.15±0.71
	Si (mg/g soil)	<0.013	<0.006	<0.019	<1.07	0.94±0.44	2.01±1.73
	Fe (mg/g soil)	<0.002	1.64±0.15	9.07±0.56	46.30±0.41	3.56±0.09	60.57±0.72
	Mg (mg/g soil)	1.67±0.74	1.42±0.37	<0.83	2.49±0.74	1.14±0.18	7.55±1.59
	Ti (mg/ g soil)	0.69±0.49	<0.003	<0.26	<0.005	0.62±0.12	1.57±0.89
	Mn (mg/g soil)	0.208±0.007	0.044±0.004	0.076±0.011	0.102±0.007	0.012±0.002	0.441±0.015
	Th (µg/g soil)	<1.4	5.0±3.7	13.6±10.3	<0.6	2.1±1.6	22.8±13.5
	U (µg/g soil)	564±17	207±9	32±1	12.1±5	7.0±3	822±19
SC6-1 8.6-9.3m Sludge	Al (mg/g soil)	<0.13	0.72±0.17	<0.33	1.65±0.33	19.19±0.34	22.02±0.69
	Si (mg/g soil)	<0.013	<0.006	<0.019	<1.14	5.32±0.81	6.46±1.92
	Fe (mg/g soil)	1.12±0.26	3.51±0.19	4.96±0.47	<0.002	7.09±0.10	16.68±0.58
	Mg (mg/g soil)	6.47±0.77	8.73±0.47	1.43±1.17	4.41±0.77	1.46±0.19	22.50±1.68
	Ti (mg/ g soil)	0.54±0.51	<0.003	<0.37	<0.01	0.66±0.13	1.57±1.06
	Mn (mg/g soil)	0.090±0.007	0.012±0.004	0.040±0.011	<0.003	0.028±0.002	0.170±0.014
	Th (µg/g soil)	<2.3	3.9±3.2	14.9±11.2	<1.7	<1.5	24.3±14.1
	U (µg/g soil)	433±18	162±7	23.2±9	9.9±4	6.6±3	635±19
SC6-2 8.6-9.3m Sludge	Al (mg/g soil)	<0.004	0.53±0.16	<0.006	1.70±0.30	25.13±0.40	27.35±0.53
	Si (mg/g soil)	<0.013	<0.006	<2.46	7.69±3.15	3.68±0.79	13.82±4.13
	Fe (mg/g soil)	<0.002	7.82±0.19	11.85±0.57	0.92±0.26	6.45±0.10	27.04±0.66
	Mg (mg/g soil)	4.44±0.75	6.96±0.43	1.46±1.15	4.12±0.75	1.62±0.19	18.59±1.63
	Ti (mg/ g soil)	<0.46	<0.003	<0.23	<0.05	0.78±0.13	1.52±1.04
	Mn (mg/g soil)	0.082±0.007	0.010±0.004	0.044±0.011	<0.003	0.028±0.002	0.167±0.0016
	Th (µg/g soil)	<1.5	3.9±3.2	14.2±10.7	<2.4	1.7±1.5	23.7±13.6
	U (µg/g soil)	392±16	178±7	26±1	10.7±4	7.7±3	614±18
SC19 2.5-3.8m	Al (mg/g soil)	0.67±0.25	2.27±0.17	<0.006	1.19±0.33	10.25±0.29	14.37±0.54

Sample	Element extracted	Reagent					Sum extracted Al, Si and Fe (mg/g) and Th and U (µg/g)
		Morgan's Solution	TAO	CDB	6M HCl	Digestion and fusion	
Sludge	Si (mg/g soil)	<0.39	<0.71	<0.019	3.73±1.81	0.86±0.45	5.68±2.71
	Fe (mg/g soil)	<0.002	7.32±0.19	7.65±0.58	<0.002	2.86±0.10	17.83±0.62
	Mg (mg/g soil)	4.99±0.77	5.65±0.41	<1.04	7.61±0.78	0.57±0.19	19.87±1.67
	Ti (mg/ g soil)	0.62±0.51	<0.13	<0.27	<0.07	0.27±0.13	1.36±1.09
	Mn (mg/g soil)	0.218±0.007	0.117±0.004	0.090±0.011	<0.003	0.010±0.002	0.435±0.014
	Th (µg/g soil)	<3.4	18.4±13.0	66.6±47.7	6.8±6.1	<1.0	96.2±50.2
	U (µg/g soil)	1576±60	1174±46	178±7	46±2	9.2±4	2984±76
SC30 2.4-5.6m Sludge	Al (mg/g soil)	1.08±0.26	3.27±0.19	<0.006	0.95±0.26	2.28±0.28	7.58±0.50
	Si (mg/g soil)	<0.013	5.66±1.60	<0.019	<0.013	1.81±0.80	7.46±1.79
	Fe (mg/g soil)	<0.002	1.90±0.16	1.26±0.39	<0.002	2.64±0.10	5.80±0.43
	Mg (mg/g soil)	5.19±0.76	2.98±0.38	<0.83	<0.75	<0.15	9.91±1.66
	Ti (mg/ g soil)	0.89±0.51	<0.15	<0.36	<0.1	<0.07	1.57±1.09
	Mn (mg/g soil)	0.236±0.007	0.202±0.004	0.162±0.011	<0.007	0.010±0.002	0.618±0.016
	Th (µg/g soil)	<3.7	9.7±6.7	59.5±42.5	13.9±9.8	<0.5	87.3±44.4
	U (µg/g soil)	2537±101	1553±63	136±6	71±3	6.9±3	4304±119
SC417b 8.2-10.2m Tailings	Al (mg/g soil)	<0.004	<0.01	<0.006	0.41±0.25	23.14±0.28	23.56±0.47
	Si (mg/g soil)	<0.013	<0.006	<0.019	<0.013	<0.33	<0.33
	Fe (mg/g soil)	<0.002	5.26±0.19	4.18±0.44	<0.002	4.52±0.10	13.96±0.49
	Mg (mg/g soil)	6.09±0.76	5.50±0.40	1.52±1.16	4.11±0.76	1.56±0.19	18.78±1.64
	Ti (mg/ g soil)	<0.44	<0.003	<0.36	<0.005	0.67±0.13	1.47±0.92
	Mn (mg/g soil)	0.038±0.007	<0.002	0.037±0.011	<0.003	0.014±0.002	0.088±0.014
	Th (µg/g soil)	<0.3	<0.5	<0.6	<0.4	<1.3	<3.2
	U (µg/g soil)	7.0±3	2.1±0.1	<1.71	<1.13	0.8±0.1	12.6±0.4

Morgan's Solution: Carbonate minerals, adsorbed trace elements; **TAO**: Amorphous minerals of Fe, Al and Si and secondary U minerals; **CDB**: Crystalline Fe oxides, hydroxides and oxyhydroxides; **6M HCl**: Clay minerals and U oxides; **Digestion and fusion**: remaining resistant minerals (quartz, muscovite).

Table A2.3: Total Al, Si, Fe, Mg, Ti, Mn, Th and U extracted by sequential extraction of samples of mixture of soil and sludge, sludge and tailings (% of total in dry sample).

Sample	Element extracted (%)	Reagent					Sum extracted Al, Si and Fe (mg/g) and Th and U (µg/g)
		Morgan's Solution	TAO	CDB	6M HCl	Digestion and fusion	
SC416b 0.45-4.3m Mixt. of soil and sludge	Al	0	4	4	16	76	29.15±0.71
	Si	1	0	1	53	47	2.01±1.73
	Fe	0	3	15	76	6	60.57±0.72
	Mg	22	19	11	33	15	7.55±1.59
	Ti	44	0	17	0	39	1.57±0.89
	Mn	47	10	17	23	3	0.441±0.015
	Th	<6	22	60	<3	9	22.8±13.5
	U	69	25	4	1	1	822±19
SC6-1 8.6-9.3m Sludge	Al	1	3	1	7	87	22.02±0.69
	Si	0	0	18	56	82	6.46±1.92
	Fe	7	21	30	0	43	16.68±0.58
	Mg	29	39	6	20	6	22.50±1.68
	Ti	34	0	24	1	42	1.57±1.06
	Mn	53	7	24	2	16	0.170±0.014
	Th	<10	16	61	<7	<6	24.3±14.1
	U	68	26	4	2	1	635±19
SC6-2 8.6-9.3m Sludge	Al	0	2	0	6	92	27.35±0.53
	Si	0	0	18	56	27	13.82±4.13
	Fe	0	29	44	3	24	27.04±0.66
	Mg	24	37	8	22	9	18.59±1.63
	Ti	30	0	15	3	51	1.52±1.04
	Mn	49	6	26	2	17	0.167±0.0016
	Th	<6	17	60	<10	7	23.7±13.6
	U	64	29	4	2	1	614±18

Sample	Element extracted (%)	Reagent					Sum extracted Al, Si and Fe (mg/g) and Th and U (µg/g)
		Morgan's Solution	TAO	CDB	6M HCl	Digestion and fusion	
SC19 2.5-3.8m Sludge	Al	5	16	0	8	71	14.37±0.54
	Si	7	13	0	66	15	5.68±2.71
	Fe	0	41	43	0	16	17.83±0.62
	Mg	25	28	5	38	3	19.87±1.67
	Ti	46	10	20	5	20	1.36±1.09
	Mn	50	27	21	1	2	0.435±0.014
	Th	<4	19	69	7	1	96.2±50.2
	U	53	39	6	2	0	2984±76
SC30 2.4-5.6m Sludge	Al	14	43	0	13	30	7.58±0.50
	Si	0	76	0	0	24	7.46±1.79
	Fe	0	33	22	0	46	5.80±0.43
	Mg	52	30	8	8	2	9.91±1.66
	Ti	57	10	23	6	4	1.57±1.09
	Mn	38	33	26	1	2	0.618±0.016
	Th	<4	11	68	16	<1	87.3±44.4
	U	59	36	3	2	0	4304±119
SC417b 8.2-10.2m Tailings	Al	0	0	0	2	98	23.56±0.47
	Si	0	0	0	0	100	<0.33
	Fe	0	38	30	0	32	13.96±0.49
	Mg	32	29	8	22	8	18.78±1.64
	Ti	30	0	24	0	46	1.47±0.92
	Mn	43	2	42	3	16	0.088±0.014
	Th	<9	<16	<19	<13	<41	<3.2
	U	56	17	13	8	6	12.6±0.4

Morgan's Solution: Carbonate minerals, adsorbed trace elements; **TAO**: Amorphous minerals of Fe, Al and Si and secondary U minerals; **CDB**: Crystalline Fe oxides, hydroxides and oxyhydroxides; **6M HCl**: Clay minerals and U oxides; **Digestion and fusion**: remaining resistant minerals (quartz, muscovite).

Appendix 3

Chemical Composition of Groundwater and Pore Water Samples

Table A3.1: Chemical composition of groundwater samples and pore water samples extracted from solid samples of core SC429 (solution concentration in mol/l).

Sample	GROUNDWATER												POREWATER		
	SC416a,b,c								SC417a,b,c				SC429		
	Mixt. S.S.		Tailings		Alluvium		Sludge		Tailings		Alluvium		Mixt. S.S. (3.2m)	Sludge (6.8m)	Tailings (8.8m)
Time of sampling	Feb 2011	Jul 2009	Feb 2011	Jul 2009	Feb 2011	Jul 2009	Feb 2011	Aug 2009	Feb 2011	Aug 2009	Feb 2011	Aug 2009	May 2011	May 2011	May 2011
pH	5.8±0.1	6.00	5.6±0.1	6.00	6.8±0.1	6.71	8.1±0.1	8.38	5.7±0.1	6.02	6.7±0.1	6.28	6.9±0.1	7.2±0.1	6.3±0.1
Eh (*in situ*) (mV)	433±20	-	441±20	-	184±20	-	357±20	-	399±20	-	225±20	-	-	-	-
Eh (lab) (mV)	233	360	241	-50	-16	117	157	273	199	310	25	53	*NA*	*NA*	*NA*
I (M)	0.70	1.43	1.23	1.64	0.07	0.21	1.31	1.65	1.12	1.68	0.06	0.39	1.84	3.02	3.05
Charge Balance (%)	62.81	80.56	57.29	-34.96	59.2	12.13	59.54	-11.62	54.18	-21.72	53.96	-15.06	-2.6	-16.2	-15.4
TC ($\cdot 10^{-3}$ mol/l)	2.56 (±0.02)	*NA*	2.78 ±0.07)	*NA*	10.94 (±0.51)	*NA*	2.75 (±0.11)	*NA*	2.96 (±0.02)	*NA*	4.83 (±0.4)	*NA*	*NA*	*NA*	*NA*
TOC ($\cdot 10^{-3}$ mol/l)	0.91 (±0.02)	*NA*	1.52 (±0.08)	*NA*	3.28 (±0.59)	*NA*	2.56 (±0.11)	*NA*	1.47 (±0.04)	*NA*	0.12 (±0.11)	*NA*	*NA*	*NA*	*NA*
TIC ($\cdot 10^{-3}$ mol/l)	1.65 (±0.01)	*NA*	1.26 (±0.04)	*NA*	7.66 (±0.29)	*NA*	0.19 (±0.01)	*NA*	1.49 (±0.4)	*NA*	4.71 (±0.11)	*NA*	*NA*	*NA*	*NA*

TC: total carbon, TIC: total inorganic carbon, TOC: total organic carbon

Burgeap analysis carried out between 30/07/2009 and 10/12/2009 (Burgeap, 2009 – CTOZ090490). The uncertainty of the analysis is not presented in the report.

Sample	GROUNDWATER												POREWATER		
	SC416a,b,c								SC417a,b,c				SC429		
	Mixt. S.S.		Tailings		Alluvium		Sludge		Tailings		Alluvium		Mixt. S.S. (3.2m)	Sludge (6.8m)	Tailings (8.8m)
Time of sampling	Feb 2011	Jul 2009	Feb 2011	Jul 2009	Feb 2011	Jul 2009	Feb 2011	Aug 2009	Feb 2011	Aug 2009	Feb 2011	Aug 2009	May 2011	May 2011	May 2011
HCO_3^- / alkalinity ($\cdot 10^{-3}$ mol/l)	8.4 (±0.03) [c]	7.0	6.4 (±0.21) [c]	11.9	38.9 (±1.50) [c]	19.2	0.96 (±0.05) [c]	33.6	7.6 (±0.19) [c]	8.4	23.94 (±0.54) [c]	33.6	2.35 [a]	0.21 [a]	2.14 [a]
Fe(II) ($\cdot 10^{-7}$ mol/l)	*< 0.29*	*NA*	*< 0.29*	*NA*	21.8 (±1.4)	*NA*	*< 0.29*	*NA*	*< 0.29*	*NA*	34.5 (±2.7)	*NA*	*NA*	*NA*	*NA*
Fe(III) ($\cdot 10^{-7}$ mol/l)	5.4 (±2.7)	*NA*	*< 0.29*	*NA*	7.5 (±1.9)	*NA*	11.7 (±1.4)	*NA*	2.3 (±1.4)	*NA*	4.0 (±3.9)	*NA*	*NA*	*NA*	*NA*
Fe total ($\cdot 10^{-7}$ mol/l)	5.4 (±2.7)	5926.6	*< 0.29*	4816.5	29.2 (±0.1)	1171.0	11.7 (±1.4)	1602.5	2.3 (±1.4)	73590	38.6 (±2.7)	7663.4	*NA*	*NA*	*NA*
NO_3 ($\cdot 10^{-1}$ mol/l)	1.85 (±0.05)	1.53	4.24 (±0.26)	23.63	0.18 (±0.01)	0.02	4.05 (±0.02)	25.73	4.39 (±0.07)	23.12	0.23 (±0.01)	2.78	13.3	24.7	25.1
NO_2 ($\cdot 10^{-5}$ mol/l)	13.28 (±0.07)	21.6	1.23 (±0.04)	7.5	0.40 (±0.03)	97.8	686.80 (±0.80)	2282.1	1.78 (±0.06)	17.6	2.25 (±0.03)	29.1	*NA*	*NA*	*NA*
SO_4 ($\cdot 10^{-3}$ mol/l)	2.75 (±0.10)	344	2.35 (±0.42)	22.71	7.54 (±0.03)	67.57	2.08 (±0.01)	9.44	2.39 (±0.10)	23.24	6.18 (±0.01)	43.53	11.0	8.13	8.27
Cl ($\cdot 10^{-2}$ mol/l)	1.20 (±0.01)	4.0	1.11 (±0.01)	2.1	0.82 (±0.02)	1.1	0.98 (±0.01)	1.1	1.31 (±0.01)	2.1	1.19 (±0.03)	2.3	2.16	92.6	1.02
F ($\cdot 10^{-4}$ mol/l)	16.96 (±0.06)	*NA*	9.90 (±1.10)	*NA*	28.77 (±11.0)	*NA*	9.03 (±0.34)	*NA*	9.90 (±1.58)	*NA*	20.96 (±0.75)	*NA*	*NA*	*NA*	*NA*

[a]The concentrations of Ca and Si were calculated in equilibrium with calcite and amorphous SiO_2, in agreement with the XRD results which showed calcite and quartz to be present in the solid phase.

[c] calculated from the concentration of total inorganic carbon

Burgeap analysis carried out between 30/07/2009 and 10/12/2009 (Burgeap, 2009 – CTOZ090490). The uncertainty of the analysis is not presented in the report.

Sample	GROUNDWATER												POREWATER		
	SC416a,b,c								SC417a,b,c				SC429		
	Mixt. S.S.		Tailings		Alluvium		Sludge		Tailings		Alluvium		Mixt. S.S. (3.2m)	Sludge (6.8m)	Tailings (8.8m)
Time of sampling	Feb 2011	Jul 2009	Feb 2011	Jul 2009	Feb 2011	Jul 2009	Feb 2011	Aug 2009	Feb 2011	Aug 2009	Feb 2011	Aug 2009	May 2011	May 2011	May 2011
pH	5.8±0.1	6.00	5.6±0.1	6.00	6.8±0.1	6.71	8.1±0.1	8.38	5.7±0.1	6.02	6.7±0.1	6.28	6.9±0.1	7.2±0.1	6.3±0.1
P ($\cdot 10^{-5}$ mol/l)	0.39[d]	-	389.8[d]	-	13.2(±5.8)	-	91.2[d]	-	*< DL*	-	6.6(±1.3)	-	*NA*	*NA*	*NA*
Organic phosphates (as P) ($\cdot 10^{-5}$ mol/l)	1.85	*NA*	1.4	*NA*	< 0.065	*NA*	15	*NA*	6.9	*NA*	1.1	*NA*	*NA*	*NA*	*NA*
Na ($\cdot 10^{-1}$ mol/l)	1.95 (±0.02)	5.37	4.56 (±0.03)	4.15	0.32 (±0.01)	0.33	4.11 (±0.03)	4.12	3.86 (±0.02)	2.83	0.39 (±0.01)	0.82	3.64	5.65	5.68
Mg ($\cdot 10^{-2}$ mol/l)	8.1 (±0.1)	6.3	6.5 (±0.1)	6.6	2.4 (±0.1)	4.3	3.6 (±0.1)	1.1	4.5 (±0.1)	7.2	1.0 (±0.1)	2.7	10.5	1.2	4.3
Ca ($\cdot 10^{-1}$ mol/l)	2.53 (±0.03)	6.71	4.71 (±0.05)	2.17	0.06 (±0.01)	0.10	5.56 (±0.06)	7.04	4.92 (±0.05)	3.18	0.13 (±0.01)	0.32	3.50	6.23	6.00
K ($\cdot 10^{-2}$ mol/l)	2.8 (±0.1)	7.5	10.0 (±0.2)	8.0	*<0.26*	0.14	8.8 (±0.2)	11.0	7.8 (±0.1)	6.2	*<0.26*	0.50	*NA*	*NA*	*NA*
Si ($\cdot 10^{-4}$ mol/l)	4.0 (±0.2)	28.0	3.3 (±0.2)	12.0	2.8 (±0.2)	4.4	<0.71	9.0	3.0 (±0.2)	25.0	2.3 (±0.2)	14.0	18.5[a]	18.2[a]	17.3[a]
V ($\cdot 10^{-5}$ mol/l)	*NA*												7.05 (±30%)	6.35 (±30%)	5.59 (±30%)

[d] single measurement above detection limit. No uncertainty calculated

Burgeap analysis carried out between 30/07/2009 and 10/12/2009 (Burgeap, 2009 – CTOZ090490). The uncertainty of the analysis is not presented in the report.

Sample	GROUNDWATER												POREWATER		
	SC416a,b,c								SC417a,b,c				SC429		
	Mixt. S.S.		Tailings		Alluvium		Sludge		Tailings		Alluvium		Mixt. S.S. (3.2m)	Sludge (6.8m)	Tailings (8.8m)
Time of sampling	Feb 2011	Jul 2009	Feb 2011	Jul 2009	Feb 2011	Jul 2009	Feb 2011	Aug 2009	Feb 2011	Aug 2009	Feb 2011	Aug 2009	May 2011	May 2011	May 2011
Cr ($\cdot 10^{-5}$ mol/l)						*NA*							1.80 (±30%)	1.77 (±30%)	1.50 (±30%)
Mn ($\cdot 10^{-5}$ mol/l)						*NA*							18.84 (±30%)	0.44 (±30%)	16.48 (±30%)
Zn ($\cdot 10^{-5}$ mol/l)						*NA*							5.70 (±30%)	5.88 (±30%)	5.41 (±30%)
Sr ($\cdot 10^{-4}$ mol/l)						*NA*							15.44 (±30%)	4.39 (±30%)	21.12 (±30%)
Zr ($\cdot 10^{-5}$ mol/l)						*NA*							1.89 (±30%)	1.97 (±30%)	1.82 (±30%)
Mo ($\cdot 10^{-5}$ mol/l)						*NA*							2.09 (±30%)	6.00 (±30%)	-
Cs ($\cdot 10^{-6}$ mol/l)						*NA*							1.63 (±30%)	2.18 (±30%)	2.13 (±30%)

Burgeap analysis carried out between 30/07/2009 and 10/12/2009 (Burgeap, 2009 – CTOZ090490). The uncertainty of the analysis is not presented in the report.

Sample	GROUNDWATER												POREWATER		
	SC416a,b,c								SC417a,b,c				SC429		
	Mixt. S.S.		Tailings		Alluvium		Sludge		Tailings		Alluvium		Mixt. S.S. (3.2m)	Sludge (6.8m)	Tailings (8.8m)
Time of sampling	Feb 2011	Jul 2009	Feb 2011	Jul 2009	Feb 2011	Jul 2009	Feb 2011	Aug 2009	Feb 2011	Aug 2009	Feb 2011	Aug 2009	May 2011	May 2011	May 2011
Cs ($\cdot 10^{-6}$ mol/l)						*NA*							1.63 (±30%)	2.18 (±30%)	2.13 (±30%)
W ($\cdot 10^{-6}$ mol/l)						*NA*							0.51 (±30%)	1.42 (±30%)	1.95 (±30%)
Re ($\cdot 10^{-7}$ mol/l)						*NA*							5.78 (±30%)	4.82 (±30%)	4.91 (±30%)
^{238}U (mol/l)	3.5(±0.1) $\cdot 10^{-5}$	1.1 $\cdot 10^{-4}$	1.1(±0.1) $\cdot 10^{-4}$	2.8 $\cdot 10^{-5}$	9.5(±0.1) $\cdot 10^{-8}$	5.5 $\cdot 10^{-7}$	<4.1 $\cdot 10^{-8}$	9.6 $\cdot 10^{-7}$	6.6(±0.1) $\cdot 10^{-5}$	6.9 $\cdot 10^{-5}$	9.6(±0.1) $\cdot 10^{-8}$	5.9 $\cdot 10^{-7}$	50.8(±0.6) $\cdot 10^{-5}$	47.7(0.5) $\cdot 10^{-8}$	47.3(±0.5) $\cdot 10^{-7}$
^{235}U (mol/l)	2.0(±0.1) $\cdot 10^{-7}$	9.3 $\cdot 10^{-7}$	6.3(±0.1) $\cdot 10^{-7}$	6.6 $\cdot 10^{-7}$	5.7(±0.1) $\cdot 10^{-10}$	4.4 $\cdot 10^{-9}$	8.4(±0.1) $\cdot 10^{-11}$	8.8 $\cdot 10^{-8}$	3.7(±0.1) $\cdot 10^{-7}$	6.6 $\cdot 10^{-7}$	6.1(±0.1) $\cdot 10^{-10}$	4.4 $\cdot 10^{-8}$	*NA*	*NA*	*NA*
^{234}U (mol/l)	1.5(±0.1) $\cdot 10^{-10}$	6.1 $\cdot 10^{-9}$	4.7(±0.1) $\cdot 10^{-10}$	2.0 $\cdot 10^{-9}$	4.0(±0.1) $\cdot 10^{-13}$	3.2 $\cdot 10^{-11}$	6.7(±0.3) $\cdot 10^{-14}$	3.9 $\cdot 10^{-11}$	2.8(±0.1) $\cdot 10^{-10}$	3.0 $\cdot 10^{-9}$	4.9(±0.5) $\cdot 10^{-13}$	3.7 $\cdot 10^{-11}$	*NA*	*NA*	*NA*
^{232}Th (mol/l)	*<4.1·10^{-9}*	*NA*	*<4.1·10^{-9}*	*NA*	*<4.1·10^{-9}*	*NA*	*<4.1·10^{-9}*	*NA*	*<4.1·10^{-9}*	*NA*	*<4.1·10^{-9}*	*NA*	*<4.1·10^{-9}*	1.1·10^{-6}	*<4.1·10^{-9}*
^{230}Th (mol/l)	*NA*	11.13 $\cdot 10^{-11}$	*NA*	1.55 $\cdot 10^{-11}$	*NA*	1.18 $\cdot 10^{-11}$	*NA*	6.80 $\cdot 10^{-11}$	*NA*	24.12 $\cdot 10^{-11}$	*NA*	3.59 $\cdot 10^{-11}$	*NA*	*NA*	*NA*

Burgeap analysis carried out between 30/07/2009 and 10/12/2009 (Burgeap, 2009 – CTOZ090490). The uncertainty of the analysis is not presented in the report.

Appendix 4

Historical Weather Data

Table A4.1: Historical rainfall data per month and year at the meteorological station of Narbonne, France (Source: www.meteonarbonne.fr).

Year	Jan	Feb	Mar	Apr	May	Jun	Jul	Aug	Sep	Oct	Nov	Dec	Annual rainfall (mm)
2015	12.6	29.2	58	46	3.6	96.5	7.6	46.5	8.4	10.4	19.5	9.4	**347.7**
2014	16.8	13	14.7	58.9	14.2	31.7	40.9	50.6	143.9	2.9	256.8	36.3	**680.7**
2013	25.8	8.5	99.4	75.1	43.5	4.3	11.5	3.8	15.5	21.7	59.4	8.3	**376.8**
2012	5	---	15.9	32.6	20	27.1	16.6	44.4	64.3	36.6	17.4	8.1	**288**
2011	63.9	24.9	69.9	43.9	26.3	13.5	26.7	31.1	0.5	61.3	129.5	11.5	**503**
2010	49.2	62.6	47.6	10.1	87.5	22.3	5.1	2.6	18.1	120.1	14	19.7	**458.9**
2009	45.9	23.4	19.2	116.9	7.1	5.9	4.4	5	6.6	32.3	5.8	10.4	**282.9**
												Minimum annual rainfall (mm)	**282.9**
												Maximum annual rainfall (mm)	**680.7**
												Average annual rainfall (mm)	**419.7**

Table A4.2: Cumulative frequency for rainfall per day between 2009 and 2015 (compiled with historical weather data for the city of Narbonne (www.meteonarbonne.fr).

Rainfall (mm/day)	2	5	10	20	30	40	>40
Frequency	474	102	56	47	9	7	13
Cumulative frequency (%)	66.95	81.36	89.27	95.90	97.18	98.16	100.00

Appendix 5

Analytical Results – Column Experiments

Table A5.1: Packed column of aged sludge. Analytical Results.

Pore volume	0.04	1.2	5.5	35.4	67.0	67.7	83.2	145.4	161.6	597.8	605.6
Sample number	1	28	40	125	258	263	310	377	421	1311	1319
Q (ml/min)	0.036	0.036	0.036	0.036	0.036	0.036	0.146	0.146	0.357	0.129	0.129
pH (± 0.1)	7.5	8.4	8.2	8.1	7.8	7.7	8.4	9.0	9.3	7.5	7.8
Eh (mV) (± 20)	415	434	439	430	419	421	505	510	498	435	454
Alkalinity (mol/l)	$7.4\cdot10^{-4}$	$9.3\cdot10^{-4}$	$6.7\cdot10^{-4}$	$4.7\cdot10^{-4}$	$5.4\cdot10^{-4}$	$5.4\cdot10^{-4}$	$4.3\cdot10^{-4}$	$(4.1\cdot10^{-4})$ *	$(7.4\cdot10^{-4})$ *	$3.6\cdot10^{-4}$	$4.8\cdot10^{-4}$
Percent Error (%)	-47.0	-3.1	-49.8	-45.1	-3.9	-4.5	3.7	-2.38	-8.29	-8.0	-24.1
Ionic Strength (mol/l)	0.38	0.07	0.04	0.04	0.04	0.04	0.04	0.01	0.01	0.001	0.001
U ($\cdot10^{-6}$ mol/l)	5.53±0.08	4.81±0.06	4.44±0.04	4.42±0.04	4.14±0.05	5.63±0.07	5.05±0.07	1.16±0.01	0.857±0.001	0.363±0.008	0.518±0.010
Th (mol/l)	$<4.3\cdot10^{-10}$	$<4.3\cdot10^{-10}$	$<4.3\cdot10^{-11}$	$<4.3\cdot10^{-11}$	$<4.3\cdot10^{-10}$	$<4.3\cdot10^{-11}$	$<4.3\cdot10^{-11}$	$<4.3\cdot10^{-11}$	$<4.3\cdot10^{-11}$	$5.2\pm0.6\cdot10^{-10}$	$4.7\pm0.7\cdot10^{-10}$
F ($\cdot10^{-4}$ mol/l)	4.50 ± 0.06	3.11 ± 0.04	2.82 ± 0.01	2.34 ± 0.01	2.49 ± 0.01	2.41 ± 0.01	2.40 ± 0.01	4.06 ± 0.01	4.65 ± 0.01	5.32 ± 0.06	4.97 ± 0.03
Cl (mol/l)	$2.61(\pm0.04)\cdot10^{-3}$	$4.58(\pm0.01)\cdot10^{-4}$	$4.41(\pm0.01)\cdot10^{-5}$	$<2.82\cdot10^{-7}$	$2.21(\pm0.03)\cdot10^{-3}$	$1.73(\pm0.01)\cdot10^{-5}$	$2.01(\pm0.01)\cdot10^{-5}$	$<2.82\cdot10^{-7}$	$<2.82\cdot10^{-7}$	$<1.41\cdot10^{-6}$	$1.52(\pm0.03)\cdot10^{-5}$
NO_2 (mol/l)	$4.05(\pm3.26)\cdot10^{-4}$	$<2.75\cdot10^{-4}$	--	--	--	--	--	--	--	--	--
NO_3 (mol/l)	$4.38(\pm0.07)\cdot10^{-1}$	$1.05(\pm0.02)\cdot10^{-2}$	$1.39(\pm0.01)\cdot10^{-4}$	$4.39(\pm0.01)\cdot10^{-5}$	$2.83(\pm0.01)\cdot10^{-5}$	$<2.17\cdot10^{-7}$	$3.90(\pm0.01)\cdot10^{-5}$	$1.82(\pm0.01)\cdot10^{-5}$	$<2.17\cdot10^{-7}$	$1.81(\pm0.09)\cdot10^{-5}$	$2.75(\pm0.06)\cdot10^{-5}$
SO_4 (mol/l)	$1.39(\pm0.02)\cdot10^{-2}$	$2.02(\pm0.03)\cdot10^{-2}$	$1.93(\pm0.03)\cdot10^{-2}$	$1.59(\pm0.02)\cdot10^{-2}$	$1.37(\pm0.02)\cdot10^{-2}$	$1.41(\pm0.02)\cdot10^{-2}$	$1.43(\pm0.02)\cdot10^{-2}$	$5.77(\pm0.08)\cdot10^{-3}$	$4.19(\pm0.06)\cdot10^{-3}$	$3.54(\pm0.04)\cdot10^{-5}$	$5.44(\pm0.03)\cdot10^{-5}$
Fe (mol/l)	--	--	$<7.77\cdot10^{-7}$	$<7.77\cdot10^{-7}$	$<7.77\cdot10^{-7}$	$<7.77\cdot10^{-7}$	$<7.77\cdot10^{-7}$	--	--	--	--
B (mol/l)	$3.3\cdot10^{-5}$	$2.2\cdot10^{-4}$	$1.5\cdot10^{-5}$	--	--	--	$1.1\cdot10^{-5}$	ND	ND	--	--
Na (mol/l)	$4.2\cdot10^{-2}$	$8.9\cdot10^{-3}$	ND	--	--	--	$6.1\cdot10^{-5}$	ND	ND	$8.2\cdot10^{-5}$	$6.9\cdot10^{-4}$
Mg (mol/l)	$9.4\cdot10^{-3}$	$3.0\cdot10^{-3}$	$6.4\cdot10^{-4}$	$8.4\cdot10^{-5}$	$1.9\cdot10^{-4}$	$1.7\cdot10^{-4}$	$1.8\cdot10^{-4}$	ND	ND	ND	ND
Al (mol/l)	--	--	--	--	--	--	--	--	--	$2.0\cdot10^{-4}$	ND
K (mol/l)	$8.3\cdot10^{-3}$	$9.5\cdot10^{-3}$	$6.9\cdot10^{-4}$	--	--	--	$1.9\cdot10^{-4}$	ND	ND	ND	ND
Ca (mol/l)	$5.4\cdot10^{-2}$	$1.3\cdot10^{-2}$	$7.9\cdot10^{-3}$	$8.1\cdot10^{-3}$	$1.4\cdot10^{-2}$	$1.3\cdot10^{-2}$	$1.5\cdot10^{-2}$	$6.0\cdot10^{-3}$	$4.2\cdot10^{-3}$	$3.7\cdot10^{-4}$	ND

Pore volume	0.04	1.2	5.5	35.4	67.0	67.7	83.2	145.4	161.6	597.8	605.6
Sample number	1	28	40	125	258	263	310	377	421	1311	1319
Mn (mol/l)	$9.1\cdot10^{-6}$	$2.0\cdot10^{-6}$	$1.2\cdot10^{-6}$	$6.0\cdot10^{-7}$	$7.6\cdot10^{-7}$	$7.7\cdot10^{-7}$	$6.6\cdot10^{-7}$	--	$1.5\cdot10^{-7}$	ND	ND
Co (mol/l)	$5.6\cdot10^{-7}$	$3.0\cdot10^{-7}$	$9.0\cdot10^{-8}$	$3.7\cdot10^{-8}$	$3.8\cdot10^{-8}$	$1.8\cdot10^{-8}$	$3.1\cdot10^{-8}$	ND	ND	ND	ND
Cu (mol/l)	$1.9\cdot10^{-5}$	ND	ND	ND	ND	ND	ND	$7.6\cdot10^{-7}$	$4.8\cdot10^{-7}$	$5.0\cdot10^{-7}$	ND
Zn (mol/l)	$1.8\cdot10^{-5}$	$8.9\cdot10^{-7}$	$1.2\cdot10^{-6}$	$2.6\cdot10^{-6}$	$3.7\cdot10^{-7}$	$2.1\cdot10^{-6}$	$2.2\cdot10^{-7}$	$6.1\cdot10^{-6}$	$7.1\cdot10^{-6}$	ND	ND
Rb (mol/l)	$1.6\cdot10^{-6}$	$4.8\cdot10^{-7}$	$1.7\cdot10^{-7}$	$4.1\cdot10^{-8}$	$4.9\cdot10^{-8}$	$3.7\cdot10^{-8}$	$3.2\cdot10^{-8}$	$2.6\cdot10^{-8}$	$2.1\cdot10^{-8}$	ND	ND
Sr (mol/l)	$5.1\cdot10^{-4}$	$6.7\cdot10^{-5}$	$5.8\cdot10^{-5}$	$6.2\cdot10^{-5}$	$6.2\cdot10^{-5}$	$5.6\cdot10^{-5}$	$5.1\cdot10^{-5}$	$1.1\cdot10^{-5}$	$8.1\cdot10^{-6}$	$4.7\cdot10^{-6}$	ND
Zr (mol/l)	$6.8\cdot10^{-7}$	$1.9\cdot10^{-7}$	$1.7\cdot10^{-7}$	$1.4\cdot10^{-7}$	$2.0\cdot10^{-7}$	$1.8\cdot10^{-7}$	$1.2\cdot10^{-8}$	$6.8\cdot10^{-8}$	$7.4\cdot10^{-8}$	$1.6\cdot10^{-7}$	$1.5\cdot10^{-6}$
Mo (mol/l)	$4.3\cdot10^{-6}$	$6.3\cdot10^{-5}$	$3.1\cdot10^{-5}$	$3.0\cdot10^{-5}$	$4.7\cdot10^{-5}$	$4.5\cdot10^{-5}$	$4.6\cdot10^{-5}$	$2.2\cdot10^{-5}$	$1.6\cdot10^{-5}$	$6.9\cdot10^{-7}$	$1.3\cdot10^{-6}$
Cd (mol/l)	--	$1.1\cdot10^{-7}$	--	--	$6.0\cdot10^{-8}$	$6.0\cdot10^{-8}$	$7.6\cdot10^{-8}$	$3.4\cdot10^{-8}$	$1.7\cdot10^{-8}$	ND	ND
Cs (mol/l)	$4.2\cdot10^{-8}$	$1.4\cdot10^{-8}$	$2.0\cdot10^{-8}$	$1.4\cdot10^{-8}$	$1.2\cdot10^{-8}$	$1.1\cdot10^{-8}$	ND	ND	ND	ND	ND
Ba (mol/l)	$1.8\cdot10^{-6}$	$6.0\cdot10^{-8}$	ND	ND	ND	ND	$1.3\cdot10^{-7}$	$2.6\cdot10^{-7}$	$2.6\cdot10^{-7}$	$2.1\cdot10^{-7}$	ND

*calculated from calcite equilibrium; --not determined; ND: not detected; the uncertainty associated with the cations and trace elements is of ±30%.

Table A5.2: Packed column of fresh sludge. Analytical Results.

Pore volume	1.1	2.4	9.6	27.5	82.2
Sample number	**10**	**23**	**60**	**173**	**325**
Q (ml/min)	0.156	0.156	0.156	0.156	0.156
pH (± 0.1)	7.1	8.0	7.7	7.1	7.1
Eh (mV) (± 20)	461	418	444	452	449
Alkalinity (mol/l)	$2.59^{\cdot 10\text{-}3}$	$1.90^{\cdot 10\text{-}3}$	$6.06^{\cdot 10\text{-}4}$	$3.64^{\cdot 10\text{-}4}$	$3.33^{\cdot 10\text{-}4}$
Percent Error (%)	98.6	-28.0	-5.7	-2.7	-2.8
Ionic Strength (mol/l)	2.59	0.47	0.04	0.04	0.02
U (mol/l)	$1.77(\pm 0.02)\cdot 10^{-5}$	$3.51(\pm 0.05)\cdot 10^{-6}$	$1.99(\pm 0.03)\cdot 10^{-6}$	$1.59(\pm 0.02)\cdot 10^{-6}$	$5.99(\pm 0.10)\cdot 10^{-7}$
Th (mol/l)	$3.45(\pm 0.24)\cdot 10^{-9}$	$3.45(\pm 1.18)\cdot 10^{-9}$	$2.54(\pm 0.19)\cdot 10^{-9}$	$1.34(\pm 0.10)\cdot 10^{-9}$	$1.08(\pm 0.12)\cdot 10^{-9}$
F (mol/l)	$4.59(\pm 1.11)\cdot 10^{-4}$	$3.49(\pm 0.05)\cdot 10^{-4}$	$2.34(\pm 0.03)\cdot 10^{-4}$	$2.51(\pm 0.01)\cdot 10^{-4}$	$4.44(\pm 0.02)\cdot 10^{-4}$
Cl (mol/l)	$1.48(\pm 0.02)\cdot 10^{-2}$	$1.39(\pm 0.03)\cdot 10^{-3}$	$2.52(\pm 0.11)\cdot 10^{-5}$	$1.76(\pm 0.05)\cdot 10^{-5}$	$1.26(\pm 0.10)\cdot 10^{-5}$
NO_2 (mol/l)	--	--	--	--	--
NO_3 (mol/l)	--	$4.49(\pm 0.06)\cdot 10^{-1}$	$3.91(\pm 0.06)\cdot 10^{-4}$	$2.26(\pm 0.01)\cdot 10^{-4}$	$1.01(\pm 0.02)\cdot 10^{-4}$
SO_4 (mol/l)	$7.97(\pm 0.13)\cdot 10^{-3}$	$1.34(\pm 0.02)\cdot 10^{-2}$	$1.68(\pm 0.03)\cdot 10^{-2}$	$1.56(\pm 0.03)\cdot 10^{-2}$	$5.53(\pm 0.26)\cdot 10^{-3}$
Fe (mol/l)	--	--	--	--	--
B (mol/l)	*ND*	*ND*	*ND*	*ND*	*ND*
Na (mol/l)	$6.33\cdot 10^{-1}$	$6.24\cdot 10^{-2}$	$1.09\cdot 10^{-3}$	$2.05\cdot 10^{-4}$	$1.34\cdot 10^{-4}$
Mg (mol/l)	$8.16\cdot 10^{-2}$	$9.79\cdot 10^{-3}$	$1.57\cdot 10^{-3}$	$6.44\cdot 10^{-4}$	$8.34\cdot 10^{-5}$
Al (mol/l)	*ND*	*ND*	*ND*	*ND*	*ND*
K (mol/l)	$1.51\cdot 10^{-1}$	*ND*	*ND*	*ND*	*ND*
Ca (mol/l)	$1.02\cdot 10^{0}$	$9.68\cdot 10^{-2}$	$1.40\cdot 10^{-2}$	$1.47\cdot 10^{-2}$	$5.59\cdot 10^{-3}$
Mn (mol/l)	*ND*	*ND*	*ND*	*ND*	*ND*
Co (mol/l)	*ND*	*ND*	*ND*	*ND*	*ND*
Cu (mol/l)	$5.06\cdot 10^{-5}$	$3.83\cdot 10^{-5}$	$3.87\cdot 10^{-6}$	$5.60\cdot 10^{-7}$	$4.15\cdot 10^{-7}$
Zn (mol/l)	*ND*	*ND*	*ND*	*ND*	*ND*

Pore volume	**1.1**	**2.4**	**9.6**	**27.5**	**82.2**
Sample number	**10**	**23**	**60**	**173**	**325**
Rb (mol/l)	$1.99 \cdot 10^{-5}$	*ND*	*ND*	*ND*	*ND*
Sr (mol/l)	$7.18 \cdot 10^{-4}$	*ND*	*ND*	$4.29 \cdot 10^{-6}$	$1.21 \cdot 10^{-6}$
Zr (mol/l)	$8.55 \cdot 10^{-6}$	$8.15 \cdot 10^{-6}$	$7.88 \cdot 10^{-7}$	$8.22 \cdot 10^{-8}$	$8.57 \cdot 10^{-8}$
Mo (mol/l)	$2.02 \cdot 10^{-5}$	$4.51 \cdot 10^{-5}$	$3.71 \cdot 10^{-5}$	$2.55 \cdot 10^{-5}$	$2.57 \cdot 10^{-5}$
Cd (mol/l)	*ND*	*ND*	*ND*	*ND*	*ND*
Cs (mol/l)	*ND*	*ND*	*ND*	*ND*	*ND*
Ba (mol/l)	$9.70 \cdot 10^{-5}$	$5.11 \cdot 10^{-6}$	*ND*	$8.46 \cdot 10^{-8}$	$8.01 \cdot 10^{-8}$

*calculated from calcite equilibrium; --not determined; ND: not detected; the uncertainty associated with the cations and trace elements is of ±30%.

Table A5.3: Undisturbed column of fresh sludge. Analytical Results.

Volume eluted (ml)	109	400	858	1277	2058	2503	2717
Sample number	22	81	174	243	370	435	484
Q (ml/min)	0.065	0.065	0.065	0.065	0.065	0.065	0.065
pH (± 0.1)	7.7	7.4	8.5	8.3	8.8	8.2	8.2
Eh (mV) (± 20)	389	421.3	398	381	319	369	369
Alkalinity (mol/l)	1.12·10-2	4.86·10-3	7.88·10-3	4.72·10-3	2.91·10-3	2.91·10-3	2.91·10-3
Percent Error (%)	-14.6	5.3	-18.7	-9.9	-11.4	-11.5	26.2
Ionic Strength (mol/l)	3.03	0.94	0.34	0.20	0.07	0.05	0.08
U (mol/l)	$4.96(\pm0.06)\cdot10^{-7}$	$3.01(\pm0.07)\cdot10^{-7}$	$1.98(\pm0.03)\cdot10^{-7}$	$2.14(\pm0.03)\cdot10^{-7}$	$1.79(\pm0.03)\cdot10^{-7}$	$1.76(\pm0.03)\cdot10^{-7}$	$3.15(\pm0.03)\cdot10^{-7}$
Th (mol/l)	*<4.31·10-10*	*<4.31·10-10*	*<4.31·10-11*	*<2.59·10-10*	*<2.59·10-10*	*<2.59·10-10*	*<2.59·10-10*
F (mol/l)	$4.24(\pm0.01)\cdot\cdot10^{-4}$	$1.57(\pm0.01)\cdot\cdot10^{-4}$	$3.29(\pm0.01)\cdot\cdot10^{-4}$	$2.62(\pm0.05)\cdot\cdot10^{-4}$	$2.90(\pm0.02)\cdot\cdot10^{-4}$	$3.11(\pm0.01)\cdot\cdot10^{-4}$	$2.48(\pm0.01)\cdot\cdot10^{-4}$
Cl (mol/l)	$4.86(\pm0.06)\cdot10^{-4}$	$1.28(\pm0.02)\cdot10^{-4}$	$6.05(\pm0.01)\cdot10^{-5}$	$3.38(\pm0.18)\cdot10^{-5}$	$1.89(\pm0.01)\cdot10^{-4}$	$8.81(\pm0.11)\cdot10^{-5}$	$7.50(\pm0.31)\cdot10^{-5}$
NO_2 (mol/l)	$2.54(\pm0.43)\cdot10^{-2}$	$7.17(\pm2.36)\cdot10^{-3}$	$2.59(\pm0.75)\cdot10^{-3}$	$2.21(\pm0.94)\cdot10^{-3}$	$5.97(\pm0.47)\cdot10^{-4}$	$3.09(\pm1.89)\cdot10^{-4}$	$1.08(\pm0.28)\cdot10^{-3}$
NO_3 (mol/l)	$2.65(\pm0.02)\cdot10^{0}$	$6.38(\pm0.05)\cdot10^{-1}$	$2.89(\pm0.05)\cdot10^{-1}$	$1.37(\pm0.03)\cdot10^{-1}$	$2.77(\pm0.02)\cdot10^{-2}$	$1.14(\pm0.01)\cdot10^{-2}$	$1.27(\pm0.01)\cdot10^{-2}$
SO_4 (mol/l)	$1.16(\pm0.01)\cdot10^{-2}$	$1.30(\pm0.01)\cdot10^{-2}$	$1.36(\pm0.01)\cdot10^{-2}$	$1.39(\pm0.01)\cdot10^{-2}$	$1.38(\pm0.01)\cdot10^{-2}$	$1.40(\pm0.01)\cdot10^{-2}$	$1.44(\pm0.01)\cdot10^{-2}$
Fe (mol/l)	*<1.33·10-6*	--	--	--	*<7.97·10-7*	--	--
B (mol/l)	$1.71\cdot10^{-4}$	$1.67\cdot10^{-4}$	$1.11\cdot10^{-4}$	$9.53\cdot10^{-5}$	$7.68\cdot10^{-5}$	$6.25\cdot10^{-5}$	$1.41\cdot10^{-4}$
Na (mol/l)	$4.20\cdot10^{-1}$	$1.62\cdot10^{-1}$	$4.24\cdot10^{-2}$	$2.17\cdot10^{-2}$	$5.04\cdot10^{-3}$	$2.38\cdot10^{-3}$	$4.23\cdot10^{-3}$
Mg (mol/l)	$2.18\cdot10^{-2}$	$9.98\cdot10^{-3}$	$3.69\cdot10^{-3}$	$4.19\cdot10^{-3}$	$1.64\cdot10^{-3}$	$1.16\cdot10^{-3}$	$2.55\cdot10^{-3}$
Si (mol/l)				$1.12\cdot10^{-4}$	$1.11\cdot10^{-4}$	$1.11\cdot10^{-4}$	$2.18\cdot10^{-4}$
K (mol/l)	$2.22\cdot10^{-1}$	$8.93\cdot10^{-2}$	$2.35\cdot10^{-2}$	$6.66\cdot10^{-3}$	$1.90\cdot10^{-3}$	$1.06\cdot10^{-3}$	$1.93\cdot10^{-3}$
Ca (mol/l)	$6.69\cdot10^{-1}$	$2.39\cdot10^{-1}$	$7.77\cdot10^{-2}$	$5.34\cdot10^{-2}$	$1.96\cdot10^{-2}$	$1.52\cdot10^{-2}$	$2.89\cdot10^{-2}$
Mn (mol/l)	$2.53\cdot10^{-5}$	$1.23\cdot10^{-5}$	$4.67\cdot10^{-6}$	$3.09\cdot10^{-6}$	$1.36\cdot10^{-6}$	$1.03\cdot10^{-6}$	$2.03\cdot10^{-6}$
Co (mol/l)	$5.28\cdot10^{-6}$	$2.06\cdot10^{-6}$	$5.85\cdot10^{-7}$	$3.09\cdot10^{-7}$	$1.49\cdot10^{-7}$	$9.91\cdot10^{-8}$	$1.78\cdot10^{-7}$
Ni (mol/l)	$6.88\cdot10^{-6}$	$1.90\cdot10^{-6}$	$4.90\cdot10^{-7}$	$3.84\cdot10^{-7}$	$2.06\cdot10^{-7}$	$1.88\cdot10^{-7}$	$2.80\cdot10^{-7}$
Cu (mol/l)	*ND*	*ND*	$6.64\cdot10^{-8}$	$3.33\cdot10^{-7}$	$9.06\cdot10^{-8}$	$6.87\cdot10^{-8}$	$1.10\cdot10^{-7}$

Volume eluted (ml)	109	400	858	1277	2058	2503	2717
Sample number	**22**	**81**	**174**	**243**	**370**	**435**	**484**
Zn (mol/l)	$1.26 \cdot 10^{-5}$	$3.72 \cdot 10^{-6}$	$4.46 \cdot 10^{-7}$	$4.10 \cdot 10^{-7}$	*ND*	$4.69 \cdot 10^{-7}$	$6.26 \cdot 10^{-7}$
As (mol/l)	$8.84 \cdot 10^{-7}$	$2.44 \cdot 10^{-7}$	$1.08 \cdot 10^{-7}$	$1.11 \cdot 10^{-7}$	$5.68 \cdot 10^{-8}$	$5.38 \cdot 10^{-8}$	$1.05 \cdot 10^{-7}$
Rb (mol/l)	$1.24 \cdot 10^{-5}$	$4.82 \cdot 10^{-6}$	$1.27 \cdot 10^{-6}$	$8.22 \cdot 10^{-7}$	$2.69 \cdot 10^{-7}$	$1.62 \cdot 10^{-7}$	$3.06 \cdot 10^{-7}$
Sr (mol/l)	$3.94 \cdot 10^{-4}$	$1.37 \cdot 10^{-4}$	$3.86 \cdot 10^{-5}$	$2.94 \cdot 10^{-5}$	$1.09 \cdot 10^{-5}$	$8.94 \cdot 10^{-6}$	$1.68 \cdot 10^{-5}$
Zr (mol/l)	$1.40 \cdot 10^{-7}$	$1.37 \cdot 10^{-7}$	$1.40 \cdot 10^{-8}$	$8.61 \cdot 10^{-9}$	$7.89 \cdot 10^{-9}$	$7.87 \cdot 10^{-9}$	$7.52 \cdot 10^{-9}$
Mo (mol/l)	$6.39 \cdot 10^{-5}$	$4.21 \cdot 10^{-5}$	$3.41 \cdot 10^{-5}$	$3.42 \cdot 10^{-5}$	$3.27 \cdot 10^{-5}$	$3.28 \cdot 10^{-5}$	$7.12 \cdot 10^{-5}$
Cd (mol/l)	$1.18 \cdot 10^{-7}$	$5.58 \cdot 10^{-8}$	$6.73 \cdot 10^{-8}$	$5.82 \cdot 10^{-8}$	$5.66 \cdot 10^{-8}$	$5.55 \cdot 10^{-8}$	$1.08 \cdot 10^{-7}$
Sn (mol/l)	$2.00 \cdot 10^{-7}$	$1.13 \cdot 10^{-7}$	$7.84 \cdot 10^{-8}$	$8.94 \cdot 10^{-8}$	$9.54 \cdot 10^{-8}$	$9.08 \cdot 10^{-8}$	$1.87 \cdot 10^{-7}$
Sb (mol/l)	*ND*	*ND*	$1.65 \cdot 10^{-9}$	$2.09 \cdot 10^{-9}$	$2.04 \cdot 10^{-9}$	$1.55 \cdot 10^{-9}$	$3.45 \cdot 10^{-9}$
Cs (mol/l)	$3.06 \cdot 10^{-7}$	$1.05 \cdot 10^{-7}$	$2.52 \cdot 10^{-8}$	$2.08 \cdot 10^{-8}$	$7.61 \cdot 10^{-9}$	$4.75 \cdot 10^{-9}$	$9.09 \cdot 10^{-9}$
Ba (mol/l)	$1.30 \cdot 10^{-5}$	$2.25 \cdot 10^{-6}$	$3.98 \cdot 10^{-7}$	$2.87 \cdot 10^{-7}$	$1.22 \cdot 10^{-7}$	$1.04 \cdot 10^{-7}$	$1.94 \cdot 10^{-7}$

*calculated from calcite equilibrium; --not determined; ND: not detected; the uncertainty associated with the cations and trace elements is of ±30%.

Table A5.4: Packed column of aged tailings. Analytical Results.

Pore volume	0.6	1.6	7.2	11.9	18.4	23.3	28.3	34.0	77.5	99.6	107.5	111.6	142.7
Sample number	1_4	1_11	2_3	2_21	2_46	3_2	3_15	3_30	3_144	3_202	4_3	4_15	4_105
Q (ml/min)													
pH (± 0.1)	6.8	7.3	7.7	7.8	7.8	7.6	7.4	7.5	8.3	8.1	8.1	8.2	8.3
Eh (mV) (± 20)	458	410	385	447	465	384	371	381	389	403	393	391	382
Alkalinity (mol/l)	--	--	$6.90 \cdot 10^{-4}$	$7.41 \cdot 10^{-4}$	$3.33 \cdot 10^{-4}$	$9.52 \cdot 10^{-4}$	$3.14 \cdot 10^{-4}$	$3.33 \cdot 10^{-4}$	$2.46 \cdot 10^{-4}$	$2.54 \cdot 10^{-4}$	$7.02 \cdot 10^{-4}$	$3.33 \cdot 10^{-4}$	$2.08 \cdot 10^{-4}$
Percent Error (%)	46.2	-94.7	-91.0	-92.1	-92.5	-84.2	-1.8	-4.7	-8.0	-7.7	-5.5	-8.7	-7.6
Ionic Strength (mol/l)	1.09	0.35	0.31	0.29	0.29	0.27	0.04	0.04	0.04	0.04	0.04	0.04	0.04
U (mol/l)	$1.28(\pm0.05) \cdot 10^{-5}$	$8.45(\pm0.07) \cdot 10^{-6}$	$1.63(\pm0.01) \cdot 10^{-5}$	$3.25(\pm0.04) \cdot 10^{-6}$	$1.38(\pm0.01) \cdot 10^{-6}$	$8.61(\pm0.07) \cdot 10^{-6}$	$1.14(\pm0.01) \cdot 10^{-6}$	$1.25(\pm0.01) \cdot 10^{-6}$	$2.62(\pm0.05) \cdot 10^{-7}$	$2.22(\pm0.04) \cdot 10^{-7}$	$1.04(\pm0.02) \cdot 10^{-6}$	$8.78(\pm0.13) \cdot 10^{-7}$	$1.83(\pm0.01) \cdot 10^{-7}$
Th (mol/l)	$2.46(\pm0.09) \cdot 10^{-10}$	$1.04(\pm0.06) \cdot 10^{-10}$	$2.84(\pm0.56) \cdot 10^{-11}$	*<4.31·10⁻¹¹*	*<4.31·10⁻¹¹*	$4.31 \cdot 10^{-11}$	*<4.31·10⁻¹¹*	*<4.31·10⁻¹¹*	*<4.31·10⁻¹¹*	*<4.31·10⁻¹¹*	*<4.31·10⁻¹¹*	*<4.31·10⁻¹¹*	*<4.31·10⁻¹¹*
F (mol/l)	$6.99(\pm0.10) \cdot 10^{-4}$	$6.99(\pm0.10) \cdot 10^{-4}$	$1.61(\pm0.02) \cdot 10^{-4}$	$1.10(\pm0.03) \cdot 10^{-4}$	$9.00(\pm0.18) \cdot 10^{-5}$	$8.39(\pm0.15) \cdot 10^{-5}$	$9.34(\pm0.21) \cdot 10^{-5}$	$1.09(\pm0.03) \cdot 10^{-4}$	$5.93(\pm0.19) \cdot 10^{-5}$	$5.45(\pm0.10) \cdot 10^{-5}$	$9.95(\pm0.19) \cdot 10^{-5}$	$4.27(\pm0.10) \cdot 10^{-5}$	$3.02(\pm0.20) \cdot 10^{-5}$
Cl (mol/l)	$3.43(\pm0.08) \cdot 10^{-3}$	$3.43(\pm0.08) \cdot 10^{-3}$	$2.45(\pm0.03) \cdot 10^{-3}$	*<2.86·10⁻⁶*	*<2.86·10⁻⁶*	*<2.86·10⁻⁶*	$2.56(\pm0.04) \cdot 10^{-3}$	$2.80(\pm0.07) \cdot 10^{-5}$	*<2.86·10⁻⁶*	*<2.86·10⁻⁶*	*<2.86·10⁻⁶*	*<2.86·10⁻⁶*	*<2.86·10⁻⁶*
NO_2 (mol/l)	--	--	--	--	--	--	--	--	--	--	--	--	--
NO_3 (mol/l)	$2.58(\pm0.02) \cdot 10^{-1}$	$2.58(\pm0.02) \cdot 10^{-1}$	$3.57(\pm0.07) \cdot 10^{-3}$	*<2.20·10⁻⁴*	*<2.20·10⁻⁴*	*<2.20·10⁻⁴*	*<2.20·10⁻⁶*	$5.97(\pm0.11) \cdot 10^{-5}$	*<2.20·10⁻⁴*	*<2.20·10⁻⁴*	*<2.20·10⁻⁴*	$3.70(\pm0.11) \cdot 10^{-5}$	$2.91(\pm0.07) \cdot 10^{-5}$
SO_4 (mol/l)	$1.09(\pm0.01) \cdot 10^{-1}$	$1.09(\pm0.01) \cdot 10^{-1}$	$1.59(\pm0.01) \cdot 10^{-1}$	$1.48(\pm0.01) \cdot 10^{-1}$	$1.50(\pm0.01) \cdot 10^{-1}$	$1.37(\pm0.01) \cdot 10^{-1}$	$1.55(\pm0.01) \cdot 10^{-2}$	$1.57(\pm0.01) \cdot 10^{-2}$	$1.58(\pm0.01) \cdot 10^{-2}$	$1.61(\pm0.01) \cdot 10^{-2}$	$1.61(\pm0.01) \cdot 10^{-2}$	$1.61(\pm0.01) \cdot 10^{-2}$	$1.63(\pm0.01) \cdot 10^{-2}$
Fe (mol/l)	*<7.77·10⁻⁷*	--		*<7.77·10⁻⁷*	--	--	--	*<7.77·10⁻⁷*	--	--	--	--	--
B (mol/l)	$1.0 \cdot 10^{-4}$	$4.4 \cdot 10^{-6}$	$8.2 \cdot 10^{-5}$	$1.0 \cdot 10^{-6}$	*ND*	$2.0 \cdot 10^{-5}$	*ND*	*ND*	*ND*	*ND*	$7.4 \cdot 10^{-6}$	*ND*	*ND*
Na (mol/l)	overflow	$4.0 \cdot 10^{-3}$	$3.4 \cdot 10^{-5}$	$3.9 \cdot 10^{-5}$	$2.8 \cdot 10^{-5}$	$8.3 \cdot 10^{-5}$	$2.4 \cdot 10^{-5}$	$2.8 \cdot 10^{-5}$	$2.0 \cdot 10^{-5}$	$2.0 \cdot 10^{-5}$	$4.8 \cdot 10^{-5}$	$3.7 \cdot 10^{-4}$	$2.1 \cdot 10^{-5}$
Mg (mol/l)	$1.1 \cdot 10^{-1}$	$2.0 \cdot 10^{-3}$	$1.0 \cdot 10^{-3}$	$3.8 \cdot 10^{-4}$	$1.8 \cdot 10^{-4}$	$5.1 \cdot 10^{-4}$	$1.8 \cdot 10^{-4}$	$1.9 \cdot 10^{-4}$	$3.2 \cdot 10^{-5}$	$3.7 \cdot 10^{-5}$	$1.8 \cdot 10^{-4}$	$5.2 \cdot 10^{-5}$	$1.5 \cdot 10^{-5}$
Si (mol7l)	$3.7 \cdot 10^{-4}$	$4.2 \cdot 10^{-5}$	$4.7 \cdot 10^{-4}$	$3.3 \cdot 10^{-4}$	$2.5 \cdot 10^{-4}$	$3.9 \cdot 10^{-4}$	$2.5 \cdot 10^{-4}$	$2.5 \cdot 10^{-4}$	$1.1 \cdot 10^{-4}$	$1.1 \cdot 10^{-4}$	$2.9 \cdot 10^{-4}$	$2.5 \cdot 10^{-4}$	$1.2 \cdot 10^{-4}$
Al (mol/l)	--	--	--	--	--	--	--	--	--	--	--	--	--
K (mol/l)	$5.5 \cdot 10^{-2}$	$1.4 \cdot 10^{-3}$	$2.7 \cdot 10^{-3}$	$1.3 \cdot 10^{-4}$	$7.6 \cdot 10^{-5}$	$9.8 \cdot 10^{-3}$	$2.8 \cdot 10^{-3}$	$5.1 \cdot 10^{-5}$	$2.7 \cdot 10^{-5}$	*ND*	$4.5 \cdot 10^{-5}$	$3.5 \cdot 10^{-5}$	$1.7 \cdot 10^{-5}$
Ca (mol/l)	$3.9^{\cdot 10^{-1}}$	$5.8 \cdot 10^{-3}$	$1.5 \cdot 10^{-2}$	$1.5 \cdot 10^{-2}$	$1.5 \cdot 10^{-2}$	$1.5 \cdot 10^{-2}$	$1.5 \cdot 10^{-2}$	$1.5 \cdot 10^{-2}$	$1.4 \cdot 10^{-2}$	$1.5 \cdot 10^{-2}$	$1.5 \cdot 10^{-2}$	$1.4 \cdot 10^{-2}$	$1.5 \cdot 10^{-2}$
Mn (mol/l)	$2.9 \cdot 10^{-4}$	$5.6 \cdot 10^{-6}$	$1.2 \cdot 10^{-5}$	$9.6 \cdot 10^{-6}$	$7.1 \cdot 10^{-6}$	$8.0 \cdot 10^{-6}$	$7.5 \cdot 10^{-6}$	$5.5 \cdot 10^{-6}$	$1.6 \cdot 10^{-6}$	$1.3 \cdot 10^{-6}$	$2.8 \cdot 10^{-6}$	$1.9 \cdot 10^{-6}$	$7.6 \cdot 10^{-7}$
Co (mol/l)	$4.1 \cdot 10^{-6}$	$1.1 \cdot 10^{-7}$	$2.7 \cdot 10^{-7}$	$1.4 \cdot 10^{-7}$	$9.4 \cdot 10^{-8}$	$1.6 \cdot 10^{-7}$	$9.8 \cdot 10^{-8}$	$8.8 \cdot 10^{-8}$	$3.1 \cdot 10^{-8}$	$3.0 \cdot 10^{-8}$	$6.6 \cdot 10^{-8}$	$3.6 \cdot 10^{-8}$	$2.5 \cdot 10^{-8}$
Ni (mol/l)	$1.6 \cdot 10^{-5}$	$4.4 \cdot 10^{-7}$	$9.2 \cdot 10^{-7}$	$4.8 \cdot 10^{-7}$	$3.2 \cdot 10^{-7}$	$6.1 \cdot 10^{-7}$	$3.1 \cdot 10^{-7}$	$2.5 \cdot 10^{-7}$	$1.6 \cdot 10^{-7}$	$1.5 \cdot 10^{-7}$	$2.9 \cdot 10^{-7}$	$1.5 \cdot 10^{-7}$	$1.4 \cdot 10^{-7}$
Cu (mol/l)	$3.5 \cdot 10^{-6}$	$2.1 \cdot 10^{-7}$	$1.8 \cdot 10^{-6}$	$3.4 \cdot 10^{-7}$	$2.0 \cdot 10^{-7}$	$1.0 \cdot 10^{-6}$	$1.6 \cdot 10^{-7}$	$1.9 \cdot 10^{-7}$	$7.3 \cdot 10^{-8}$	$6.5 \cdot 10^{-8}$	$1.2 \cdot 10^{-6}$	$1.0 \cdot 10^{-7}$	$6.3 \cdot 10^{-8}$
Zn (mol/l)	$6.0 \cdot 10^{-6}$	$2.5 \cdot 10^{-7}$	$1.3 \cdot 10^{-6}$	$7.9 \cdot 10^{-7}$	$3.8 \cdot 10^{-7}$	$9.7 \cdot 10^{-7}$	$1.4 \cdot 10^{-6}$	$1.2 \cdot 10^{-6}$	$3.0 \cdot 10^{-7}$	$4.1 \cdot 10^{-7}$	$2.4 \cdot 10^{-6}$	$5.5 \cdot 10^{-7}$	$5.7 \cdot 10^{-7}$

Pore volume	0.6	1.6	7.2	11.9	18.4	23.3	28.3	34.0	77.5	99.6	107.5	111.6	142.7
Sample number	1_4	1_11	2_3	2_21	2_46	3_2	3_15	3_30	3_144	3_202	4_3	4_15	4_105
As (mol/l)	$5.2\cdot10^{-7}$	$3.7\cdot10^{-8}$	$7.3\cdot10^{-8}$	$2.2\cdot10^{-8}$	$8.4\cdot10^{-9}$	$5.3\cdot10^{-8}$	$1.1\cdot10^{-8}$	$9.3\cdot10^{-9}$	*ND*	*ND*	$2.3\cdot10^{-8}$	*ND*	$9.8\cdot10^{-9}$
Rb (mol/l)	$4.9\cdot10^{-6}$	$1.2\cdot10^{-7}$	$1.4\cdot10^{-7}$	$5.9\cdot10^{-8}$	$4.2\cdot10^{-8}$	$1.7\cdot10^{-7}$	$7.0\cdot10^{-8}$	$4.3\cdot10^{-8}$	$2.3\cdot10^{-8}$	$2.1\cdot10^{-8}$	*ND*	$4.2\cdot10^{-8}$	$1.9\cdot10^{-8}$
Sr (mol/l)	$3.7\cdot10^{-3}$	$5.6\cdot10^{-5}$	$1.1\cdot10^{-4}$	$8.4\cdot10^{-5}$	$5.9\cdot10^{-5}$	$9.2\cdot10^{-5}$	$5.5\cdot10^{-5}$	$5.1\cdot10^{-5}$	$2.2\cdot10^{-5}$	$2.1\cdot10^{-5}$	$5.1\cdot10^{-5}$	$3.0\cdot10^{-5}$	$2.0\cdot10^{-5}$
Zr (mol/l)	$9.3\cdot10^{-9}$	$8.3\cdot10^{-9}$	$3.2\cdot10^{-9}$	$4.6\cdot10^{-9}$	$6.1\cdot10^{-9}$	$3.9\cdot10^{-9}$	$5.8\cdot10^{-9}$	$4.2\cdot10^{-9}$	$7.1\cdot10^{-9}$	$5.0\cdot10^{-9}$	$5.0\cdot10^{-9}$	$6.8\cdot10^{-9}$	$5.1\cdot10^{-9}$
Mo (mol/l)	$5.2\cdot10^{-6}$	$8.4\cdot10^{-7}$	$4.5\cdot10^{-6}$	$1.4\cdot10^{-6}$	$7.4\cdot10^{-7}$	$2.8\cdot10^{-6}$	$5.1\cdot10^{-7}$	$7.5\cdot10^{-7}$	$1.4\cdot10^{-7}$	$1.1\cdot10^{-7}$	$1.4\cdot10^{-6}$	$1.3\cdot10^{-7}$	$8.1\cdot10^{-8}$
Cd (mol/l)	$2.6\cdot10^{-8}$	*ND*	$8.1\cdot10^{-9}$	$2.8\cdot10^{-9}$	*ND*	$3.4\cdot10^{-9}$	*ND*	*ND*	*ND*	*ND*	$3.4\cdot10^{-9}$	*ND*	*ND*
Cs (mol/l)	$1.5\cdot10^{-7}$	$2.8\cdot10^{-9}$	$2.6\cdot10^{-9}$	$8.9\cdot10^{-10}$	$8.9\cdot10^{-10}$	$2.9\cdot10^{-9}$	$9.2\cdot10^{-10}$	$5.8\cdot10^{-10}$	*ND*	*ND*	$4.5\cdot10^{-10}$	$4.1\cdot10^{-10}$	*ND*
Ba (mol/l)	$1.3\cdot10^{-5}$	$1.4\cdot10^{-7}$	$1.6\cdot10^{-7}$	$1.4\cdot10^{-7}$	$1.6\cdot10^{-7}$	$2.2\cdot10^{-7}$	$1.6\cdot10^{-7}$	$1.8\cdot10^{-7}$	$1.7\cdot10^{-7}$	$1.6\cdot10^{-7}$	$2.0\cdot10^{-7}$	$1.8\cdot10^{-7}$	$1.6\cdot10^{-7}$
Pb (mol/l)	$1.7\cdot10^{-8}$	*ND*	$7.2\cdot10^{-9}$	*ND*	*ND*	$1.5\cdot10^{-7}$	$3.4\cdot10^{-8}$	$1.7\cdot10^{-9}$	$9.5\cdot10^{-10}$	$5.1\cdot10^{-10}$	$3.5\cdot10^{-9}$	$8.7\cdot10^{-10}$	$5.2\cdot10^{-10}$

*calculated from calcite equilibrium; --not determined; ND: not detected; the uncertainty associated with the cations and trace elements is of ±30%.

Table A5.5: Packed column of fresh tailings. Analytical Results.

Pore volume	0.9	13.3	29.3	49.5	316.6
Sample number	**3**	**45**	**73**	**107**	**647**
Q (ml/min)	0.154	0.154	0.154	0.154	0.154
pH (± 0.1)	7.8	7.6	7.6	7.3	7.4
Eh (mV) (± 20)	412	420	423	423	449
Alkalinity (mol/l)	$1.30 \cdot 10^{-2}$	$1.61 \cdot 10^{-3}$	$1.07 \cdot 10^{-3}$	$9.17 \cdot 10^{-4}$ *	$7.37 \cdot 10^{-4}$ *
Percent Error (%)	-20.9	-52.9	20.8	18.4	24.6
Ionic Strength (mol/l)	0.58	0.05	0.07	0.06	0.07
U (mol/l)	$2.39(\pm 0.04) \cdot 10^{-5}$	$8.19(\pm 0.13) \cdot 10^{-7}$	$5.42(\pm 0.03) \cdot 10^{-7}$	$4.58(\pm 0.04) \cdot 10^{-7}$	$8.45(\pm 0.16) \cdot 10^{-8}$
^{233}U (mol/l)	*ND*	*ND*	*ND*	*ND*	$8.12(\pm 0.27) \cdot 10^{-9}$
Th (mol/l)	--	--	--	--	--
F (mol/l)	$1.34(\pm 0.06) \cdot 10^{-3}$	$3.34(\pm 0.11) \cdot 10^{-4}$	$5.02(\pm 0.07) \cdot 10^{-5}$	*$<5.26 \cdot 10^{-6}$*	*$<5.26 \cdot 10^{-6}$*
Cl (mol/l)	$1.70(\pm 0.03) \cdot 10^{-2}$	$<2.82 \cdot 10^{-6}$	$2.54(\pm 0.04) \cdot 10^{-4}$	$2.48(\pm 0.04) \cdot 10^{-4}$	$1.06(\pm 0.04) \cdot 10^{-4}$
NO_2 (mol/l)	--	--	--	--	--
NO_3 (mol/l)	$6.21(\pm 0.10) \cdot 10^{-4}$	$5.29(\pm 0.08) \cdot 10^{-3}$	$5.07(\pm 0.17) \cdot 10^{-3}$	$5.02(\pm 0.18) \cdot 10^{-3}$	$5.56(\pm 0.09) \cdot 10^{-3}$
SO_4 (mol/l)	$2.56(\pm 0.04) \cdot 10^{-1}$	$1.96(\pm 0.03) \cdot 10^{-2}$	$1.86(\pm 0.03) \cdot 10^{-2}$	$1.83(\pm 0.03) \cdot 10^{-2}$	$1.72(\pm 0.02) \cdot 10^{-2}$
Fe (mol/l)	--	--	--	--	--
B (mol/l)	*ND*	*ND*	*ND*	*ND*	*ND*
Na (mol/l)	$1.26 \cdot 10^{-1}$	$1.28 \cdot 10^{-2}$	$6.68 \cdot 10^{-3}$	$6.52 \cdot 10^{-3}$	$5.83 \cdot 10^{-3}$
Mg (mol/l)	$1.40 \cdot 10^{-1}$	*ND*	$7.49 \cdot 10^{-3}$	$7.23 \cdot 10^{-3}$	$7.00 \cdot 10^{-3}$
Al (mol/l)	*ND*	*ND*	*ND*	*ND*	*ND*
K (mol/l)	*ND*	*ND*	*ND*	*ND*	$3.03 \cdot 10^{-3}$
Ca (mol/l)	*ND*	*ND*	$1.85 \cdot 10^{-2}$	$1.73 \cdot 10^{-2}$	$1.79 \cdot 10^{-2}$
Mn (mol/l)	$1.16 \cdot 10^{-4}$	<	$3.91 \cdot 10^{-5}$	$2.19 \cdot 10^{-5}$	$3.66 \cdot 10^{-6}$
Co (mol/l)	*ND*	*ND*	*ND*	*ND*	*ND*
Cu (mol/l)	*ND*	*ND*	*ND*	*ND*	*ND*

Pore volume	**0.9**	**13.3**	**29.3**	**49.5**	**316.6**
Sample number	**3**	**45**	**73**	**107**	**647**
Zn (mol/l)	*ND*	$6.61 \cdot 10^{-4}$	*ND*	*ND*	$5.34 \cdot 10^{-6}$
Rb (mol/l)	*ND*	*ND*	*ND*	*ND*	*ND*
Sr (mol/l)	$1.08 \cdot 10^{-4}$	$1.19 \cdot 10^{-4}$	$6.12 \cdot 10^{-5}$	$5.42 \cdot 10^{-5}$	$4.66 \cdot 10^{-5}$
Zr (mol/l)	$1.51 \cdot 10^{-5}$	1.51·10-5	$1.30 \cdot 10^{-6}$	$1.50 \cdot 10^{-6}$	$1.54 \cdot 10^{-7}$
Mo (mol/l)	$1.00 \cdot 10^{-5}$	$4.49 \cdot 10^{-6}$	$5.53 \cdot 10^{-7}$	$4.57 \cdot 10^{-7}$	$4.31 \cdot 10^{-8}$
Sn (mol/l)	$2.19 \cdot 10^{-6}$	*ND*	*ND*	$2.12 \cdot 10^{-7}$	$4.30 \cdot 10^{-8}$
Sb (mol/l)	*ND*	$5.75 \cdot 10^{-9}$	*ND*	*ND*	*ND*
Ba (mol/l)	*ND*	*ND*	$8.81 \cdot 10^{-7}$	$8.79 \cdot 10^{-7}$	$7.78 \cdot 10^{-7}$
Eu (mol/l)	*ND*	$3.96 \cdot 10^{-7}$	$3.79 \cdot 10^{-8}$	$3.83 \cdot 10^{-8}$	$4.30 \cdot 10^{-9}$

*calculated from calcite equilibrium; --not determined; ND: not detected; the uncertainty associated with the cations and trace elements is of ±30%.

Appendix 6

Chemical Speciation Results – Column Experiments

Table A6.1: Packed column of aged sludge. Saturation indices of major minerals.

Sample number	Pore volume	Q (ml/min)	Calcite	Dolomite	Magnesite (natural)	Manganite	Rhodochrosite	Barite	Celestite	Gypsum	NaF(s)
1	**0.04**	**0.036**	0.30	0.07	0.04	-2.62	-2.04	0.65	-0.22	-0.06	-4.71
28	**1.2**	**0.036**	0.79	1.13	0.61	-0.39	-1.73	-0.20	-0.33	-0.06	-5.31
40	**5.5**	**0.036**	0.36	-0.19	-0.28	-0.96	-2.14	--	-0.30	-0.18	--
125	**35.4**	**0.036**	0.11	-1.59	-1.42	-1.69	-2.56	--	-0.30	-0.20	--
258	**67.0**	**0.036**	0.18	-1.33	-1.24	-2.69	-2.70	--	-0.41	-0.05	--
263	**67.7**	**0.036**	0.05	-1.61	-1.39	-2.93	-2.75	--	-0.43	-0.07	--
310	**83.2**	**0.146**	0.53	-0.67	-0.93	0.47	-2.42	0.12	-0.49	-0.04	-7.54
377	**145.4**	**0.146**	--	--	--	7.76	--	--	-6.21	--	--
421	**161.6**	**0.357**	--	--	--	8.08	--	--	-8.07	--	--
1311	**597.8**	**0.129**	-1.36	--	--	--	--	-1.33	-3.33	-3.44	-6.92
1319	**605.6**	**0.129**	--	--	--	--	--	--	--	--	-6.01

--not determined; cells highlighted in green show calculated saturation index (SI) of between -1 and 1. Cells highlighted in orange represent calculated SI of -3<SI<-1 and 1<SI<3

Table A6.2: Packed column of aged sludge. Aqueous speciation of U and Th complexes (in % of total dissolved U and Th).

Sample number	Pore volume	Q (ml/min)	$Ca_2UO_2(CO_3)_3$	$CaUO_2(CO_3)_3^{2-}$	$UO_2(CO_3)_3^{4-}$	$UO_2(CO_3)_2^{2-}$	$UO_2(CO_3)$	UO_2F^+	$Th(OH)_3(CO_3)^-$	$Th(OH)_2(CO_3)_2^{2-}$	$Th(OH)_4$	$Th(OH)_3^+$	$Th(OH)_2^{2+}$	ThF_4	ThF_3^+
1	**0.04**	**0.036**	88.73	10.82	0.41	0.04	0.00	0.00	48.18	8.40	37.03	3.84	0.02	0.90	0.07
28	**1.2**	**0.036**	82.80	16.88	0.30	0.02	0.00	0.00	54.25	7.71	37.25	0.47	0.00	0.00	0.00
40	**5.5**	**0.036**	77.30	22.20	0.42	0.08	0.00	0.00	51.23	5.71	41.90	0.75	0.00	0.00	0.00
125	**35.4**	**0.036**	79.76	19.78	0.30	0.13	0.01	0.00	43.85	3.36	51.02	1.27	0.00	0.00	0.00
258	**67.0**	**0.036**	88.34	11.49	0.10	0.06	0.01	0.00	47.03	4.44	45.17	2.26	0.00	0.05	0.00
263	**67.7**	**0.036**	87.65	12.14	0.11	0.09	0.01	0.00	46.76	4.41	44.61	2.80	0.01	0.11	0.01
310	**83.2**	**0.146**	88.70	11.18	0.09	0.03	0.00	0.00	35.56	1.86	61.57	0.79	0.00	0.00	0.00
377	**145.4**	**0.146**	0.00	0.00	0.00	0.00	0.00	0.00	0.00	0.00	0.00	0.00	0.00	0.00	0.00
421	**161.6**	**0.357**	0.00	0.00	0.00	0.00	0.00	0.00	0.00	0.00	0.00	0.00	0.00	0.00	0.00
1311	**597.8**	**0.129**	36.96	41.92	0.99	7.87	3.12	0.06	28.37	1.57	35.00	3.10	0.01	29.72	0.75
1319	**605.6**	**0.129**	0.00	0.00	8.25	27.46	4.39	0.03	47.10	3.42	43.88	2.03	0.00	2.22	0.06

Table A6.3: Packed column of aged sludge. Saturation indices of U and Th minerals.

Sample number	Pore volume	Q (ml/min)	Uranophane	UO2(OH)2(beta)	Clarkeite	Schoepite	Schoepite (des)	Becquerelite (natural)	Rutherfordine	Soddyite (synt 1)	Na-Boltwoodite	Na-Weeksite	ThO2(aged)	ThO2(coll)	ThO2(fresh)
1	**0.04**	**0.036**	1.49	-19.09	-1.81	-4.34	-3.38	-6.19	-4.90	-3.37	-0.95	-2.80	-0.89	-3.49	-1.69
28	**1.2**	**0.036**	2.10	-18.48	-1.85	-4.65	-3.69	-6.84	-5.96	-4.00	-0.98	-2.88	-0.89	-3.49	-1.69
40	**5.5**	**0.036**	2.95	-17.63	--	-3.96	-3.00	-3.22	-5.17	-2.62	--	--	-1.84	-4.44	-2.64
125	**35.4**	**0.036**	3.74	-16.84	--	-3.44	-2.48	-0.36	-4.65	-1.58	--	--	-1.76	-4.36	-2.56
258	**67.0**	**0.036**	2.40	-18.18	--	-3.96	-3.00	-3.76	-4.78	-2.61	--	--	-0.81	-3.41	-1.61
263	**67.7**	**0.036**	2.74	-17.84	--	-3.67	-2.71	-2.27	-4.39	-2.04	--	--	-1.82	-4.42	-2.62
310	**83.2**	**0.146**	4.07	-16.51	-3.08	-3.72	-2.76	-1.12	-5.39	-2.13	-2.21	-5.34	-1.68	-4.28	-2.48
377	**145.4**	**0.146**	--	--	--	-5.17	-4.21	--	--	-5.03	--	--	--	--	--
421	**161.6**	**0.357**	--	--	--	-5.44	-4.48	--	--	-5.57	--	--	--	--	--
1311	**597.8**	**0.129**	3.38	-17.20	-2.64	-2.57	-1.61	2.79	-3.13	0.18	-1.77	-4.46	-0.84	-3.44	-1.64
1319	**605.6**	**0.129**	--	--	-0.97	-2.11	-1.15	--	-2.82	1.09	-0.10	-1.12	-0.78	-3.38	-1.58

--not determined; cells highlighted in green show calculated saturation index (SI) of between -1 and 1. Cells highlighted in orange represent calculated SI of -3<SI<-1 and 1<SI<3

Table A6.4: Packed column of fresh sludge. Saturation indices of major minerals.

Sample number	Pore volume	Q (ml/min)	Calcite	Dolomite	Magnesite (natural)	Manganite	Rhodochrosite	Barite	Celestite	Gypsum	NaF(s)
10	**1.1**	**0.156**	1.01	1.08	0.34	--	--	1.35	-1.13	-0.01	-3.95
23	**2.4**	**0.156**	1.33	1.89	0.83	--	--	0.97	-99.99	0.04	-4.66
60	**9.6**	**0.156**	0.13	-0.52	-0.37	--	--	-99.99	-99.99	-0.02	-6.31
173	**27.5**	**0.156**	-0.65	-2.47	-1.56	--	--	-0.06	-1.54	-0.01	-6.99
325	**82.2**	**0.156**	-0.91	-3.47	-2.29	--	--	-0.20	-2.24	-0.59	-6.87

--not determined; cells highlighted in green show calculated saturation index (SI) of between -1 and 1. Cells highlighted in orange represent calculated SI of -3<SI<-1 and 1<SI<3

Table A6.5: Packed column of fresh sludge. Aqueous speciation of U and Th complexes (in % of total dissolved U and Th).

Sample number	Pore volume	Q (ml/min)	$Ca_2UO_2(CO_3)_3$	$CaUO_2(CO_3)_3^{2-}$	$UO_2(CO_3)_3^{4-}$	$UO_2(CO_3)_2^{2-}$	$UO_2(CO_3)$	UO_2F^+	$Th(OH)_3(CO_3)^-$	$Th(OH)_2(CO_3)_2^{2-}$	$Th(OH)_4$	$Th(OH)_3^+$	$Th(OH)_2^{2+}$	ThF_4	ThF_3^+
10	**1.1**	**0.156**	97.49	2.43	0.08	0.00	0.00	0.00	46.95	20.77	20.26	7.20	0.19	0.95	0.20
23	**2.4**	**0.156**	92.55	7.24	0.21	0.00	0.00	0.00	56.37	22.42	19.79	0.71	0.00	0.00	0.00
60	**9.6**	**0.156**	86.86	12.92	0.13	0.08	0.01	0.00	50.00	5.69	40.47	2.45	0.01	0.07	0.01
173	**27.5**	**0.156**	87.26	11.73	0.10	0.43	0.27	0.01	27.41	1.89	36.21	8.69	0.08	21.14	1.58
325	**82.2**	**0.156**	81.02	16.22	0.14	1.07	0.85	0.04	7.02	0.42	9.66	2.20	0.02	76.98	2.84

Table A6.6: Packed column of fresh sludge. Saturation indices of U and Th minerals.

Sample number	Pore volume	Q (ml/min)	Uranophane	UO2(OH)2(beta)	Clarkeite	Schoepite	Schoepite (des)	Becquerelite (natural)	Rutherfordine	Soddyite (synt 1)	Na-Boltwoodite	Na-Weeksite	ThO2(aged)	ThO2(coll)	ThO2(fresh)
10	**1.1**	**0.156**	-1.29	-4.75	-2.56	-5.79	-4.82	-14.75	-5.76	-6.25	-1.71	-4.31	-0.23	-2.83	-1.03
23	**2.4**	**0.156**	-1.53	-5.40	-3.27	-6.44	-5.47	-17.60	-7.13	-7.56	-2.41	-5.72	-0.26	-2.86	-1.06
60	**9.6**	**0.156**	1.47	-3.29	-3.11	-4.32	-3.36	-6.14	-4.99	-3.33	-2.24	-5.39	-0.09	-2.69	-0.89
173	**27.5**	**0.156**	2.43	-2.23	-3.37	-3.26	-2.30	-0.92	-3.54	-1.21	-2.50	-5.91	-0.41	-3.01	-1.21
325	**82.2**	**0.156**	2.29	-2.17	-3.47	-3.20	-2.24	-0.83	-3.47	-1.09	-2.60	-6.11	-1.08	-3.68	-1.88

--not determined; cells highlighted in green show calculated saturation index (SI) of between -1 and 1. Cells highlighted in orange represent calculated SI of -3<SI<-1 and 1<SI<3

Table A6.7: Undisturbed column of fresh sludge. Saturation indices of major minerals.

Sample number	Volume eluted (ml)	Q (ml/min)	Calcite	Dolomite	Magnesite (natural)	Manganite	Rhodochrosite	Barite	Celestite	Gypsum	Fluorite
22	**109**	**0.065**	2.17	3.39	1.50	-1.89	-0.41	-0.03	-1.54	0.07	1.59
81	**400**	**0.065**	1.36	1.60	0.51	-2.25	-0.75	0.25	-1.27	0.11	0.79
174	**858**	**0.065**	2.29	3.45	1.44	-0.76	-0.84	0.01	-1.33	0.06	1.36
243	**1277**	**0.065**	1.88	2.85	1.24	-1.54	-1.08	0.06	-1.24	0.06	1.13
370	**2058**	**0.065**	1.86	2.83	1.24	-1.59	-1.40	-0.02	-1.30	-0.05	1.04
435	**2503**	**0.065**	1.31	1.67	0.64	-2.57	-1.78	-0.03	-1.30	-0.07	1.04
484	**2717**	**0.065**	1.51	2.14	0.90	-2.10	-1.37	0.14	-1.16	0.07	1.03

--not determined; cells highlighted in green show calculated saturation index (SI) of between -1 and 1. Cells highlighted in orange represent calculated SI of -3<SI<-1 and 1<SI<3

Table A6.8: Undisturbed column of fresh sludge. Aqueous speciation of U and Th complexes (in % of total dissolved U and Th).

Sample number	Pore volume	Q (ml/min)	$Ca_2UO_2(CO_3)_3$	$CaUO_2(CO_3)_3^{2-}$	$UO_2(CO_3)_3^{4-}$	$UO_2(CO_3)_2^{2-}$	$UO_2(CO_3)$	UO_2F^+	$Th(OH)_3(CO_3)^-$	$Th(OH)_2(CO_3)_2^{2-}$	$Th(OH)_4$	$Th(OH)_3^+$	$Th(OH)_2^{2+}$	ThF_4	ThF_3^+
22	**109**	**0.065**	96.18	3.62	0.19	0.00	0.00	0.00	18.25	41.09	1.59	0.10	0.00	0.00	0.00
81	**400**	**0.065**	94.89	4.95	0.16	0.00	0.00	0.00	41.94	48.50	5.79	0.93	0.01	0.00	0.00
174	**858**	**0.065**	92.45	7.38	0.17	0.00	0.00	0.00	39.41	52.39	3.89	0.05	0.00	0.00	0.00
243	**1277**	**0.065**	92.47	7.42	0.11	0.00	0.00	0.00	49.60	42.69	6.83	0.13	0.00	0.00	0.00
370	**2058**	**0.065**	89.06	10.83	0.12	0.00	0.00	0.00	60.80	23.35	15.53	0.08	0.00	0.00	0.00
435	**2503**	**0.065**	87.73	12.14	0.12	0.00	0.00	0.00	57.97	31.14	10.13	0.21	0.00	0.00	0.00
484	**2717**	**0.065**	92.17	7.76	0.06	0.00	0.00	0.00	58.17	29.63	11.42	0.24	0.00	0.00	0.00

Table A6.9: Undisturbed column of fresh sludge. Saturation indices of U and Th minerals.

Sample number	Volume eluted (ml)	Q (ml/min)	Uranophane	UO2(OH)2(beta)	Clarkeite	Schoepite	Schoepite (des)	Becquerelite (natural)	Rutherfordine	Soddyite (synt 1)	Na-Boltwoodite	Na-Weeksite	ThO2(aged)	ThO2(coll)	ThO2(fresh)
22	**109**	**0.065**	-10.58	-8.71	-6.18	-9.76	-8.78	-37.48	-9.63	-15.37	-6.55	-17.58	-2.21	-4.81	-3.01
81	**400**	**0.065**	-9.22	-7.53	-5.65	-8.57	-7.60	-31.32	-8.25	-13.03	-6.02	-16.62	-1.69	-4.29	-2.49
174	**858**	**0.065**	-9.75	-8.67	-6.24	-9.70	-8.74	-36.35	-10.28	-15.36	-6.63	-17.97	-2.87	-5.47	-3.67
243	**1277**	**0.065**	-8.69	-7.92	-5.93	-8.95	-7.99	-32.28	-9.46	-13.84	-6.32	-17.31	-1.85	-4.45	-2.65
370	**2058**	**0.065**	-6.54	-7.18	-5.24	-8.21	-7.25	-27.11	-9.50	-12.41	-5.66	-16.13	-1.49	-4.09	-2.29
435	**2503**	**0.065**	-7.23	-6.88	-5.90	-7.91	-6.95	-26.70	-8.39	-11.77	-6.28	-17.23	-1.68	-4.28	-2.48
484	**2717**	**0.065**	-6.56	-6.97	-5.75	-8.00	-7.04	-26.97	-8.55	-11.66	-5.84	-15.49	-1.63	-4.23	-2.43

--not determined; cells highlighted in green show calculated saturation index (SI) of between -1 and 1. Cells highlighted in orange represent calculated SI of -3<SI<-1 and 1<SI<3

Table A6.10: Packed column of aged tailings. Saturation indices of major minerals.

Sample number	Pore volume	Q (ml/min)	Calcite	Dolomite	Magnesite (natural)	Manganite	Rhodochrosite	Barite	Celestite	Gypsum	NaF(s)
1_4	0.6	0.037	--	--	--	-1.89	--	1.79	0.97	1.04	--
1_11	1.6	0.037	--	--	--	-4.03	--	0.27	-0.26	-0.21	-5.43
2_3	7.2	0.126	-0.45	-1.85	-1.13	-2.00	-1.24	0.39	0.16	0.26	-7.45
2_21	11.9	0.126	-0.23	-1.84	-1.34	-0.62	-1.04	0.31	0.04	0.27	-8.24
2_46	18.4	0.126	-0.59	-2.87	-2.02	-0.35	-1.42	0.37	-0.11	0.27	-8.47
3_2	23.3	0.331	-0.29	-1.85	-1.29	-2.28	-1.13	0.51	0.07	0.28	-8.01
3_15	28.3	0.331	-0.45	-2.63	-1.92	-3.01	-1.55	0.20	-0.44	-0.02	-8.39
3_30	34.0	0.331	-0.29	-2.30	-1.74	-2.68	-1.64	0.27	-0.45	-0.01	-8.24
3_144	77.5	0.331	0.28	-1.89	-1.91	-0.69	-1.50	0.24	-0.82	-0.01	-8.63
3_202	99.6	0.331	0.13	-2.15	-2.01	-1.08	-1.69	0.23	-0.83	0.00	-8.67
4_3	107.5	0.396	0.60	-0.55	-0.88	-1.21	-1.24	0.33	-0.45	0.00	-8.04
4_15	111.6	0.396	0.31	-1.64	-1.68	-0.90	-1.38	0.28	-0.67	-0.01	-7.50
4_105	142.7	0.396	0.24	-2.33	-2.30	-0.97	-1.78	0.23	-0.86	0.01	-8.90

--not determined; cells highlighted in green show calculated saturation index (SI) of between -1 and 1. Cells highlighted in orange represent calculated SI of -3<SI<-1 and 1<SI<3

Table A6.11: Packed column of aged tailings. Aqueous speciation of U and Th complexes (in % of total dissolved U and Th).

Sample number	Pore volume	Q (ml/min)	$Ca_2UO_2(CO_3)_3$	$CaUO_2(CO_3)_3^{2-}$	$UO_2(CO_3)_3^{4-}$	$UO_2(CO_3)_2^{2-}$	$UO_2(CO_3)$	UO_2F^+	$Th(OH)_3(CO_3)^-$	$Th(OH)_2(CO_3)_2^{2-}$	$Th(OH)_4$	$Th(OH)_3^+$	$Th(OH)_2^{2+}$	ThF_4	ThF_3^+
1_4	**0.6**	**0.037**	0.00	0.00	0.00	0.00	0.00	1.42	0.00	0.00	46.12	27.77	1.09	19.41	4.07
1_11	**1.6**	**0.037**	0.00	0.00	0.00	0.00	0.00	1.10	0.00	0.00	32.82	5.19	0.04	59.54	2.28
2_3	**7.2**	**0.126**	43.63	43.47	11.47	1.00	0.06	0.00	49.87	8.49	37.79	2.71	0.01	0.01	0.00
2_21	**11.9**	**0.126**	46.80	42.85	9.72	0.60	0.02	0.00	53.19	10.81	33.23	1.84	0.01	0.00	0.00
2_46	**18.4**	**0.126**	45.59	42.55	9.94	1.34	0.11	0.00	38.76	3.54	54.02	2.99	0.01	0.00	0.00
3_2	**23.3**	**0.331**	50.15	41.15	7.98	0.65	0.03	0.00	54.96	13.93	27.19	2.37	0.01	0.00	0.00
3_15	**28.3**	**0.331**	87.59	11.86	0.11	0.27	0.11	0.00	35.35	2.15	53.33	7.06	0.03	0.04	0.01
3_30	**34.0**	**0.331**	87.83	11.79	0.10	0.19	0.05	0.00	37.34	2.38	53.42	5.22	0.02	0.02	0.00
3_144	**77.5**	**0.331**	87.66	12.15	0.11	0.05	0.00	0.00	30.95	1.31	66.40	1.10	0.00	0.00	0.00
3_202	**99.6**	**0.331**	87.78	12.01	0.11	0.07	0.01	0.00	32.48	1.50	63.96	1.68	0.00	0.00	0.00
4_3	**107.5**	**0.396**	88.09	11.78	0.10	0.02	0.00	0.00	53.31	6.77	38.37	0.96	0.00	0.00	0.00
4_15	**111.6**	**0.396**	87.50	12.32	0.11	0.05	0.00	0.00	37.60	2.20	58.59	1.25	0.00	0.00	0.00
4_105	**142.7**	**0.396**	87.84	11.96	0.11	0.06	0.00	0.00	27.37	0.97	70.34	1.12	0.00	0.00	0.00

Table A6.12: Packed column of aged tailings. Saturation indices of U and Th minerals.

Sample number	Pore volume	Q (ml/min)	Uranophane	UO2(OH)2(beta)	Clarkeite	Schoepite	Schoepite (des)	Becquerelite (natural)	Rutherfordine	Soddyite (synt 1)	Na-Boltwoodite	Na-Weeksite	ThO2(aged)	ThO2(coll)	ThO2(fresh)
1_4	**0.6**	**0.037**	7.15	0.62	--	-0.41	0.55	16.62	--	3.78	--	--	-1.03	-3.63	-1.83
1_11	**1.6**	**0.037**	4.68	0.75	1.04	-0.29	0.68	16.54	--	3.08	0.25	-5.39	-1.58	-4.18	-2.38
2_3	**7.2**	**0.126**	3.31	-1.49	-2.19	-2.52	-1.56	4.16	-3.23	-0.34	-1.94	-6.64	-2.07	-4.67	-2.87
2_21	**11.9**	**0.126**	1.09	-2.56	-3.80	-3.59	-2.63	-2.03	-4.33	-2.65	-3.71	-10.66	-1.94	-4.54	-2.74
2_46	**18.4**	**0.126**	2.19	-1.88	-3.27	-2.91	-1.95	2.02	-4.00	-1.42	-3.30	-10.21	-1.73	-4.33	-2.53
3_2	**23.3**	**0.331**	1.39	-2.30	-3.40	-3.33	-2.37	-0.84	-3.76	-2.05	-3.24	-9.50	-2.03	-4.63	-2.83
3_15	**28.3**	**0.331**	0.66	-2.48	-4.28	-3.51	-2.55	-1.88	-4.11	-2.60	-4.31	-12.24	-1.74	-4.34	-2.54
3_30	**34.0**	**0.331**	0.61	-2.63	-4.24	-3.66	-2.70	-2.57	-4.37	-2.91	-4.27	-12.14	-1.74	-4.34	-2.54
3_144	**77.5**	**0.331**	-0.34	-3.51	-4.50	-4.54	-3.58	-6.30	-6.19	-5.03	-4.89	-14.47	-1.64	-4.24	-2.44
3_202	**99.6**	**0.331**	-0.71	-3.51	-4.70	-4.54	-3.58	-6.68	-5.95	-5.01	-5.08	-14.81	-1.66	-4.26	-2.46
4_3	**107.5**	**0.396**	-1.22	-4.20	-5.00	-5.23	-4.27	-10.80	-6.23	-5.99	-4.96	-13.33	-1.88	-4.48	-2.68
4_15	**111.6**	**0.396**	0.60	-3.28	-3.11	-4.31	-3.35	-5.12	-5.71	-4.21	-3.14	-9.91	-1.70	-4.30	-2.50
4_105	**142.7**	**0.396**	-0.16	-3.47	-4.43	-4.50	-3.54	-6.03	-6.25	-4.93	-4.79	-14.17	-1.62	-4.22	-2.42

--not determined; cells highlighted in green show calculated saturation index (SI) of between -1 and 1. Cells highlighted in orange represent calculated SI of -3<SI<-1 and 1<SI<3

Table A6.13: Packed column of fresh tailings. Saturation indices of major minerals.

Sample number	Pore volume	Q (ml/min)	Calcite	Dolomite	Magnesite (natural)	Manganite	Rhodochrosite	Barite	Celestite	Gypsum	NaF(s)
3	**0.9**	**0.154**	--	--	2.27	-1.45	-0.04	--	0.09	--	-4.00
45	**13.3**	**0.154**	--	--	--	--	--	--	0.04	--	-5.06
73	**29.3**	**0.154**	0.33	0.44	0.38	-0.73	-0.08	0.91	-0.45	0.02	-6.34
107	**49.5**	**0.154**	0.00	-0.20	0.07	-1.52	-0.44	0.91	-0.49	0.00	--
647	**316.6**	**0.154**	0.00	-0.23	0.04	-1.63	-1.23	0.84	-0.58	-0.01	--

--not determined; cells highlighted in green show calculated saturation index (SI) of between -1 and 1. Cells highlighted in orange represent calculated SI of -3<SI<-1 and 1<SI<3

Table A6.14: Packed column of fresh tailings. Aqueous speciation of U and Th complexes (in % of total dissolved U and Th).

Sample number	Pore volume	Q (ml/min)	$Ca_2UO_2(CO_3)_3$	$CaUO_2(CO_3)_3^{2-}$	$UO_2(CO_3)_3^{4-}$	$UO_2(CO_3)_2^{2-}$	$UO_2(CO_3)$	UO_2F^+	$Th(OH)_3(CO_3)^-$ *	$Th(OH)_2(CO_3)_2^{2-}$ *	$Th(OH)_4$ *	$Th(OH)_3^+$ *	$Th(OH)_2^{2+}$ *	ThF_4 *	ThF_3^+ *
3	**0.9**	**0.154**	0.00	0.00	99.79	0.21	0.00	0.00	--	--	--	--	--	--	--
45	**13.3**	**0.154**	0.00	0.00	80.96	17.50	0.67	0.00	--	--	--	--	--	--	--
73	**29.3**	**0.154**	88.17	11.65	0.13	0.04	0.00	0.00	--	--	--	--	--	--	--
107	**49.5**	**0.154**	87.57	12.17	0.14	0.10	0.01	0.00	--	--	--	--	--	--	--
647	**316.6**	**0.154**	88.08	11.67	0.13	0.09	0.01	0.00	--	--	--	--	--	--	--

*no Th analysis were carried out for this experiment

Table A6.15: Packed column of fresh tailings. Saturation indices of U and Th minerals.

Sample number	Pore volume	Q (ml/min)	Uranophane	UO2(OH)2(beta)	Clarkeite	Schoepite	Schoepite (des)	Becquerelite (natural)	Rutherfordine	Soddyite (synt 1)	Na-Boltwoodite	Na-Weeksite	ThO2(aged) *	ThO2(coll) *	ThO2(fresh) *
3	**0.9**	**0.154**	--	-4.56	-2.37	-5.59	-4.63	--	-5.12	-5.86	-1.50	-3.91	--	--	--
45	**13.3**	**0.154**	--	-2.09	-0.91	-3.12	-2.16	--	-3.25	-0.92	-0.04	-0.98	--	--	--
73	**29.3**	**0.154**	-1.19	-4.55	-3.72	-5.58	-4.62	-13.82	-5.89	-5.84	-2.85	-6.61	--	--	--
107	**49.5**	**0.154**	-0.90	-4.14	-3.56	-5.17	-4.21	-11.91	-5.30	-5.04	-2.69	-6.30	--	--	--
647	**316.6**	**0.154**	-2.02	-4.78	-4.18	-5.81	-4.85	-15.60	-6.11	-6.32	-3.31	-7.54	--	--	--

--not determined; cells highlighted in green show calculated saturation index (SI) of between -1 and 1. Cells highlighted in orange represent calculated SI of -3<SI<-1 and 1<SI<3

*no Th analysis were carried out for this experiment